ANALYSIS OF RHOH FUNCTION *IN VIVO*

TATJANA DORN

MÜNCHEN 2007

Hiermit erkläre ich, dass ich die vorliegende Dissertation selbständig und ohne unerlaubte Hilfe angefertigt habe. Ich habe weder anderweitig versucht, eine Dissertation einzureichen oder eine Doktorprüfung durchzuführen, noch habe ich diese Dissertation oder Teile derselben einer anderen Prüfungskommission vorgelegt.

Tatjana Dorn
München, 13.06.2007

Die vorliegende Arbeit wurde zwischen Januar 2004 und Mai 2007 unter Anleitung von Prof. Dr. Cord Brakebusch am Max-Planck-Institut für Biochemie in Martinsried und an der Universität von Kopenhagen durchgeführt.

Wesentliche Teile dieser Arbeit sind in folgender Publikation veröffentlicht:

Dorn, T., Kuhn, U., Bungartz, G., Stiller, S., Bauer, M., Ellwart, J., Peters, T., Scharffetter-Kochanek, K., Semmrich, M., Laschinger, M., Holzmann, B., Klinkert, W.E.F., Straten, P.T., Køllgaard, T., Sixt, M. and Brakebusch, C. (2007). RhoH is important for positive thymocyte selection and T cell receptor signaling. *Blood* 109: 2346-2355.

Promotionsgesuch eingereicht am: 13.06.2007

Tag der mündlichen Prüfung am: 01.08.2007

Erster Gutachter: Prof. Dr. Charles N. David

Zweiter Gutachter: Prof. Dr. Michael Schleicher

Sondergutachter: Prof. Dr. Cord Brakebusch

Table of contents

Abbreviations

aa	amino acid		**HSC**	hematopoietic stem cell
ADP	adenosin 5'-diphosphate		**ICAM**	intercellular cell adhesion molecule
APC	antigen presenting cell		**Ig**	immunoglobulin
APS	ammonium persulfate		**ITAM**	immunotyrosine activation motif
ATP	adenosine 5'-triphosphate		**IP$_3$**	inositol-1,4,5-trisphosphate
BCL6	B cell lymphoma 6		**kD**	kilo dalton
BCR	B cell receptor		**KLH**	keyhole limpet hemocyanin
BM	bone marrow		**ko**	mutant samples/mice (in figures)
bp/kb	base pairs/1000 bases		**LAT**	linker of activation in T cells
BrdU	bromodeoxyuridine		**LB**	Luria Bertoni
BSA	bovine serum albumin		**LFA-1**	lymphocyte function-associated antigen 1
c.a.	constitutively active		**LN**	lymph node
CIP	calf intestine phosphatase		**Mg**	magnesium
CLP	common lymphoid progenitor		**Mn**	manganese
cDNA	complementary DNA		**MeOH**	methanol
DAG	diacylglycerol		**MHC**	major histocompatibility complex
DC	dendritic cell		**min**	minute
ddH$_2$O	double-distilled water		**MKK6**	MAP kinase kinase 6
DEPC	diethylpyrocarbonate		**NADPH**	nicotinamide adenine dinucleotide phosphate
DH	Dbl homology		**NFAT**	nuclear factor of activated T cells
DL1	delta like 1		**NF-κB**	nuclear factor κB
DLBCL	diffuse large B cell lymphoma		**NHL**	Non-Hodgkin's lymphoma
DMSO	dimethylsulfoxide		**NK**	natural killer
DN	double negative		**NKT**	natural killer T
d.n.	dominant negative		**NP$_{20}$-CG**	nitrophenyl-chicken-γ-globulin
dNTP	deoxynucleotide triphosphates		**OD**	optical density
DP	double positive		**o/n**	over night
DMRIE-C	1,2-dimyristyloxypropyl-3-dimethyl-hydroxyl ethyl bromide ammonium bromide-cholesterol		**PCR**	polymerase chain reaction
			PBS	phosphate-buffered-saline
E. coli	*Escherichia coli*		**PE**	phycoerythrin
e.g.	for example (*lat.* exempli gratia)		**PKC θ**	protein kinase C θ
EDTA	ethylene-diamine-tetraacetic acid		**PFA**	paraformaldehyd
ES cells	embryonic stem cells		**PI-3K**	phosphoinositide kinase 3
EtOH	ethanol		**PIP$_2$**	phosphatidylinositol-(4,5)-bisphosphate
FACS	fluorescence activated cell sorter		**PIP$_3$**	phosphatidylinositol-(3,4,5)-trisphosphate
FCS	fetal calf serum			
FITC	fluorescein isothiocyanate		**PH**	pleckstrin homology
GAPDH	glyceraldehyde-3-phosphate dehydrogenase		**PLCγ1**	phospholipase C γ1
GAPs	GTPase activating proteins		**PMA**	phorbol-12-myristate-13-acetate
GDIs	guanine nucleotide dissociation inhibitors		**PS**	phosphatidylserine
GEFs	guanine nucleotide exchange factors		**PVDF**	polyvinylidene fluoride
GS	glutathion-sepharose		**RAG**	recombination activating gene
GST	glutathione-S-transferase		**Rho**	Ras homolog
GTP	guanosine triphosphate		**RNase**	ribonuclease
GTPase	guanosine triphosphatase			
HL	Hodgkin's lymphoma			

HPC	hematopoietic progenitor cell	**rpm**	rotations per minute
RT	room temperature	**SP**	single positive
RT-PCR	reverse transcription PCR	**TAP**	tandem affinity purifcation
SDS	sodium dodecyl sulphate	**TCR**	T cell receptor
SDS-PAGE	SDS-polyacrylamide gel electrophoresis	**TBS**	tris-buffered saline
sec	second	**TD**	T cell dependent
ROS	reactive oxygen species	**TI**	T cell independent
SHM	somatic hypermutation	**Tris**	tris-hydroxymethyl-aminomethane
SLP-76	SH2-domain containing leukocyte protein of 76 kD	**U**	unit of enzyme activity
		ZAP70	ζ-chain-associated protein of 70 kD

1 Summary

Rho GTPases are small GTPases that regulate cytoskeletal organization, proliferation, survival and cell polarization. They are present in an active GTP-bound form and an inactive GDP-bound form. Only in the GTP-bound conformation can they interact with a wide range of effector molecules including serine-threonine kinases, lipid kinases and cytoskeletal proteins. RhoH is a small GTPase that is expressed only in the hematopoietic system. RhoH was found to have no intrinsic GTPase activity and is suggested to be constitutively active, and to be controlled only at the transcriptional level. In diffuse large B cell lymphoma the *RhoH* gene is frequently mutated in the non-coding region, which might affect mRNA stability or translation efficiency. Functionally, RhoH was proposed to be a negative regulator of Rho GTPases and integrins.

Using mice with a targeted disruption of the *RhoH* gene, we demonstrate that RhoH is crucial for thymocyte development and that it is a positive regulator of pre-TCR and TCR signaling.

In the absence of RhoH, thymocyte maturation was partially blocked at the DN3 to DN4 transition and at the transition from DP to CD4SP and CD8SP cells, where β-selection and positive selection take place, respectively. In line with defects in β-selection and positive selection, proliferation of RhoH-null DN3 and DN4 cells was reduced, while apoptosis of DN4, DP, CD4SP and CD8SP cells was increased. Furthermore, RhoH-deficient DN3 and DN4 thymocytes exhibited a severely impaired ability to differentiate and expand *in vitro*. Analysis of RhoH-null mice expressing an ovalbumin specific MHC class II restricted TCR confirmed that RhoH is important for positive selection, since no increase in positively selected CD4SP thymocytes was observed, in contrast to controls. The defects in thymocyte development, as well as the aberrant expression of maturation markers in the absence of RhoH, indicated a significant role of RhoH in pre-TCR and TCR signaling. The examination of TCR signaling *in vitro* revealed that while RhoH is not required for TCR-induced proximal signaling events, such as activation of ZAP70, it is crucial for distal signaling events, such as phosphorylation of LAT, PLCγ1, and Vav1, the activation of Erk, and calcium influx. These data suggest that RhoH is important for pre-TCR and TCR signaling by allowing the efficient interaction of ZAP70 with the LAT signalosome, thus regulating thymocyte development.

2 Introduction

2.1 Family of Rho GTPases

2.1.1 Overview of Rho GTPase family

Ras homologous (Rho) proteins belong to the Ras superfamily of 20-30 kD small guanosine triphosphates (GTPases) and are required for various cellular processes. GTPases function as molecular switches cycling between an active GTP-bound and inactive GDP-bound form, and they possess an intrinsic ability to hydrolyse GTP. In the active state GTPases interact with a target protein and generate a response until GTP hydrolysis returns the switch to the inactive state (Figure 1; Etienne-Manneville and Hall, 2002).
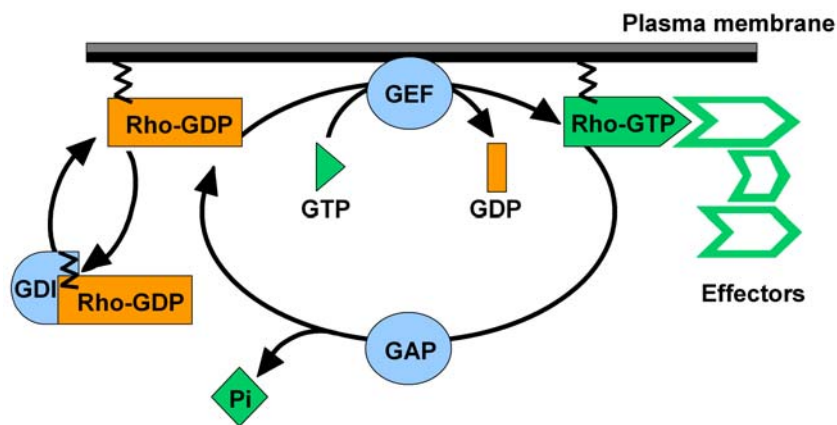
Figure 1. The Rho GTPase cycle. Rho GTPases cycle between an active (GTP-bound) and an inactive (GDP-bound) state. In the active state, they interact with effector proteins involved in a variety of cellular processes. The cycle is tightly regulated by three classes of protein: GEFs (guanine nucleotide exchange factors), which catalyze the loading of the Rho GTPases with GTP, GAPs (GTPase activating proteins), that accelerate the GTP hydrolysis, and GDIs (guanine nucleotide dissociation inhibitors), which negatively regulate the Rho GTPases by sequestration (from Etienne-Manneville and Hall, 2002).

The Ras superfamily comprises over 150 members in humans and is divided into five major families on the basis of sequence and functional similarities: Ras, Rho, Rab, Ran and Arf (Wennerberg et al., 2005). 22 mammalian genes have been identified encoding Rho GTPases that can be further classified into nine different subfamilies based on the primary amino acid (aa) sequence identity, structural motifs and biological function, with similar but not identical properties (Figure 2; Wennerberg and Der, 2004): RhoA-related subfamily (RhoA, RhoB, RhoC), Rac1-related subfamily (Rac1, Rac1b, Rac2, Rac3, RhoG), Cdc42-related subfamily (Cdc42, G25K, TC10, TCL, Wrch-1, Chp/Wrch-2), Rnd subfamily (Rnd1, Rnd2, Rnd3/RhoE), RhoBTB subfamily (RhoBTB1, RhoBTB2, RhoBTB3), Miro subfamily (Miro1, Miro2), Rif/RhoF, RhoD and RhoH/TTF. Of these, the RhoBTB and the Miro family are

considered as atypical. Most typical Rho GTPases are small (190-250 aa), however some of the more atypical family members can be more than 700 aa long.
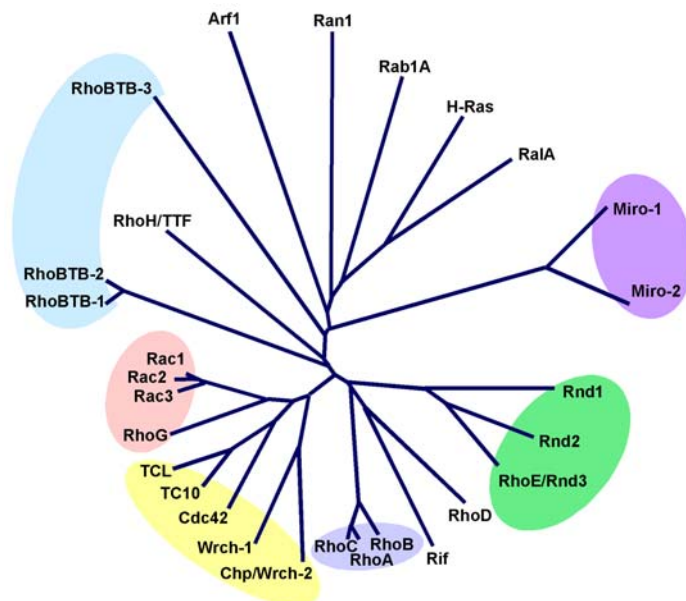
Figure 2. Phylogenetic tree of the Rho GTPases and other members of the Ras superfamily. Based on the sequence similarity and functional data nine Rho subfamilies can be distinguished (modified from Wennerberg and Der, 2004).

Rho family proteins are defined by a presence of a Rho-type GTPase-like domain, flanked by short N-terminal and C-terminal extensions. The GTPase domain consists of a mixed six-stranded β-sheet and five α-helices, connected with loops (Figure 3A and Figure 15). A structural feature that distinguishes Rho proteins from other small GTPases is the Rho insert domain of 13 aa located between the fifth β-strand and the fourth α-helix in the small GTPase domain (Figure 3A; Valencia, 1991; Wennerberg and Der, 2004; Nassar et al., 2006). Within their GTPase domains, the Rho proteins share approximately 40-95% identity and there is 30% identity with the Ras protein GTPase domains.
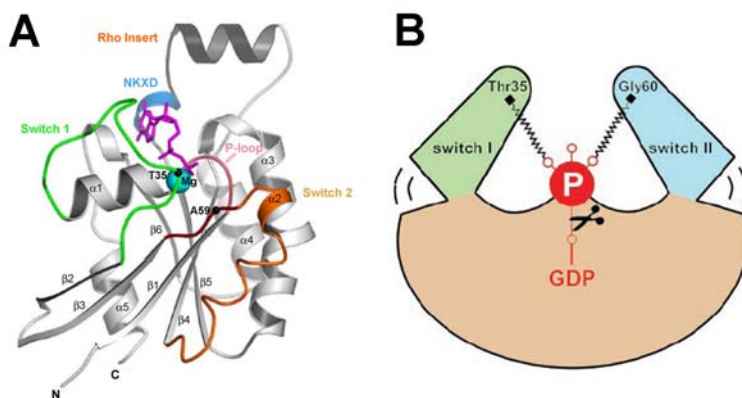
Figure 3. Structure of Rho GTPases. (A) Ribbon plot of the GTPase (Rac) with the conserved sequence elements and the switch regions in different colours as indicated. The nucleotide and Mg^{2+} ion are shown in ball-and-stick representation (modified from Nassar et al., 2006). (B) Schematic diagram of the universal loaded spring mechanism where the switch I and II domains are bound to the γ-phosphate via the NH groups of the invariant Thr and Gly residues. Release of γ-phosphate after GTP hydrolysis allows the switch regions to relax into a different conformation (from Vetter and Wittinghofer, 2001).

The most important contributions in binding of a nucleotide to the GTPase are made by the interaction of a base with the N/TKXD motif and the interaction of the β- and γ-phosphates with the conserved phosphate-binding loop, the GxxxxGKS/T motif (Figure 3A; Vetter and Wittinghofer, 2001). The loading of the GTPase with GTP involves a conformational change

that can be described as the loaded spring mechanism where the switch I and II domains are bound to the γ-phosphate via the main chain of NH groups of the invariant threonine (Thr) and glycine (Gly) residues (Figure 3B; Vetter and Wittinghofer, 2001). This process is dependent on the presence of magnesium (Mg^{2+}) which is then bound by the side chain of threonine. GTP hydrolysis releases the γ-phosphate allowing the switch regions to relax into a different GDP-bound conformation. The aa glycine at the position 14 and glutamine at the position 63, in the phosphate binding loop and switch II region, respectively, are important for the GTPase activity (RhoA numbering; Vetter and Wittinghofer, 2001).

2.1.2 Regulation of Rho GTPases

2.1.2.1 Regulation by GEFs, GAPs and GDIs

The GDP/GTP cycle of the Rho GTPases is tightly regulated by three classes of protein: (1) guanine nucleotide exchange factors (GEFs), which stimulate the weak intrinsic exchange activity of Rho proteins to promote an exchange of the bound GDP to GTP and thus formation of active Rho-GTP and association with downstream effectors; (2) GTPase activating proteins (GAPs), which accelerate the intrinsic GTP hydrolysis of Rho proteins and thereby promote the formation of the inactive GDP-bound protein; and (3) guanine dissociation inhibitors (GDIs), which negatively regulate GTPases (Figure 1; Etienne-Manneville and Hall, 2002).

Currently, around 80 GEFs, 70 GAPs and 3 GDIs have been identified in mammalian cells. A regulator can be specific for only one Rho GTPase, but it can also recognize multiple GTPases, and a GTPase can interact with several regulators, too.

GEFs interact strongly with the switch I and II, the β2- and β3-strands as well as with the phosphate-binding loop and Mg^{2+}-binding area and stabilize nucleotide-depleted GTPases (Figure 3A and Figure 4). In cells, GTP concentration is higher than GDP, and these nucleotide-depleted complexes rapidly dissociate into GTP-bound GTPases and free GEFs. The GEF family encompasses the larger Dbl subfamily and the smaller Dock/CZH subfamily with 69 and 11 members, respectively (Rossman et al., 2005; Meller et al., 2005). The Dbl GEF proteins contain the Dbl homology (DH) domain, which is required for the catalysis of the GDP/GTP exchange in the target GTPase, and the adjacent C-terminal pleckstrin homology (PH) domain, that binds to phosphoinositides and therefore is important for membrane localization of the GEFs and also modulates DH domain activity (Rossman et al., 2005). The Dock family members lack the DH domain. Instead they possess the Dock-homology region-1 and -2 (DHR1 and DHR2, known also as CZH1 and CZH2 domains) that

promote guanine nucleotide exchange (Meller et al., 2005). A novel class of GEFs, SWAP70 and SLAT, have been recently identified (Shinohara et al., 2002; Gupta et al., 2003a; Gupta et al., 2003b). They contain a DH domain with a low degree of homology with the Dbl GEFs and an N-terminal PH domain.

The RhoGAP family is defined by the presence of a conserved RhoGAP domain with at least 20% sequence identity with other family members. It is often accompanied by a number of functional domains (Moon and Zheng, 2003). The interaction between RhoGAP and Rho GTPase is mostly mediated by both the switch I and II regions and the phosphate-binding loop of the Rho GTPase (Figure 3A and Figure 4; Moon and Zheng, 2003). RhoGAP provides a so-called catalytic arginine finger for the active site of glutamine at the position 63 of the GTPase (RhoA numbering) and thus accelerates GTP hydrolysis. However, mechanisms of GAP-assisted GTP hydrolysis independent of arginine and glutamine also exist.

Emerging evidence indicates that GEF and GAP activities are regulated by a wide variety of mechanisms, such as lipid binding, phosphorylation, proteolytic degradation and protein-protein interaction representing indirect mechanisms of regulation of GTPases (Tcherkezian and Lamarche-Vane, 2007).
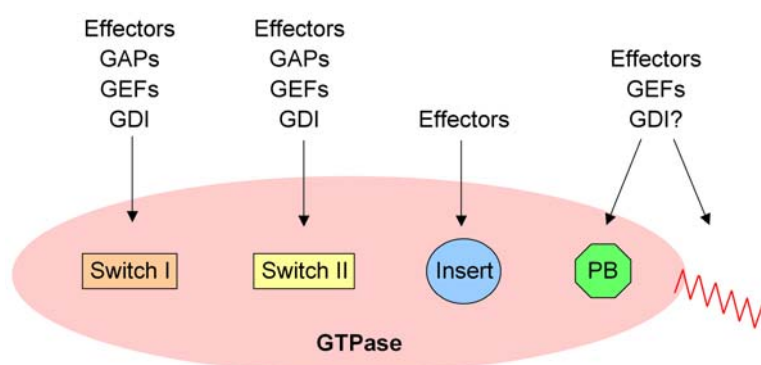
Figure 4. Schematic representation of the structural domains of Rho GTPases. Regulatory and effector partners of Rho GTPases physically interact with several regions in Rho GTPases [switch I, switch II, Rho insert, "polybasic domain" (PB) and the C-terminal CAAX motif] (modified from DerMardirossian and Bokoch, 2005).

An additional level of regulation for Rho GTPases is based on GDIs. GDIα, GDIβ, GDIγ, and a few other proteins are suggested to have GDI activity towards Rho GTPases (DerMardirossian and Bokoch, 2005). Three distinct mechanisms of inhibition of Rho GTPases have been described for Rho GDIs. First, they inhibit the dissociation of GDP from GTPases, maintaining the GTPase in the inactive form and preventing GTPase activation by GEFs. Second, GDIs bind GTP-loaded GTPases, inhibiting GTP hydrolysis and blocking interactions with effector proteins. Finally, GDIs sequester Rho GTPases in the cytosol, removing them from the GDP/GTP cycle. In addition, GDIs are suggested to function as shuttles transporting Rho GTPases between different intracellular membranes (DerMardirossian and Bokoch, 2005). The physical interaction of GDIs with Rho GTPases occurs via the switch I

and II regions, the "polybasic domain" and the terminal "CAAX motif" of the Rho GTPases (Figure 4; DerMardirossian and Bokoch, 2005). GDIs can also be regulated by phosphorylation, which can affect their association with GTPases.

2.1.2.2 Regulation by lipid modification

The activity of Rho GTPases is dependent on their localization to membranes. This property is achieved by the posttranslational lipid modification of the C-terminal CAAX motif by farnesylation, geranylation or methylation, as summarized in Figure 5A (Wennerberg and Der, 2004; DerMardirossian and Bokoch, 2005).
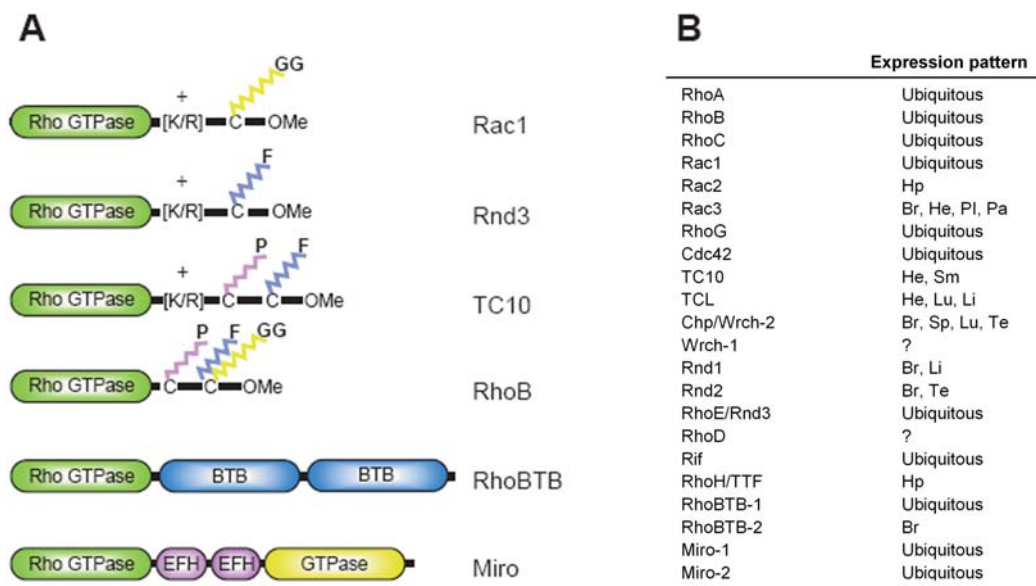
Figure 5. Posttranslational modification and expression pattern of the Rho GTPases. (A) Representation of different C-termini, which are posttranslationally lipid modified, and the additional membrane targeting signals of Rho GTPases ([K/R]: polybasic sequence). CAAX sequence is modified by either farnesyl (F) or geranyl-geranyl (GG) at the cysteine, followed by proteolytic removal of AAX residues and carboxymethylation (OMe) of the now-terminal cysteine. Palmytoylation (P) of the cysteine upstream of CAAX is possible. RhoBTB contains two BTB domains, no CAAX motif and does not undergo any posttranslational modifications. Miro comprises two EFH domains and one additional GTPase domain, and also does not terminate with CAAX motif. RhoBTB, Miro and Chp can however still associate with membranes. Here, Rac1 is also representative for Rac2, Rac3, RhoA, RhoC and Cdc42. (B) Overview of expression pattern of the Rho GTPases. Abbreviations: Hp, hematopoietic; Br, brain; He, heart; Pl, placenta; Pa, pancreas; Sm, skeletal muscle; Lu, lung; Li, liver; Sp, spleen; Te, testis (modified from Wennerberg and Der, 2004).

2.1.2.3 Regulation by gene expression

In addition to the aforementioned regulation mechanisms by GEFs, GAPs, GDIs, and lipid modification, Rho GTPases are also controlled by gene expression. Some Rho GTPases are ubiquitously expressed, whereas other Rho proteins are restricted to specific tissues. Figure 5B summarizes the expression pattern of the Rho GTPases. Furthermore, regulation of transcription and/or translation of the Rho GTPases represents another important regulation

mechanism. For instance, RhoG transcription is induced after growth factor stimulation (Vincent et al., 1992; Wennerberg and Der, 2004). The transcriptional control is especially critical for GTPases that are assumed to be constitutively active, such as Rnd subfamily and RhoH (Chardin, 2006; Li et al., 2002).

2.1.2.4   Regulation by phosphorylation and ubiquitinylation

Phosphorylation of Rho GTPases was shown to affect their binding affinity towards Rho GDIs. When phosphorylated at serine 188 within the "polybasic domain" by protein kinase A, RhoA and Cdc42 reveal an increased affinity for Rho GDIs, resulting in the increase of these GTPases within the cytosolic fraction and thus their inhibition (Forget et al., 2002). Ubiquitinylation with subsequent degradation of Rho GTPases has been recently shown as another regulation mechanism of Rho GTPases. In response to stimuli, RhoA can be ubiquitinylated by Smurf1, an E3 ubiquitin ligase, and degraded (Wang et al., 2003).

2.1.2.5   Crosstalk between Rho GTPases

Besides the described regulation of Rho GTPases above, observations have been made on the crosstalk between Rho family proteins, where one family member reduces the activity of another by stimulating a GAP, or increases activity by stimulating a GEF. In addition, there are proteins like Bcr and Abr, that contain both GAP and GEF domains for different Rho members. Finally, the interplay between family members is also mediated by interactions between their respective downstream signaling pathways (Burridge and Wennerberg, 2004).

2.1.3   Biological function of Rho GTPases

Diverse receptor-initiated signals of growth factor receptors, G protein-coupled receptors, integrins or mechanical stress (tension, compression and fluid shear) act upon GEFs, GAPs and GDIs to regulate the activation state of Rho GTPases. In the active conformation, Rho GTPases interact with a number of effectors leading to stimulation of downstream signaling pathways. Figure 6 depicts the major effector pathways of Rho, Rac and Cdc42. The main function of Rho GTPases is to regulate the assembly and organization of the actin and microtubule cytoskeleton. Therefore, Rho GTPases play an important role in a variety of cellular processes that are dependent on the actin cytoskeleton, such as cytokinesis, phagocytosis, pinocytosis, cell migration, formation of lamellipodia and filopodia, cell polarity, morphogenesis, and axon guidance (Hall, 1998; Bishop and Hall, 2000; Jaffe and Hall, 2005). In addition, Rho GTPases are involved in a series of biochemical pathways

including regulation of serum response factor and nuclear factor κB (NF-κB) leading to alterations in gene expression, the *c-Jun* N-terminal kinase (JNK) and p38 mitogen-activated protein kinase pathways, the phagocytic NADPH oxidase complex, G1 cell-cycle progression, the assembly of cadherin-containing cell-cell contacts and secretion in mast cells (Bishop and Hall, 2000; Jaffe and Hall, 2005).
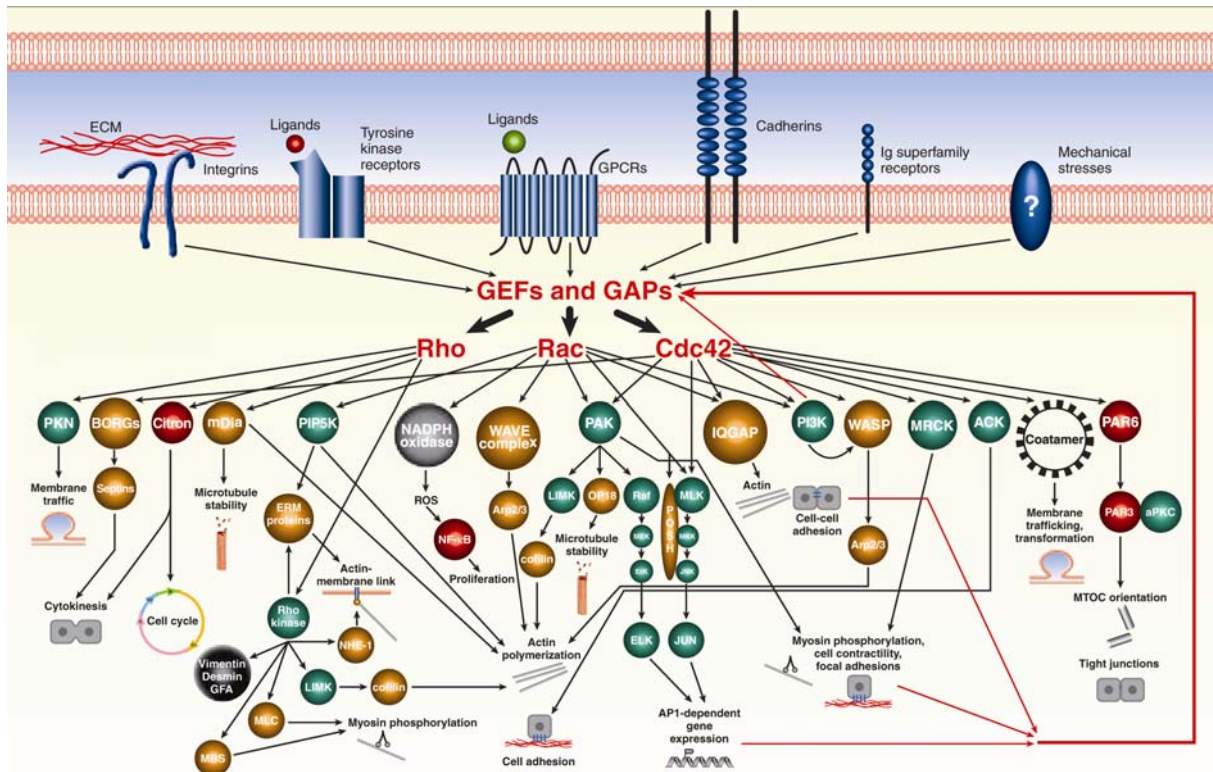
Figure 6. Overview of the activation of Rho GTPases and their effector pathways (modified from Schwartz, 2004).

Rho GTPases bind to effector proteins mostly through the switch I region. The switch II region, the C-terminus and the Rho insert domain are also involved, but to a lesser degree (Figure 4; Karnoub et al., 2004). Common GTPase-binding domains in effectors are the CRIB (Cdc42/Rac-interactive binding) motif, which is present in many Rac- und Cdc42 binding effectors (e.g. WASP, N-WASP, PAK, ACK), the REM motif (Rho effector homology motif/class-1 Rho-binding motif), which is present in rhophilin and rhotekin, and the RKH motif (class-2 Rho-binding motif), which is present in ROK and kinectin (Bishop and Hall, 2000). Other motifs for Rho GTPase binding in target proteins might also exist.

The most utilized mechanism of effector activation by Rho GTPases is the disruption of intramolecular autoinhibitory interactions, which leads to exposure of functional domains within the effector protein. For example, the kinase activity of PAK1-3 serine-threonine kinases is inhibited by binding of the kinase domain to an intramolecular regulatory domain.

Upon GTPase binding this regulatory domain is displaced, liberating the kinase domain (Bokoch, 2003). Similar mechanisms are used by many scaffold-like targets of Rho GTPases such as Dia, WASP and N-WASP (Bishop and Hall, 2000).

2.2   Hematopoiesis

Hematopoiesis, the development of blood cells, requires hematopoietic stem cells (HSCs), which have the capacity to self-renew and differentiate into all hematopoietic lineages. Hematopoiesis is developmentally regulated and occurs in distinct anatomical locations. In mouse, the first HSCs emerge in the blood islands of the extra-embryonic yolk sac and in the aorta/gonad/mesonephros of the embryo proper at embryonic day 7.5 (E7.5). With the onset of systemic circulation at E8.5, HSCs seed the fetal liver, which becomes at E12 the major site of hematopoiesis. Soon after birth, liver-derived cells colonize the bone marrow (BM), which represents the predominant organ of hematopoiesis in adulthood (Kondo et al., 2003). HSCs give rise to myeloid, erythroid and lymphoid lineages. Based on their self-renewal capacity, HSCs can be subdivided into long-term (LT) HSCs and short-term (ST) HSCs, giving rise to multipotent progenitors (MPPs). MPPs have completely lost self-renewal potential, but are still able to develop into all hematopoietic lineages. MPPs branch into common myeloid progenitors (CMPs) and common lymphoid progenitors (CLPs) (Figure 7; Kondo et al., 2003; Rosenbauer and Tenen, 2007).

2.2.1   Development of myeloid and erythroid cells

CMPs give rise to granulocytes, monocytes, dendritic cells (DCs), mast cells, erythrocytes and platelets. Granulocytes, the polymorphnuclear leukocytes, comprise neutrophils, eosinophils, and basophils and can be detected by their expression of Gr-1 (Hestdal et al., 1991). Monocytes differentiate to macrophages in the tissues and are the major phagocytic cells of the immune system. Granulocytes, monocytes and macrophages express the integrin Mac1 ($\alpha4\beta2$/CD11CD18). Megakaryocytes differentiate into platelets and erythroid progenitors develop in the BM into erythroblasts, which finally mature to erythrocytes. The erythroid development is characterized by the expression of Ter119 and CD71 (Socolovsky et al., 2001).
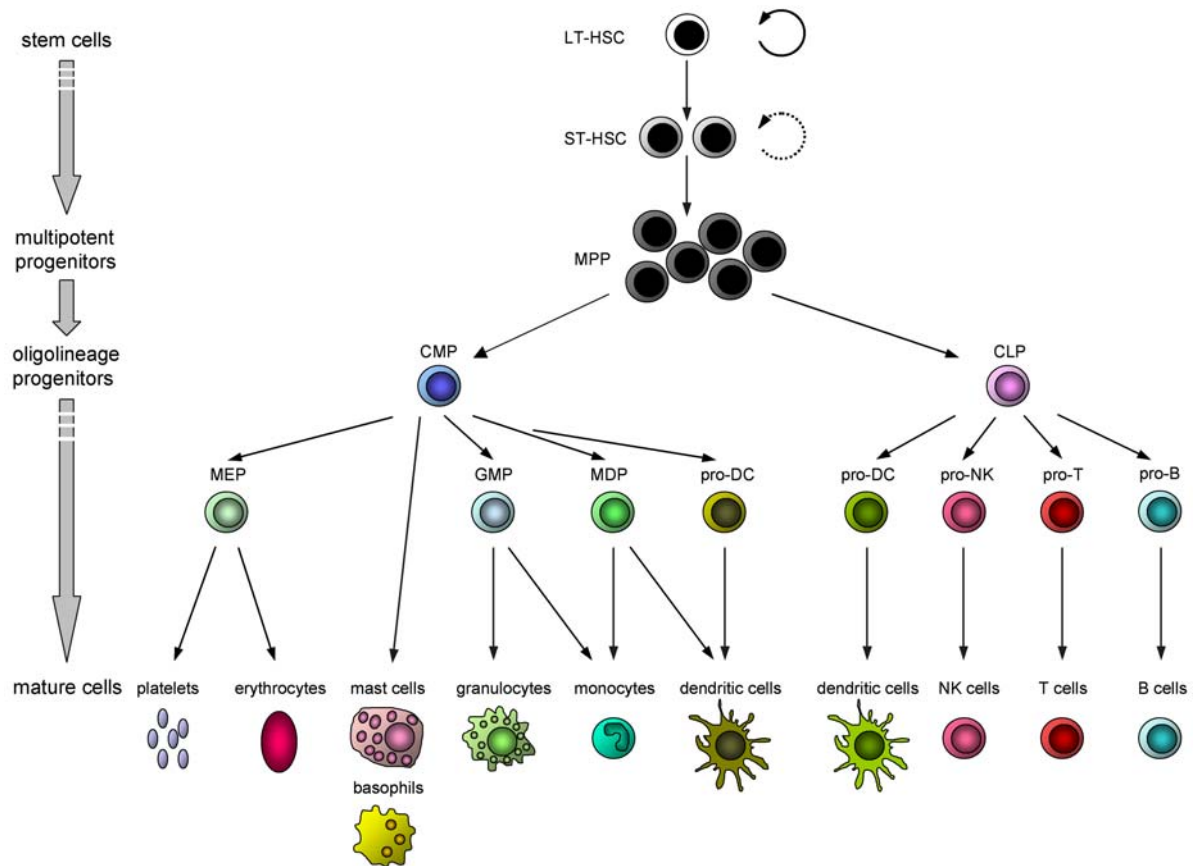
Figure 7. Development of hematopoietic lineages. According to the model established by the Weissman group, long-term hematopoietic stem cells (LT-HSCs) develop to short-term hematopoietic stem cells (ST-HSCs) and further into multipotent progenitors (MPPs), that generate common myeloid progenitors (CMPs) and common lymphoid progenitors (CLPs). CMPs give rise to granulocytes, monocytes, dendritic cells (DCs), mast cells, erythrocytes and platelets. CLPs give rise to B, T, natural killer (NK) cells and DCs (Kondo et al., 2003; Rosenbauer and Tenen, 2007).

2.2.2 Development of lymphoid cells

CLPs are thought to give rise to T, B, natural killer (NK) cells and dendritic cells (DCs). Recent data, however, point towards a progenitor that is distinct from CLPs giving rise to T cells (Rosenbauer and Tenen, 2007).

2.2.2.1 B cells

B cells are generated in the BM and migrate to the spleen at the transitional B cell stage, to complete their maturation and finally to recirculate to the BM. The stages of B cell development in mouse are characterized by certain cell surface markers (Figure 8). B220 is the first marker to be expressed on B cell precursors and is present throughout B cell maturation. B cell precursors can be subdivided into four groups according to their differential expression of a range of markers (pre-pro B; pro-B; pre-B I and II cells). All these stages do

not express cell surface immunoglobulin (Ig) (Figure 8). During these stages, genes for the Ig heavy and light chain which form the B cell receptor (BCR) are rearranged, and the BCR IgM is then expressed on immature B cells. They exit the BM and are transported by the blood stream to the spleen, where they express cell surface IgD along wih IgM and become mature (Nagasawa, 2006).
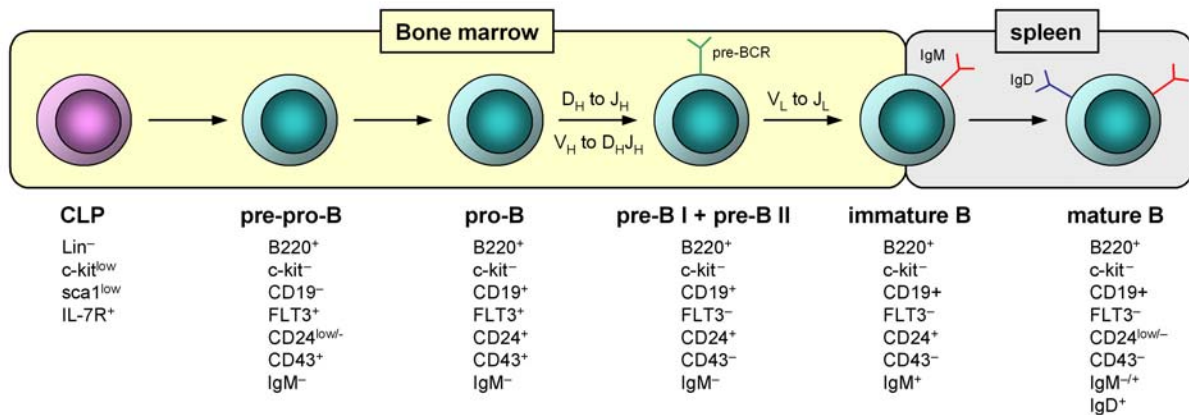
Figure 8. Overview of B cell development. B cell development from CLPs begins in the BM and is completed in the spleen. Stages of B cell development are characterized by differential expression of cell surface markers B220, CD19, CD117 (c-kit), FLT3, CD24, CD43, IgM and IgD (modified from Nagasawa, 2006).

2.2.2.2   NK cells

NK cells belong to the innate immune system and are characterized by cytotoxic activity and the capability to rapidly produce cytokines. NK precursors (NKPs), which arise from early lymphoid progenitors and CLPs, develop into immature and mature NK cells. NKPs are found in the BM, thymus, spleen and lymph nodes, however the precise sites of NK cell maturation have not been fully defined (Di Santo, 2006). Several markers describe NK cells, including NK1.1, CD122, DX5 (α2), and Mac1. NK cells can be identified as CD3-NK1.1+CD122+. In mouse strains that are NK1.1-, NK cells can be detected as CD3-DX5+CD122+.

2.2.2.3   T cells

The thymus, which is divided into cortex and medulla, is the primary lymphoid organ where T cells are generated (Ceredig and Rolink, 2002). The thymus is a non-self renewing hematopoietic organ and is therefore continually seeded with hematopoietic precursors from the BM that maintain the production of thymocytes for a 6 to 8 week period (Bhandoola and Sambandam, 2006). Two lineages of T cells are generated in the thymus: T cells expressing $\alpha\beta$ TCR and T cells expressing $\gamma\delta$ TCR (Figure 9 and Figure 10).

Hematopoietic precursors enter the thymus at the cortico-medullary junction (Figure 10) and proceed through the double negative (DN; CD4-CD8-) stage, which can be subdivided on the basis of differential expression of the surface markers CD25 and CD44 into DN1 (CD25-CD44+), DN2 (CD25+CD44+), DN3 (CD25+CD44-) and DN4 (CD25-CD44-). In the $\alpha\beta$ lineage, DN4 thymocytes express small amounts of CD8 and become subsequently immature single positive cells (ISPs), which rapidly upregulate CD4, forming the double positive (DP; CD4+CD8+) population (Figure 9). Finally, DP thymocytes differentiate into single positive CD4 (CD4SP) or CD8 (CD8SP) thymocytes. After brief proliferation SP thymocytes migrate to the periphery to function as mature $\alpha\beta$ T cells (Hayday and Pennington, 2007).
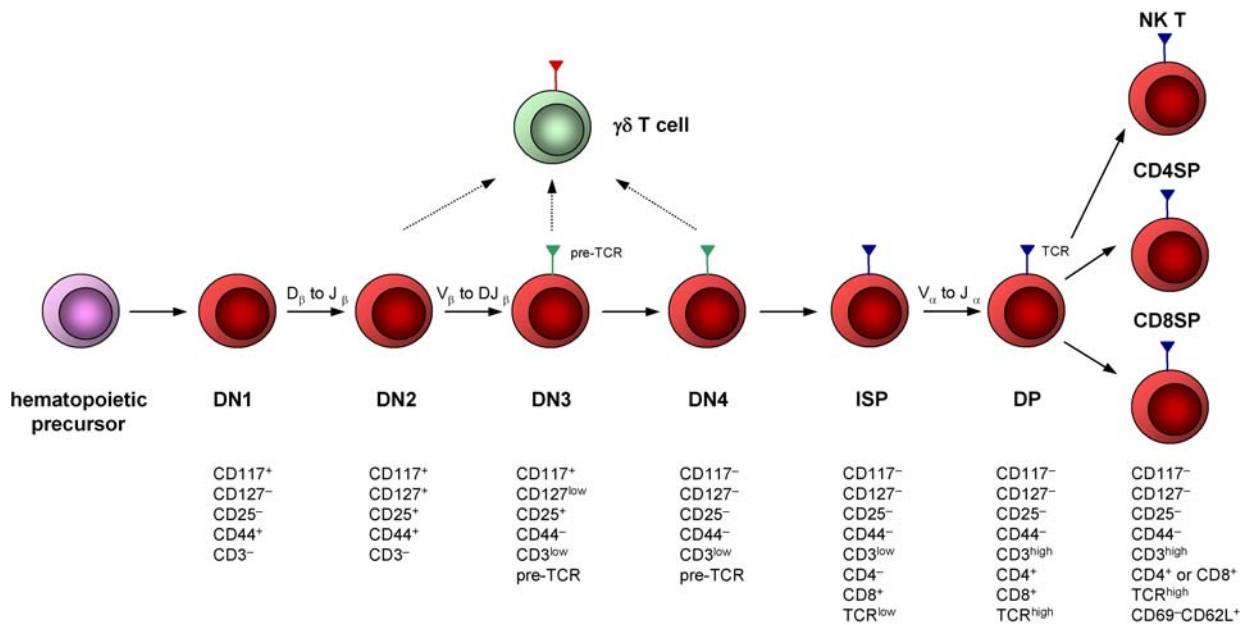
Figure 9. Overview of T cell development. Thymocyte differentiation is characterized by the expression of cell surface markers, including CD4, CD8, CD25, CD44, CD117, CD127, CD3, TCR, CD69, CD62L (modified from Ceredig and Rolink, 2002).

DN thymocytes constitute approximately ~5% of all thymocytes, while DP cells comprise ~80% of all thymocytes, thus representing the major thymocyte subpopulation. ~10% express only CD4 co-receptor and ~5% express only CD8 co-receptor. Within the DN fraction, ~10-15% are DN1, ~2-3% are DN2, ~50-70% are DN3 and 10-20% are DN4 cells (Ceredig and Rolink, 2002).

Although the precise identity of the early thymocyte progenitors is unknown, the earliest precursors are considered to be found in the DN1 subpopulation. The DN1 fraction is a heterogeneous population with a multi-lineage potential for T, B, NK, myeloid cells and DCs (Bhandoola and Sambandam, 2006). Recently, on the basis of CD24 and CD117 (IL-7Rα) expression, five DN1 subsets have been characterized (DN1a-DN1e) that can all give rise to T

cells, but that differ in their ability to diverge into other lineages and display different kinetics of differentiation and proliferative capacity (Porritt et al., 2004; Hayday and Pennington, 2007). DN1a (CD24-CD117+CD127-) cells have been suggested to be the earliest intrathymic progenitors, although they may still give rise to NK, myeloid cells, and to a limited degree, to B cells (Porritt et al., 2004; Hayday and Pennington, 2007).
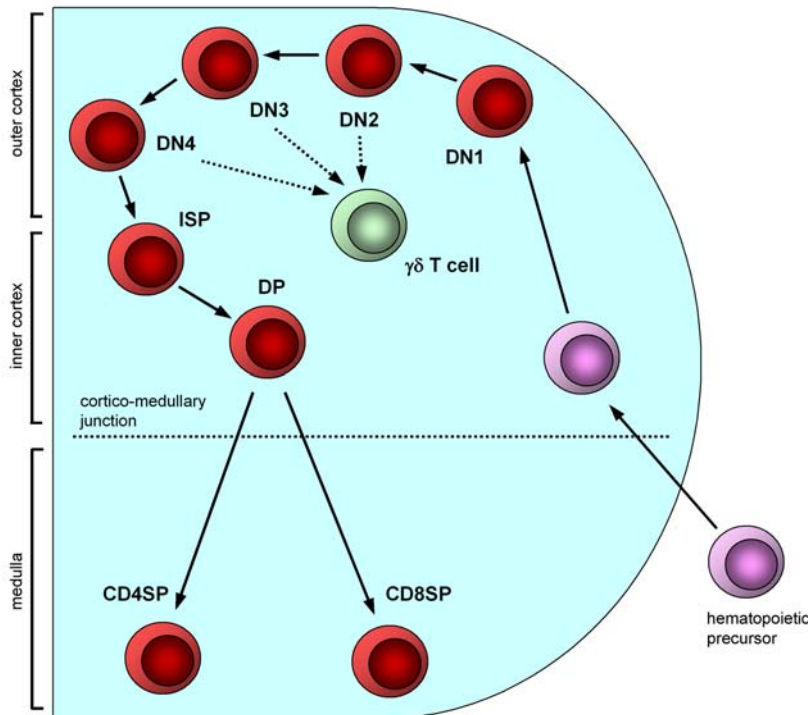
Figure 10. Overview of thymocyte migration. A hematopoietic precursor enters the thymus at the cortico-medullary junction and proceeds through the DN stages migrating outwards from the cortex to the subcapsular region (Takahama, 2006; Ladi et al., 2006). Emerging αβ DP cells in the cortex interact with cortical epithelial cells for positive selection. Positively selected SP thymocytes migrate into the medulla, where autoreactive cells are eliminated by negative selection, and undergo further maturation. γδ T cells, a second lineage of T cells, diverge from αβ thymocytes at the DN stage (modified from Zuniga-Pflücker, 2004).

Somatic rearrangement of the genes encoding the TCRβ chain begins in the DN2 stage and is completed during the DN3 stage. If productively rearranged, TCRβ chain is expressed and forms together with an invariant pre-Tα chain and CD3 molecules the pre-TCR complex. Assembly of the pre-TCR initiates pre-TCR signaling that creates a survival signal and drives the proliferation and further differentiation of DN3 thymocytes (Figure 9). Cells that have not successfully recombined the *TCRβ* gene and do not express the pre-TCR, are eliminated by apoptosis. Pre-TCR signaling therefore establishes a key checkpoint in early thymocyte development which has been defined as "β-selection". The surviving DN3 thymocytes down-regulate CD25, become DN4 cells and rearrange TCRα chain loci. The recombination of the *TCRα* gene is completed at the DP stage (Figure 9).

The majority of DP thymocytes (97%) die by apoptosis because they cannot recognize the major histocompatibility complex (MHC) expressed on the thymic epithelial cells and thus do not receive a survival signal (Figure 11 and Figure 12A). The remaining thymocytes (3%) which recognize MHC, can bind to self-antigen presented in the context of MHC on thymic epithelial cells either with a high or low affinity (Werlen et al., 2003). Thymocytes expressing

TCR that bind with high affinity to MHC-self-peptide-complex are negatively selected and die by apoptosis (Werlen et al., 2003; Palmer, 2003). Thereby, potential autoreactive T cells are eliminated in the thymus before migrating to the periphery where they can be activated by self-antigens and cause autoimmunity (Figure 11). T cells, expressing TCR that bind MHC-self-peptide-complex with low affinity, are positively selected: They receive a survival signal and can further differentiate into CD8SP or CD4SP thymocytes, expressing MHC class I and II restricted TCR, respectively (Figure 12A; Werlen et al., 2003).
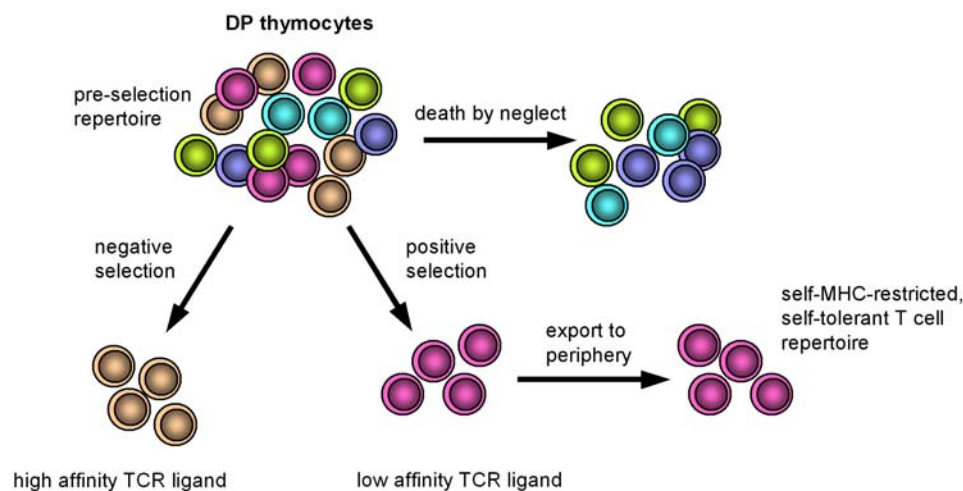
Figure 11. Positive and negative selection of developing thymocytes. The majority of DP thymocytes express TCRs, that cannot recognize MHC-self-antigen-complex, and die by neglect due to the absence of survival signal. DP thymocytes expressing TCRs that recognize MHC-self-antigen-complex with high affinity undergo apoptosis (negative selection), whereas DP cells expressing TCRs that bind MHC-self-antigen-complex with low affinity are positively selected and differentiate into SP thymocytes (modified from Palmer, 2003).

How does a thymocyte discriminate between the MHC-peptide-complex of differing affinity? One suggested model is kinetic proofreading. This assumes that a receptor can measure ligand affinity by "reading" its occupancy time of the TCR. Low-affinity ligands have short occupancy time, whereas high-affinity ligands bind the TCR for a longer time. Thus, low- and high-affinity ligands would induce different activation kinetics of certain effectors and therefore translate into different outcomes: positive or negative selection of T cells, respectively (Werlen et al., 2003). The distinction between selection signals may lie in the kinetics of Erk activation (Werlen et al., 2003). Positively selecting ligands induce a slow and sustained accumulation of Erk activity, whereas negatively selecting ligands generate a strong and transient Erk activation. p38 and JNK are activated with similar kinetics by both positively and negatively selecting ligands. Thus, during positive selection, Erk is activated after p38 and JNK, whereas negative selecting ligands induce Erk activation before p38 and JNK. This decides between survival and apoptosis of thymocytes (Werlen et al., 2003).

The commitment of thymocytes to CD4 or CD8 lineage occurs parallel to the positive and negative selection and involves a series of transitional stages with intermediate CD4 and CD8 expression (Figure 12B; Kappes et al., 2005). A quantitative instructive model was proposed which describes that signal duration and strength of a TCR engaged with a MHC-antigen-complex and its matched co-receptor regulates the downmodulation of the inappropriate co-receptor (Kappes et al., 2005). Strong and long signals favour development of CD4 lineages, while weak and short signals drive to the CD8 lineage. The differences in signal intensities are explained by two models. According to the classical signal strength model, the difference in signal intensity is based on the stronger association of lck, a critical mediator of TCR signaling, with the CD4 co-receptor than with the CD8 co-receptor, resulting in a stronger TCR signal. According to the kinetic signaling model, different signal intensities come from developmentally programmed reduction in CD8 expression at the CD4+CD8low stage, which selectively impairs signaling by MHC class I restricted TCRs (He and Kappes, 2006).
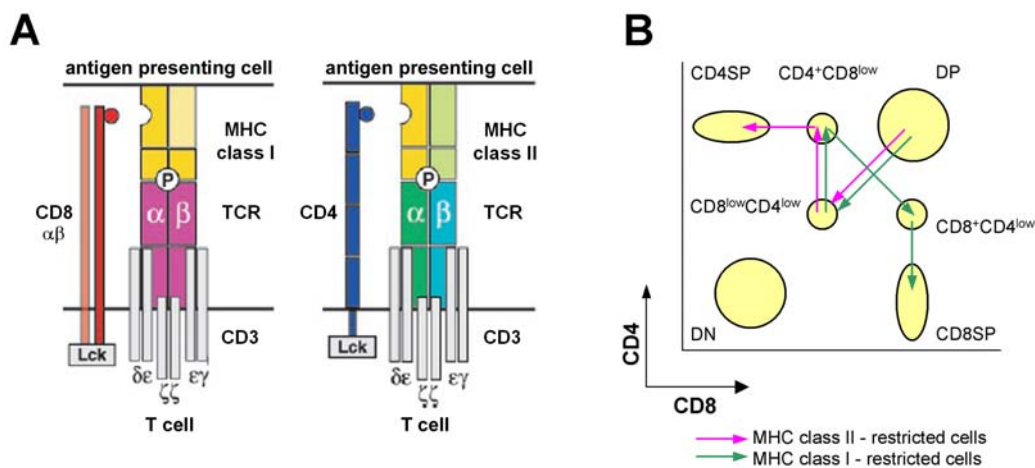
Figure 12. CD4-CD8 developmental stages and schematic representation of a TCR binding to a MHC-antigen-complex. (A) A schematic diagram shows the interaction of a MHC class I or II restricted TCR and a CD8 or CD4 co-receptor on the T cell with a MHC class I-antigen-complex or MHC class II-antigen-complex on the antigen presenting cell (from Werlen et al., 2003). (B) Flow cytometry diagram represents thymocytes stained with anti-CD4 and anti-CD8 antibodies and demonstrates the developmental pathways of CD4-CD8 differentiation. The development is asymmetrical since both MHC class I and II restricted thymocytes pass through CD4+CD8low stage (modified from Kappes et al., 2005).

2.2.2.4   Natural killer T cells

Natural killer T (NKT) cells constitute a sublineage of $\alpha\beta$ T cells and differ from conventional T cells in the feature that they express both a TCR and NK1.1, a marker specific for NK cells. More recently, NKT cells have been defined as cells that nearly always have an invariant Vα14-Jα18 rearrangement and reactivity to the glycosphingolipid α-galactosyl-ceramide (αGalCer) when presented by the class I-like molecule CD1d (Kronenberg, 2005).

NKT cells arise in the thymus and are positively selected by the CD1d-expressing BM-derived cells. NKT cells do not express CD8 co-receptor but some express CD4 co-receptor. In humans however, NKT cells expressing CD8 have been detected. Upon activation, NKT cells rapidly produce cytokines and can lead to either suppression or stimulation of immune responses.

2.2.2.5 γδ T cells

T cells that express γδ TCR represent a second lineage of T cells besides those expressing αβ TCR. γδ T cells constitute 1-5% of circulating T cells, and many of them reside in epithelial layers of tissues, such as skin, intestinal epithelial, lung and tongue, where they are mostly involved in innate immune response (Pennington et al., 2005). The diversity of the repertoire of the TCR is much more limited in these locations than that of γδ or αβ T cells in secondary lymphoid organs (Xiong and Raulet, 2007). γδ and αβ T cells have a common progenitor in the thymus. The differentiation of γδ T cells also begins at the DN stage (Figure 9), but it is not determined by pre-TCR or CD4-CD8 co-expression and extensive proliferation. Instead, γδ T cells remain DN, undergo little or no proliferation, and express the mature γδ TCR (Hayes and Love, 2007; Xiong and Raulet, 2007). The precise DN stage at which γδ T cell commitment happens is unclear. Some evidence has suggested that lineage specification into γδ or αβ T cells occurs at the DN2 stage and that IL-7R and IL-7 play an important role in the development of γδ T cells (Pennington et al., 2005).

2.3 TCR signaling

Pre-TCR and TCR signaling mark two critical checkpoints during thymocyte development in the progression of DN3 to DN4 stage and of DP to SP stage, respectively. Pre-TCR and TCR signaling lead to proliferation, differentiation, survival or induction of cell death.

The TCR consists of a ligand-binding subunit, the α and β chains, and the signaling subunit, which contains three dimers, the CD3εγ, CD3εδ and TCRζζ (Figure 12A; Werlen et al., 2003). CD3ε, γ, and δ have each one immunotyrosine activation motif (ITAM), whereas each TCRζ chain has three, thus contributing 10 ITAMs to one TCR. An ITAM contains two tyrosines separated by 9-12 aa and the ITAM sequence is $YXX[L/V]X_{6-9}YXX[L/V]$. The pre-TCR is composed of a TCRβ chain paired with the pre-Tα and CD3 chains.

The pre-TCR and TCR are considered to trigger similar, if not identical, intracellular responses (Sommers et al., 2004). However, no ligand has been identified for the pre-TCR, and it has been suggested that signaling is initiated by assembly of the pre-TCR (Sommers et al., 2004).

The first recognizable event upon TCR ligation, is the activation of the Src kinases lck and fyn, which phosphorylate ITAMs (Figure 13). Lck is constitutively associated with the CD4 and CD8 co-receptors and fyn interacts with CD3ε and TCRζ upon receptor clustering. The activity of lck and fyn is regulated by the phosphorylation of regulatory tyrosines in the kinase domain and the C-terminal region. Phosphorylation of the kinase domain results in the activation of the Scr kinase and phosphorylation at the C-terminal region leads to inhibition of the protein activity. Phosphorylation of the inhibitory tyrosine is mainly achieved by Csk kinase, which is constitutively active. The inhibitory phosphate is removed by the phosphatase CD45 leading to unfolding and activation of Src. The balance between Csk and CD45 determines the kinase activity of lck and fyn in response to TCR engagement (Palacios and Weiss, 2004).

ζ-chain-associated protein of 70 kD (ZAP70), a Syk family kinase, is recruited to the ITAMs through its two SH2-domains (Figure 13). ZAP70 is activated through phosphorylation by lck and autophosphorylation. Along with ZAP70, lck regulates activity of Tec kinases by phosphorylation, the third class of kinases involved in TCR signaling. Once activated, ZAP70 phosphorylates two major adaptor proteins, LAT (linker of activation in T cells) and the SH2-domain containing leukocyte protein of 76 kD (SLP-76). LAT is a transmembrane protein of 36-38 kD that has nine tyrosines which can be differentially phosphorylated and serve as inducible binding domains for various proteins containing SH2-motifs (Werlen et al., 2003), including phospholipase C γ1 (PLCγ1), Grb2, phosphoinositide kinase 3 (PI-3K), and Gads (Figure 13). LAT provides a scaffold to the TCR signaling molecules, which is termed the LAT signalosome.

PI-3K associates directly with LAT via its SH2-domain or indirectly via the adaptor TRIM (Okkenhaug et al., 2004), and is phosphorylated by lck. PI-3K catalyzes the phosphorylation of phosphatidylinositol-(4,5)-bisphosphate (PIP_2) to yield phosphatidylinositol-(3,4,5)-tris-phosphate (PIP_3), a secondary messenger that accumulates in the lipid bilayer. The pleckstrin homology (PH) domain containing Tec kinases are then recruited to PIP_3 in the membrane, and this localization is essential for subsequent phosphorylation and activation of Tec kinases by Src kinases and ZAP70 (Okkenhaug et al., 2004; Berg et al., 2005).

SLP-76 phosphorylation results in the recruitment of the SH2-motif containing GEF Vav1 and the adaptor protein Nck, as well as ADAP, which might contribute to the regulated changes in the T cell actin cytoskeleton (Clements, 2003). The Tec kinase Itk binds through its SH2-domain to phosphorylated SLP-76. The interaction between Itk and SLP-76 is mediated also in part via the Itk SH3-domain and SLP-76 proline residues. In addition, the proline-rich region of SLP-76 constitutively binds to the SH3-domains of the Grb2-like adapter Gads. As a consequence of the inducible association between the SH2-domain of Gads and phosphorylated tyrosines of LAT, SLP-76 is recruited from the cytosol to the membrane (Clements, 2003), serving along with LAT as a second docking platform in the LAT signalosome.
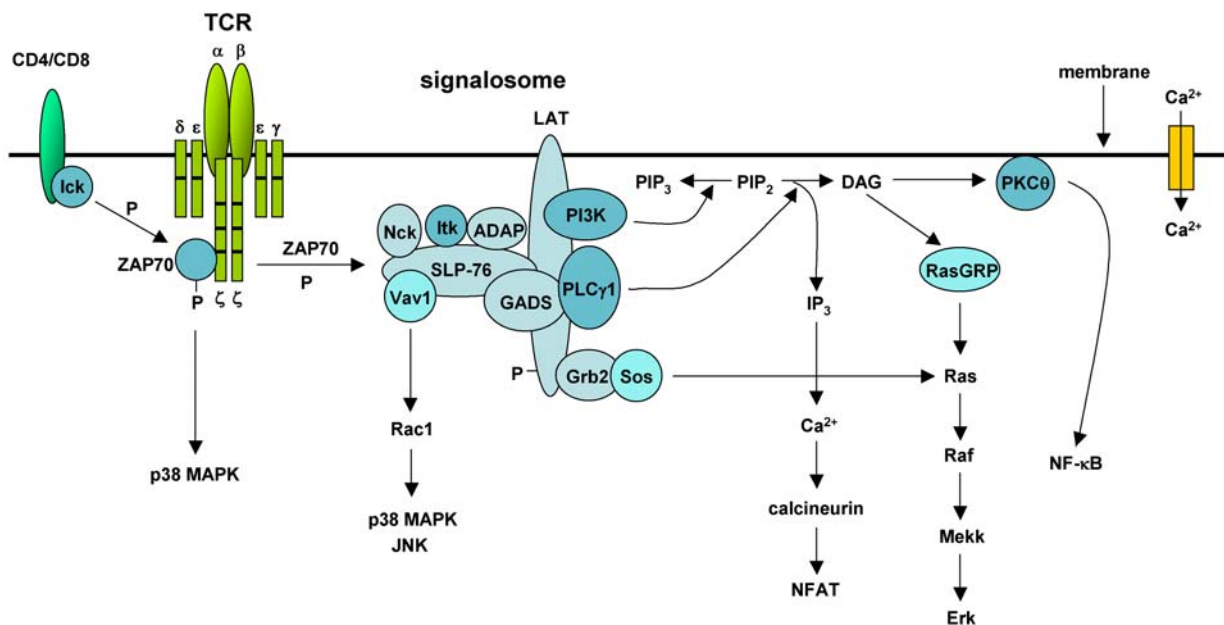
Figure 13. Schematic outline of TCR signaling. Upon engagement of a TCR by a ligand (MHC-peptide-complex), the associated Scr kinases lck and fyn are activated and phosphorylate the ITAMs of the CD3 and TCRζ cytoplasmic tails. The Syk kinase ZAP70 is subsequently recruited to phosphorylated ITAMs, phosphorylated by lck and autophosphorylated, resulting in activation. Active ZAP70 phosphorylates two major adaptors LAT and SLP-76, which provide a scaffold for the inducible binding of the SH2-motif containing proteins (PLCγ1, Grb2, PI-3K, and Gads) forming the LAT signalosome. Proteins associated with the LAT signalosome are activated by phosphorylation through ZAP70, and partially through Tec kinases (e.g. PLCγ1) or lck/fyn, and initiate signaling cascades leading to activation of Erk, p38, JNK, NFAT and NF-κB. p38 can also be activated independent of the LAT signalosome (modified from Dr. Cord Brakebusch).

The proteins bound to LAT can be subsequently phosphorylated by ZAP70 and/or Tec kinases and become activated. PLCγ1 is phosphorylated by Itk and ZAP70 and cleaves PIP_2 into the secondary messengers inositol-1,4,5-trisphosphate (IP_3) and diacylglycerol (DAG). IP_3 releases Ca^{2+} from endoplasmatic reticulum, and when these stores are depleted, extra-cellular Ca^{2+}-influx is taking place through the Ca^{2+}-dependent channels in the surface membrane. Increased intracellular Ca^{2+} activates calcineurin, a calcium-modulin-dependent

serine phosphatase that dephosphorylates NFAT (nuclear factor of activated T cells), resulting in nuclear translocation of NFAT (Nel., 2002). In the nucleus, NFAT acts as a transcriptional regulatory protein leading to activation of genes involved in proliferation and differentiation (Macian, 2005).

DAG together with Ca^{2+} activates protein kinase C θ (PKCθ), which is involved in NF-κB activation (Nel, 2002; Nel and Slaughter, 2002). In addition, DAG recruits RasGRP, a GEF for Ras, through binding to C1 domain (Ebinu et al., 1998), thus activating the MAPK cascade. RasGRP stimulates GTP loading of Ras. Active Ras activates the serine-threonine kinase Raf, which in turn phosphorylates Mek kinase (Mekk). Active Mekk phosphorylates and activates Erk, which translocates into the nucleus and finally phosphorylates the transcription factor family Ets. Ras can also be activated via another GEF, Sos. Sos is recruited to the TCR in a complex with the adaptor protein Grb2, which binds tyrosine-phosphorylated LAT through its SH2-domain (Figure 13; Alberola-Ila and Hernandez-Hoyos, 2003).

Vav1, which contains a proline-rich and DH-domain as well as SH3- and SH2-domains, has adaptor and GEF functions (Tybulewicz, 2005). It is recruited to the LAT signalosome by binding to phosphorylated SLP-76. Phosphorylation by ZAP70 stimulates GEF activity of Vav1, which can then activate Rac1 and thereby induce a MAPK cascade. This cascade finally results in the activation of p38 and c-JNK kinases that in turn phosphorylate transcription factors (Ashwell, 2006). p38 has been demonstrated to be activated independently of the LAT signalosome, via direct phosphorylation by ZAP70 and subsequent autophosphorylation, inducing kinase activity (Figure 13; Salvador et al., 2005).

Taken together, pre-TCR and TCR signaling are crucial during thymocyte development. The receptors differ slightly in their composition and ligand requirement, but utilize similar transduction molecules. The pre-TCR and TCR intracellular transduction cascade can be structured into three main sequential activation steps, the proximal, distal and downstream events and is mostly based on the induced binding of the SH2-domain containing proteins to phosphorylated tyrosine residues in signaling molecules.

Activation of the Src kinase lck, which phosphorylates ITAM motifs in the cytoplasmic tails of both receptors upon pre-TCR assembly or TCR stimulation on one hand, and subsequent phosphorylation and activation of ZAP70 kinase on the other hand, belong to the proximal signaling events. Activated ZAP70 induces distal signaling steps. It phosphorylates a series of proteins such as LAT, SLP-76, PLCγ1, Grb2, Gads, Vav1 and Tec kinases. Together they form the LAT signalosome with LAT as a scaffold. Activated components of the LAT

signalosome initiate downstream events resulting in activation of Erk, NF-κB, p38, JNK and NFAT (Figure 13).

2.4   Role of Rho GTPases in hematopoiesis

Rho GTPases play an important role in directional migration, proliferation, survival, differentiation and biological functions of hematopoietic cells under physiological and pathological conditions (van Hennik and Hordijk, 2005). The best characterized members of the Rho GTPase family in hematopoietic cells are Rac1, Rac2, RhoA and Cdc42.

2.4.1   Migration and adhesion

Migration and adhesion require a coordinated remodelling of the actin cytoskeleton and microtubules. Rac2 was shown to be important for directed migration of neutrophils. Furthermore, it can compensate for Rac1-deficiency, since in Rac1-null neutrophils chemotaxis is not affected. However, in double Rac1/Rac2-deficient neutrophils migration is stronger diminished than in Rac2-single knockout cells (Bokoch, 2005).

In the BM Rac1, but not Rac2 is required for the engraftment of HSCs, because Rac1-deficient HSCs do not rescue hematopoiesis after transplantation into lethally irradiated mice. Deletion of Rac1 after engraftment of HSCs does not impair hematopoiesis and Rac2-deficient mice display only a modest mobilization of HSCs into circulating blood. However, post-engraftment ablation of both Rac1 and Rac2 causes massive mobilization of HSCs from the BM, resulting in an ineffective hematopoiesis (Cancelas et al., 2005).

RhoA appears to antagonize the effect of Rac GTPases, since dominant negative inhibition of RhoA results in increased HSC engraftment (Ghiaur et al., 2006).

Cdc42-deficient HSCs cannot properly adhere, home and lodge leading to a massive release of HSCs from the BM into the blood and engraftment failure, indicating a crucial role of Cdc42 in these processes (Yang, et al., 2007).

2.4.2   Differentiation, proliferation and survival

Rho GTPases do not only regulate the actin cytoskeleton, adhesion and migration, but also modulate the size of the HSC compartment, as well as the differentiation of various hematopoietic lineages (van Hennik and Hordjik, 2005).

In HSCs Rac1, but not Rac2, is important for growth factor-stimulated proliferation *in vitro*. However, ablation of both Rac1 and Rac2 has an even more severe reduction in proliferation of HSCs than of Rac1 alone. In contrast, RhoA inhibits proliferation of HSCs (Ghiaur et al.,

2006). Cdc42 was suggested to coordinate the quiescence of stem cells, since Cdc42-deficient mice revealed an increased number of HSCs in the BM that enter active cell cycle (Yang et al., 2007). Survival of HSCs was shown to be dependent on Rac2 (Gu et al., 2003).

Moreover, Rac2 was reported to play a crucial role in B cell development. In the absence of Rac2, multiple defects in B cell development are observed, leading to reduced numbers of peripheral B cells and IgM-secreting plasma cells and a severe reduction in the number of marginal zone and peritoneal B1 cells (Croker et al., 2002). In contrast, B cell specific deletion of Rac1 does not result in abnormal B cell development. However, the double Rac1/Rac2-deficient mice reveal an aggravated B cell phenotype of Rac2-deficient mice, excluding the redundancy of both proteins (Walmsley et al., 2003). Both GTPases were demonstrated to be required to transduce BCR signals leading to proliferation and survival that are crucial during B cell development (Walmsley et al., 2003).

In T cells, Rac2 is important for activation (Yu et al., 2001). In addition, Rac2 was reported to be involved in Th1 differentiation by activating Th1-specific signaling and IFN-γ production, which is decreased in the absence of Rac2 (Li et al., 2000). T cell specific expression of constitutively active Rac2 was shown to induce a high rate of apoptosis in thymocytes leading to severe atrophy of the thymus (Lores et al., 1997). With regard to Rac1, studies on constitutively active Rac1 mutant pointed out that Rac1 controls pre-T cell proliferation and differentiation (Gomez et al., 2000). In addition, constitutively active Rac1 was shown to divert the cell fate of DP and SP thymocytes from positive to negative selection (Gomez et al., 2001).

Inactivation of RhoA function in thymus by C3 transferase, which selectively ADP-ribosylates Rho within its effector domain and thereby abolishes its activity, leads to maturational, proliferative and survival defects during T cell development, indicating that this GTPase is a critical signaling molecule during thymocyte development (Galandrini et al., 1997; Henning et al., 1997). Mice expressing a constitutively active form of RhoA have enhanced TCR-mediated responses revealing that RhoA is a positive regulator of TCR signaling (Corre et al., 2001).

Constitutively active Cdc42 causes a dramatic reduction of thymocyte numbers and mature T cells, which can be explained by the massive apoptosis of these cells (Na et al., 1999). Interestingly, the phenotype of these mice resembles that of transgenic mice expressing constitutively active Rac2 in thymus, suggesting that both Rac2 and Cdc42 might induce the same downstream signaling.

2.4.3 Phagocytosis and production of reactive oxygen species

Phagocytosis, the uptake of particles, is a crucial function of neutrophils, macrophages and other phagocytic leukocytes in the innate immune response. Phagocytosis requires an ordered assembly of actin cytoskeleton, which was shown to be regulated by Rho GTPases (Bokoch, 2005). Structurally different phagocytic processes are dependent on different Rho GTPases: while phagocytosis mediated by Fc receptor (FcR) has been demonstrated to rely on both Rac and Cdc42, but not RhoA activity, phagocytosis mediated by complement receptor requires RhoA, but not Rac or Cdc42 (Bokoch, 2005).

The production of reactive oxygen species (ROS) by the phagocytes is an integral component in the host defence against pathogens and is mediated by NADPH oxidase. Rac2 was shown to assemble into the membrane-localized NADPH oxidase, and the deficiency of Rac2, but not Rac1, leads to a significant reduction in ROS generation in neutrophils and macrophages (Roberts et al., 1999; Kim et al., 2001; Bokoch, 2005). Cdc42 seems, however, to antagonize Rac2-mediated activation of NADPH (Diebold et al., 2004).

Taken together, despite the high degree of similarity on the aa level among the Rho GTPases, distinct roles have been assigned to each of them. They have been shown to be involved in chemokine directed migration of neutrophils, monocytes and HSCs. Furthermore, Rho GTPases are required for retention of the HSCs in the BM. The importance of Rho GTPases in homing and engraftment of HSCs has also been revealed. In addition, Rho GTPases are critical for proliferation, differentiation and survival of various hematopoietic lineages and for phagocytosis in neutrophils and macrophages.

2.5 RhoH function

RhoH/TTF is a hematopoietic member of the Rho GTPase family and was shown to be expressed at very high levels in thymus, less abundant in spleen, and least abundant in the BM (Li et al., 2002). The highest RhoH expression is detected in lymphocytes, while hemato-poietic progenitor cells (HPCs), myeloid lineages, including neutrophils and *in vitro* BM-derived mast cells, (Li et al., 2002; Gu et al., 2005a) display lower expression. In erythroid cell lines RhoH is expressed at the lowest levels (Lahousse et al., 2004). RhoH seems not to be expressed in non-hematopoietic tissues.

The *RhoH* gene is located on chromosome 4 and 5 in humans and mice, respectively. The *RhoH* gene was first identified as a fusion transcript of *LAZ3/BCL6* (B cell lymphoma 6) oncogene as a result of a t(3;4)(q27;p11-13) translocation in the B cell non-Hodgkin's lymphoma (NHL) cell line and in other NHL cases (Dallery et al., 1995; Preudhomme et al.,

2000). *LAZ3/BCL6* gene encodes a sequence-specific zinc finger transcriptional inhibitor (Albagli et al., 1995). It has been suggested that LAZ3/BCL6 is important for the repression of genes involved in the control of lymphocyte activation, differentiation, and apoptosis, and for the formation of germinal centre B cells, where its downregulation is further necessary for B cells to exit the germinal centres (Pasqualucci et al., 2003; Ohno, 2006). Often, LAZ3/BCL6 remains constitutively active in lymphomas. With respect to the *RhoH LAZ3/BCL6* rearrangement, Preudhomme et al., 2000 reported two fusion products, a *RhoH-LAZ3/BCL6* and a *LAZ3/BCL6-RhoH*, placing each gene under the control of the partner gene promoter. This exchange suggests a deregulated expression of both the *LAZ3/BCL6* and the *RhoH* gene. In multiple myeloma, which develops from malignant, differentiated B lymphocytes accumulating in the BM, another *RhoH* translocation t(4;14)(p13;q32) was isolated, involving the *IgH* gene. The transposition of *RhoH* into the *Ig* locus conceivably also results in the deregulation of the *RhoH* gene expression (Preudhomme et al., 2000).

Recently, the *RhoH* gene along with three other genes (*PIM1*, *MYC* and *PAX5*) was discovered to be hypermutated in 46% of the diffuse large B cell lymphomas (DLBCLs), the most typical subtype of NHL (Pasqualucci et al., 2001). Mutations were also reported to occur in other subtypes of B cell NHL (Gaidano et al., 2003; Deutsch et al., 2007; Bödor et al., 2005; Dijkman et al., 2006). In contrast, *RhoH* gene is rarely affected by mutations in Hodgkin's lymphoma (HL) (Liso et al., 2006).

The mutations are introduced by the aberrant somatic hypermutation (SHM) mechanism. Normally, this mechanism selectively targets the variable regions of *Ig* genes of the antigen-activated B cells which undergo clonal expansion in germinal centres during humoral immunity response, and inserts nucleotide substitutions to generate variants of Igs with higher affinity for antigen. The SHM is not only restricted to the *Ig* loci, but brings in mutations also into *BCL6*, *CD95/Fas*, *CD79a* and *CD79b* genes (Peng et al., 1999; Shen et al., 1998; Pasqualucci et al., 2001; Muschen et al., 2000; Gordon et al., 2003). The significance of these mutations is not known. RhoH, however, is not hypermutated in normal germinal B cells.

Interestingly, the tumour specific mutations of the *RhoH* gene are introduced into the 5' untranslated region, in the intron between exon 1b and exon 2. This further suggests that RhoH expression might be deregulated in lymphomas (Pasqualucci et al., 2001).

The expression analysis of the human *RhoH* gene in cell lines of different hematopoietic lineages demonstrated transcriptional regulation of the *RhoH* gene (Lahousse et al., 2004). The human *RhoH* gene consists of 7 exons (X1, 1a, X2, 1b, X3, X4, 2) and the coding region is located within exon 2 (Figure 14; Lahousse et al., 2004). The gene structure is characterized

by an intronless open reading frame (ORF), preceded by a very large 5' region about 50 kb in length. Several transcription initiation sites were detected, and a high 5' end heterogeneity of mRNAs was observed due to alternative splicing of some 5' exons. Moreover, different transcription start sites are used in different hematopoietic cell lines (Figure 14; Lahousse et al., 2004; Preudhomme et al., 2000). In addition, RhoH might be controlled at the post-transcriptional level since multiple polyadenylation sites and "AU"-rich elements were identified, which could regulate mRNA stability by differential polyadenylation. The presence of two transcripts at 1.8 and 2.2 kb indeed might reflect the usage of two different polyadenylation sites.
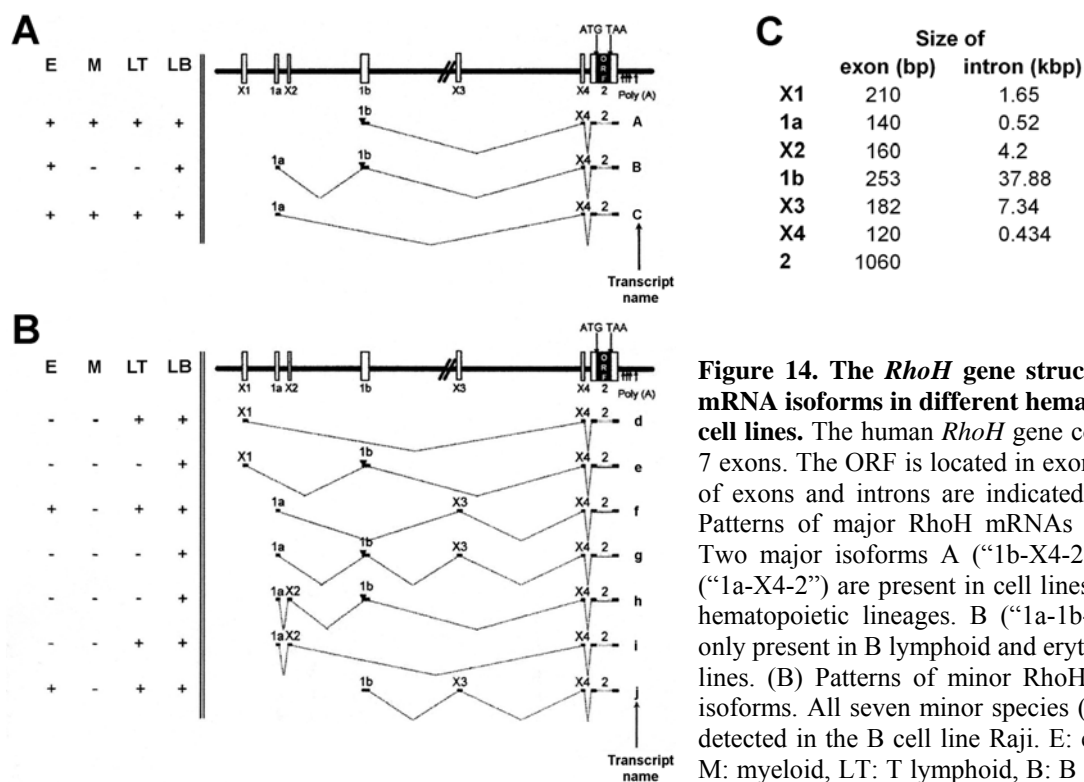
Figure 14. The *RhoH* gene structure and mRNA isoforms in different hematopoietic cell lines. The human *RhoH* gene consists of 7 exons. The ORF is located in exon 2. Sizes of exons and introns are indicated (C). (A) Patterns of major RhoH mRNAs isoforms. Two major isoforms A ("1b-X4-2") and C ("1a-X4-2") are present in cell lines from all hematopoietic lineages. B ("1a-1b-X4-2) is only present in B lymphoid and erythroid cell lines. (B) Patterns of minor RhoH mRNAs isoforms. All seven minor species (d-j) were detected in the B cell line Raji. E: erythroid, M: myeloid, LT: T lymphoid, B: B lymphoid (modified from Lahousse et al., 2004).

The transcriptional regulation of *RhoH* was demonstrated in Jurkat cells, a human T cell leukemia line, and in T cells. In Jurkat cells, phorbol-12-myristate-13-acetate (PMA) treatment decreased RhoH mRNA by 80% within 60 to 80 min, and the activation of the TCR in T cells reduced RhoH transcript levels within a few hours (Li et al., 2002).

At highly conserved positions in the aa sequence RhoH has different aa when compared to other Rho GTPases: at the position 13, serine instead of glycine and at the position 62, asparagine instead of glutamine. The aa glycine and glutamine are crucial for GTP hydrolysis (Figure 15). Similar to RhoH, Rnd3/RhoE GTPase has also different aa at these positions (serines at both positions) and is known to be deficient in GTPase activity. Therefore, it is assumed that RhoH has no intrinsic GTPase activity and is constitutively active. RhoH was

shown that it cannot autohydrolyze GTP and cannot hydrolyze GTP in the presence of RhoGAP p50, a potent GAP for RhoA, Rac and Cdc42 (Li et al., 2002).

RhoH was demonstrated to bind to all three known GDIs, which are capable of extracting Rho GTPases from membranes, implying a possible role in regulation of subcellular localization of RhoH. At the C-terminus, RhoH contains a typical CAAX motif (SKIF), which is most likely geranylated, like other Rho GTPases. Such geranylation should allow its association with membranes. However, RhoH was found to be mainly distributed to the cytoplasm (Li et al., 2002).

Functionally, RhoH was proposed to be a negative regulator of Rho GTPases. RhoH antagonizes Rac1-, RhoA- and Cdc42-mediated activation of NF-κB and p38 when transfected into Jurkat and 293 cells, while having no effect on JNK or Erk in these cells (Li et al., 2002). In addition, RhoH overexpression in HPCs suppresses Rac1 activation in response to stem cell factor (Gu et al., 2005a).

In contrast to other Rho GTPases, RhoH does not exert a significant role on the actin cytoskeleton reorganization in non-hematopoietic 293 cells (Li et al., 2002). However, in HPCs, overexpression of RhoH is associated with defective assembly and polarization of F-actin and reduced chemokine-induced cell migration *in vitro* (Gu et al., 2005a). Furthermore, in hematopoietic Jurkat cells and human peripheral blood cells, RhoH was demonstrated to be required to maintain the integrin lymphocyte function-associated antigen 1 (LFA-1), αLβ2-integrin, in a non-adhesive state (Cherry et al., 2004).

Retrovirus-mediated overexpression of RhoH resulted in reduced activity of HPCs to engraft into the BM of lethally irradiated mice, as well as in decreased HPC proliferation and increased HPC apoptosis *in vivo*. Knockdown of RhoH expression in HPCs led to increased HPCs proliferation, survival and migration activities, implying that RhoH is a negative regulator of proliferation and survival (Gu et al., 2005a).

PAK5, a member of the serine-threonine protein kinase family, has recently been identified as an effector protein binding to RhoH (Wu and Frost, 2006). PAK5 localizes to mitochondria and is thought to be important for protecting cells from apoptosis (Cotteret et al., 2003; 2006). However, the biological function of the interaction between RhoH and PAK5 is unclear (Wu and Frost, 2006).

In conclusion, the Rho GTPase family member RhoH displays a hematopoietic expression, preferentially in lymphoid cells and to a lesser extent in myeloid lineages (Li et al., 2002; Gu et al., 2005a; Lahousse et al., 2004). RhoH was suggested to be constitutively active and thus regulated transcriptionally (Li et al., 2002). Deregulation of RhoH expression probably occurs

in various lymphomas, where the *RhoH* gene is often mutated in the non-coding region or translocated into the locus of other genes (Pasqualucci et al., 2001; Preudhomme et al., 2000). Functionally, RhoH was shown to inhibit Rho GTPases and integrins (Li et al., 2002; Gu et al., 2005a; Cherry et al., 2004).

2.6   Aim of the project

RhoH is a hematopoietic member of Rho GTPase family. Based on overexpression and knockdown studies, several inhibitory functions were assigned to RhoH. First, RhoH was shown to have a suppressive effect on activation of Rac1 and Rac1-mediated signaling (Li et al., 2002; Gu et al., 2005a). Second, RhoH was revealed to inhibit proliferation and survival, and third, RhoH was demonstrated to be required to maintain the integrin LFA-1 in a non-adhesive state on lymphocytes (Gu et al., 2005a; Cherry et al., 2004). However, the function of RhoH in hematopoiesis was completely unknown when this study was initiated.

The aim of this project was to investigate the physiological role of RhoH in hematopoiesis and to verify the aforementioned effects of RhoH on Rac1-mediated signaling, proliferation, survival and adhesion, using RhoH-deficient mice. Since mutations of the *RhoH* gene were associated with a variety of lymphomas, one further aim was to examine whether RhoH-deficiency results in lymphoma formation.

3 Materials and methods

3.1 Materials

Chemicals were from Sigma, Roth or Merck. Restriction enzymes were purchased from New England Biolabs or Fermentas.

3.2 Generation of the RhoH-deficient mice

RhoH-deficient mice were generated by Ursula Kuhn and Dr. Cord Brakebusch using procedures as described previously (Talts et al., 1999). Briefly, as a targeting vector a 6.9 kb EcoRI-EcoRI genomic DNA fragment, cloned in pBluescript II KS (+/-), was used, in which a 0.9 kb HindIII-AatII fragment encoding the first 42 aa of the RhoH protein was replaced by an inverted neomycin resistance expression cassette. The vector was electroporated into embryonic stem cells (ES; 129/Sv) and cells with a stable integration of the targeting vector were selected by geneticin (G418; Invitrogen). The DNA of these clones was analyzed by Southern blot for homologous recombination.

Finally, two independent ES cell clones, positive for homologous recombination, were injected into C57BL6 blastocysts which were then transferred into the uterus of foster mice (carried out by Dr. Michael Bösl, Transgenic Facility, MPI for Biochemistry, Martinsried) and developed to chimeric mice. The contribution of ES cells to the chimeric mice was assessed by coat colour of the chimeric mice. ES cells are derived from agouti 129/Sv mice and blastocysts from black C57BL6 mice, and therefore the percentage of agouti coat colour indicates the contribution of ES cells. Germ-line transmission was tested by mating male chimeras showing a high ES cell contribution to female C57BL6 mice. Since agouti is dominant over black coat colour, the offsprings derived from ES-cell-germ-line will have the agouti coloured coat.

To obtain RhoH-deficient mice, heterozygous RhoH+/- aguti mice were mated.

3.3 Mice

Wild type and RhoH heterozygous knockout mice were kept as 129Sv/C57BL6 outbreds. β2-integrin-deficient mice (Scharffetter-Kochanek et al., 1998) and RhoH-null mice were inter-crossed to obtain RhoH-β2-null-double knockouts. RhoH-mutant mice backcrossed for 6 generations to C57BL6 were mated with OT-II transgenic mice (Barnden et al., 1998) to obtain RhoH-null/OT-II mice. The mice were weaned at the age of 3-4 weeks and separated according to gender. For matings, female mice older then 6 weeks and male mice older than 9

weeks were used. All mice were kept in a barrier facility (SPF: specific pathogen free) of the Max Planck Institute of Biochemistry in Martinsried according to the German and in the quarantine according to Danish rules of animal welfare.

3.4 Generation of the RhoH antibody

3.4.1 Immunization of a rabbit with the RhoH peptide

For the generation of a polyclonal anti-RhoH antibody, a rabbit was immunized with RhoH peptide and upon development of the immune response bled for serum preparation. 10 mg of RhoH peptide NRRKLFSINE-OH spanning 10 aa in C-terminus of the RhoH protein were synthesized by Dr. Stefan Übel in the department of Bioorganic Chemistry in the Max Planck Institute of Biochemistry in Martinsried, Germany. An additional cysteine was added at the N-terminus of the peptide to provide a sulfhydryl group for the conjugation with the keyhole limpet hemocyanin (KLH; Imject Maleimide Activated mcKLH; Pierce). 2 mg RhoH peptide in 280 µl PBS were mixed with 2 mg KLH in 220 µl H_2O and incubated for 2 h at RT to form a conjugate. A peptide (hapten) alone cannot stimulate an immune response, however when coupled to a carrier protein, for example KLH, it will induce a strong immune reaction. The conjugate was purified by gel filtration in order to remove EDTA, which is an anti-coagulant and should not be injected into animals. The peptide-KLH mixture was applied on a D-Salt Polyacrylamide Desalting column (Pierce), which was pre-equilibrated with Purification Buffer Salts (Pierce), and the hapten-carrier conjugate was eluted with 8x 0.5 ml aliquots of Purification Buffer Salts. The fractions, containing the KLH-RhoH peptide conjugate, were determined by measurement of absorbance at 280 nm, pooled, divided into 5 samples and stored at -20°C. The quantification of conjugation was done according to the protocol of manufacturer's.

One aliquot of a peptide-KLH-conjugate in 500 µl PBS was mixed with 500 µl complete Freund's adjuvant (Sigma) using two 2 ml syringes connected by an adaptor (Braun) until emulsion was developed. The emulsion was subsequently injected subcutaneously into a rabbit (carried out by the Animal Core Facility). On day 14, 28, 42 the rabbit was boosted with peptide-KLH-conjugate mixed with the incomplete Freund's adjuvant and blood was collected on day 54. On day 21, 35 and 49 the rabbit was bled to prepare an anti-serum aliquot for monitoring the development of a specific antibody response in ELISA. Following the incubation for 30-60 min at 37°C, the blood was incubated over night (o/n) at 4°C. The anti-serum was separated by centrifugation for 10 min at 4000 rpm, 4°C and subsequent

centrifugation of the supernatant for 10 min at 10000 rpm, 4°C. Anti-serum was aliquoted and stored at -20°C.

3.4.2 ELISA of the rabbit anti-serum

96-well flat bottom plate was coated with 100 µl 0.01 mg/ml RhoH peptide in PBS (1 µg peptide per well) o/n at RT (s. scheme). Next day, the liquid was removed and the plate blocked with 100 µl 1% BSA in PBS for 1.5 h at RT. After washing the plate 3x with 200 µl PBS and addition of 100 µl of anti-serum serially diluted in 1% BSA/PBS, the plate was incubated for 1 h at RT. Subsequently, the plate was washed 3x with 200 µl PBS, and incubated with 100 µl goat anti-rabbit-HRP diluted 1:1000 in 1% BSA/PBS for 1 h at RT. The plate was again washed 3x with 200 µl PBS and incubated with 100 µl substrate (3.3 µl H_2O_2 added to 10 ml of 1 mg/ml 5-aminosalicylic acid in 20 mM phosphate buffer pH 6.8) for 10-20 min at RT. Reaction was stopped by adding 100 µl 1 N NaOH and the plate read at 490 nm.

Scheme

	1	2	3	4	5	6	7	8	9	10	11	12
	preserum	preserum	preserum	preserum	1st bleed	1st bleed	1st bleed	1st bleed	2nd bleed	2nd bleed	2nd bleed	2nd bleed
A	1:500	1:500	1:500	1:500	1:500	1:500	1:500	1:500	1:500	1:500	1:500	1:500
B	1:1000	1:1000	1:1000	1:1000	1:1000	1:1000	1:1000	1:1000	1:1000	1:1000	1:1000	1:1000
C	1:2000	1:2000	1:2000	1:2000	1:2000	1:2000	1:2000	1:2000	1:2000	1:2000	1:2000	1:2000
D	1:5000	1:5000	1:5000	1:5000	1:5000	1:5000	1:5000	1:5000	1:5000	1:5000	1:5000	1:5000
E	1:10000	1:10000	1:10000	1:10000	1:10000	1:10000	1:10000	1:10000	1:10000	1:10000	1:10000	1:10000
F	1:20000	1:20000	1:20000	1:20000	1:20000	1:20000	1:20000	1:20000	1:20000	1:20000	1:20000	1:20000
G	1:40000	1:40000	1:40000	1:40000	1:40000	1:40000	1:40000	1:40000	1:40000	1:40000	1:40000	1:40000
H	PBS	PBS	PBS	PBS	PBS	PBS	PBS	PBS	PBS	PBS	PBS	PBS

coated with peptide   coated with peptide   coated with peptide

3.5 Bacteria culture

3.5.1 Bacteria strains

For cloning, *Escherichia coli* (*E. coli*) DH5α strain (F', endA1, hsdR, hsdM, sup44, thi-1, gyrA1, gyrA96, relA1, recA1, lacZΔM15) was used.

E. coli BL21(DE3)pLys (B, F⁻, dcm, ompT, hsdS(r_B^- m_B^-), gal λ(DE3) [pLys Cam^r]) strain was used for expression of recombinant proteins.

3.5.2 Media and conditions for bacteria culture

Bacteria were grown in Luria-Bertoni medium (LB; 0.5% yeast extract, 1% bactotryptone, 1% NaCl, autoclaved) at 37°C with shaking at 200 rpm or on LB plates (1.5% agar in LB medium) at 37°C. Bacteria transformed via electroporation method were cultured in SOC

medium (0.5% yeast extract, 2% bactotryptone, 10 mM NaCl, 2.5 mM KCl, 10 mM MgCl$_2$, 20 mM MgSO$_4$, 20 mM glucose). Following antibiotics were used for selecting of bacteria: 100 µg/ml ampicillin, 25 µg/ml kanamycin or 34 µg/ml chloramphenicol.

3.6 Molecular biology methods

3.6.1 Primers

The following primers synthetized by Metabion, Germany, were used.

primer name	Sequence (5' – 3')	application
Rh1	GTG TAC GAG AAT ACG GGT GT	genotyping (RhoH wt allele, fw)
Rh2	GTG GCC ACA ACC AGC ACC	genotyping (RhoH wt, ko allele, rev)
Rh4	CTT GTG TAG CGC CAA GTG C	genotyping (RhoH ko allele, fw)
oIMR1825	GCT GCT GCA CAG ACC TAC T	genotyping (OTII)
oIMR1826	CAG CTC ACC TAA CAC GAG GA	genotyping (OTII)
CD18.1	AGG ACA GCA AGG GGG AGG ATT	genotyping (β2 ko allele)
CD18.2	GCC CAC ACT CAC TGC TGC TTG	genotyping (β2 wt, ko allele)
CD18.3	CCC GGC AAC TGC TGA CTT TGT	genotyping (β2 wt allele)
TD1	GCG GAA TTC GAT GCT GAG CTC AAT CAA GTG C	probe for Northern blotting (fw)
TD2	GCG GGA TCC CTT AGA AGA TCT TGC ATT CAT TGA T	probe for Northern blotting (rev)
rt-1-fw	TTA CAT GGC GTG GAG AGC TA	qRT-PCR (RhoH exon1-exon2-border, fw)
rt-2-rv	TCT CAG CCA CTT TGG GAA CT	qRT-PCR (RhoH exon1-exon2-border, rev)
rt-3-fw	AGT CAT CGC ACA CCA GTT G	qRT-PCR (RhoH exon2-exon3-border, fw)
rt-4-rv	AGT CTG CCC AGG TGA GAA AC	qRT-PCR (RhoH exon2-exon3-border, rev)
rt-5-fw	AGT TCC AAA GTG GCT GAG A	qRT-PCR (RhoH exon1-exon2-exon3-border, fw)
rt-6-rv	CAA CTG GTG TGC GAA TGA CT	qRT-PCR (RhoH exon1-exon2-exon3-border, rev)
GAPDH_sense	TCG TGG ATC TGA CGT GCC GCC TG	qRT-PCR (GAPDH, fw)
GAPDH_anti	CAC CAC CCT GTT GCT GTA GCC GTA T	qRT-PCR (GAPDH, rev)
TD3	GCG GGA TCC ATG CTG AGC TCA ATC AAG TGC	cloning of RhoH in pRK5-myc (fw)
TD4	GCG GAA TTC TTA GAA GAT CTT GCA TTC ATT GAT	cloning of RhoH in pRK5-myc (rev)
Rh EcoRI Fw	GCG GAA TTC ATG CTG AGC TCA ATC AAG TGC GT	cloning of RhoH in pCR3.V64-Met-Flag-Stop (fw)
Rh XhoI Rv	CCG CTC GAG TTA GAA GAT CTT GCA TTC ATT GAT	cloning of RhoH in pCR3.V64-Met-Flag-Stop (rev)
TD18B	GCG CTC GAG CTG CCA CCA TGC TGA GCT CAA TCA AGT G	cloning of RhoH in pCMV-N-terminal-TAP (fw)
TD21	GCG GGA TCC TTA GAA GAT CTT GCA TTC ATT GAT GG	cloning of RhoH in pCMV-N-terminal-TAP (rev)
TD19	CTT CTG AAG GCG TCC AGG CCG GCA GTG TC	cloning of RhoH-N62L in pCMV-N-terminal-TAP (rev)
TD20	CGC ACC AAC AGT GAG TTT TTC CCC ACA GCA C	cloning of RhoH-T18N in pCMV-N-terminal-TAP (rev)
T7	GTA ATA CGA CTC ACT ATA GGG C	cloning of RhoH-T18N in pCMV-N-terminal-TAP (fw)
UK7	GCG GAA TCC TGC TGA GTT TCA GAC ATC TAC	cloning of 3' external RhoH probe
UK8	GCG GGA TCC ACA GCA AAC ACC AGA ACA TAC	cloning of 3' external RhoH probe

3.6.2 Determination of DNA concentration

The DNA concentration and quality was measured with UV spectrophotometer (Gene Quant II, Amersham Pharmacia Biotech) using quarz cuvette against H$_2$O as a reference. The absorbance of 1 at 260 nm will correspond to a DNA concentration of 50 µg/ml. The measurement of DNA quality is based on a ratio between the absorbance at 260 nm and 280 nm (A_{260}/A_{280}). Clean DNA has a A_{260}/A_{280} ratio between 1.8 and 2.

3.6.3 Agarose gel electrophoresis

Agarose gel electrophoresis was used for separating and analyzing DNA fragments in an electric field. 0.8-2.5% agarose (Invitrogen) was dissolved in 1x TAE buffer (50x TAE: 242 g Tris, 57.1 ml glacial acetic acid, 100 ml 0.5 M EDTA pH 8 filled up to 1 l with ddH$_2$O, was

diluted to 1x TAE) by boiling in the microwave. The choice of the agarose gel concentration depended on the size of the DNA fragments to be separated. Large DNA fragments (5-10 kb) show a good separation in 0.8% agarose gel, small fragments (0.2-1 kb) are resolved in 2% agarose gel. After cooling down to 60°C, ethidium bromide was added to a final concentration of 0.5 µg/ml and agarose solution was poured into a gel chamber. DNA mixed 1:6 with 6x DNA loading buffer (30% glycerol, 0.3% bromphenol blue) was loaded into the slots and separated in 1x TAE buffer at 80-120V. DNA with intercalated ethidium bromide was visualized under UV light at 254 nm and the gel was photographed. With the DNA standard size marker (1 kb ladder; Invitrogen) applied on the gel, the sizes of the resolved DNA fragments could be estimated.

3.6.4   DNA digestion

Analytical digests were performed in 20 µl reaction volume as follows: 5 µl of mini-prep-DNA were digested in 2 µl 10x specific restriction enzyme buffer, 2 µl 1 mg/ml BSA, 2.5 U restriction enzymes. Preparative digests were carried out in 50 µl reaction volume as follows: 5 µg plasmid-DNA or 30 µl PCR-product were cut in 5 µl 10x specific restriction enzyme buffer, 2 µl 1 mg/ml BSA, 50 U restriction enzymes. The samples were incubated for 2 h at 37°C. PCR-products were digested o/n at 37°C.

3.6.5   DNA ligation

The ligation of two compatible DNA fragments was achieved by T4 DNA ligase, which catalyzes the ATP-dependent formation of phosphodiester bound between 3'-OH and 5'-phosphate ends. The ligation was performed as follows: 0.5-1 µl digested and purified vector DNA, 7 µl purified insert DNA, 2 µl 5x T4 ligase buffer (Invitrogen), 1 µl T4 DNA ligase (Invitrogen) were mixed and incubated for 1-4 h RT or o/n at 16°C.

3.6.6   Dephosphorylation of the vector

To prevent the religation of a vector, digested with compatible enzymes, the 5'-phosphates were removed with alkaline calf intestinal phosphatase (CIP; Roche). 1 µl CIP was directly added to DNA after restriction digestion and incubated for 30 min at 37°C. 1 µl CIP was added and the sample was again incubated for 30 min at 37°C. CIP was inactivated for 10 min at 65°C and DNA was purified from agarose gel by QIAquick Gel Extraction Kit (s. 3.6.7).

3.6.7 Extraction of DNA fragments from agarose gel

The desired DNA fragment was excised from the agarose gel with a scalpel under a long wave UV light and isolated using QIAquick Gel Extraction Kit (Qiagen) or DNA Extraction Kit (Fermentas) according to manufacturer's protocol. An aliquot of 2-3 µl purified DNA was analyzed on agarose gel to verify the quality of DNA purification and to estimate the amount of purified DNA using the standard marker as a reference.

3.6.8 Cloning of RhoH constructs

Coding region of RhoH was amplified by PCR from pBluescript II KS (+/-) (pBS)-RhoH-EcoRI-EcoRI with primers TD1 and TD2, digested with EcoRI and BamHI and cloned into pBS, which was also digested with EcoRI and BamHI.

RhoH-myc was constructed by amplifying RhoH from pBS-RhoH-EcoRI-EcoRI by PCR with primers TD3 and TD4, digested with BamHI and EcoRI and cloned into pRK5, which was also digested with BamHI and EcoRI.

RhoH-Flag was constructed by amplifying RhoH from pBS-RhoH-EcoRI-EcoRI by PCR with primers Rh EcoRI Fw and Rh XhoI Rv, digested with EcoRI and XhoI and cloned into pCR3.V64-Met-Flag-Stop (PS080), which was also digested with EcoRI and XhoI.

RhoH-TAP-tag was constructed by amplifying RhoH from pBS-RhoH-EcoRI-EcoRI by PCR primers with TD18B and TD21, digested with XhoI and BamHI and cloned in pCMV-N-terminal-TAP, which was also digested with XhoI and BamHI.

A mutation N to L of RhoH at the position 62 was introduced via mutagenesis PCR as follows: RhoH was amplified from pBS-RhoH-EcoRI-EcoRI by PCR with primers TD18B and TD19, carrying the mutation. The PCR product was used as a 5'-megaprimer in the subsequent PCR with TD21 as a 3'-primer and pBS-RhoH-EcoRI-EcoRI as a template. The PCR product was digested with XhoI and BamHI and cloned in pCMV-N-terminal-TAP, which was also digested with XhoI and BamHI.

A mutation T to N of RhoH at the position 18 was introduced via mutagenesis PCR as follows:

RhoH was amplified from RhoH-Flag-PS080 with T7 and TD20, carrying the mutation. The PCR product was used as a 5'-megaprimer in the subsequent PCR with Rh XhoI Rv and RhoH-Flag-PS080 as a template. The amplified DNA was digested with BamHI and EcoRI and cloned into pCR3.V64-Met-Flag-Stop (PS080), which was also digested with BamHI and EcoRI. The resulting vector was used as a template in a PCR with TD18B and TD21, digested

with XhoI and BamHI and cloned in pCMV-N-terminal-TAP, which was also digested with XhoI and BamHI.

3.6.9 Mini-preparation of plasmid DNA

For analytical preparation of plasmid DNA up to 20 μg, a single bacterial colony was inoculated in 3 ml LB, supplemented with antibiotics and incubated o/n at 37°C with vigorous shaking. Next day, 1.5 ml bacteria were harvested by centrifugation for 30 sec, 14000 rpm, RT. After removing the supernatant, the pellet was resuspended in 200 μl P1 (50 mM Tris pH 8, 10 mM EDTA, 100 μg/ml RNAse A). 200 μl P2 (200 mM NaOH, 1% SDS) were added and the samples were mixed. Following incubation for 5 min at RT, 200 μl P3 (3 M potassium acetate pH 5.5) were added to neutralize the solution. The samples were mixed and incubated for 5 min on ice. Subsequently, the samples were centrifuged for 5 min, 14000 rpm, RT and the supernatant was transferred into new tubes. After addition of 500 μl isopropanol, the samples were mixed again and DNA was precipitated by centrifugation for 5 min, 14000 rpm, RT. The pellet was washed with 70% EtOH and centrifuged for 5 min, 14000 rpm, RT. After removing the supernatant, the DNA was air-dried and resuspended in 30 μl ddH$_2$O. DNA was stored at -20°C.

3.6.10 Maxi-preparation of plasmid DNA

QIAGEN Maxi prep kit was used for preparative isolation of plasmid DNA up to 500 μg. The protocol was carried out according to the manufacturer's procedure. DNA concentration was determined and DNA was stored at -20°C.

3.6.11 Polymerase chain reaction

Polymerase chain reaction (PCR) is a method to specifically amplify defined DNA fragments (Saiki et al., 1988).

The PCR was prepared in 20 μl reaction volume (or 50 μl for preparative PCR) containing 2 μl of 10x PCR buffer, 0.6 μl 50 mM MgCl$_2$, 0.4 μl 10 mM dNTPs, 0.2 μl 10 μM forward primer, 0.2 μl 10 μM reverse primer, 0.2 μl *Taq* DNA polymerase, 2 μl genomic DNA (or 0.1 -1 μg vector DNA), 14.4 μl ddH$_2$O, and run on a PCR machine (Biometra). RhoH- and β2-mutant mice with genotyped with a touchdown PCR with the annealing temperature 65°C to 55°C and 63°C to 53°C, respectively, as follows:

1. Denaturation   95°C, 3 min
2. Denaturation   95°C, 30 sec
3. Annealing   65°C (or 63°C), 30 sec
4. Elongation   72°C, 30 sec
5. Steps 2, 3 and 4 were repeated 9 times. The annealing temperature was decreased each cycle by 1°C.

6.	Denaturation	95°C, 30 sec
7.	Annealing	55°C (or 53°C), 30 sec
8.	Elongation	72°C, 30 sec
9.	Steps 6, 7 and 8 were repeated 35 times.	
10.	Elongation	72°C, 5 min
11.	Pause	4°C

OT-II mice were genotyped using the PCR program with the annealing temperature of 60°C without the touchdown step.

For cloning, the PCR was carried out with the High Fidelity PCR System (Roche) or with the pfu DNA polymerase (Fermentas), containing a DNA polymerase with a proof-reading activity, and using the reaction buffers supplied by the manufactures.

3.6.12 DNA sequencing

To verify the sequence of DNA, 600 ng plasmid DNA together with 2 µl Big dye terminator premixture, 1 µl 10 pmol/µl given primer in 10 µl total volume were subjected to a PCR (program: 95°C 30 sec, 50°C 10 sec, 60°C 4 min, 30 cycles) and stored at 4°C prior to sequencing. 10 µl PCR-reactions were sequenced at Max Planck Institute, Martinsried, Germany. Alternatively, 1-2 µg air-dried DNA together with 10 pmol (10 µl of 10 µM) primer were sent to MWG Biotech AG (http://www.mwg-biotech.com/html/all/index.php). The sequences were viewed with Chromas software, version 1.45.

3.6.13 Preparation of competent bacteria

3.6.13.1 Preparation of heat shock competent DH5α

For o/n culture, 5 ml LB medium supplemented with 0.02 M MgSO$_4$ and 0.01 M KCl were inoculated with DH5α *E. coli* bacteria and incubated o/n at 37°C on the shaker. Next day, 150 ml pre-warmed LB medium supplemented with 0.02 M MgSO$_4$ and 0.01 M KCl were inoculated with 1 ml DH5α o/n culture and grown at 37°C on the shaker to OD$_{600}$ of 0.3-0.4. Bacteria were then transferred into four pre-chilled 50 ml tubes and kept in the ice bath for 10 min. After centrifugation for 10 min at 6000 rpm, 4°C, the pellets were gently resuspended in 37.5 ml ice-cold TFB1 (25 mM KAc, 50 mM MnCl$_2$, 100 mM RbCl, 100 mM CaCl$_2$, sterile filtered and 87% autoclaved glycerol were added to a final concentration of 15%) each and incubated for 10 min on ice. Again, the cells were centrifuged for 10 min at 6000 rpm, 4°C and each pellet was gently resuspended in 3 ml ice-cold TFB2 (10 mM MOPS, 75 mM CaCl$_2$, 10 mM RbCl, 15% glycerol, autoclaved). 50 µl aliquots of the bacteria (240 aliquots result from 150 ml culture) were frozen in dry ice/isopropanol bath and stored at -80°C.

3.6.13.2 Preparation of electrocompetent BL21(DE3)

5 ml LB medium supplemented with 34 µg/ml chloramphenicol were inoculated with BL21 *E. coli* bacteria and incubated o/n at 37°C with vigorous shaking. Next day, 250 ml LB medium + chloramphenicol were inoculated with 2.5 ml o/n culture and grown at 37°C with vigorous shaking until the OD_{600} was between 0.5 and 1.0. After the desired OD_{600} was reached, the bacteria were cooled on ice for 15 min, transferred into four pre-chilled tubes and centrifuged for 10 min at 4000 rpm, 4°C. The pellets were resuspended in 125 ml cold sterile ddH_2O each and centrifuged for 15 min at 4000 rpm, 4°C. Again, the pellets were resuspended in 62.5 ml sterile ddH_2O each and centrifuged for 15 min at 4000 rpm, 4°C. The bacteria were then resuspended in 10 ml 15% cold sterile glycerol in total and transferred into one tube. After centrifugation for 15 min at 4000 rpm, 4°C, the supernatant was decanted and the pellet was resuspended in residual glycerol and transferred into a 1.5 ml tube. Subsequently, the cells were centrifuged for 5 min at 14000 rpm, 4°C and resuspended in 1-1.5 ml cold 15% glycerol. 50 µl aliquots of the bacteria were frozen in dry ice / ethanol bath and stored at -80°C.

3.6.14 *E.coli* transformation

3.6.14.1 Heat shock

Competent DH5α *E. coli* bacteria (s. 3.6.13.1) were thawed on ice and 10 µl of ligation reaction (s. 3.6.5) or 1 µl (10 ng) of plasmid DNA were added. Following the incubation on ice for 30 min, the cells were heat shocked for 2 min at 42°C. The cells were immediately transferred on ice and 1 ml LB medium containing no antibiotics was added. The tubes were placed on a shaker and incubated for 30-60 min at 37°C. Next, the cells were pelleted and 800 µl supernatant were removed. The cells were resuspended in the residual 200 µl medium and distributed on a LB plate containing the appropriate antibiotic with a Drygalski spatula. The plates were inverted and incubated o/n at 37°C.

3.6.14.2 Electroporation

Electrocompetent BL21(DE3) *E. coli* bacteria (s. 3.6.13.2) were thawed on ice and 1 µl of 5 pg/µl to 0.5 µg/µl DNA was added. Bacteria were then transferred into pre-chilled electroporation cuvette and kept on ice for 10 min. Immediately after the electrical pulse of 25 µF, 2.5 kV, 200 W with a time constant higher than 4.1 (ideally close to 5.0) initiated through the electroporator (Biorad), 1 ml of SOC or LB medium was added to the cuvette and the bacteria were transferred into 1.5 ml tube. The cells were incubated for 30-60 min at 37°C

with gentle shaking and then plated on LB plates containing the appropriate antibiotic using the same procedure as described above (s. 3.6.14.1).

3.6.15   Genomic DNA extraction

3.6.15.1   DNA extraction from tail pieces

For genotyping mice were marked with ear-tags and 5 mm long tail pieces were clipped. Tails were either stored at -20°C or processed immediately by incubation in 500 µl tail lysis buffer (100 mM Tris pH 8.5, 5mM EDTA, 0.2% SDS, 200 mM NaCl, containing freshly added 100 µg/ml Proteinase K) at 55°C o/n. Next day, the samples were stored at -20°C or directly processed further: The tail debris were pelleted for 5 min, 14000 rpm, RT and supernatant was transferred into new tubes and mixed with 500 µl isopropanol to precipitate DNA. After vigorous shaking the samples were centrifuged for 5 min, 14000 rpm, RT and the supernatant was removed. Precipitated DNA was washed with 500 µl 70% EtOH and centrifuged for 5 min, 14000 rpm, RT. Again, the supernatant was removed and DNA was air-dried for 10 min, RT. Finally, the DNA was resuspended in 300 µl ddH$_2$O and incubated at 55°C for 2 h or o/n to dissolve and then stored at 4°C.

3.6.15.2   DNA isolation from tail pieces for Southern blot

For Southern blotting tail pieces were lysed in 500 µl tail lysis buffer (s. 3.6.15.1) at 55°C o/n. Next day, the tail debris were pelleted for 10 min, 14000 rpm, RT and supernatant transferred into new tubes. DNA was extracted by adding 250 µl phenol (equilibrated with TE, pH 8) and 250 µl chloroform. After vigorous shaking the samples were centrifuged for 5 min, 14000 rpm, RT and the aqueous phase containing DNA was precipitated with 500 µl isopropanol in new tubes. Followed vigorous shaking, DNA was pelleted for 5 min, 14000 rpm, RT and washed with 500 µl 70% EtOH. After centrifigution for 5 min, 14000 rpm, RT and air-drying, the DNA was resuspended in 50-100 µl TE and incubated at 55°C o/n to dissolve and then stored at 4°C.

3.6.16   Southern blotting

Southern blotting technique was used for detection of a specific DNA sequence in the genome. DNA was digested with restriction enzymes and separated by the agarose gel electrophoresis, followed by the transfer on a membrane. The specific DNA sequences were detected by hybridization with radioactively labeled DNA probes.

3.6.16.1 Genomic digestion and DNA gel electrophoresis

Genomic tail DNA was digested with HindIII in 30 µl total volume at 37°C o/n (20 µl tail DNA, 3 µl 1 mg/ml BSA, 3 µl 10x buffer 2, 1 µl 40 U/µl HindIII, 3 µl ddH$_2$O). Digested DNA and 1 kb DNA ladder were separated on 0.8% agarose gel, at 30 V o/n, RT. Next day, the gel with a ruler laid alongside the gel was photographed on a UV transilluminator at 366 nm. The double stranded DNA was denatured into single strands by incubation of the gel in a denaturation solution (0.5 M NaOH, 1.5 M NaCl) for 45 min, RT, with gentle agitation. After rinsing the gel for several times with water, the gel was neutralized in a neutralization solution (0.5 M Tris-HCl, 0.5 M NaCl, pH 7).

Subsequently, the chamber for DNA transfer was prepared. A glass plate was placed on a dish filled with 10x SSC (20x SSC: 175.2 g NaCl (3 M), 88.2 g Na$_3$-citrate x 2H$_2$O (0.3 M) filled up to 1 l, pH 7; diluted 1:2). The gel was arranged on two pieces of Whatman (3MM) paper of the same size as the width of the glass plate. The Whatman paper protruded into the dish and was soaked with 10x SSC. The air bubbles were squeezed out by rolling a pipette over the surface. A positively charged HybondXL membrane (Amersham Biosciences) of the size of the gel was wetted in 10x SSC and laid on top of the gel. The free space on the Whatman paper was covered by plastic wrap to avoid the drying out of the paper and to ensure the DNA transfer. The membrane was covered with two layers of 10x SSC wetted gel-sized Whatman paper. The air bubbles between gel, membrane and Whatman paper were removed by rolling a pipette over the surface. A 10 cm stack of paper tissues and a glass plate with 0.5 kg weight was placed on top of the Whatman paper to ensure a good contact throughout the structure. The transfer was carried out o/n at RT.

After transfer the slots were marked on the membrane with the pencil and the membrane was put on a Whatman paper and UV crosslinked (120 J/cm2) in a crosslinker (UV Stratalinker 2400, Stratagene). The membrane was then backed for 2 h at 80°C and stored in a plastic foil at 4°C.

3.6.16.2 Labeling of the DNA probe

The DNA probe was radioactively labeled with ^{32}P. 5 µl DNA probe (2.5-25 ng) were mixed with 40 µl TE and denatured for 5 min at 95°C. The DNA was transferred immediately on ice and incubated for 3 min on ice. Next, the DNA was added to a Rediprime II reaction mix (Amersham Biosciences) containing an improved exonuclease free Klenow fragment. 5 µl Redivue [^{32}P dCTP] (Amersham Biosciences) were added to this mixture and incubated for 30 min at 37°C. In the meantime, sepharose columns was prepared. 1 ml syringe plugged with 2 layers of glass microfibre filter was filled with 1 ml sepharose (Sephadex G50 powder

dissolved in ddH$_2$O), placed in 15 ml tube and centrifuged for 3 min, 2000 rpm, RT to remove the residual H$_2$O. The syringe had to be filled with around 0.7 ml sepharose. 50 µl TE were added to the labeled DNA probe and the sample was applied onto the sepharose column. After centrifugation for 3 min, 2000 rpm, RT, DNA probe was eluted, whereas non-incorporated nucleotides bound to the sepharose column. 1 µl labeled DNA was measured in a scintillation counter.

3.6.16.3 Hybridization, washing, autoradiography

During the labeling of the DNA probe the membrane was pre-hybridized in a closed box with Church buffer (0.5 M NaPi, 7% SDS, 1 mM EDTA, 100 mg/ml salmon sperm ssDNA, 1% BSA) for 1 h at 65°C with gentle agitation. DNA probe (s. 3.6.16.2) was denatured again for 3 min at 95°C and added to membrane in the pre-hybridization solution (Church buffer). The hybridization was peformed o/n at 65°C with gentle agitation.

Next day, the hybridization solution was removed, and the membrane washed 2x 20 min with Church wash buffer (40 mM NaPi, 1% SDS) at 65°C with gentle agitation. The membrane was placed in a plastic wrap and exposed to an autography film (Kodak) for 4 h or up to 4 days at -80°C. The films were developed in a developing machine.

3.6.17 RNA

3.6.17.1 RNA isolation

BM, spleen, thymus and lymph nodes (LN) were isolated from RhoH+/+, RhoH+/- and RhoH-/- mice and single cell suspensions were prepared as described in 3.9.1.1. 1 ml TRIzol reagent (Invitrogen) was used per 5-10x10^6 cells. 40x10^6 BM cells, splenocytes and thymocytes were resuspended in 4 ml TRIzol reagent. 10x10^6 LN cells were resuspended in 1 ml TRIzol and incubated for 5 min at RT to permit the dissociation of nucleoprotein complexes. 800 µl or 200 µl chloroform were added to BM cells, splenocytes and thymocytes or LN cells, respectively. The samples were shaked vigorously and incubated for 5 min at RT. Following the centrifugation for 20 min, 4000 rpm, 4°C, the mixture separated into lower red, phenol-chloroform phase, an interphase, and colorless upper aqueous phase. Aqueous phase containing RNA was transferred into a new tube and precipitated with 0.5 ml isopropanol per 1 ml TRIzol. The samples were mixed and incubated for 10 min at RT. After centrifugation for 30 min, 4000 rpm, 4°C, the gel-like pellet was washed with 1 ml 80% EtOH per 1 ml TRIzol. The samples were vortexed and centrifuged for 15 min, 4000 rpm, 4°C. Lastly, the

RNA was air-dried, dissolved in 200 µl (for BM cells, splenocytes, thymocytes) or 50 µl H$_2$O$_{DEPC}$ (for LN cells) and incubated for 10 min at 55°C. RNA was stored at -80°C.

Absolutely RNA Microprep Kit (Stratagene) was used to isolate RNA from less than 5x10^5 and RNeasy Mini Kit (Qiagen) from 5x10^5 to 1x10^7 cells according to manufacturer's protocol.

3.6.17.2   Determination of RNA concentration

RNA concentration was measured with the same UV spectrophotometer as for determining DNA concentration. The absorbance of 1 at 260 nm will correspond to a RNA concentration of 40 µg/ml.

3.6.18   Northern blotting

Northern blotting technique was used for detection of gene expression. RNA, isolated via TRIzol method, was separated by the agarose gel electrophoresis, followed by the transfer on a membrane. The specific RNA sequences were detected by hybridization with radioactively labeled DNA probes similar as for the Southern blotting.

3.6.18.1   Preparation of RNA samples

5 µg RNA in 12 µl H$_2$O$_{DEPC}$ were prepared. If RNA concentration was too low, RNA was precipitated with 1 µl tRNA, 0.1 volume 4 M LiCl and 2.5 volume 100% EtOH for at least 1 h at -80°C. The RNA was pelleted for 30 min, 14000 rpm, 4°C, washed with 500 µl 80% EtOH and resuspended in appropriate volume H$_2$O$_{DEPC}$.

5 µg RNA in 12 µl H$_2$O were incubated with 1 µl 40x MOPS, 20.25 µl formamide, 6.6 µl 37% formaldehyde for 7 min at 55°C, vortexed and incubated for additional 7 min at 55°C. After spinning down, the samples were transferred onto ice and 4.5 µl of ethidium bromide-mixture [1 µl 1 mg/ml ethidium bromide + 3.5 µl 10x RNA-loading dye (50% glycerol, 10 mM EDTA pH 8, 0.25% bromphenol blue, stored at -20°C)] were added.

3.6.18.2   RNA agarose gel electrophoresis

RNA was fractionated on 0.8% agarose gel. For 100 ml agarose gel, 0.8 g agarose in 81 ml H$_2$O$_{DEPC}$ were weighed and boiled. After boiling the weight was determined again and, if necessary, H$_2$O$_{DEPC}$ was added to achieve the original weight. The agarose was cooled down for 2 min, and 2.5 ml 40x MOPS (167,6 g MOPS (0.8 M), 27,2 g Na-acetate x 3H$_2$O (0.2 M), 80 ml 0.5 M EDTA (40 mM EDTA), adjusted with NaOH to pH 7.2, filled up to 1 l with H$_2$O$_{DEPC}$) and 16.5 ml 37% formaldehyde were added. Following mixing, the agarose gel was

poured into a gel chamber treated with 1 M NaOH for 30 min and thoroughly washed with H_2O_{DEPC}.

The gel was pre-run in 1x MOPS (40x MOPS diluted 1:40) buffer at 70 V for 15 min at 4°C. RNA was separated at 70 V for 4-5 h at 4°C. The ethidium bromide stained RNA was visualized on a UV transilluminator at 366 nm and photographed with a ruler laid alongside the gel so that the RNA band sizes could be later identified and calculated on the membrane. Two bands corresponding to 28S (4,72 kbp) and 18S (1,87 kbp) rRNA were visible on the gel.

3.6.18.3   RNA blotting

After electrophoretic fractionation of RNA, the gel was equilibrated in 10x SSC for 20 min at RT with gentle agitation. Meanwhile the chamber for RNA transfer was prepared. The blotting structure and procedure was the same as for Southern blot (s. 3.6.16.1). The transfer was carried out for 5-6 h at RT.

After transfer the slots were marked on the membrane with the pencil, RNA was crosslinked (s. 3.6.16.1) and membrane was stored in a plastic foil at 4°C.

3.6.18.4   Labeling of the DNA probe

s. 3.6.16.2

3.6.18.5   Hybridization, washing, autoradiography

s. 3.6.16.3

3.6.18.6   Removal of the probes from Northern blots

Hybridization probes could be removed from Northern blots by incubating the membrane in the 85°C pre-warmed stripping buffer (100 ml H_2O_{DEPC}, 100 ml TE, 1 ml 20% SDS) for 30 min at 85°C with gentle agitation. After stripping, the membrane was washed 2x 20 min with Church wash buffer at 65°C and could be re-used for another pre-hybridization and a hybridization with the second probe.

3.6.19   Real-time-PCR

To analyze the expression of RhoH in thymocyte subpopulations, splenic T and B cells, and BM granulocytes, real-time-PCR was performed. Wild type DN thymocytes enriched via MACS (Miltenyi) were sorted for DN1, DN2, DN3 and DN4 with FACSAria (BD). DP, CD4SP and CD8SP thymocytes were sorted with FACSAria, while CD4+, CD8+, B220+ splenocytes and Gr-1+ BM cells were enriched via MACS. Absolutely RNA Microprep Kit

(Stratagene) was used to isolate RNA from DN1, DN2, DN4 and CD8SP, and RNeasy Mini Kit (Qiagen) was used to isolate RNA from DN3, DP, CD4SP, CD4+, CD8+, B220+, and Gr-1+ cells according to manufacturer's protocol. cDNA was generated from 15 ng RNA using the iScript cDNA Synthesis Kit (Bio-Rad) in 20 µl volume (4 µl 5x reaction mix, 1 µl reverse transcriptase, 15 ng RNA, H_2O_{DEPC}) according to the following program: 5 min at 25°C, 30 min at 42°C, 5 min at 85°C, cool to 4°C. 1 µl cDNA was subjected to real-time-PCR using the iQ SYBR Green Supermix (Bio-Rad) on the iCycler (Bio-Rad) in 25 µl volume in 96-well plate (Bio-Rad). Two Mastermixes were prepared:

Mastermix 1:		Mastermix 2:	
CyBrGreen	12.5 µl	cDNA	1 µl
sense primer 10 µM	1 µl	ddH$_2$O	9.5 µl
anti primer 10 µM	1 µl	Σ	10.5 µl
Σ	14.5 µl		

14.5 µl of Matermix 1 were mixed with 10.5 µl of Mastermix 2 in one well, centrifuged and PCR was performed on the iCycler.

The primers fwd-3 and rev-4 spanning the exon 2 – exon 3 border were used to amplify the cDNA. The *RhoH* gene expression was quantified with Gene Expression Analysis Program for iCycler iQ Real-Time-PCR Detection System (Bio-Rad). *GAPDH* was used as a reference gene to normalize the *RhoH* gene expression and the *RhoH* expression level in DP cells was set to 1. cDNA generated from keratinocytes was used as a negative control. Real-time-PCR was performed in triplicates.

3.7   Cell culture

3.7.1   Cell lines

OP9 (Kodama et al., 1994; kindly provided by Juan Carlos Zuniga-Pflücker): Adherent murine stromal cell line derived from BM of *OP/OP* mice, which are deficient in macrophage colony-stimulating factor. OP9 cells support B cell development from HSCs *in vitro*.

OP9-DL1 (Schmitt and Zuniga-Pflücker, 2002; kindly provided by Juan Carlos Zuniga-Pflücker): Adherent cell line derived from OP9 cells retrovirally transduced to express the Notch ligand delta-like 1 (DL1), which can support T cell differentiation from HSCs *in vitro*.

293 (ATCC): Adherent epithelial cell line derived from human embryonic kidney.

Jurkat TAg (Northrop et al., 1993; kindly provided by Dr. Anders Woetmann, Copenhagen, Denmark): Derivate of Jurkat cell line (Gillis and Watson, 1980) stably transfected with SV40 large T antigen. Jurkat cells in suspension originated from human T cell leukemia.

3.7.2 Culture conditions

OP9-DL1 cells were maintained in α-minimal essential medium (α-MEM, GlutaMAX^{TM} I, Ribonucleosides and Desoxyribonucleosides; Invitrogen) containing 20% heat inactivated foetal calf serum (FCS; Invitrogen), 100 U/ml penicillin G (Invitrogen) and 100 µg/ml streptomycin sulfate (Invitrogen).

293 cells were cultured in Dulbecco's modified Eagle medium (DMEM, GlutaMAX^{TM} I, 4500 mg/L D-Glucose, Sodium Pyruvate; Invitrogen) supplemented with 10% FCS, 100 U/ml penicillin G and 100 µg/ml streptomycin sulfate.

Jurkat TAg cells were grown in RPMI 1640 medium supplemented with 10% FCS, 2 mM L-Glutamine (Invitrogen), 100 U/ml penicillin G and 100 µg/ml streptomycin sulfate.

All cells were cultured in a tissue incubator at 37°C and 5% CO_2.

3.7.3 Passaging of cells

Jurkat TAg cells in suspension were propagated in 25 or 75 cm^2 tissue culture flasks. For subculturing, the cells were diluted with fresh medium.

Adherent cell lines 293, OP9 and OP9-DL1 were grown in 25 or 75 cm^2 tissue culture flasks or 10 cm tissue culture plates. Subculturing was done by trypsinization: the cells were washed with phosphate-buffered-saline (PBS) and incubated with 1x trypsin solution (0.05% trypsin, 0.02% EDTA, prepared from 10x solution; Invitrogen) for 5 min at 37°C. The trypsin activity was stopped by adding pre-warmed growth medium, containing FCS, and the detached cells were centrifuged for 5 min at 1200 rpm, RT. The cell pellet was resuspended in growth medium and the appropriate volume of cells was transferred to a new culture dish.

The OP9 and OP9-DL1 cells, usually cultured on 10 cm dishes, were split every 2-3 days 1:4 or 1:5 when they were 80-90% confluent. If the cells were not split, then the medium was changed.

3.7.4 Freezing of cells

For freezing, cells were pelleted and resuspended in a pre-cooled freezing medium [90% growth medium and 10% (v/v) dimethyl-sulfoxide (DMSO; Sigma)]. Cells aliquoted into 1.5 ml cryo-vials (Corning) were immediately placed on dry-ice and then transferred to -80°C. For longer storage, frozen cells were kept in a liquid nitrogen tank. OP9 and OP9-DL1 cells were frozen in 90% FCS and 10% DMSO.

3.7.5 Thawing of cells

Thawing of cells was carried out by placing the frozen cryo-vial into a 37°C water bath. The thawed cells were then transferred into a falcon tube with 10 ml pre-warmed growth medium, centrifuged at 1200 rpm for 5 min, RT to remove DMSO, resuspended in growth medium and seeded on culture dishes.

3.7.6 Transfection

3.7.6.1 Calcium phosphate transfection

293 cells were transfected using the calcium precipitation method. $2x10^6$ 293 cells were seeded in a well of a 6-well plate the day before the transfection. Next day, 2 μg DNA in 80 μl TE were mixed with 20 μl 1 M $CaCl_2$ and 100 μl 2x HBS (HEPES buffered saline: 16.4 g NaCl, 11.9 g HEPES, 0.21 g Na_2HPO_4, filled up with ddH_2O to 1 l and pH adjusted to 7.05 with NaOH, filtered, aliquoted and stored at -20°C) were added drop wise. The sample was gently mixed and incubated for 5 min at 37°C. The DNA-Ca-phosphate-mixture was added drop wise to the cells in a 6-well plate. The cells were incubated at 37°C, 5% CO_2. 8 h later the medium was changed. 48 h after the transfection, the 293 cells were used for assays.

3.7.6.2 DMRIE-C transfection

DMRIE-C reagent (Invitrogen) which is 1:1 liposome formulation of the cationic lipid DMRIE (1,2-dimyristyloxypropyl-3-dimethyl-hydroxy ethyl ammonium bromide) and cholesterol in membrane-filtered water was used to transfect Jurkat cells. The procedure was carried out according to the manufacturer's protocol. Briefly, Jurkat cells were split to $2x10^5$ cells/ml the day before the transfection. Next day, 0.5 ml 1640 RPMI medium without FCS were mixed with 4 μl DMRIE-C reagent in a well of a 6-well plate and 0.5 ml 1640 RPMI medium without FCS containing 4 μg DNA were added and mixed by swirling. The sample was incubated for 30 min at RT to allow the formation of DNA-lipid-complexes. During this incubation step $2x10^6$ cells were washed 3x with 50 ml 1640 RPMI medium without FCS to remove the FCS since the serum inhibits the interaction of the lipid with DNA. The centrifugation between the washing steps was carried out for 5 min, 1200 rpm, RT. The Jurkat cells were resuspended in 0.2 ml 1640 RPMI medium without FCS, added to the well with DMRIE-C and DNA and mixed gently. After incubation for 4.5-5 h at 37°C, 5% CO_2, 2 ml of 1640 RPMI medium containing 10% FCS were added to the cells. 48 h later the cells were used for assays.

3.8 Histological methods

3.8.1 Embedding for cryosections and cutting of tissue

For embedding, a part of a spleen was transferred into a plastic container (tissue teks, Sakura) filled with O.C.T.^{TM} (Sakura) embedding medium with the section side towards the bottom of the container. The latter was placed on copper plate on dry ice and after freezing stored at -80°C.

The tissue was cut in 8 µm slices at -20°C with cryostate (Microm) and transferred to positively charged glass microscope slides (SuperFrostPlus, Menzel-Gläser), air-dried for 30 min, RT and stored at -80°C.

3.9 Immunological and cell biological methods

3.9.1 Flow cytometry

3.9.1.1 FACS of surface antigens

Single cell suspensions were prepared by gentle disaggregation of the dissected organs (spleen, thymus and lymph nodes) through 70 µm cell strainers (BD) in a petri dish with 10 ml PBS. Cells were then transferred into a 50 ml Falcon tube and the petri dish was rinsed with 10 ml PBS. BM was flushed out of the femuri using 10 ml syringes and 23G x 1¼″ needle (Terumo neolus). After subsequent centrifugation for 5 min, 1300 rpm at 4°C the cells from spleen, thymus and BM were resuspended in 10 ml FACS-buffer (1% BSA in PBS), LN cells were resuspended in 2 ml FACS-buffer and counted in a hemacytometer (Hausser Scientific). For phenotypic analysis, 1×10^6 cells from BM, spleen, thymus and lymph nodes were incubated in a round-bottomed 96-well plate with primary antibodies diluted 1:200 in 50 µl FACS-buffer for 30 min at 4°C in the dark. The following primary antibodies conjugated to fluorescein (FITC), phycoerythrin (PE), allophycocyanin or biotin (all BD unless otherwise specified) were used: rat anti-B220 (RA3-6B2), rat anti-IgM (R6-60.2), rat anti-IgD (11-26c.2a), rat anti-Gr-1 (RB6-8C5), rat anti-Mac1 (CD11b; α_M, M1-70), rat anti-Ter119, mouse anti-NK1.1 (PK136), rat anti-CD4 (H129.19), rat anti-CD8 (53-6.7), rat anti-CD5 (53-7.3), hamster anti-TCRβ (H57-597), hamster anti-TCRγδ (GL3), hamster anti-CD69 (H1.2F3), rat anti-Vα2 (B20.1), rat anti-CD62L (MEL-14). After a washing step with 200 µl FACS-buffer, cells were centrifuged for 5 min, 1300 rpm at 4°C and incubated with secondary antibodies in 50 µl FACS-buffer for 15 min at 4°C in the dark. Biotinylated antibodies were detected by streptavidin Cy-5 or streptavidin-PE (Jackson Immunoresearch, 1:500 dilution). Afterwards, cells were washed again with 200 µl FACS-buffer and centrifuged for 5 min, 1300 rpm at

4°C. Finally cells were resuspended in 200 µl FACS-buffer, transferred into FACS tubes (Alpha Laboratories Ltd.) and analyzed on a FACSCalibur (BD) with CellQuest software (BD). Dead cells were excluded by forward-scatter (FSC) and side-scatter (SSC) profiles and by counterstaining with 1 µg/ml propidium iodide added just prior the measurement. Erythrocytes and debris were excluded by FSC/SSC gating.

For the characterization of DN thymocytes, 5×10^6 cells were stained with primary biotinylated antibodies for B220, CD4, CD8, NK1.1, Mac1, Gr-1, Ter119 and CD25-FITC or allophycocyanin (7D4) and CD44-PE (IM7) diluted 1:100 in 100 µl FACS-buffer. Subsequently, biotinylated antibodies were detected by streptavidin-Cy-Chrom diluted 1:100 in 100 µl FACS-buffer. For the analysis of DN1, DN2, DN3 and DN4 cells thymocytes were gated for lineage negative B220, CD4, CD8, NK1.1, Mac1, Gr-1, Ter119 cells and plotted in a diagram for CD25 versus CD44.

In all dot plot analyses the percentage of cells in the respective quadrant is indicated. The cells in the lower left quadrant show no staining significantly distinct from the autofluorescence of these cells.

3.9.1.2   FACS analysis of proliferation

For proliferation assays mice were given an intraperitoneal injection of 1 mg of BrdU (BD) (100 µl of 10 mg/ml BrdU-solution) and killed 2 h later. In this method, BrdU (an analogon of DNA precursor thymidine is incorporated into newly synthesized DNA by cells entering and progressing through the S phase (DNA synthesis) of the cell cycle. BrdU incorporation of thymocytes was determined using the BrdU Flow kit containing the specific anti-BrdU antibody labeled with FITC (BD). The levels of cell-associated BrdU were then measured by flow cytometry. Staining for CD4 and CD8 antigens or cells surface markers of DN cells allowed for distinguishing BrdU-incorporated cells within thymocyte subpopulations (s. 3.9.1.1). BrdU staining was carried out according to BrdU Flow kit protocol.

3.9.1.3   FACS analysis of apoptosis

AnnexinV which binds specifically to phosphatidylserine (PS) in the presence of calcium was used for the detection of apoptosis. Apoptosis is characterized by the loss of membrane asymmetry. In healthy cells PS is located on inner leaflet of the cell membrane, whereas in apoptotic cells PS is found mainly on the outer leaflet of the membrane. Hence, apoptotic events can be detected by binding of AnnexinV-Alexa488 to the exposed PS. Staining for CD4 and CD8 antigens or cell surface markers of DN cells allowed for distinguishing of apoptotic cells within thymocyte subpopulations.

Cells were stained with antibodies specific for cell-surface markers as described in 3.9.1.1. After the last washing step the thymocytes were resuspended in 100 µl binding buffer (10 mM Hepes pH 7.4, 140 mM NaCl, 2.5 mM $CaCl_2$) and 5 µl AnnexinV-Alexa488 (final dilution 1:1000; kindly provided by Dr. Ernst Pöschl, Erlangen, Germany) were added. Following the incubation for 15 min at RT in the dark, 200 µl of binding buffer were added and the samples were analyzed in flow cytometry within one hour. Since AnnexinV can pass through the membrane of nectrotic cells, a counterstain with 1 µg/ml propidium iodide just prior the measurement was carried out to discriminate between apoptotic and nectrotic events.

3.9.1.4   Intracellular FACS

$5x10^6$ fresh isolated thymocytes were incubated in eppendorf tubes with 5 µg/ml biotinylated anti-CD3ε (145-2C11) and anti-CD4 antibodies or anti-CD3ε antibody alone in 50 µl PBS for 30 min at 4°C and washed with 300 µl cold PBS. Subsequently, cells were centrifuged for 5 min, 300xrcf, 4°C. Crosslinking of the bound antibodies was carried out by addition of 37°C pre-warmed 5-10 µg/ml streptavidin (Sigma) in 50 µl PBS and incubation of the samples for 5 min at 37°C resulting in TCR signaling induction. After stimulation, cells were directly fixed in an equal volume of 37°C pre-warmed 4% paraformaldehyde (PFA) in PBS for 10 min at 37°C. The PFA was added while vortexing the sample to avoid clumping of the cells. Thymocytes were then washed twice with cold 300 µl PBS and centrifuged for 5 min, 300xrcf, 4°C. Next, cells were resuspended by drops while vortexing in 200 µl ice-cold 90% methanol and permeabilized for 30 min on ice. Afterwards, thymocytes were pelleted by centrifugation for 5 min 300xrcf, 4°C, washed twice with 200 µl cold PBS and centrifuged for 5 min, 300xrcf, 4°C. Finally, the cells were stained with fluorescently labeled anti-CD4, anti-CD8 and anti-phospho-ZAP70 (Y319)/Syk(Y352) or anti-phospho-Lck (Y505) or anti-phospho-Erk1/2 (T202/Y204) or anti-phospho-p38 MAPK (T180/Y182) for 1 h at RT and washed with 200 µl FACS buffer (phospho-antibodies were purchased from BD). After centrifugation step for 5 min, 300xrcf, 4°C thymocytes were resuspended in 200 µl FACS buffer and analyzed by FACS.

3.9.1.5   Calcium influx

For measurement of influx calcium, $40x10^6$ thymocytes or splenocytes in 2 ml PBS were loaded with 2.5 µM Fluo-4 acetoxymethyl ester dye (F14201, Molecular Probes/ Invitrogen) for 25 min at 37°C in a water bath in dark. For this purpose, 9 µl DMSO were added to a vial containing 50 µg Fluo-4, mixed, and 1 to 2 µl aliquots were stored at -20°C. Aliquots were diluted with an equal volume of 20% Pluronic, and 2 µl of this mixture were used for loading

of cells. Fluo-4 exhibits a fluorescence intensity increase on binding Ca^{2+}. It is an analogon of Fluo-3 with the two chlorine substitutes replaced by fluorines which result in increased fluorescence excitation at 488 nm. The acetoxymethyl ester modification allows the dye to permeate cell membrane. Once inside the cell the acetoxymethyl ester group is cleaved by non-specific esterases, resulting in a charged form that leaks out of the cell far more slowly than its parent compound. Addition of the non-ionic detergent pluronic facilitates the dispersion of the nonpolar acetoxymethyl ester in aqueous media.

Subsequently, 10 ml cold RPMI 1640 (Gibco; without phenol red and with 25 mM HEPES) were added to loaded cells and the cells were centrifuged for 10 min, at 1200 rpm, 4°C. Pelleted cells were washed again with 10 ml cold RPMI 1640 and centrifuged for 10 min, at 1200 rpm, 4°C. Cells were resuspended in 800 µl cold RPMI 1640 to a concentration of $5x10^7$ cells/ml and 100 µl ($5x10^6$ cells) per well were transferred into 96-well round bottom plate. After centrifugation for 5 min, 1200 rpm, 4°C cells were stained with anti-CD8α-allophycocyanin (53-6.7) (eBiosciences; 1:100 dilution), anti-CD4-PE-Cy5.5 (RM4-5) (Caltag; 1:100 dilution) and 5 µg/ml biotinylated anti-CD3ε or 5 µg/ml biotinylated anti-CD4 or a combination of both in 50 µl RPMI 1640 for 30 min at 4°C. Afterwards, cells were washed with 200 µl cold RPMI 1640 and centrifuged for 5 min, 1200 rpm, 4°C. Eventually, cells were resuspended in cold RPMI 1640 to a concentration of $5x10^6$ cells/ml and transferred to FACS tubes (BD). Cells were warmed to 37°C and analyzed for 20 sec to establish baseline calcium levels. Then CD3ε was crosslinked by the addition of 10 µg/ml streptavidin and calcium influx was measured at 37°C in FL1 channel for 2.5 min (During the measurement the tube containing the sample was placed in glass with 37°C warmed water). The flow cytometric analysis was performed with FACSCalibur using FlowJo (TreeStar).

3.9.2   MACS separation and FACSAria/Vantage sorting

Single cell suspensions from wild type spleen, thymus and BM were prepared as mentioned in 3.9.1.1.

$5x10^7$ splenocytes were stained with 5 µl B220-biot, CD4-biot or CD8-biot in 500 µl MACS-buffer (2 mM EDTA in PBS); $3x10^7$ BM cells were stained with 3 µl Gr-1-biot in 300 µl MACS-buffer and incubated for 30 min at 4°C. Splenocytes and BM cells were washed with 5 ml or 3 ml MACS-buffer, respectively, and centrifuged for 10 min, 1300 rpm, 4°C. Magnetic sorting was carried out with microbeads according to the manufacturer's instructions (Miltenyi biotec). Briefly, splenocytes and BM cells were resuspended in 450 µl or 270 µl MACS-bufffer and 50 µl or 30 µl streptavidin microbeads were added, respectively.

After 15 min incubation at 4°C the splenocytes and BM cells were washed with 5 ml or 3 ml MACS-buffer, respectively, and centrifuged for 10 min, 1300 rpm, 4°C. After resuspending cells in 500 µl MACS-buffer, cells were applied to a MiniMACS separation column attached to the MiniMACS separation unit (magnet) equilibrated with 500 µl MACS-buffer and placed at the MACS Multistand. A 10 µl aliquot of stained cells was saved for later FACS analysis (Fraction A). The column was washed three times with 500 µl buffer to remove all unlabeled cells. Negative fraction and washing fractions were collected and a 100 µl aliquot for later FACS analysis was saved (Fraction B). Then the MACS column was removed from the magnet and placed on a collection tube. To elute all cells, 1 ml MACS-buffer was applied to the column and firmly flushed out using the plunger supplied with the column. 20 µl aliquot of the positive fraction was saved for later FACS analysis (Fraction C). The purity of MACS separated splenocytes was determined by staining the fraction A and C with streptavidin-Cy5, and fraction B with anti-CD4-FITC, anti-CD8-FITC or anti-B220-FITC and subsequent analysis with flow cytometry. The purity of MACS separated BM cells was determined by staining the fraction A and C with streptavidin-Cy5, and fraction B with anti-Gr-1-FITC followed by analysis with flow cytometry.

For the isolation of DN cells, $2x10^9$ thymocytes were stained with 25 µl CD4-biot, CD8-biot, 5 µl B220-biot, Ter119-biot, Gr-1-biot, and Mac1-biot in 1.5 ml MACS-buffer for 30 min at 4°C. Cells were washed with 10 ml MACS-buffer and centrifuged for 10 min, 1300 rpm, 4°C. Subsequently, thymocytes were resuspended in 2 ml MACS-buffer and 400 µl streptavidin microbeads were added, mixed and incubated for 15 min at 4°C. After washing with 10 ml MACS-buffer and centrifugation for 10 min, 1300 rpm, 4°C, cells were resuspended in 2 ml MACS-buffer (10 µl fraction was saved for later FACS analysis, Fraction A) and applied on LS column equilibrated with 5 ml MACS-buffer. The column was washed with 3x 5 ml MACS-buffer and the negative and washing fractions were collected and 100 µl aliquot was saved for later FACS analysis (Fraction B). The cells were eluted with 5 ml of MACS and 20 µl aliquot was saved for later FACS analysis (Fraction C). Fraction A, B and C were stained with streptavidin-Cy5 and analyzed with flow cytometry. Negative fraction was centrifuged for 5 min, 1300 rpm, 4°C and the DN thymocytes were incubated with 10 µl CD25-FITC, CD44-PE and streptavidin-CyChr in 500 µl FACS-buffer for 30 min at 4°C. Next, cells were washed with 10 ml FACS-buffer und resuspended in 4 ml FACS-buffer. Finally, cells were sorted for DN1, DN2, DN3 and DN4 with FACSAria.

For the isolation of DP and SP cells, $3x10^9$ wild type thymocytes were stained with 30 µl anti-CD4-PE and anti-CD8-FITC in 1 ml FACS-buffer for 30 min at 4°C. After washing with 10

ml FACS-buffer and centrifugation for 5 min, 1300 rpm, 4°C, the cells were resuspended in 8 ml FACS-buffer and sorted by FACSAria (BD).

For TCR signaling $3x10^9$ wild type and RhoH-deficient thymocytes were stained with 30 µl anti-CD4-PE and anti-CD8-FITC in 1 ml RPMI 1640 medium, 2 mM EDTA, 0.5% BSA for 30 min at 4°C. After washing step with 10 ml RPMI 1640 medium, 2 mM EDTA, 0.5% BSA and centrifugation for 5 min, 1300 rpm, 4°C, cells were resuspended in 8 ml RPMI 1640 medium, 2 mM EDTA, 0.5% BSA and by sorted by FACSAVantage (BD).

3.9.3   T cell development *in vitro*

In vitro T cell development on OP9-DL1 stromal cells was carried out as described previously (Schmitt and Zuniga-Pflücker, 2002). Control and RhoH-deficient DN thymocytes enriched via MACS (s. 3.9.2) were sorted for DN3 and DN4 populations with FACSAria. For co-cultures, OP9-DL1 cells from one 10 cm dish were seeded in two or three 24-well plates 1-2 days before. $5x10^4$ DN3 and $2.5x10^4$ DN4 thymocytes were plated on a subconfluent OP9-DL1 monolayer in a 24-well plate and cultured in the presence of 5 ng/ml Flt3 ligand (Peprotech) and 1 ng/ml IL-7 (Peprotech), which support early lymphogenesis, for 8 days. The medium with cytokines was replaced after 4 days. Developmental progression of cultured cells was assessed by flow cytometry after 4 and 8 days. Cells were harvested by forceful pipetting, filtered through a 70 µM cell strainer to remove OP9-DL1 cells and counted with hemacytometer.

3.9.4   Immunofluorescence staining on cryosections

Prior to staining, the section slides were warmed for 1 h at RT. The specimen were surrounded with a Pap-pen and fixed for 20 min with 4% PFA in PBS in a metal humid box. After washing 3x with PBS in a glass slide container, 5 min each, the sections were blocked with 1% BSA in PBS for 30 min at RT in a metal humid box. Next, the sections were incubated with 50 µl fluorescently labeled and/ or biotinylated antibodies in 1% BSA in PBS for 1.5 h, RT in a metal humid box, dark. The sections were washed 3x with PBS, 5 min, in a glass slide container, dark. If a biotinylated antibody was used, the sections were incubated with 50 µl streptavidin-Cy5 in 1% BSA in PBS for 1 h, RT, in a metal humid box, dark. In the last 5 min of the antibody incubation, 50 µl of 4,6-diamidino-2-phenylindole (DAPI, Sigma), diluted 1:10000 in PBS were added to the sections and incubated for 5 min. Following washing 3x with PBS, 5 min, the slides were carefully dried around the specimen, mounted in

elvanol and covered with glass coverslips. The slides were air-dried and stored in a box at -20°C.

Following antibodies were used in 1:100 dilution: rat anti-B220-FITC (RA3-6B2) and rat anti-Thy1.2-biot. (30-H12). Streptavidin-Cy5 was used in 1:200 dilution.

3.9.5   Immune response

In order to determine the functionality of RhoH-deficient T cells *in vivo*, antibody titer in sera of mice immunized with a T cell dependent antigen was analyzed.

Nitrophenyl-chicken-γ-globulin (NP$_{20}$-CG; kindly provided by Dr. Ari Waisman, Köln, Germany), was diluted to 1 mg/ml with PBS, and an equal volume of Alum Imject (PIERCE) was added. After incubation for 30 min at RT with vortexing every 3 min, 100 µg Alum-precipitated NP$_{20}$-CG (200 µl NP$_{20}$-CG-Alum-emulsion) were intraperitoneally injected into 2 month old control and RhoH-deficient mice on day 0. The groups of control and mutant mice consisted of 5-6 animals. 50 µl blood was taken from the eye using the 50 µl capillary (Blaubrand®) before the immunization (day 0) and on day 7, 14, 21, 28, and 42 after immunization. For memory response, mice were immunized with 10 µg soluble NP$_{20}$-CG in PBS on day 42, and blood was collected on the day 49, 56, 63, and 70.

Sera were prepared by incubating the blood samples for 2-3 h at RT and centrifugation for 15 min, 14000 rpm, 4°C. The supernatant (serum) was transferred into new tubes and stored at –20°C. The anti-NP$_{20}$-CG specific titers for IgM, IgG1, IgG2a, IgG3, Igκ and Igλ were determined by means of ELISA carried out with Claudia Utthoff-Hachenberg in the laboratory of Dr. Ari Waisman, Köln, Germany. Briefly, round bottom 96-well microtiter plates were coated with 50 µl 10 µg/ml NP$_{14}$-BSA in PBS at 4°C o/n in a box covered with moisted towel preventing the plates from drying out. Next day the antigen coating solution was removed and the plates were washed 3x with 200 µl tap water or PBS. The plates were incubated for 5 min at RT between the washing steps. The solution in wells was removed by flicking the plate over a sink. The remaining drops were removed by patting the plate on a paper towel. The unspecific binding sites of the antigen were blocked by adding 200 µl PBS/0.5% BSA/0.01% NaN$_3$ into the wells and incubating the plates for 30 min at RT. Sera and standard primary NP-specific antibody dilutions of IgM, IgG1, IgG2a, IgG3, Igκ and Igλ (10 µg/ml, in PBS/0.5% BSA/0.01% NaN$_3$) were diluted in 1:8 steps (1:50 as starting dilution, 1:400, 1:3200, 1:25600, 1:204800, 1:1638400) in 96-well plate. In the first and 7th column 245 µl were added, and 210 µl PBS/0.5% BSA/0.01% NaN$_3$ in the remaining wells of the plate. In the first (B-H) and 7th (B-H) row 5 µl of 14 different sera samples and in A7 5 µl

of standard primary NP-specific antibody were added and mixed. 30 µl diluted sera from the first row were transferred into 2nd row (dilution 1:400), mixed, and again 30 µl were transferred into 3rd row (1:3200 diution), mixed and so forth till the 6th row. The same dilution scheme was conducted with the sera in the 7th row and with the standard primary NP-specific antibody starting from A7 (s. dilution scheme below). Row A1-6 was only filled with PBS/0.5% BSA/0.01% NaN_3 (blank row). 30 µl solution from 6th and 12th column were discarded. After incubation for 1 h at 37°C, the sera and antibody dilutions were removed and the plates washed 3x with 200 µl tap water or PBS.

50 µl of biotinylated antibody against IgM, IgG1, IgG2a, IgG3, Igκ or Igλ (1:500 dilution in PBS/0.5% BSA/0.01% NaN_3) were added to the wells and the plates were incubated o/n at 4°C in moisture boxes.

Next day, the antibody solution was removed and the plates were washed 3x with 200 µl tap water or PBS. 50 µl of streptavidin conjugated alkaline phosphatase (1:3000 dilution in PBS/0.5% BSA/0.01% NaN_3; Boehringer) were added and the plates were incubated for 1 h in moisted chamber. Subsequently, the solution was removed and the plates were washed 3x with 200 µl tap water or PBS.

Then 50 µl of the 0.4 mg/ml substrate p-Nitrophenyl phosphate in the substrate buffer (1 M diethanolamine, 0.5 mM $MgCl_2$, pH 9.8) were added and the plates were incubated for 0.5-1 h at RT in the moisted chamber. The absorbance was measured with microtiter plate spectrometer at 405 nm and with the reference filter at 570 nm.

Dilution scheme

	1	2	3	4	5	6	7	8	9	10	11	12
A	blank	blank	blank	blank	blank	blank	standard					
B	sera 1						sera 8					
C	sera 2						sera 9					
D	sera 3						sera 10					
E	sera 4						sera 11					
F	sera 5						sera 12					
G	sera 6						sera 13					
H	sera 7						sera 14					
	245 µl buffer + 5 µl sera	210 µl buffer	210 µl buffer	210 µl buffer	210 µl buffer	210 µl buffer	245 µl buffer + 5 µl sera	210 µl buffer	210 µl buffer	210 µl buffer	210 µl buffer	210 µl buffer
	1:50	1:400	1:3200	1:25600	1:1638400	1:13107200	1:50	1:400	1:3200	1:25600	1:1638400	1:13107200

3.10   Adhesion assays

3.10.1   Adhesion assays to ICAM-1 and VCAM-1

In order to determine the binding of RhoH-deficient thymocytes to ICAM-1, adhesion assays were performed in collaboration with Dr. Melanie Laschinger, Dr. Monika Semmrich, and Dr. Bernhard Holzmann, Klinikum rechts der Isar, Munich, Germany.

96-well polystyrene flat bottom plates were coated with purified ICAM-1(D1-2)-Fc (1.5 µg/well), VCAM-1-Fc (0.8 µg/well) or Fcγ1 fragments (1.0 µg/well) in PBS o/n at 4°C. Next day, liquid in wells was removed by inverting the plates. Next, the plates were washed with 100 µl HBSS (Sigma). Subsequently, the plates were blocked with 1% BSA in HBSS for 1 h at 37°C. Thymocytes were isolated and labeled for 30 min at 37°C in a water bath with 4 µl 6 µg/ml H33342 dye (Calbiochem) in 2 ml HBSS. Following the DNA labeling, the cells were centrifuged for 5 min, 1500 rpm, RT and resuspended in 5 ml HBSS. Again, the thymocytes were centrifuged for 5 min, 1500 rpm, RT and resuspended in 5 ml HBSS. After counting with trypan blue, the cells were centrifuged for 5 min, 1500 rpm, RT and resuspended in HBSS to a density of 2.5×10^6 cells/ml in HBSS containing 5 mM Mg^{2+} or 2 mM Mn^{2+}. PMA (Sigma) stimulation was carried out for 30 min at 37°C with 100 ng/m. Subsequently, cells were washed to remove PMA. Alternatively, cells were resuspended in HBSS and preincubated with 2 mM EDTA, 5 mM Mg^{2+}, 1 mM Mn^{2+}, 20 ng/ml PMA, or a combination of both for 10 min at 37°C and then plated on ICAM-1 and VCAM-1. 100 µl of stimulated cells (2.5×10^5 cells) were distributed in triplicates into wells of the coated plate and gently centrifuged for 10 min, 10xg ~300 rpm, RT. Cells were allowed to adhere for 30 min at 37°C and the fluorescence of cells labeled with H33342 was measured at 360/490 nm to determine the total cell number. The plates were drowned in PBS and sealed with plastic foil (Peske). Eventually, non-adherent cells were removed by inverse centrifugation for 10 min at 50xg and the plastic foil was detached. The PBS in the wells was carefully removed by inverting the plates on tissue paper and residual liquid was sucked off. The wells were filled with 100 µl HBSS and fluorescence was measured again at 360/490 nm to determine the number of adherent cells. As control for binding, adhesion of β1-integrin to VCAM-1 was performed. Relative adhesion was calculated as follows: fluorescence of adherent cells/fluorescence of total cells, and average of triplicates was built. For all experiments, non-specific adhesion to Fcγ1 fragments was subtracted from adhesion to ICAM-1(D1-2)-Fc or VCAM-1-Fc to calculate the fraction of cells adhering specifically to integrin ligands.

3.10.2   Adhesion assays to bEnd.5 and bEndI1.1 endothelial cells

Adhesion assays with bEnd.5 and bEndI1.1 endothelial cells were performed using 16-well glass chamber slides (Nunc) [performed by Dr. Melanie Laschinger]. The endothelioma cell lines bEnd5 and bEndI1.1 (Reiss et al., 1998) were kindly provided by Britta Engelhardt (Bern, Switzerland).

Chamber slides were coated with 2.5 µg/well fibronectin (Roche) and cultured with $2x10^4$ endothelial cells per well for 2 days. Depending on the experiment, endothelial cells were incubated with 20 ng/ml TNF per well for the last 16 h of culture. To stimulate T cell adhesion, splenic cells were activated with 2.5 µg/ml Concanavalin A (Sigma) for 16 h and isolated on a Nycoprep gradient (Nycoprep 1.077A, Progen). After removal of the cytokine, endothelial cells were coincubated with $1x10^5$ Concanavalin A-activated T cells in 100 µl adhesion medium (DMEM containing 5% FCS and 25 mM Hepes) for 30 min on a rocking platform. Assays were washed twice in PBS and fixed in 2.5% glutaraldehyde in PBS at 4°C for 2 h. Bound cells per pre-defined field were determined by counting three fields per well. FD441.8 (Biosource) and PS/2 (from hybridoma) antibodies were used to block αL-integrin and α4-integrin, respectively. Mouse IgG2b (BD) was used as a control antibody. Tests were performed in triplicates for each value.

3.11   Biochemical methods

3.11.1   Protein extraction

Protein extracts were prepared by lysing cells in a lysis buffer (s. 3.11.6.1, 3.11.7, 3.11.8.1, 3.11.8.2, 3.11.9, 3.11.10, 3.11.11) on ice for 20 min and centrifugation for 15 min at 14000 rpm, 4°C.

3.11.2   Determination of protein concentration

The protein concentration in cell extracts was determined using the BCA^{TM} Protein Assay Kit (Pierce) based on a colorimetric detection of protein. This method combines the reduction of Cu^{+2} to Cu^{+1} by protein in alkaline medium (biuret reaction) with the detection of Cu^{+1} by bicinchoninic acid (BCA) forming a water-soluble purple-coloured complex with a strong absorbance at 562 nm. The absorbance is nearly linear with increasing protein concentrations over a broad working range (20-2000 µg/ml).

Briefly, the protein standards of known concentrations were prepared by serially diluting the 2 mg/ml BSA stock (2; 1; 0.5; 0.25; 0.125; 0.065; 0.0325; 0 mg/ml) in lysis buffer (s. 3.11.6.1, 3.11.7, 3.11.8.1, 3.11.8.2, 3.11.9, 3.11.10, 3.11.11). 5 µl of protein standards and protein

extracts were transferred in triplicates into flat bottom 96-well plate and 200 µl of a mixture of 1:50 diluted solution B to A were added. After incubation of the plate for 30 min at 37°C, the absorbance was measured at 562 nm with ELISA reader (Dynatech) and the protein concentration was calculated according to the protein standard reference curve.

3.11.3   SDS electrophoresis

Protein extracts were denatured with 4x sample buffer (200 mM Tris-HCl pH 6.8, 4 mM EDTA, 40% glycerol, 4% β-mercaptoethanol, 0.1 mg/ml bromphenol blue) for 5 min at 95°C and separated on 1.5 mm 10-12% or 5-15% gradient SDS-PAGE in 1x running buffer (10x running buffer: 30.3 g Tris, 144 g glycine, 10 g SDS filled up to 1 l with ddH$_2$O; diluted 1:10) using Mini Protein II System (BioRad) at 120-150 V for 1-1.5 h in the presence of the protein molecular weight marker (Broad range BioRad®) to estimate the protein sizes. The SDS-PAGE gels consisted of two different polyacrylamide gels: the lower resolving gel (10 or 12% or 5-15%) and the upper stacking gel (5 or 4%). Separated proteins were either visualized by non-specific binding of Coomassie brilliant blue dye solution or transferred to PVDF membrane (s. 3.11.4). The gels were incubated for 1 h or o/n in the Coomassie brilliant blue solution (40% methanol, 10% acetic acid, 0.025% Coomassie brilliant blut R-250) with gentle agitation and destained with several changes in 10% acetic acid to remove the non-bound dye.

Resolving gel 10% and 12% (2 gel sizes; 20 ml)			**Stacking gel 5% (2 gel sizes; 8 ml)**	
	10%	**12%**		
ddH$_2$0	7.9 ml	6.6 ml	ddH$_2$0	5.5 ml
Tris-HCl pH 8.8	5 ml	5 ml	Tris-HCl pH 6.8	1 ml
30% Bisacrylamide	6.7 ml	8 ml	30% Bisacrylamide	1.3 ml
10% SDS	200 µl	200 µl	10% SDS	80 µl
10% APS	200 µl	200 µl	10% APS	80 µl
TEMED	8 µl	8 µl	TEMED	8 µl

For 5-15% gradient gel, 15 and 5% resolving gel solutions were mixed and poured.

Resolving gel 5% and 15% (2 gel sizes; 20 ml)			**Stacking gel 4% (2 gel sizes; 8 ml)**	
	5%	**15%**		
ddH$_2$0	11.3 ml	4.6 ml	ddH$_2$0	5.8 ml
Tris-HCl pH 8.8	5 ml	5 ml	Tris-HCl pH 6.8	1 ml
30% Bisacrylamide	3.3 ml	10 ml	30% Bisacrylamide	1 ml
10% SDS	200 µl	200 µl	10% SDS	80 µl
10% APS	200 µl	200 µl	10% APS	80 µl
TEMED	16 µl	8 µl	TEMED	8 µl

3.11.4   Western blotting

After SDS-PAGE the proteins were transferred onto a PVDF membrane (Immobilon–P, Millipore) using wet blotting system of Mini Trans-Blot cell, BioRad. A "sandwich" in a grid consisting of a sponge, Whatman paper, PVDF membrane, gel, Whatman paper and sponge, was placed in a chamber containing 1x blotting buffer (10x blotting buffer: 30.2 g Tris, 144 glycine filled up to 1 l with ddH$_2$O, diluted 1:10 by adding 20% MetOH) with the membrane facing the anode. Sponges, Whatman paper were pre-wetted in the blotting buffer and the PVDF membrane was first activated for 20 sec in MetOH and then equilibrated for 10 min in the blotting buffer. After the electrophoretic transfer for 1,5 h at 100 V, 4°C or o/n at 30 V, 4°C the membrane was rinsed in ddH$_2$0 and stained in Ponceau S Solution for 2 min to visualize the transferred proteins and the weight marker which was subsequently labeled with pen on the membrane. All following incubation steps were carried out on a shaker with gentle mixing. The membrane was washed 3x 5 min to remove Ponceau S and blocked for 1 h at RT or o/n at 4°C either in 3-5% skim milk/TBST or 3-5% BSA/TBST depending on the primary antibody. The membrane was incubated with the primary antibody o/n at 4°C (s. 3.11.5.1). Was the blocking solution different from the solution containing the primary antibody, a washing step of 3x 5min with TBST was integrated between the incubation of blocking and primary antibody solution. After primary antibody incubation the membrane was washed 3x 5 min with TBST and incubated with secondary antibody (s. 3.11.5.2) conjugated to horseradish peroxidase (HRP) in 5% skim milk/TBST for 1 h at RT. After that, again the membrane was washed 3x 5 min with TBST and the proteins were detected by ECL^{TM} Western blotting detection reagent (Perkin Elmer) by applying a mixture of equal volume of solution A and B onto the membrane and incubating it for 1 min at RT. The membrane was finally covered by plastic foil and exposed to a film (Kodak) which was subsequently developed in a developing machine. The films were scanned and the quantification analysis of densitometry was performed with the BioProfile software. The same membrane could be re-used for detection of several proteins with antibodies from the same species by stripping the previous antibody with stripping buffer (32.5 mM Tri-HCl pH 6.7, 2% SDS, 100 mM β-mercaptoethanol) for 30 min at 55°C with occasional agitation, washing the membrane with TBST 3x 10 min, blocking and incubating with the other primary antibody. If, however, the first and second primary antibodies were from different species, then the first antibody was removed by incubating the membrane in 15% H$_2$O$_2$ for 30 min at RT with gentle agitation, followed by washing with TBST 3x 10 min and probing with the second primary antibody.

3.11.5 Antibodies

3.11.5.1 Primary antibodies

antibody	species	source	dilution for WB	dilution for IP	blocking solution; blocking time	antibody solution; incubation time
PY-7E1	mouse	Zymed	1 µg/ml (1:500)		5% BSA/TBST; 4°C, o/n	5% BSA/TBST; 4°C, o/n
Vav1 (C-14)	rabbit	Santa Cruz	1:2500	1.2 µg	5% milk/TBST; RT, 1 h	5% milk/TBST; 4°C, o/n
Vav1 (D-7)	mouse	Santa Cruz	1:1000		5% milk/TBST; RT, 1 h	5% milk/TBST; 4°C, o/n
phospho-Vav2(Tyr172)-R	rabbit	Santa Cruz	1:1000		5% milk/TBST; RT, 1 h	5% milk/TBST; 4°C, o/n
Vav2 (H-200)	rabbit	Santa Cruz	1:1000		5% milk/TBST; RT, 1 h	5% milk/TBST; 4°C, o/n
phospho-Vav3(Tyr173)	rabbit	Biosource	1:1000		5% BSA/TBST; 4°C, o/n	3% BSA/TBST; RT, 2 h
Vav3 (K-19)	goat	Santa Cruz	1:1000		5% milk/TBST; RT, 1 h	5% milk/TBST; 4°C, o/n
phospho-ZAP70(Tyr319)	rabbit	Cell Signaling	1:1000		5% milk/TBST; RT, 1 h	5% BSA/TBST; 4°C, o/n
ZAP70 (99F2)	rabbit	Cell Signaling	1:1000		5% milk/TBST; RT, 1 h	5% BSA/TBST; 4°C, o/n
phospho-PLCγ1(Tyr783)	rabbit	Cell Signaling	1:1000		5% milk/TBST; RT, 1 h	5% BSA/TBST; 4°C, o/n
PLCγ1	rabbit	Cell Signaling	1:1000		5% milk/TBST; RT, 1 h	5% BSA/TBST; 4°C, o/n
LAT	rabbit	Upstate	1:1000	3 µg	3% milk/TBST; RT, 1 h	3% milk/TBST; 4°C, o/n
phospho-LAT(Tyr191)	rabbit	Cell Signaling	1:1000		5% milk/TBST; RT, 1 h	5% BSA/TBST; 4°C, o/n
LAT(11B.12)	mouse	Upstate	1:1000		5% milk/TBST; RT, 1 h	5% milk/TBST; RT, 2.5 h
phospho-p44/p42(T202/Tyr204)	rabbit	Cell Signaling	1:1000		5% milk/TBST; RT, 1 h	5% milk/TBST; 4°C, o/n
p44/p42	rabbit	Cell Signaling	1:1000		5% milk/TBST; RT, 1 h	5% milk/TBST; 4°C, o/n
phospho-p38(T180/Tyr182)	rabbit	Biosource	1:1000		5% BSA/TBST; 4°C, o/n	3% BSA/TBST; RT, 2 h
p38(SAPK2a/p38) (2F11)	rabbit	Biosource	1:1000		4.5% BSA/TBST; 4°C, o/n	1% % BSA/TBST; RT, 2 h
Rac1	mouse	BD Bioscience	1:1000		5% milk/TBST; RT, 1 h	5% milk/TBST; 4°C, o/n
Rac2	rabbit	Upstate	1:5000		5% milk/TBST; RT, 1 h	5% milk/TBST; 4°C, o/n
Myc (9E10)	mouse	Upstate	1:1000	4 µg	3% milk/TBST; RT, 1 h	3% milk/TBST; 4°C, o/n
cortactin	mouse	Upstate		4 µg		
Flag (F1804)	mouse	Sigma	1:1000		5% milk/TBST; RT, 1 h	3% milk/TBST; 4°C, o/n
tubulin	rat	J.Wehland, Braunschweig, Germany	1:10000		5% milk/TBST; RT, 1 h	5% milk/TBST; 4°C, o/n
RhoH (H00000399-A01)	mouse	Abnova	1:1000		5% milk/TBST; RT, 1 h	5% milk/TBST; 4°C, o/n
RhoH (N-20)	goat	Santa Cruz	1:1000		5% milk/TBST; RT, 1 h	5% milk/TBST; 4°C, o/n
myc	mouse	Upstate	1:1000	4 µg	3% milk/TBST; RT, 1 h	3% milk/TBST; RT, 1 h

3.11.5.2 Secondary antibodies

antibody	species	source	dilution	antibody solution; incubation time
anti-mouse-IgG(H+L)-HRP	donkey	Jackson Immunoresearch	1:10000	5% milk/TBST; RT, 1 h
anti-rabbit-IgG(H+L)-HRP	goat	Jackson Immunoresearch	1:10000	5% milk/TBST; RT, 1 h
anti-goat-IgG(H+L)-HRP	donkey	Jackson Immunoresearch	1:10000	5% milk/TBST; RT, 1 h
anti-rat-IgG(H+L)-HRP	donkey	Jackson Immunoresearch	1:10000	5% milk/TBST; RT, 1 h

3.11.6 TCR signaling

3.11.6.1 Stimulation of DP thymocytes

1×10^7 DP thymocytes were sorted by FACSVantage (BD) as described in 3.9.2 and incubated with 5 µg/ml biotinylated anti-CD3ε (145-2C11) and anti-CD4 in 50 µl PBS for 30 min at 4°C. Cells were washed with 200 µl cold PBS and centrifuged for 5 min, 300xrcf, 4°C. Crosslinking of the bound antibodies was carried out by addition of 50 µl 37°C pre-warmed 5 µg/ml streptavidin (Sigma) and incubation of the samples for 5 min at 37°C. After washing

step with 200 µl cold PBS and centrifugion for 5 min, 300xrcf, 4°C, thymocytes were lysed in 100 µl 50 mM Tris pH 7.4, 100 mM NaCl, 1% Nonidet P-40, 10% glycerol, 2 mM $MgCl_2$, 1 mM Na_3VO_4, 100 mM NaF containing a protease inhibitor cocktail (Complete Mini, EDTA free, Roche) for 20 min on ice. Next, lysates were cleared by centrifugation at 14000 rpm for 15 min at 4°C and the protein concentration was determined (s. 3.11.2).

3.11.6.2 Stimulation of Jurkat TAg cells

$4x10^6$ Jurkat TAg cells were resuspended in 500 µl 1640 RPMI medium and 1-3 µl 180 µg/ml anti-TCR F101.01 antibody (kindly provided by Dr. Carsten Geisler, Copenhagen, Denmark) were added. The samples were incubated for 5 min at 37°C and the stimulation was stopped by addition of 500 µl cold PBS and transferring the cells on ice. After the centrifugation for 5 min, 300xg, 4°C the supernatant was removed and cells lysed in 100 µl lysis buffer as described in 3.11.10 and 3.11.11. Next, lysates were cleared by centrifugation at 14000 rpm for 15 min at 4°C and the protein concentration was determined (s. 3.11.2).

3.11.7 Rac1 and Rac2 pulldown

For detection of active Rac1 $1x10^7$ DP thymocytes were stimulated as indicated in 3.11.6.1 by crosslinking of biotinylated CD3 and CD4 antibodies with streptavidin for 30 sec, 1 min or 5 min at 37°C. The cells were washed with 200 µl cold PBS, centrifuged for 5 min, 300xg, 4°C and lysed in 300 µl GST-fish lysis buffer [Tris-HCl pH 7.4, NaCl, 1% NP-40, 2 mM $MgCl_2$, 10% glycerol, supplemented with 1 mM Na_3VO_4, 100 mM NaF, protease inhibitor cocktail (Complete Mini, EDTA free, Roche)] containing 2 µl 2mg/ml biotinylated PAK-CRIB peptide for 20 min on ice. The lysates were centrifuged at 14000 rpm, 15 min, 4°C. 20 µl were denatured with 4x sample buffer at 95°C for later analysis of total Rac1 level. The streptavidin beads were washed 3x with 1 ml GST-fish lysis buffer and centrifuged for 30 sec, 6000 rpm, 4°C between the washing steps. The lysates were added to 30 µl strepavidin beads and rotated for 1 h at 4°C. After binding of biotinylated PAK-CRIB peptide to activated Rac1 and to streptavidin coated beads, the samples were centrifuged for 30 sec, 6000 rpm, 4°C and the supernatant was removed. Following three washing steps with 1 ml GST-fish lysis buffer and centrifugation steps for 30 sec, 6000 rpm, 4°C, the beads were resuspended in 40 µl 1x sample buffer and denatured at 95°C. The samples with total protein extract and active Rac1 were subsequently analyzed by SDS-PAGE and Western blotting. The membranes were probed with anti-Rac1 antibody and the level of active Rac1 was normalized to total level of Rac1.

3.11.8 GST-pulldown

3.11.8.1 Purification of RhoH-GST fusion protein and GST

BL21(DE3) *E. coli* bacteria transformed with RhoH-GST or GST were inoculated in 2 ml LB (containing ampicillin and chloramphenicol) and grown o/n at 37°C with vigorous shaking. Next morning, 100 ml LB (containing ampicillin and chloramphenicol) were inoculated with 2 ml o/n culture and grown for 2 h at 37°C until OD_{600} reached 0.5-0.6. The bacteria were cooled down for 15 min on ice and 100 μl 1 M IPTG (final concentration 1 mM) were added to bacteria to induce the protein production. The cells were grown for 6 h at 26°C or o/n at 18°C with shaking. For monitoring protein expression, small aliquot of bacteria suspensions were saved before IPTG induction and after protein production, centrifuged and resuspended in 4x sample buffer. After protein synthesis, the bacteria were centrifuged in 2x 50 ml tubes for 10 min at 4000 rpm, 4°C. The pellets were washed with 20 ml cold buffer A (50 mM Tris pH 7.4, 5 mM $MgCl_2$, 50 mM NaCl), combined in one tube and centrifuged for 10 min at 4000 rpm, 4°C. The supernatant was removed and the pellet frozen on dry ice / EtOH bath and stored at -80°C. Alternatively, the pellet was directly processed without freezing. Bacteria were resuspended in 5 ml cold buffer A+ (buffer A, supplemented freshly with 1 mM PMSF, 1 mM DTT, protease inhibitor cocktail) (if the pellet was frozen, it was thawed at 37°C), sonicated 4x for 15 sec (Gerhard Heinemann, Laboratoriums-Ausrüstungen; small tip, output control 5) with 30 sec pausing and placing the tube on ice between the pulses. 50 μl Triton X-100 (final concentration 1%) and the samples were tumbled for 20 min at 4°C. Then 550 μl glycerol (final concentration 10%) were added and the samples were distributed into 5-6 1.5 ml tubes. The lysates were cleared by centrifugation for 15 min at 14000 rpm, 4°C and the supernatants pooled. Bacterial extracts were aliquoted, frozen on dry ice / EtOH and stored at -80°C.

To bind GST proteins to glutathione sepharose (GS) beads Glutathion Sepharose 4 Fast Flow; Amersham Pharmacia Biotech; GS-beads), 40 μl of GS-beads slurry per sample were centrifuged for 1 min, 13000 rpm, 4°C, and washed 4x with 1 ml cold CLB+ buffer (50 mM Tris pH 7.4, 5 mM $MgCl_2$, 200 mM NaCl, 1% NP40, 10% glycerol, freshly added 1 mM PMSF, 2 mM Na_3VO_4, protease inhibitor cocktail) (centrifugation steps in between 1 min, 13000 rpm, 4°C) and incubated with 2 ml RhoH-GST bacterial extract for 1 h at 4°C on a rotary wheel. After binding, the GS-beads were washed 3x with 2 ml CLB+ buffer and kept on ice until incubating with the thymocyte extracts. In case with GST protein, 100 μl bacterial extract were used, and after binding the beads were washed 3x with 1 ml CLB+ buffer.

For monitoring the protein purification and binding to GS-beads, a small aliquot of bacteria lysate was resuspended in 4x sample buffer, the pellet after centrifugation, and the GS-beads after incubation with bacterial extracts were resuspended in 1x sample buffer, boiled at 95°C for 5 min and subjected to SDS-PAGE and Coomassie stain.

3.11.8.2 Pulldown

Since GEFs bind preferentially to the nucleotide-depleted state compared with GTP- or GDP-bound states, nucleotide-depleted condition was used to precipitate GEFs binding to RhoH. Nucleotide-loaded condition was used to precipitate effectors binding to RhoH.

Wild type thymocytes were stimulated as described in 3.11.6.1 or left non-stimulated and $6x10^7$ cells were lysed in 600 µl lysis buffer: 50 mM Tris pH 7.4, 100 mM NaCl, 1% Nonidet P-40, 10% glycerol, 1 mM Na_3VO_4, 100 mM NaF, containing a protease inhibitor cocktail supplemented either with 2 mM EDTA (nucleotide-depleted condition) to chelate magnesium, an essential co-factor for nucleotide binding, or 5 mM $MgCl_2$ (nucleotide-loaded condition) to maintain nucleotide binding. The thymocyte lysates were pre-cleared with 100 µl GS-beads for 1 h at 4°C on a rotary wheel to remove extract components which bind non-specifically to GS-beads. The GS-beads were washed before incubation with thymocyte lysate 3x with 1 ml lysis buffer.

Meanwhile, recombinantly expressed GST and RhoH-GST attached to GS-beads (s. 3.11.8.1) were incubated with 1 ml 50 mM Tris pH 7.5, 1 mM DTT, supplemented either with 5 mM EDTA or 5 mM $MgCl_2$ and 40 µM GTPγS (Sigma) for 10 min at 30°C. After centrifugation step for 1 min at 13000 rpm, 4°C, the beads were incubated with corresponding thymocyte lysate for 4 h or o/n at 4°C on a rotary wheel.

The GS-beads were washed 3x with the lysis buffer (supplemented either with EDTA or $MgCl_2$), resuspended in 40 µl 1x sample buffer and denatured at 95°C for 5 min.

3.11.9 Myc-IP

Non-transfected 293 cells and 293 cells, transfected with RhoH-myc via calcium phosphate method (s. 3.7.6.1), were harvested 48 h later: the cells were trypsinized (s. 3.7.3) and lysed in 400 µl lysis buffer 50 mM Tris pH 7.4, 100 mM NaCl, 1% Nonidet P-40, 10% glycerol, 1 mM Na_3VO_4, 100 mM NaF, containing a protease inhibitor cocktail, supplemented either with 2 mM EDTA (nucleotide-depleted condition) or 5 mM $MgCl_2$ (nucleotide-loaded condition). A small aliquot was saved for later analysis of transfection efficiency in Western blotting.

Meanwhile, IgG beads (40 µl slurry per sample) were washed 3x with 1 ml lysis buffer, supplemented either with 2 mM EDTA or loaded with 5 mM MgCl$_2$ and 40 µM GTPγS (s. 3.11.8.2) and incubated with the protein extract of 293 cells and 4 µg 9E10 antibody (Upstate), cortactin (4F11, Upstate) antibody or no antibody for 2 h at 4°C on a rotary wheel. After binding, the IgG beads were washed 3x with 1 ml lysis buffer, containing either EDTA or MgCl$_2$, and rocked with lysate of non-stimulated or stimulated thymocytes (s. 3.11.6.1) o/n at 4°C. Subsequent steps including washing and resuspending the IgG beads in 1x sample buffer were carried out according to 3.11.8.2.

3.11.10 Flag-IP

1×10^7 Jurkat TAg cells were harvested 48 h after DMRIE-C transfection (s. 3.7.6.2) of RhoH-Flag or empty PS080 vector and stimulated with F101.01 as described in 3.11.6.2. After stimulation the cells were washed with 500 µl cold PBS, centrifuged for 5 min, 300xrcf, 4°C and lysed in 300 µl 50 mM Tris pH 7.4, 100 mM NaCl, 1% Nonidet P-40, 10% glycerol, 1 mM Na$_3$VO$_4$, 100 mM NaF, containing a protease inhibitor cocktail, supplemented either with 2 mM EDTA or 5 mM MgCl$_2$ for 20 min on ice. The lysates were cleared by centrifugation at 14000 rpm for 15 min at 4°C. 30 µl were denatured with 4x sample buffer at 95°C and stored at -20°C for later analysis of stimulation and transfection status. Meanwhile, 40 µl anti-Flag M2 beads (Sigma) were washed with 3x with 1 ml cold TBS. The centrifugation steps were carried out for 1 min, 10000 rpm, 4°C. The protein extract was added to the beads and rotated for 2 h at 4°C. After binding of RhoH-Flag to the beads, the samples were centrifuged for 1 min, 10000 rpm, 4°C, the flow through was saved for later analysis of binding efficiency of RhoH-Flag to the beads and the beads were washed 3x with 1 ml cold TBS. Next, the beads were either denatured in 40 µl 1x sample buffer at 95°C or the RhoH-Flag and putative associated proteins were eluted from anti-Flag M2 beads by competing with 6 µl 5 µg/ml 3xFlag peptide (Sigma) in 50 µl TBS for 30 min on ice with gentle mixing every 2 min. Then the beads were centrifuged for 1 min, 10000 rpm, 4°C and the eluat was denatured in 4x sample buffer at 95°C. The elution efficiency was controlled by analyzing the beads, denatured in 1x sample buffer at 95°C, on SDS-PAGE.

3.11.11 TAP-tag-pulldown

1×10^7 Jurkat TAg cells were harvested 48 h after DMRIE-C transfection (s. 3.7.6.2) of RhoH-TAP-tag, RhoH-N62L-TAP-tag, RhoH-T18N-TAP-tag or empty pCMV-N-terminal-TAP-tag vector and stimulated with F101.01 as described in 3.11.6.2. After stimulation the cells were washed with 500 µl cold PBS, centrifuged for 5 min, 300xrcf, 4°C and lysed in the same lysis

buffer, supplemented either with EDTA (nucleotide-depleted condition) or MgCl$_2$ (nucleotide-loaded condition), which was used for Flag-IP (s. 3.11.10). 30 µl were denatured with 4x sample buffer at 95°C and stored at -20°C for later analysis of stimulation and transfection status.

Meanwhile, 40 µl of IgG sepharose 6 Fast Flow beads (GE Healthcare/Amersham Pharmacia Biotech) were washed with 1 ml HAc (adjusted to pH 3.4 with NH$_4$Ac), centrifuged for 1 min, 6000 rpm, 4°C, washed with 1 ml TBS, washed again with 1 ml Hac pH 3.4 and 1 ml TBS. The beads were subsequently equilibrated with 3x 1 ml lysis buffer, containing either EDTA or MgCl$_2$, and blocked with 1 ml 1% BSA in lysis buffer at 4°C on a rotary wheel. After blocking, the beads were washed 3x with 1 ml lysis buffer, containing either EDTA or MgCl$_2$. The Jurkat TAg protein extract was added to the beads and the samples were rotated for 2 h at 4°C. Next, the samples were centrifuged for 1 min, 6000 rpm, 4°C, the flow through was saved for later analysis of binding efficiency of RhoH-TAP-tag to the beads and the beads were washed 3x with 1 ml cold lysis buffer, supplemented with EDTA or MgCl$_2$. The beads were resuspended in 40 µl 1x sample buffer and denatured at 95°C for 5 min.

3.12 Microscopy

Cell and tissue morphology was analysed with phase contrast microscope Axioskop + Leica DC500 (Zeiss). Fluorescence microscopy was done with Leica DMRA2 + Hamamatsu ORCA-ER camera (Leica) and confocal Leica DMIRE2 + Leica TSC SP2 (Leica).

3.13 Statistical evaluation

All averages are shown with standard deviation. Student's t-test (p) was performed to assess the significance of observed differences. Differences with $p<0.05$ are significant.

4 Results

4.1   Characterization of the RhoH antibodies

4.1.1   Anti-RhoH peptide rabbit polyclonal antibody

4.1.1.1   Generation of the anti-RhoH peptide rabbit polyclonal antibody

To generate a rabbit polyclonal anti-RhoH antibody, C-terminal peptide NRRKLFSINE corresponding to the residues 178-187 of the murine RhoH protein was synthesized and an additional cysteine at the N-terminus was added to provide a sulfhydryl group (-SH). The hydroxyl group (-OH) at the C-terminus should enhance the solubility of the peptide. The C-terminal stretch of aa was chosen as an immunogen because of its low similarity to the other small Rho GTPases which elsewhere show a high homology to RhoH through the whole aa sequence (Figure 15). The antibodies generated against this region should specifically recognize RhoH but not Cdc42, Rac1, Rac2 or RhoA.

Since a hapten-peptide alone cannot stimulate a strong immune response, RhoH peptide was coupled to KLH carrier protein to increase its immunogenity. The coupling was achieved via disulfide bridge formation between the sulfhydryl groups of KLH and the N-terminal cysteine of the RhoH peptide. The rabbit was immunized with the KLH-RhoH-peptide-conjugate together with the complete Freund's adjuvant and boosted three times together with the incomplete Freund's adjuvant. The first boost was done two weeks after the initial immunization, the second and third boost with one week interval between the preceding injection. Finally, the rabbit was bled and the serum was analyzed by ELISA and Western blotting for the presence of anti-RhoH specific antibodies.
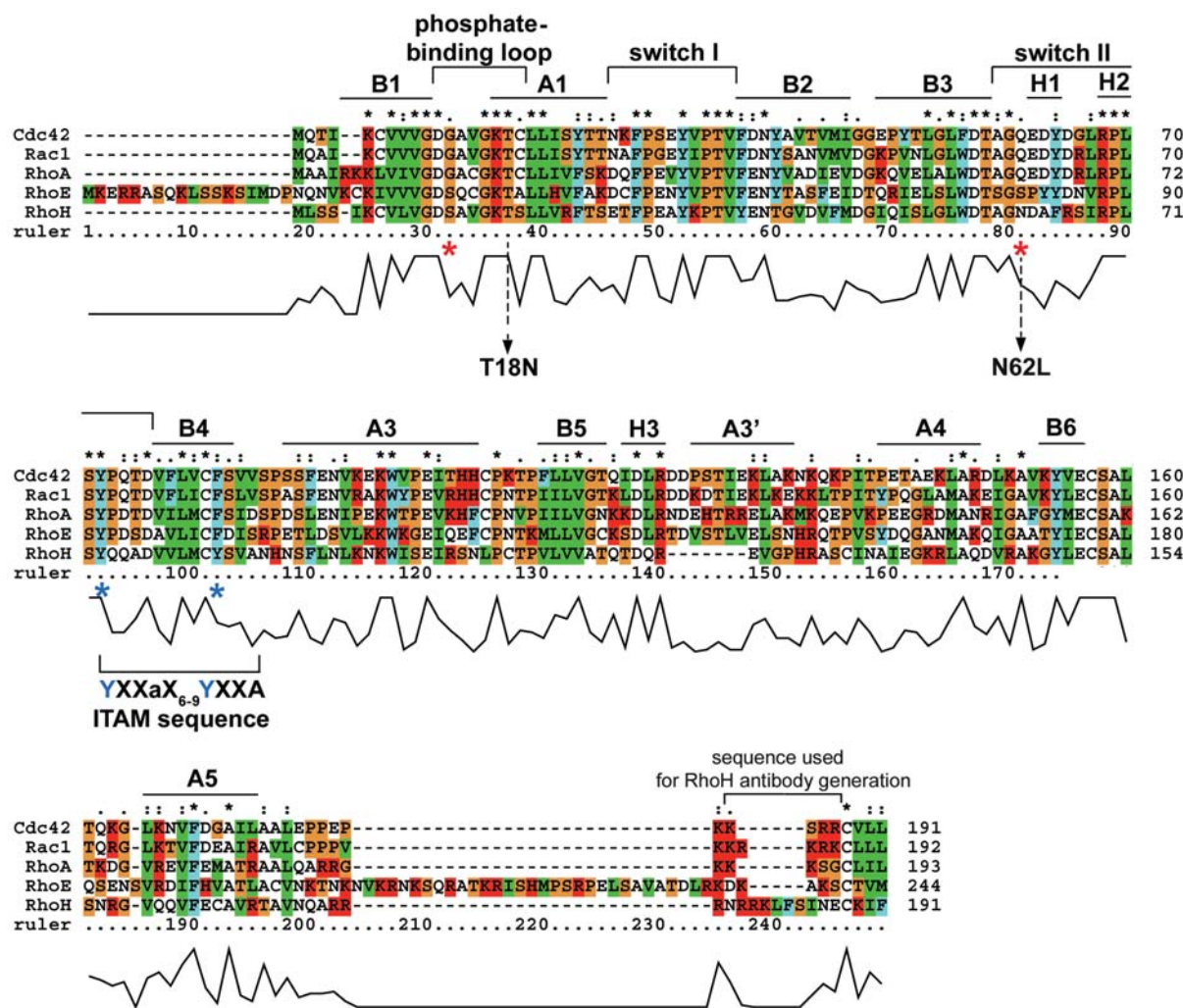
Figure 15. Alignment of murine Rho GTPases Cdc42, Rac1, RhoA, RhoE and RhoH. Alignment of aa sequences of murine Cdc42, Rac1, RhoA, RhoE and RhoH using ClustalX. Aa sequence of the RhoH protein, which was chosen for peptide synthesis, is indicated. The secondary structure elements (α-helices: A1-A5; the extended β: B1-B6, 3_{10}-helices: H1-H3) and the functional regions (switch I and II, phosphate binding loop) of Rho GTPases are shown at the top of the sequences according to Ihara et al. 1998. The histogram below the sequences demonstrates the similarity degree. "*" indicates positions which have a single, fully conserved residue. ":" indicates that one of the following 'strong' groups is fully conserved: STA, NEQK, NHQK, NDEQ, QHRK, MILV, MILF, HY, FYW. "." indicates that one of the following 'weaker' groups is fully conserved: CSA, ATV, SAG, STNK, STPA, SGND, SNDEQK, NDEQHK, NEQHRK, FVLIM, HFY. Colour code of the aa: orange: GPST, red: HKR, blue: FWY, green: ILMV. RhoH has different residues at two key sites critical for the GTPase activity indicated by a red star (serine at the position 13 instead of glycine and asparagine at the position 62 instead of glutamine as present in RhoA, Rac and Cdc42). An arrow indicates a mutation threonine to asparagine at the position 18 and asparagine to leucine at the position 62 introduced into the RhoH sequence to generate potential c.a. and d.n. form, respectively. A conserved ITAM in the RhoH aa sequence at 73 to 86 is shown as identified by Gu et al. (Gu et al, 2006).

4.1.1.2   Characterization of the anti-RhoH peptide rabbit polyclonal antibody

Before the rabbit was immunized with the RhoH peptide, a serum aliquot (pre-immune serum) was taken and tested by Western blot for the presence of antibodies which can recognize proteins at the size of approximately 21 kD, the molecular weight of RhoH. If those antibodies were present in the pre-immune serum of the rabbit, they would mask specific

antibodies against RhoH induced upon immunization with the RhoH peptide. Then another rabbit should be selected for the peptide immunization.

BM, spleen, thymus and lymph node protein extracts were subjected to Western blotting for analysis of the rabbit pre-immune serum. No proteins were detected in the range of 20-25 kD by the rabbit pre-immune serum (Figure 16), and the rabbit was used for the immunization with the RhoH peptide.
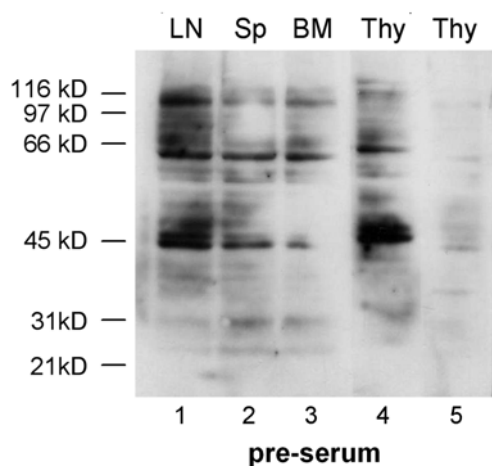

Figure 16. Rabbit pre-immune serum does not recognize proteins of 20-25 kD. Lysates of BM, spleen (Sp), thymus (Thy) and lymph nodes (LN) were subjected to Western blotting and probed with the rabbit pre-immune serum of two different dilutions (lanes 1-4, 1:5000; lane 5, 1:10000).

To monitor the development of specific RhoH peptide antibodies during the immune response, ELISA of the pre-immune serum and anti-sera after 2nd and 3rd boost was performed. A plate was coated with the RhoH peptide and incubated with serial dilutions of the rabbit anti-sera. The specific binding of the anti-sera to the RhoH peptide was determined by subsequent incubation with the anti-rabbit-HRP antibody and photometric detection of the HRP-substrate reaction. An increase in the level of specific antibodies present in the anti-sera will correspond to an increase in the absorbance. The pre-immune serum did not contain any RhoH-specific antibodies as referred by the low absorbance values (Figure 17). After initial immunization, RhoH-specific antibodies were produced. After the 2nd boost, the titer of the RhoH-specific antibodies reached its highest level and did not increase further after the 3rd boost as recorded by the similar absorbance values of sera after the 2nd and 3rd immunization (Figure 17).

The RhoH peptide rabbit anti-serum (after the 3rd boost) was analyzed in Western blot using BM, spleen, thymus and lymph node lysates of wild type and RhoH knockout mice (Figure 18A). The anti-serum was further purified against the RhoH peptide (the purification was kindly performed by Dr. Walter Göring) and analyzed by Western blotting as well (Figure 18B). Both the non-purified and affinity purified anti-sera recognized a protein in spleen, thymus and lymph nodes of approximately the same size as RhoH, at 23 kD. However, this protein is unlikely to be RhoH, since the signal corresponding to the protein of 23 kD was present both in the tissue lysates of RhoH-deficient mice and in the liver and epidermis lysates (kindly provided by Dr. Xunwei Wu). The latter tissues do not express RhoH. Interestingly, no signal for a 23 kD protein was obtained with the BM lysates.

Taken together, the generated RhoH peptide anti-serum did not work in Western blot, though it showed binding to the RhoH peptide in ELISA.
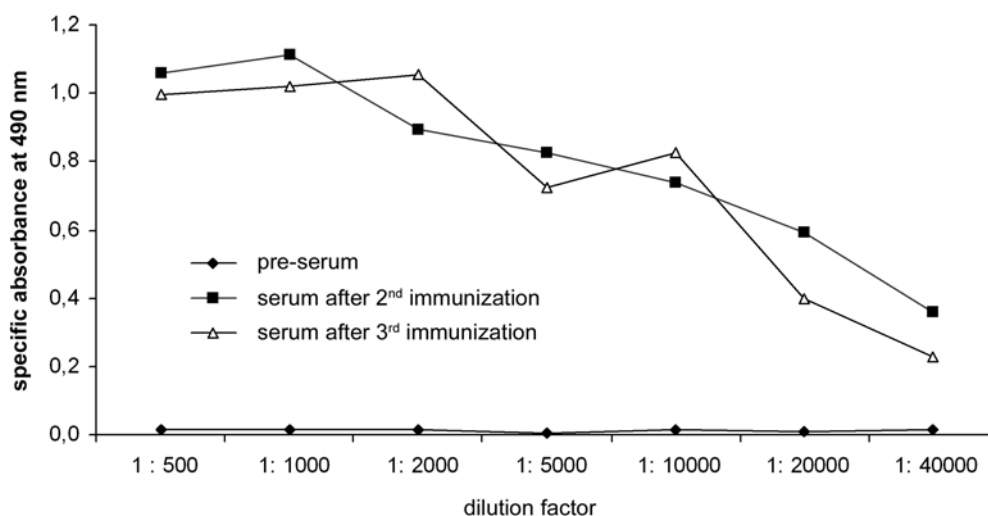
Figure 17. Specific binding of the rabbit anti-sera to the RhoH peptide in ELISA. The specific binding of the anti-sera to the RhoH peptide before the immunization and after the 2nd and 3rd boost was assessed by ELISA and evaluated photometrically. Non-specific absorbance of the anti-sera to uncoated wells was subtracted from absorbance of the anti-sera to wells coated with the RhoH peptide. Uncoated wells incubated with PBS were used as blank in the measurement.
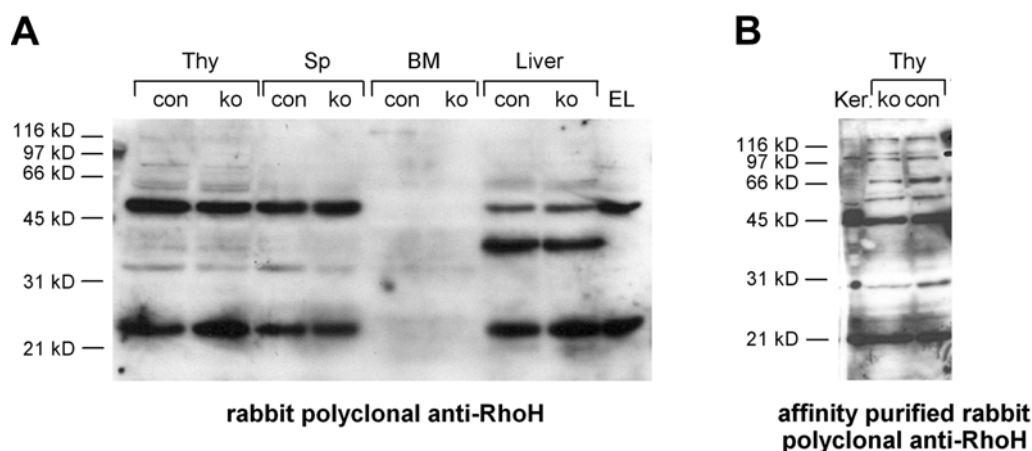
Figure 18. The RhoH peptide anti-serum does not recognize RhoH in Western blot. (A) Wild type and RhoH-null (ko) lysates of BM, spleen (Sp), thymus (Thy), and liver were probed with the non-purified RhoH peptide anti-serum. The anti-serum recognized a protein of 23 kD both in the wild type and RhoH-null lysates as well in the liver and epidermis lysates, the tissues, which do not express RhoH, suggesting that the obtained signal does not correspond to RhoH. EL, epidermal lysate. (B) Wild type (con) and RhoH-null (ko) lysates of thymus (Thy) as well as wild type keratinocyte lysate (Ker.) were probed with the affinity purified RhoH peptide anti-serum. The purified anti-serum gave a similar signal pattern as the non-purified anti-serum.

4.1.2 Characterization of the Abnova and Santa Cruz anti-RhoH antibodies

Two anti-RhoH antibodies available on the market were purchased from Abnova (anti-RhoH mouse polyclonal antibody H00000399-A01) and Santa Cruz (anti-RhoH goat polyclonal antibody N-20) and analyzed by Western blotting using wild type epidermis lysates and BM, spleen, thymus, lymph node and liver lysates from both wild type and RhoH-null mice. The anti-RhoH antibody from Abnova recognized a protein of 21-22 kD both in control and RhoH-null lysates and in epidermis lysates, suggesting that this antibody was not specific for RhoH (Figure 19A). The anti-RhoH antibody from Santa Cruz did not work either: it did not recognize any proteins at the size of 20-25 kD in BM, spleen, thymus and lymph nodes, however, it recognized RhoH-myc transfected in 293 cells (Figure 19B).

These data suggest that both the Abnova and Santa-Cruz anti-RhoH antibodies did not recognize endogenous RhoH protein in Western blot.
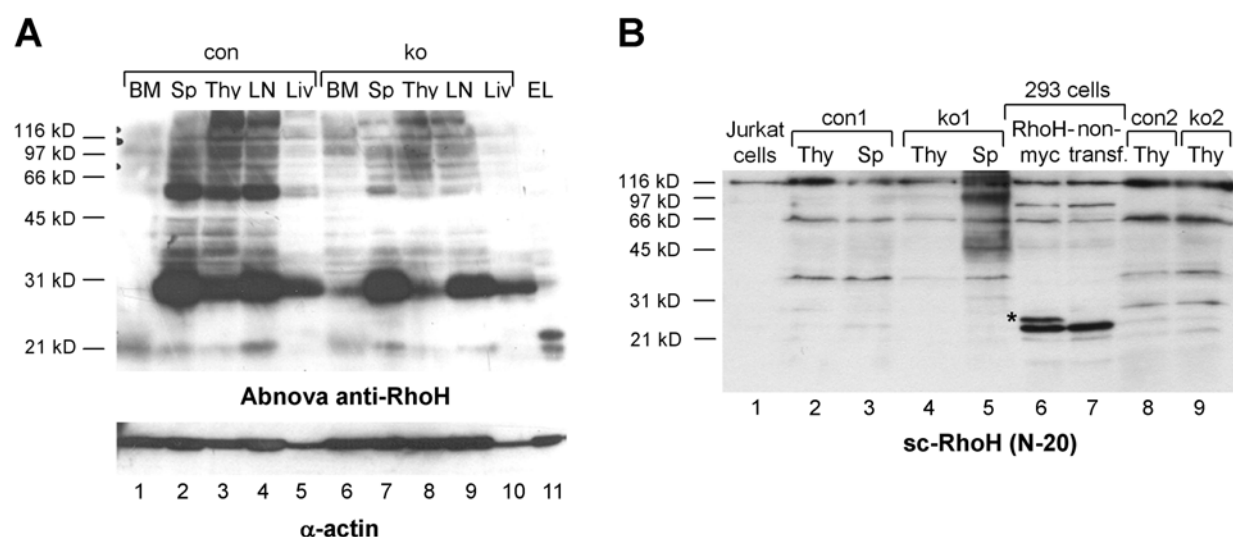
Figure 19. Anti-RhoH mouse polyclonal antibody from Abnova and anti-RhoH goat polyclonal antibody from Santa Cruz do not recognize RhoH in Western blot. (A) Wild type (con) and RhoH-null (ko) lysates of BM, spleen (Sp), thymus (Thy), lymph nodes (LN) and liver (Liv) were probed with Abnova anti-RhoH antibody (H00000399-A01). The antibody recognized a protein of 21-22 kD in the wild type and RhoH-null (ko) lysates as well in the liver and epidermis lysates, suggesting that the antibody was not specific for RhoH. (B) Lysates of thymus (Thy), spleen (Sp) of control (con1 and con2) and RhoH-deficient (ko1 and ko2) mice, Jurkat cells and 293 cells, transfected with RhoH-myc or non-transfected (non-transf.), were probed with Santa Cruz anti-RhoH (N-20) antibody. The antibody did not recognize RhoH in tissue lysates of control mice, however it gave a signal for transfected RhoH-myc as indicated by the asterisk.

4.2   Generation of RhoH knockout mice

4.2.1   The *RhoH* gene structure and knockout strategy

The murine *RhoH* gene is spread over 30 kb and consists of three exons (Figure 20A). The complete coding region of 573 bp is found within exon 3. Dr. Cord Brakebusch and Ursula Kuhn, MPI, Martinsried, Germany, generated RhoH-deficient mice using homologous recombination technique. The ES cells were targeted by a vector containing a 6.9 kb EcoRI-EcoRI genomic RhoH DNA (including 2nd and 3rd exon), where the genomic sequence of 336 bp (HindIII-AatII fragment) corresponding to the first 42 aa was replaced by an inverted neomycin expression cassette (Figure 20B).

The stably transfected ES cells (derived from 129/Sv mice) were verified by Southern blot for homologous recombination (Figure 20C). Genomic DNA was digested with HindIII and hybridized with an external probe generated with primers UK7 and UK8 binding to a 3' flank of the HindIII restriction site. A fragment of 6.3 kb was expected for the wild type and 8.6 kb for the recombined gene. The deleted sequence encodes the translation start and the switch I region, which in Rho GTPases is crucial for the interaction with GEFs, GAPs and effectors (DerMardirossan and Bokoch, 2005; Vetter and Wittinghofer, 2001; Ihara et al., 1998), implying that even if a truncated RhoH protein was produced, it would not be functional. Two ES cell clones positive for one mutated allele were injected into blastocysts and transferred into foster mice. The male offspring chimeric mice were mated to female C57BL6 to assess the germ-line transmission and to obtain RhoH heterozygous mice. RhoH homozygous mice were derived from matings of heterozygous mice. The disruption of the *RhoH* gene in mice was confirmed by Southern blot as described above for the ES cells (Figure 20D). Mice were genotyped by a genomic touchdown PCR with forward primers Rh1 detecting the wild type allele or Rh4 identifying the knockout allele and the common reverse primer Rh2, amplifying 240 and 325 bp, respectively (Figure 20E).
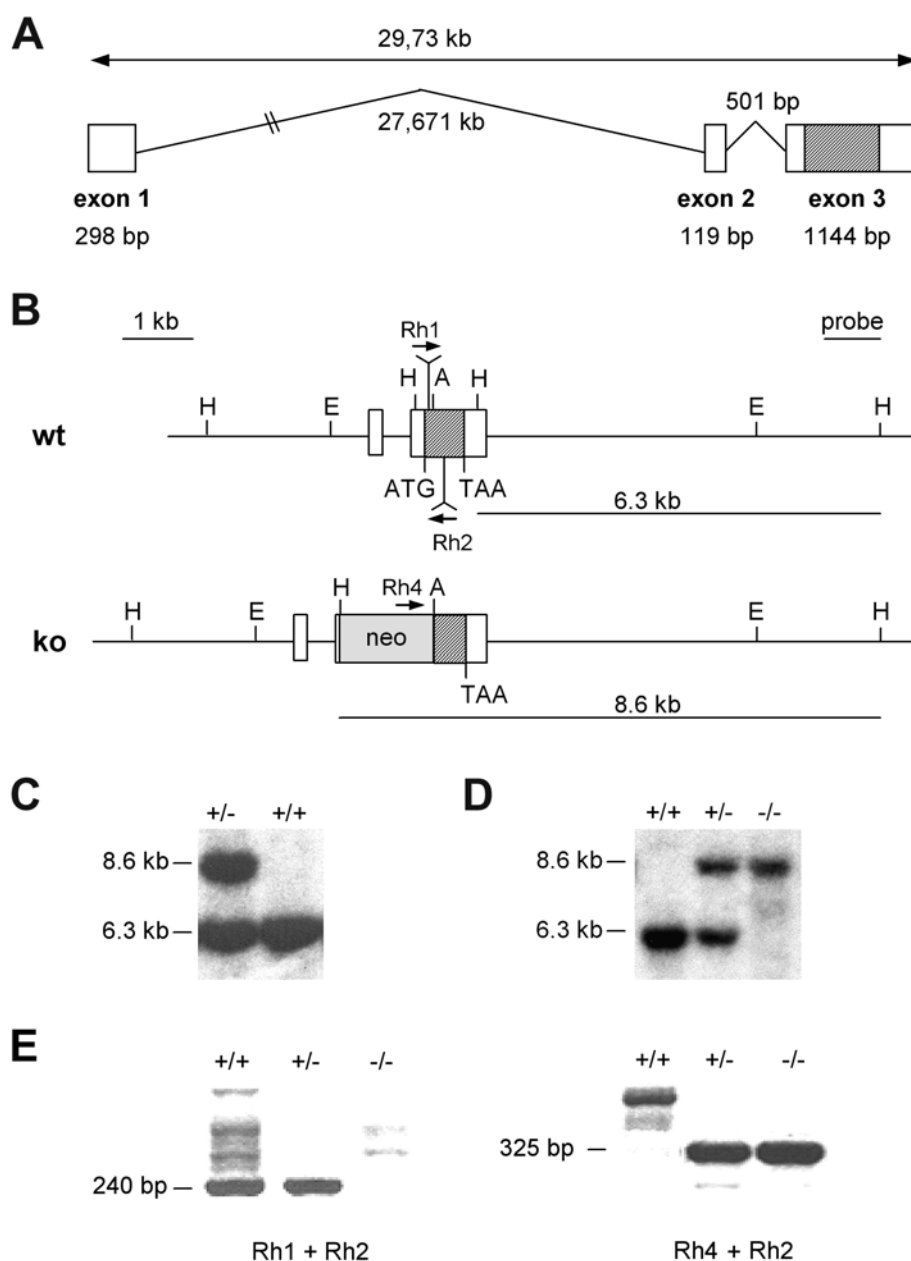
Figure 20. Structure of the *RhoH* gene and generation of the RhoH-deficient mice. (A) Schematic presentation of the *RhoH* gene structure. The gene is located on chromosome 5 and consists of three exons. The complete coding region is in exon 3. (B) Schematic presentation of the *RhoH* gene before (wt) and after (ko) homologous recombination of the targeting vector (EcoRI-EcoRI fragment of ko gene, containing 2nd and 3rd exons). Homologous recombinants were identified by digestion of genomic DNA with HindIII and Southern blot hybridization with the indicated probe, resulting in a 6.3 kb fragment for wild type and an 8.6 kb fragment for the recombined gene. Mice were genotyped using a genomic PCR with forward primers specific for wt (Rh1) or ko (Rh4) and a common reverse primer (Rh2). Exons are boxed and coding region of the *RhoH* gene is hatched (neo: neomycin resistance expression cassette; A: AatII; H: HindIII; E: EcoRI; ATG: translation start site; TAA: stop codon). (C) Southern blot analysis of ES cell DNA as described in 20B, identifying homologously recombined ES cells. (D) Southern blot analysis of mouse tail DNA as described in 20B, identifying wild type (+/+), heterozygous (+/-) and homozygous (-/-) RhoH mutants. (E) Genomic PCR of mouse tail DNA, identifying wild type (+/+), heterozygous (+/-) and homozygous (-/-) RhoH mutants. The indicated sizes are corresponding to the expected ones according to the genomic map.

4.2.2 Analysis of the RhoH transcript in the mutant mice

To examine a putative RhoH transcript in the RhoH-mutant mice, RNA from BM, spleen and thymus of wild type, heterozygous and homozygous mice was isolated and a Northern blot was performed using RhoH coding region and neomycin resistance cassette as probes. The membrane was subsequently re-hybridized with a probe recognizing the house-keeping gene *GAPDH* as a control for loading and transfer. Northern blot analysis indicated the expression of a transcript of 2.5 kb in wild type and heterozygous mice and a long transcript 4.2 kb in heterozygous and RhoH-null mice (Figure 21). The long RhoH transcript contained the sequence of the inverted *neomycin resistance* gene with at least 6 Kozak box "ATGs" followed by an in frame stop codon and the truncated RhoH coding region. These open reading frames should prevent any expression of a truncated RhoH protein. Endogenous RhoH mRNA levels in heterozygous mutant mice were about 50% of homozygous wild type mice.
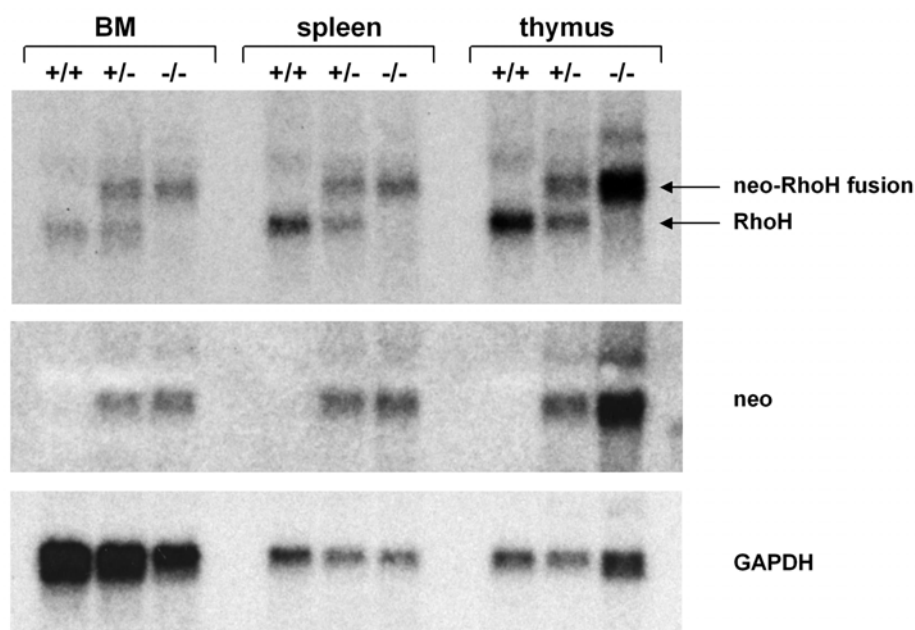
Figure 21. A long transcript containing the inverted *neomycin resistance cassette* and the truncated *RhoH* gene is expressed in the RhoH-mutant mice. Northern blot analysis was carried out with total RNA isolated from BM, spleen, and thymus of wild type (+/+), heterozygous (+/-) or homozygous (-/-) RhoH-mutant mice. The blot was hybridized sequentially with a probe for RhoH (top panel), neomycin resistance (neo; medium panel), and GAPDH (bottom panel). Transcripts for the endogenous RhoH mRNA (RhoH; 2.5 kb), and the neo-RhoH fusion transcript (neo-RhoH fusion; 4.2 kb) are indicated. In heterozygous animals equal amounts of the neo-RhoH fusion and the endogenous RhoH were detected, indicating a 50% decreased expression of the endogenous wild type RhoH.

Due to the lack of functional antibodies (s. 4.1), confirmation of the loss of RhoH on protein level was not possible. Genotyping of 214 adult offsprings derived from heterozygous matings revealed a mendelian ratio of genotypes (+/+: 23.2%; +/-: 50.8%; -/-: 26.0%) indicating

no embryonic lethality of RhoH-null mice. The RhoH heterozygous and homozygous mutant mice had normal weight, normal life span, were fertile and not distinguishable from their wild type littermates.

Wild type and RhoH heterozygous mice were used as controls with indistinguishable results in all assays.

4.2.3   Reduced thymus and spleen cellularity

Since RhoH is expressed in hematopoietic system (Li et al., 2002; Gu et al., 2005a), we analyzed the cellularity of lymphoid organs in 2 month old control and RhoH-mutant mice. BM cellularity was not significantly different between RhoH-null and control mice, while splenocytes were reduced in RhoH-deficient mice (Figure 22). Lymph node cellularity varied but tended to be lower in mutant mice (Figure 22). Cellularity of the thymus, the organ where T cell development takes place, was about 60% lower in RhoH-null mice than in control animals (Figure 22), indicating a possible role of RhoH in T cell production.
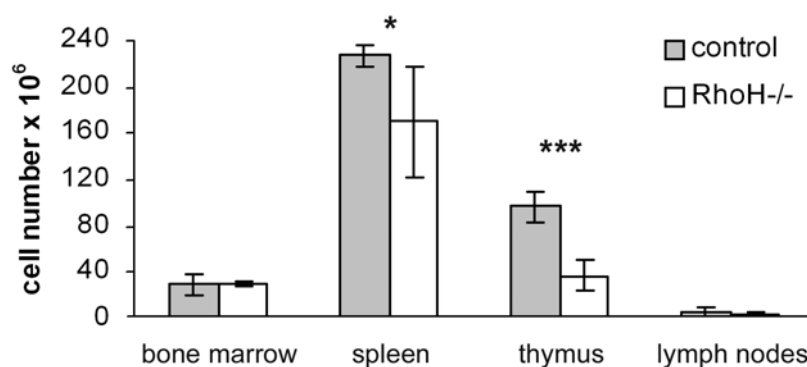
Figure 22. Decreased cellularity of the thymus and spleen in the absence of RhoH. Cellularity of the BM, spleen, thymus and lymph nodes of 2 month old RhoH-null and control mice (*: $p<0.05$; ***: $p<0.001$; n=5/5).

Similar to 2 month old mice, no significant difference in BM cellularity [control $(48.48\pm9)x10^6$ cells; RhoH-/- $(56.06\pm13)x10^6$ cells] was observed between 6 month old control and RhoH-mutant mice. In contrast to 2 month old mice, no significant difference in spleen cellularity [control $(143.64\pm72)x10^6$ cells; RhoH-/- $(138.98\pm68)x10^6$ cells] was found between 6 month old control and RhoH-null mice. However, a very high standard deviation makes it difficult to draw a firm conclusion about the spleen cellularity. More mice need to be analyzed to clarify this point. Thymus cellularity [control $(50.66\pm20)x10^6$ cells; RhoH-/- $(39.92\pm9)x10^6$ cells] of 6 month old control and RhoH-mutant mice appeared not be changed, on the contrary to 2 month data. However, age dependent thymus involution might have masked the differences between control and RhoH-null mice. The significant decrease of

lymph node cellularity [control $(8.37\pm4)x10^6$ cells; RhoH-/- $(3.73\pm2)x10^6$ cells] in 6 month old RhoH-mutant mice supported a role for RhoH in maintaining lymph node cellularity as already suggested by the data from 2 month old mice.

4.3 Analysis of RhoH expression in hematopoietic cells

To determine whether RhoH is expressed during T cell development, thymocyte subpopulations (DN1, DN2, DN3, DN4, DP, CD4SP, CD8SP) and splenic T cells (CD4+, CD8+) were sorted, tested for purity by FACS (the purity was approximately 90-95%) and analyzed for RhoH expression by real-time RT-PCR. In addition, RhoH expression was assessed in splenic B cells and BM granulocytes. RhoH was found to be expressed both throughout the thymocyte development and in mature T cells in periphery (Figure 23). RhoH transcript was also detected in splenic B cells (B220+) and marginally in BM granulocytes (Gr-1+), confirming previous observations (Figure 23; Li et al., 2002; Gu et al., 2005a; Lahousse et al., 2004).
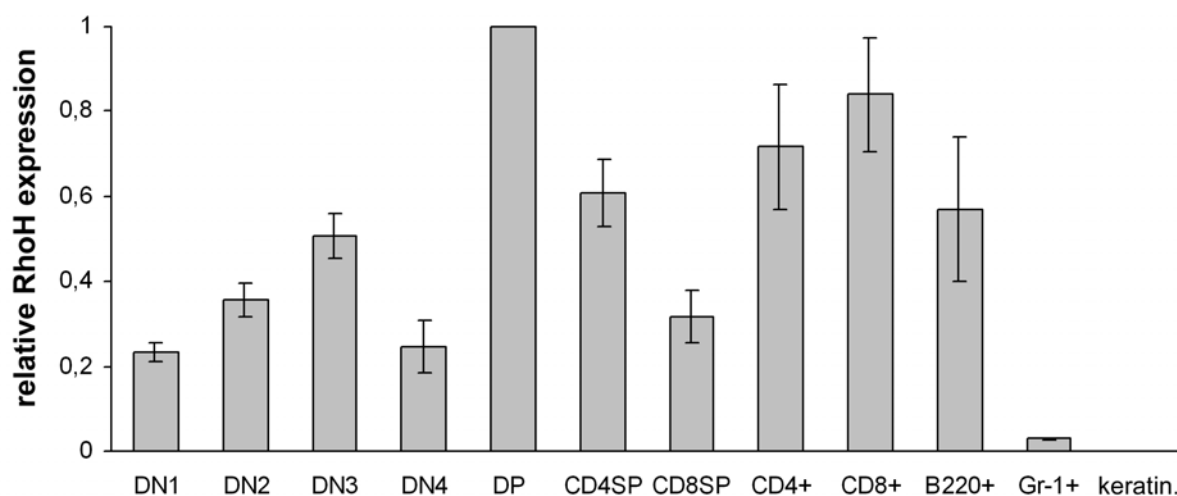
Figure 23. RhoH is expressed at all stages of T cell development. Relative expression of RhoH was determined by qRT-PCR of total RNA isolated from sorted DN1, DN2, DN3, DN4, DP, CD4SP, CD8SP, splenic CD4+, CD8+, B220+ and BM Gr-1+ cells as indicated. RhoH was expressed in thymocytes at all developmental stages, in mature B (B220+) and T cells (CD4+, CD8+), but only weakly in granulocytes (Gr-1+) and not detectably in keratinocytes (keratin.). *GAPDH* was used as a reference gene to normalize the *RhoH* gene expression. The *RhoH* gene expression level in DP cells was set to 1. Diagram shows results of 4 real-time-PCR reactions performed with cDNA generated from RNA from cells of 2 independent sorts.

The real-time-PCR analysis suggested that RhoH expression is regulated during T cell development. In the DN compartment, RhoH expression rises from DN1 to DN3, while it decreases in DN4 fraction (Figure 23). The RhoH transcript is present in DP cells at the highest level, whereas it is reduced in CD4SP and even more in CD8SP cells (Figure 23). The

peripheral splenic CD4+ and CD8+ T cells express comparable levels of RhoH as CD4SP cells in thymus (Figure 23).

4.4   Analysis of hematopoesis in the absence of RhoH

As RhoH was reported to be expressed in HPCs, lymphoid, and myeloid cells, we examined the development of different blood lineages in RhoH-mutant and control mice. The absolute numbers of lymphoid, myeloid and erythroid populations in hematopoietic organs are summarized in table 1 and table 2.

4.4.1   Normal myeloid and erythroid development

Population sizes of granulocytes (Mac1+Gr-1+), monocytes (Mac1+Gr-1-) and erythroblasts (Ter119+) in BM were similar in 2 month old mutant and control mice (Figure 24A, B; table 1), indicating that RhoH is not crucial for development of myeloid and erythroid lineages. Splenic granulocyte and erythroblast numbers were unpertubed, while splenic monocytes were slightly increased in 2 month old RhoH-deficient mice (Figure 24A, B; table 1). To investigate whether HSCs and HPCs continuously produce myeloid and erythroid cells, 6 month old mutant and control mice were analyzed. No significant changes were found in the numbers of BM granulocytes, monocytes and erythroblasts between 6 month old mutant and control mice (table 2), implying that the HSCs and HPCs can be maintained without RhoH. Splenic granulocyte and monocyte populations were similar in 6 month old control and RhoH-deficient mice, while the number of splenic Ter119+ erythroblasts was enlarged in mutant mice (table 2).

4.4.2   Normal B cell development

The B cell development was monitored in BM, spleen and lymph nodes of 2 month old RhoH-null and control mice by FACS using surface markers specific for B220, IgM and IgD. ProB + preB (B220+IgM-), immature (B220+IgM+), mature (B200+IgM+IgD+) B cell numbers in BM were similar in mutant and control mice (Figure 24C, table 1), suggesting that RhoH is not essential for the differentiation of B cells. B cell numbers (IgD+) in peripheral lymphoid organs as spleen and lymph nodes were also not changed in RhoH-null mice when compared to controls (Figure 24D, E; table 1). 6 month old mutant mice still had normal B cell numbers in BM, spleen and lymph nodes (table 2), indicating that RhoH is not crucial for the maintenance of HSCs.
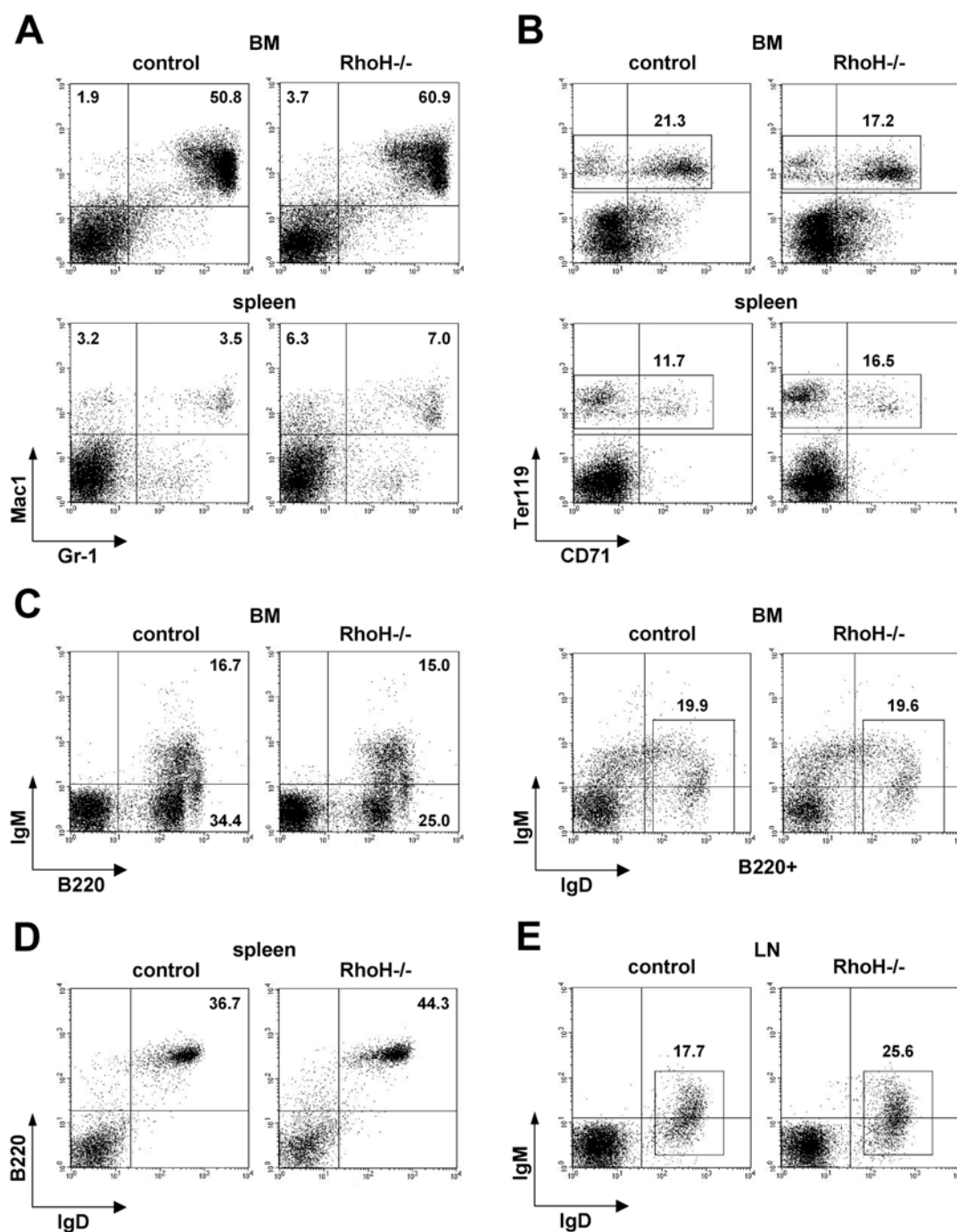
Figure 24. Normal myeloid, erythroid and B cell development in the absence of RhoH. Cells from BM, spleen and lymph nodes (LN) of 2 month old RhoH-null and control mice were stained with antibodies against Mac1, Gr-1 (A); Ter119 and CD71 (B), B220, IgM and IgD (C-D) and analyzed by FACS. Absolute numbers of granulocytes, monocytes, erythroblasts and B cells are presented in table 1 (n=5/5).

4.4.3 Increased frequency of NK1.1+ cells

The number of NK1.1+ cells including NK and NKT cells was elevated in BM and spleen of 2 month old mutant mice (Figure 25, table 1). However, in 6 month old RhoH-null mice the number of NK1.1+ cells was not significantly changed in BM and spleen (table 2).
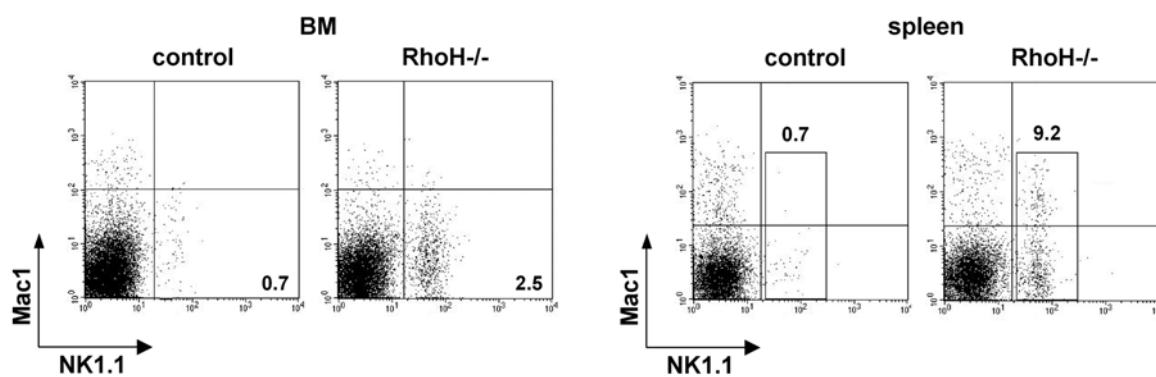
Figure 25. Increased frequency of NK1.1+ cells in BM and spleen in the absence of RhoH. Single cell suspensions of BM and spleen of 2 month old RhoH-null and control mice were stained with antibody against NK1.1 and analyzed by FACS. Absolute numbers of NK1.1+ cells are presented in table 1 (n=5/5).

Table 1 and table 2. Absolute sizes of myeloid, erythroid and lymphoid populations in hematopoietic organs of 2 (table 1) and 6 (table 2) month old mice.

Table 1	control		RhoH-/-		
	average	stdev	average	stdev	
Bone marrow (x 10^6 cells)					
Mac1+ Gr-1+	**14,849**	2,357	**14,889**	1,501	
Mac1+ Gr-1-	**1,679**	0,594	**1,360**	0,466	
Ter119+	**7,131**	4,622	**6,733**	4,560	
NK1.1+	**0,151**	0,100	**0,355**	0,092	**
CD4+	**0,218**	0,123	**0,101**	0,021	*
CD8+	**0,225**	0,159	**0,054**	0,007	*
B220+IgM-	**2,377**	1,110	**2,620**	0,745	
B220+IgM+	**1,602**	0,645	**2,084**	0,591	
B220+IgM+IgD+	**0,740**	0,183	**0,971**	0,422	
Spleen (x 10^6 cells)					
Mac1+ Gr-1+	**10,192**	3,666	**9,721**	4,169	
Mac1+ Gr-1-	**5,879**	1,351	**8,971**	2,366	*
Ter119+	**24,934**	5,423	**26,361**	8,124	
NK1.1+	**2,791**	1,337	**7,816**	2,617	**
CD4+	**64,082**	7,282	**23,471**	5,426	***
CD8+	**27,418**	3,342	**7,500**	0,743	***
IgD+	**97,934**	12,041	**89,384**	7,611	
Lymph nodes (x 10^6 cells)					
CD4+	**4,163**	3,649	**1,855**	1,105	
CD8+	**1,603**	1,506	**0,281**	0,226	
IgM+IgD+	**1,077**	0,646	**0,959**	0,434	

| Table 2	control		RhoH-/-		
	average	stdev	average	stdev	
Bone marrow (x 10^6 cells)					
Mac1+ Gr-1+	**28,053**	7,660	**34,815**	6,358	
Mac1+ Gr-1-	**3,865**	1,191	**3,687**	3,324	
Ter119+	**6,882**	2,184	**8,870**	3,309	
NK1.1+	**0,448**	0,249	**0,561**	0,294	
CD4+	**0,717**	0,381	**0,398**	0,241	
CD8+	**0,482**	0,385	**0,135**	0,096	
B220+IgM-	**3,392**	1,746	**3,829**	1,818	
B220+IgM+	**2,361**	1,323	**3,043**	2,005	
B220+IgM+IgD+	**1,678**	1,079	**1,197**	0,798	
Spleen (x 10^6 cells)					
Mac1+ Gr-1+	**4,420**	2,637	**7,150**	2,565	
Mac1+ Gr-1-	**9,542**	4,128	**7,964**	4,431	
Ter119+	**13,099**	2,144	**24,964**	5,132	**
NK1.1+	**4,152**	3,913	**3,988**	2,502	
CD4+	**35,980**	17,154	**16,754**	10,400	*
CD8+	**20,818**	12,091	**7,710**	4,107	*
IgD+	**59,688**	32,042	**71,711**	34,165	
Lymph nodes (x 10^6 cells)					
CD4+	**4,114**	1,992	**1,171**	0,493	*
CD8+	**1,747**	1,069	**0,441**	0,280	*
IgM+IgD+	**1,468**	0,820	**1,430**	1,267	

Presented are the absolute numbers of cell populations carrying indicated surface markers with standard deviation (stdev) in single cell suspensions of BM, spleen, and lymph nodes of 2 (table 1) and 6 month (table 2) old control and RhoH-null mice (*: p< 0.05; **: p<0.01; ***: p<0.001; n=5/5).

4.4.4 Defective T cell development

4.4.4.1 Impaired thymocyte development

The reduced thymus cellularity suggested that the development of T cells might be impaired in the RhoH-null mice. To test the hypothesis whether thymocyte development is defective in the absence of RhoH, we analyzed thymocytes of 2 month old control and mutant mice by co-staining for surface markers CD4 and CD8 in FACS (Figure 26A). In mutant mice, the relative and absolute number of DN (CD4-CD8-) population, containing the early thymic

immigrants, was increased more than twofold, while the absolute number of DP (CD4+CD8+) thymocytes was reduced by 60%, indicating an incomplete developmental block between DN and DP stage (Figure 26A). The relative amount of DP cells was similar in mutant and control mice. However, the relative amount of CD4SP and CD8SP was decreased by 50% in RhoH-null mice, implying an additional defect during the development from DP to SP stage, where positive selection takes place. The absolute numbers of CD4SP and CD8SP were reduced even further by 80% and 85%, respectively (Figure 26A).

Figure 26. Impaired thymocyte development in the absence of RhoH in 2 month old mice. (A) Thymocytes of 2 month old mice were analyzed for the expression of CD4 and CD8 by FACS. Bar graph presents the absolute cell number of each population (**: $p<0.01$; ***: $p<0.001$; n=11/11). (B) Thymocytes of 2 month old mice were gated for lineage negative (B220, CD4, CD8, NK1.1, Mac1, Gr-1, Ter119) cells and analyzed for the expression of CD25 and CD44. [DN1 (CD25-CD44+); DN2 (CD25+CD44+); DN3 (CD25+CD44-); DN4 (CD25-CD44-)]. Bar graph presents the absolute cell number of each population (*: $p<0.05$; n=4/4).

To define the block during DN to DP development in more detail, the DN population was further subdivided into DN1 (CD25-CD44+), DN2 (CD25+CD44+), DN3 (CD25+CD44-) and DN4 (CD25-CD44-) cells. The relative and absolute numbers of the DN1 cells were not significantly different between control and mutant mice, suggesting normal migration of T cells from the BM to the thymus (Figure 26B). Relative as well as absolute numbers of a very small DN2 population were not altered in RhoH-mutant mice. However, the DN3 cells in relative numbers were increased, and in absolute numbers, nearly threefold elevated in RhoH-null mice. The relative amount of the DN4 cells was reduced by approximately 50%, whereas the absolute size of the DN4 population was not significantly different between control and

mutant mice. The accumulation of thymocytes at the DN3 stage suggested an incomplete developmental block at the transition from DN3 to DN4, leading to the increase of total DN cell numbers.

Also 6 month old mutant mice showed a decrease in CD4SP and CD8SP cells and an increase in DN3 thymocytes (Figure 27). These differences were, however, less pronounced than in 2 month old mice. DP cell numbers were only slightly reduced in 6 month old mutant mice (Figure 27A).
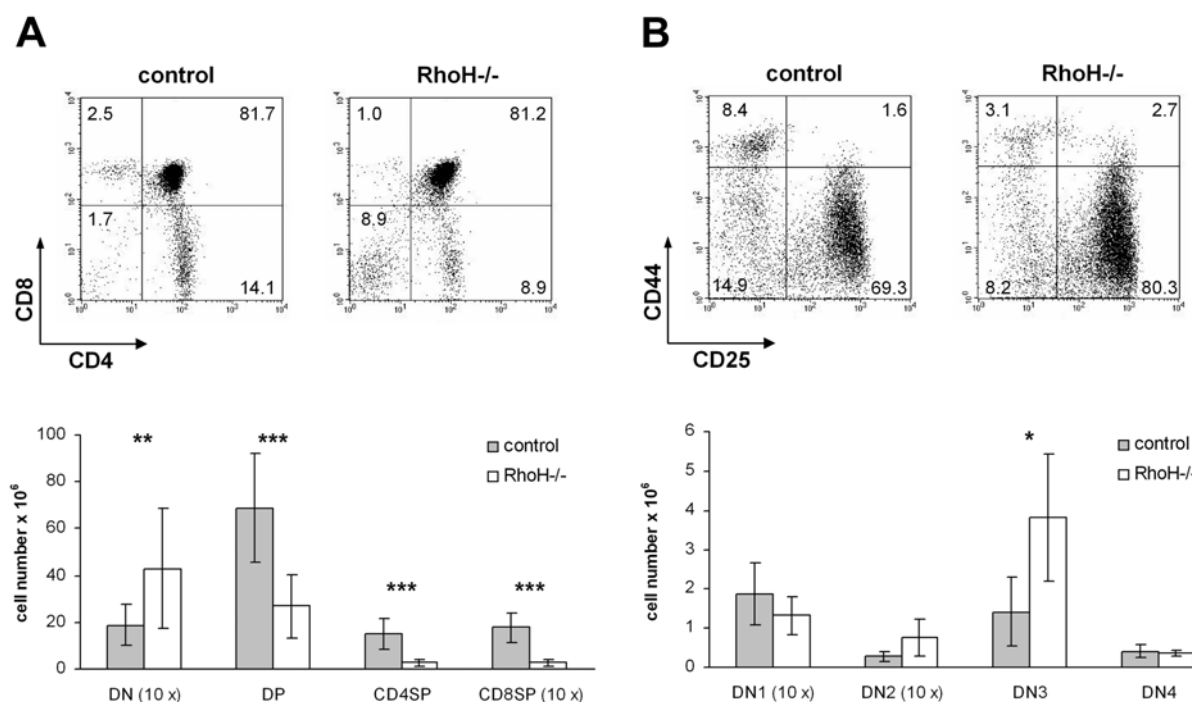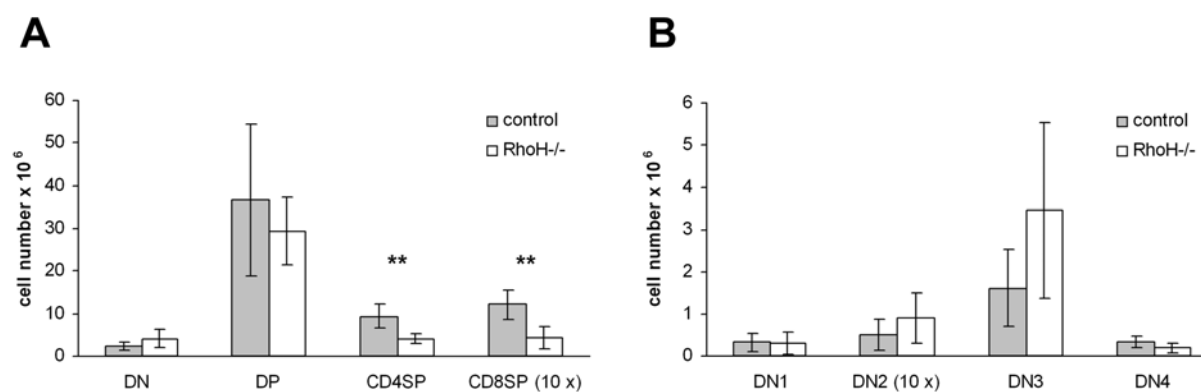

Figure 27. Impaired thymocyte development in the absence of RhoH in 6 month old mice. (A) Thymocytes of 6 month old mice were analyzed for the expression of CD4 and CD8 by FACS (**: $p<0.01$; n=5/5). (B) Thymocytes of 6 month old mice were gated for lineage negative (B220, CD4, CD8, NK1.1, Mac1, Gr-1, Ter119) cells and analyzed for the expression of CD25 and CD44. (DN1 (CD25-CD44+); DN2 (CD25+CD44+); DN3 (CD25+CD44-); DN4 (CD25-CD44-); n=4/4).
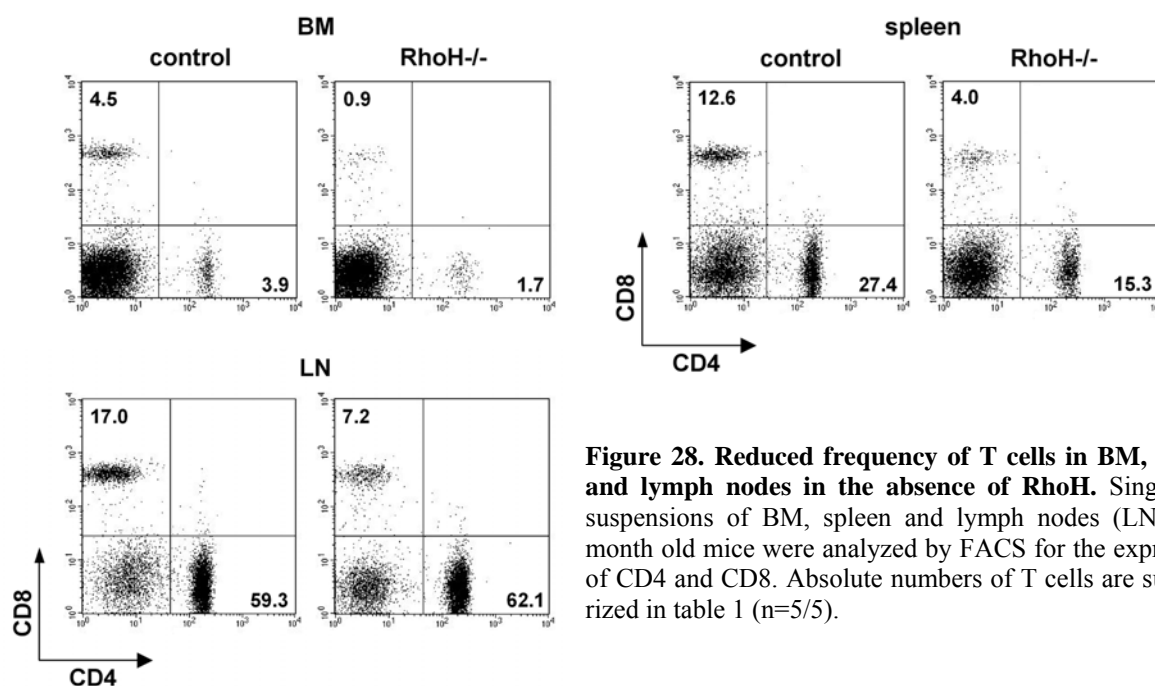
Figure 28. Reduced frequency of T cells in BM, spleen and lymph nodes in the absence of RhoH. Single cell suspensions of BM, spleen and lymph nodes (LN) of 2 month old mice were analyzed by FACS for the expression of CD4 and CD8. Absolute numbers of T cells are summarized in table 1 (n=5/5).

Due to defective thymocyte development, the T cells were strongly decreased in BM, spleen and lymph nodes in 2 month old RhoH-deficient mice: CD8+ T cells were reduced by about 75%, while CD4+ T cells were reduced by 50% (Figure 28, table 1). CD4+ and CD8+ T cells were also reduced in BM, spleen and lymph nodes in 6 month old mutant mice (table 2).

4.4.4.2   Normal numbers of γδ thymocytes

While the majority of T cells express αβ TCR, a very small population of the T cell pool expresses γδ TCR. To investigate γδ T cells, thymocytes, splenocytes and lymph node cells were stained with antibodies against CD3 and TCRγδ.
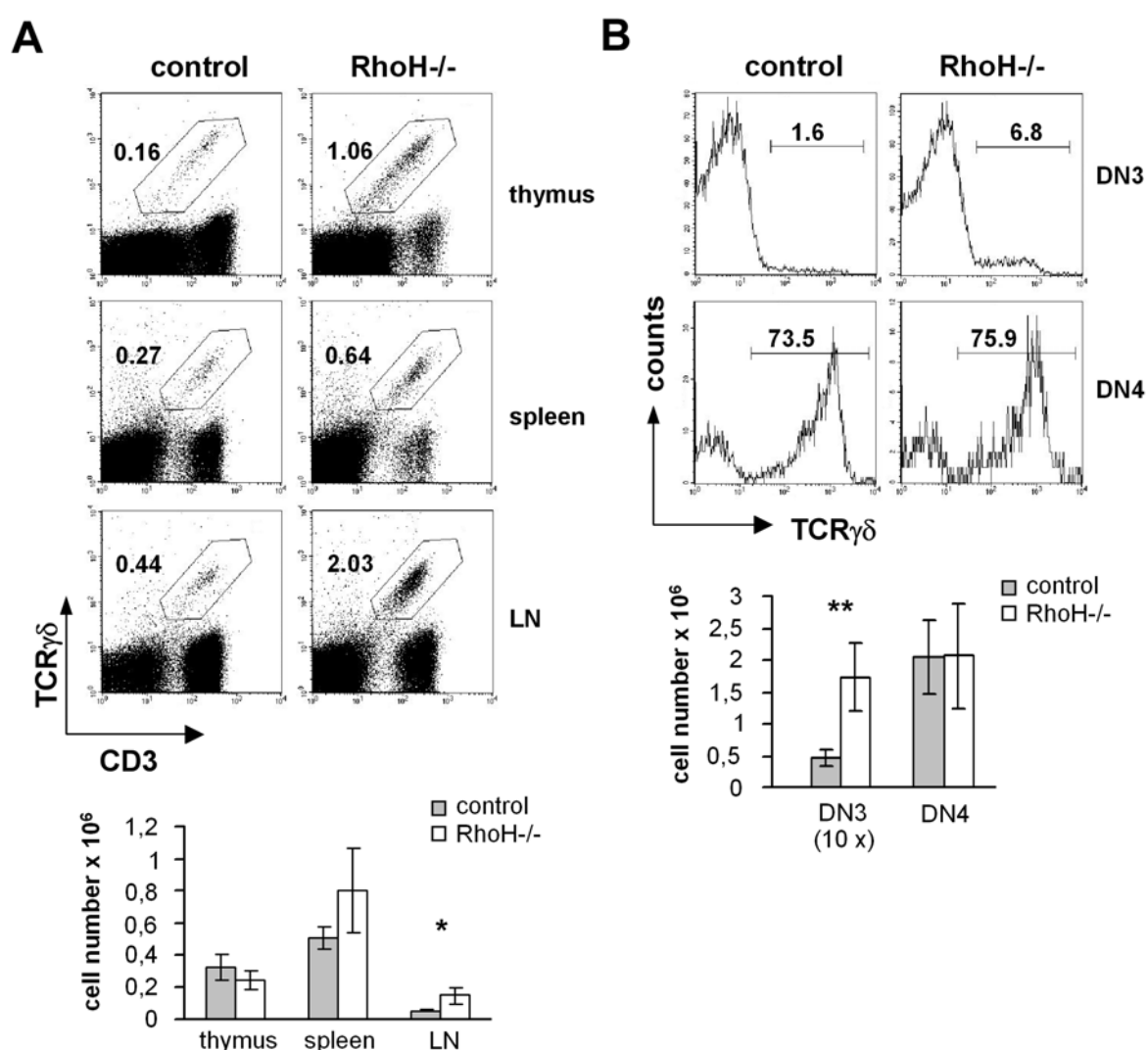
Figure 29. RhoH is not required for the development of γδ T cells. (A) Single cell suspensions of thymus, spleen and lymph nodes (LN) of 2 month old mice were analyzed by FACS for the expression of TCRγδ and CD3. Total cell numbers of TCRγδ expressing cells (TCRγδ+CD3+) are shown in bar graph. RhoH-null mice had normal number of γδ T cells in thymus and spleen and increased levels in LN (*: p<0.05; n=3/3). (B) In the absence of RhoH, the amount of TCRγδ expressing DN4 cells was unaltered, while the small population of TCRγδ+ DN3 cells was significantly elevated in RhoH-null mice. Bar graph presents the absolute number of TCRγδ expressing cells in DN3 and DN4 population (**: p<0.01; n=4/3).

Total amount of thymocytes expressing TCR$\gamma\delta$ (CD3+TCR$\gamma\delta$+) was normal in the absence of RhoH, suggesting that RhoH is not crucial for production of $\gamma\delta$ T cells (Figure 29A).

However, the very small population of DN3 cells expressing TCR$\gamma\delta$ was increased, while the amount of DN4 cells carrying TCR$\gamma\delta$ was not altered (Figure 29B). This implies that there might be an incomplete developmental block at the transition from DN3 to DN4, which is later compensated for leading to normal numbers of $\gamma\delta$ thymocytes. $\gamma\delta$ T cells were slightly increased in spleen and significantly in lymph nodes (Figure 29A).

Taken together, these data indicate that RhoH is required for the development of T cells carrying $\alpha\beta$ TCR and maybe for the early development of $\gamma\delta$ T lymphocytes.

4.4.4.3 Increased frequences of peripheral T cells with activated phenotype

The defects in thymocyte development leading to reduced numbers of peripheral T cells in the absence of RhoH prompted us to investigate the homeostasis of splenic and lymph node T cells in RhoH-mutant mice. Under normal conditions, wild type mice, not deliberately immunized with an antigen contain mostly naïve T cells (CD62L^{high}CD44^{low}), but also some CD4+ and CD8+ T cell with the characteristics of the activated (CD62L^{low}CD44^{high}) and memory (CD62L^{high}CD44^{high}) phenotype. These cells are probably produced in response to environmental antigens from sources as the gut flora or food (Swanson et al., 2002).

Peripheral T cells in spleen and lymph nodes of RhoH-null mice exhibited a significantly increased amount of cells with cell surface characteristics of activated effector T cells when compared to controls, and more CD8+ T cells demonstrated memory phenotype (Figure 30).
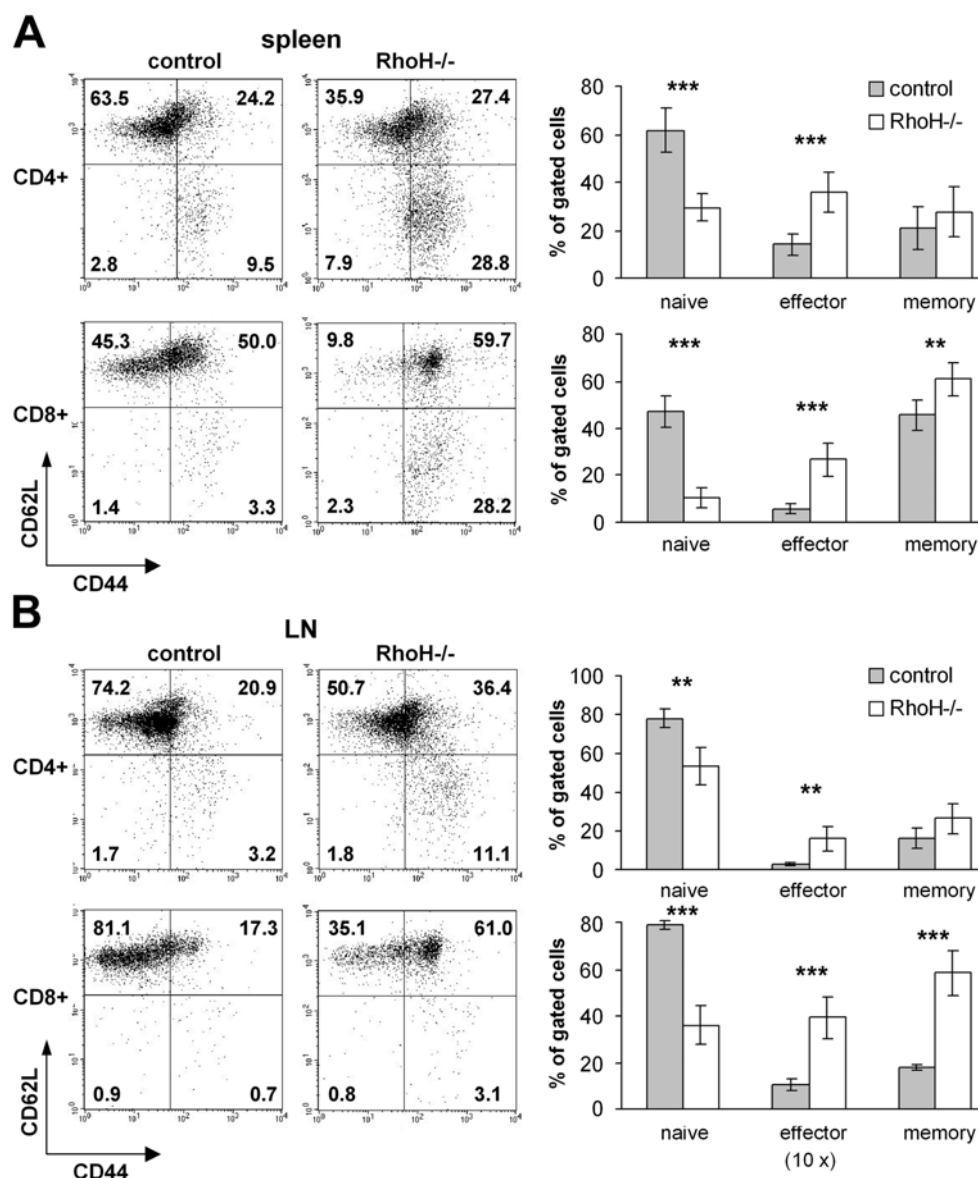
Figure 30. Reduced frequences of naive peripheral T cells. Splenocytes (A) and lymph node cells (LN; B) of 4-8 week old mice were analyzed for the expression of CD4, CD8, CD62L and CD44 by FACS. In the absence of RhoH, the percentages of naive cells (CD62L^{high}CD44^{low}) were decreased, whereas the relative amounts of effector (CD62L^{low}CD44^{high}) and CD8+ memory cells (CD62L^{high}CD44^{high}) were increased. The percentages of cells marked in histograms are shown in bar graph (**: $p<0.01$; ***: $p<0.001$; A; n=7/7; B; n=4/4).

4.4.4.4 Normal distribution of T and B cells within a peripheral lymphoid organ

Within secondary lymphoid organs, B and T cell areas are clearly distinguishable. In order to investigate whether T cells can localize properly within peripheral lymphoid organs, distribution of T cells in spleen of RhoH-mutant mice was analyzed. Cryosections of spleen of 2 month old control and RhoH-null mice were stained with antibodies against B cell marker B220 and T cell marker Thy1.2 to visualize B and T cell areas, respectively. No obvious differences between control and mutant mice were observed in the distribution of B

and T cells, implying that normal localization of T cells within secondary lymphoid organs can occur in in the absence of RhoH (Figure 31).
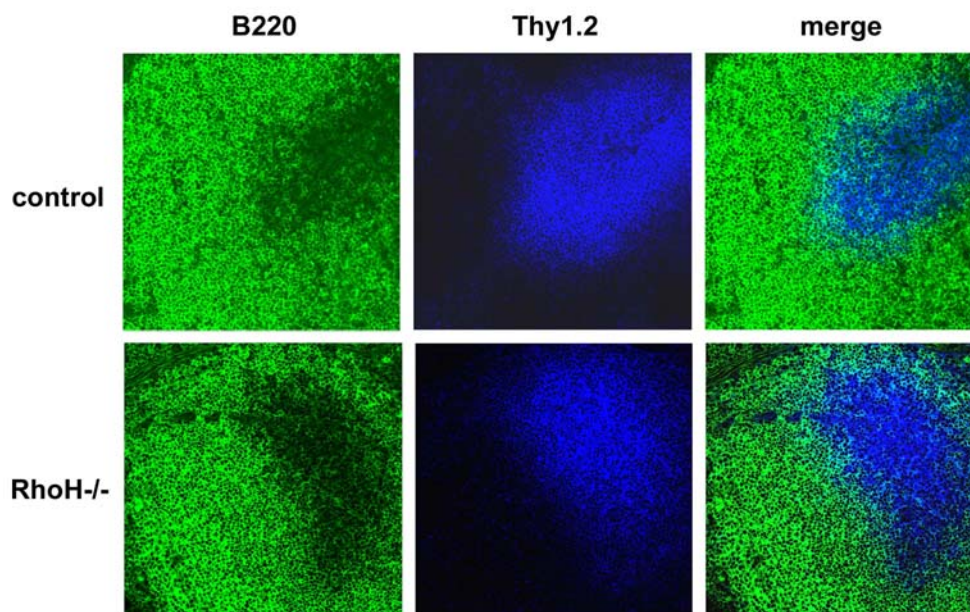
Figure 31. 2 month old RhoH-mutant mice showed normal B and T cell distribution within spleen. Spleen cryosections of 2 month old control and RhoH-mutant mice were stained with antibodies against B220 to detect B cells and Thy1.2 to detect T cells. RhoH-deficient T and B cells showed normal distribution in spleen. Picture magnification is 20x.

4.4.4.5   Aberrant proliferation and survival of thymocytes

To determine whether the impaired thymocyte development in the absence of RhoH is caused by defective proliferation or increased apoptosis, we assessed cell proliferation by measuring the incorporation of BrdU and apoptosis by examining the AnnexinV binding to thymocyte subpopulations.

The percentage of BrdU-incorporating, proliferating DN1 and DN2 thymocytes was not significantly different between control and mutant mice (Figure 32A). However, DN3 and DN4 cells showed significantly decreased proliferation in the absence of RhoH (Figure 32A), suggesting an impaired β-selection. Proliferation of DP cells was unchanged, while CD4SP and CD8SP cells showed increased proliferation (Figure 32A).

In DN1, DN2 and DN3 cells apoptosis was not significantly different between RhoH-null and control mice (Figure 32B). In contrast, RhoH-deficient DN4 cells displayed increased apoptosis (Figure 32B). Also DP, CD4SP and CD8SP thymocytes showed a higher percentage of AnnexinV+ apoptotic cells which might indicate that fewer cells are positively selected (Figure 32B).

Taken together, in the absence of RhoH, proliferation and apoptosis of thymocytes were deregulated which might explain the defects determined during T cell development. These data also suggest that RhoH regulates proliferation and cell survival independently and in a cell type and differentiation stage specific manner.
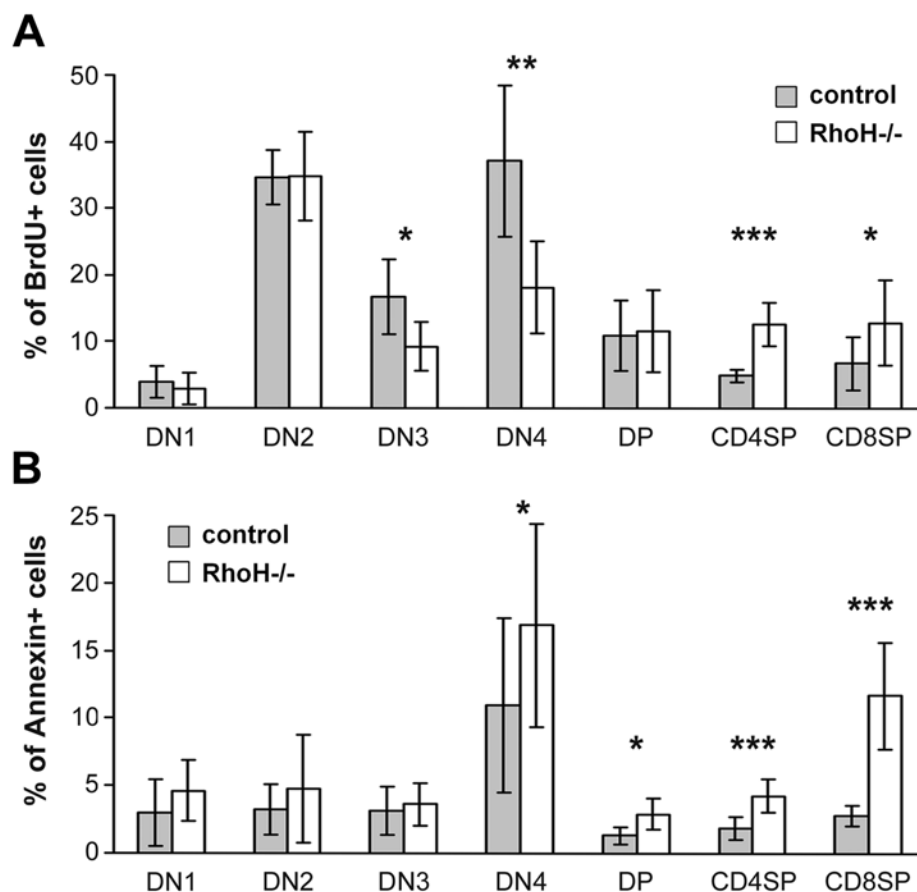
Figure 32. Impaired proliferation and survival of RhoH-null thymocytes. (A) Thymocytes of 2 month old mice were analyzed for proliferating, BrdU-incorporing cells. Different thymocyte populations were distinguished (s. Figure 26A, B; *: $p<0.05$; **: $p<0.01$; ***: $p<0.001$; DN1-DN4 n=6/10; DP, CD4SP, CD8SP n=8/10). (B) Thymocytes of 2 month old mice were analyzed for apoptotic, AnnexinV+ cells. Different thymocyte populations were distinguished (s. Figure 26A, B; *: $p< 0.05$; **: $p<0.01$; ***: $p<0.001$; DN1-DN4 n=10/10; DP, CD4SP, CD8SP n=8/9).

4.4.4.6   Altered expression of maturation markers on thymocytes

Having demonstrated that the survival and proliferation of thymocytes were affected in RhoH-deficient mice, we examined the differentiation status of thymocyte subpopulations by FACS using maturation markers TCRβ, CD5 and CD69. During thymocyte development the expression of TCRβ, CD5 and CD69 is tightly regulated by pre-TCR and TCR signaling.

TCRβ is part of the pre-TCR and TCR complex and is essential for thymocyte development. Surface expression of TCRβ chain and its association with pre-Tα in the DN3 cells is critical

for the transition of DN to DP thymocytes. Later, during positive selection, the surface expression of TCRβ increases after TCR engagement on DP and even more on CD4SP and CD8SP (Yamashita et al., 1993).

In RhoH-null mice, the number of more mature, TCRβhigh thymocytes was significantly decreased among DP, CD4SP and CD8SP cells as determined by flow cytometry, suggesting an impaired positive selection and decreased TCR signaling (Figure 33).

Figure 33. Impaired expression of TCRβ maturation marker in RhoH-null thymocytes. Thymocytes of 2 month old mice were analyzed for the expression of CD4, CD8, and TCRβ by FACS. The percentages of cells marked in histograms are shown in bar graph (**: $p < 0.01$; ***: $p < 0.001$; n=4/4).

Low levels of CD5 are expressed on immature DN thymocytes independent of TCR gene rearrangement (Azzam et al., 1998). CD5 surface expression is then upregulated on DN cells by pre-TCR signaling and maintained at intermediate levels on DP thymocytes by low affinity TCR-MHC interactions (Azzam et al., 1998). High-level expression of CD5 on DP and SP thymocytes is induced by engagement of the αβ TCR by positively or negatively selecting ligands. Relatively high levels of CD5 are maintained on mature peripheral T cells. The CD5 expression was found to directly parallel the signaling intensity of TCR-MHC-ligand interaction (Azzam et al., 1998). Investigation of CD5 surface expression on DN thymocyte subset revealed a higher percentage of cells with low CD5 levels in RhoH-deficient mice, suggesting reduced pre-TCR signaling (Figure 34A). At the DP stage the CD5 surface expression did not increase but remained significantly low on RhoH-null cells in contrast to control cells, indicating a defective TCR signaling (Figure 34A). In addition, the percentage of CD5low cells within CD4SP and CD8SP population in RhoH-deficient mice was increased, supporting the notion of defective TCR signaling (Figure 34A). Also in the periphery, the percentage of CD5low splenic T cells was increased in the absence of RhoH. Among the CD4+ splenocytes, the amount of CD5low cells increased from 2% to 24%, and among the CD8+ cells it rose from 4% to 18% (Figure 34C).

These findings indicate that RhoH is critical for pre-TCR and TCR signaling at the transition from DN3 to DN4 and from DP to SP thymocytes, respectively, thus regulating β-selection and positive selection. Furthermore, RhoH is also important for TCR signaling in mature T cells in the periphery.

Figure 34. Impaired expression of CD5 in RhoH-null thymocytes and splenic T cells. (A) Thymocytes of 2 month old mice were analyzed for the expression of CD4, CD8, and CD5 by FACS. The percentages of cells marked in histograms are shown in bar graph (***: p<0.001; n=9/9). (B) Thymocytes of 2 month old mice were analyzed for the expression of TCRγδ, CD3 and CD5 by FACS. The percentages of cells marked in histograms are shown in bar graph (**: p<0.01; n=2/2). (C) Splenocytes of 4-8 week old mice were analyzed for the expression of CD4, CD8, and CD5 by FACS. The percentages of cells marked in histograms are shown in bar graph (**: p<0.01; ***: p<0.001; n=5/4).

Within the γδ T cell subset the number of cells with low CD5 expression was likewise elevated in RhoH-null mice (Figure 34B), reflecting a possible defect in γδ TCR signaling. CD69, an 'activation marker' that is rapidly induced on mature T cells after stimulation through the TCR was also found to be upregulated on thymocytes during positive selection in response to TCR signaling (Swat et al., 1993): the low expression of CD69 on DP cells increases during the transition to SP thymocytes. RhoH-deficient DP thymocytes included significantly fewer CD69high cells in contrast to control as measured by FACS and less CD4SP and CD8SP thymocytes were CD69high in RhoH-deficient mice (Figure 35A),

indicating that positive selection might be impaired in RhoH-null thymocytes. No difference was found in the number of CD69high CD4+ and CD8+ T cells in spleen (Figure 35B).

The diminished expression of CD69 on RhoH-deficient thymocytes suggests that RhoH is important for TCR signaling and positive selection.
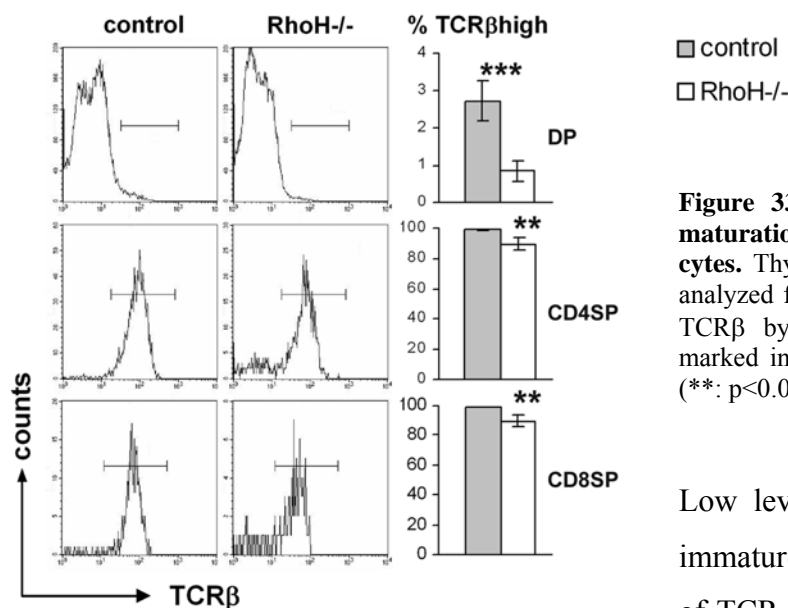

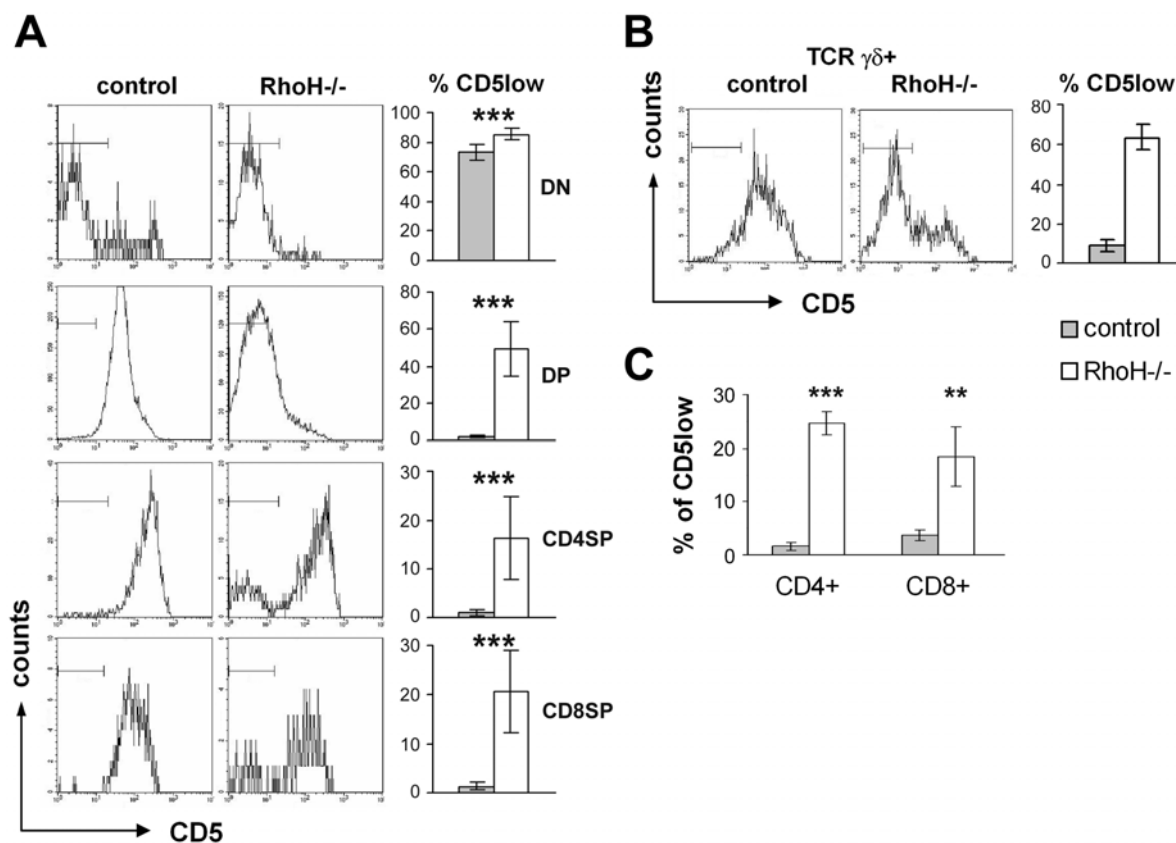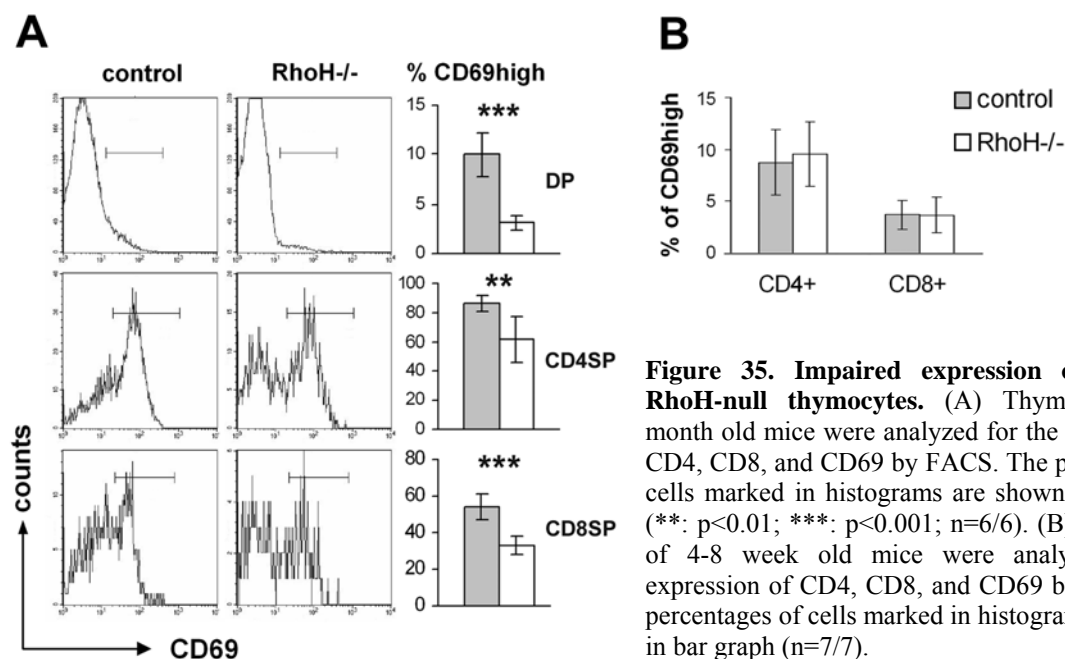**Figure 35. Impaired expression of CD69 in RhoH-null thymocytes.** (A) Thymocytes of 2 month old mice were analyzed for the expression of CD4, CD8, and CD69 by FACS. The percentages of cells marked in histograms are shown in bar graph (**: p<0.01; ***: p<0.001; n=6/6). (B) Splenocytes of 4-8 week old mice were analyzed for the expression of CD4, CD8, and CD69 by FACS. The percentages of cells marked in histograms are shown in bar graph (n=7/7).

4.5 T cell development *in vitro* and thymocyte positive selection in the absence of RhoH

4.5.1 Defective differentiation of DN thymocytes *in vitro*

To directly assess the differentiation potential of DN thymocytes in the absence of RhoH, the OP9-DL1 *in vitro* system for T cell development was applied. The BM OP9 epithelial cell line is derived from a macrophage colony-stimulating factor-deficient mouse (*op/op*) and is capable of supporting B cell development from HPCs (Kodama et al., 1994; Carlyle et al., 1997). The OP9 cell line transduced with the Notch ligand delta-like 1 (DL1) can no longer support B cell development, but induce T cell differentiation of both αβ and γδ lineages (Schmitt and Zuniga-Pflücker, 2002). The αβ T cell development on OP9-DL1 cells resembles that *in vivo*: T cell progenitors proceed through DN stages, reach the DP phase and become SP cells (Schmitt and Zuniga-Pflücker, 2002). OP9-DL1 cells express MHC class I but do not express MHC class II (Schmitt and Zuniga-Pflücker, 2002). Although a small number of mature CD8SP cells displaying high expression of TCR can be detected on OP9-DL1 cells, it is not clear to which extent OP9-DL1 cells can induce positive and negative selection of the CD8SP cells. (Schmitt and Zuniga-Pflücker, 2002). CD4SP cells most likely

do not receive a survival signal and die by neglect. However, CD4SP cells expressing low to intermediate TCR levels can be still generated on OP9-DL1 cells. These CD4SP cells probably represent developmental intermediates during CD4–CD8 commitment (Schmitt and Zuniga-Pflücker, 2002). All these observations suggest that the efficiency of positive selection appears to be low in this system and other factors unique to thymic stroma may be required for the positive and negative selection (Schmitt and Zuniga-Pflücker, 2006).

Since the partial block in the development of RhoH-deficient thymocytes occurred during DN3 to DN4 and during DN4 to DP transition, and no obvious defects in DN1 and DN2 stages in mutant mice were observed, we analyzed the differentiation capacity of DN3 and DN4 thymocytes. DN3 and DN4 subpopulations were sorted and differentiated *in vitro* on OP9-DL1 stroma for 4 and 8 days.

RhoH-deficient DN3 cells showed a significantly reduced ability to differentiate into DN4 and DP cells compared to controls after 4 and 8 days in culture (Figure 36A, C). In addition, the total cell number was severely lower in the absence of RhoH, indicating an impaired expansion potential (Figure 36A, C). Also, RhoH-null DN4 cells showed after 4 and 8 days a strongly reduced ability to develop into DP cells compared to controls and did not expand as well as the controls (Figure 36B, D).

These data demonstrate that in the absence of RhoH, the differentiation and expansion potential of both DN3 and DN4 are decreased, confirming the *in vivo* data. They furthermore prove that this is a cell autonomous defect of RhoH-null thymocytes.

When comparing the frequency of RhoH-deficient CD4SP and CD8SP cells developing from DN3 and DN4 thymocytes to control cells, no apparent defect in the differentiation of RhoH-mutant SP cells was observed, in contrast to differentiation of SP cells in RhoH-deficient mice (Figure 36). Contrasting results between *in vitro* and *in vivo* might be explained by the fact that positive and negative selection takes place *in vivo* but is not efficient *in vitro* in the OP9-DL1 system.

Figure 36. Impaired differentiation of RhoH-null DN3 and DN4 cells *in vitro*. Sorted DN3 cells were cultured for 4 (A) or 8 days [d] (C) on OP9-DL1 cells in the presence of IL-7 and Flt3 ligand. Differentiation from DN3 to DN4 was tested by FACS analysis of lineage negative cells for the expression of CD44 and CD25. RhoH-null cells showed a significantly higher percentage of DN3 cells and lower percentage of DN4 population. FACS staining for CD4 and CD8 revealed significantly increased levels of DN cells and reduced levels of DP cells in the absence of RhoH. Furthermore, cellularity of the RhoH-null cultures was about 5-fold (A) or 9-fold (C) decreased, indicating defective expansion in the absence of RhoH (**: $p<0.01$, ***: $p<0.001$; A, n=2/3; C, n=5/6). Sorted DN4 cells were cultured for 4 (B) or 8 days (D) on OP9-DL1 cells in the presence of IL-7 and Flt3 ligand. FACS staining for CD4 and CD8 revealed significantly increased levels of DN cells and reduced levels of DP cells in the absence of RhoH. Furthermore, cellularity of the RhoH-null cultures was about 15-fold (B) or 4-fold (D) decreased, indicating defective expansion of DN4 cells in the absence of RhoH (**: $p<0.01$; B, n=3/4; D, n=3/3).

A 4d culture of DN3 sorted thymocytes

B 4d culture of DN4 sorted thymocytes

C 8d culture of DN3 sorted thymocytes

D 8d culture of DN4 sorted thymocytes
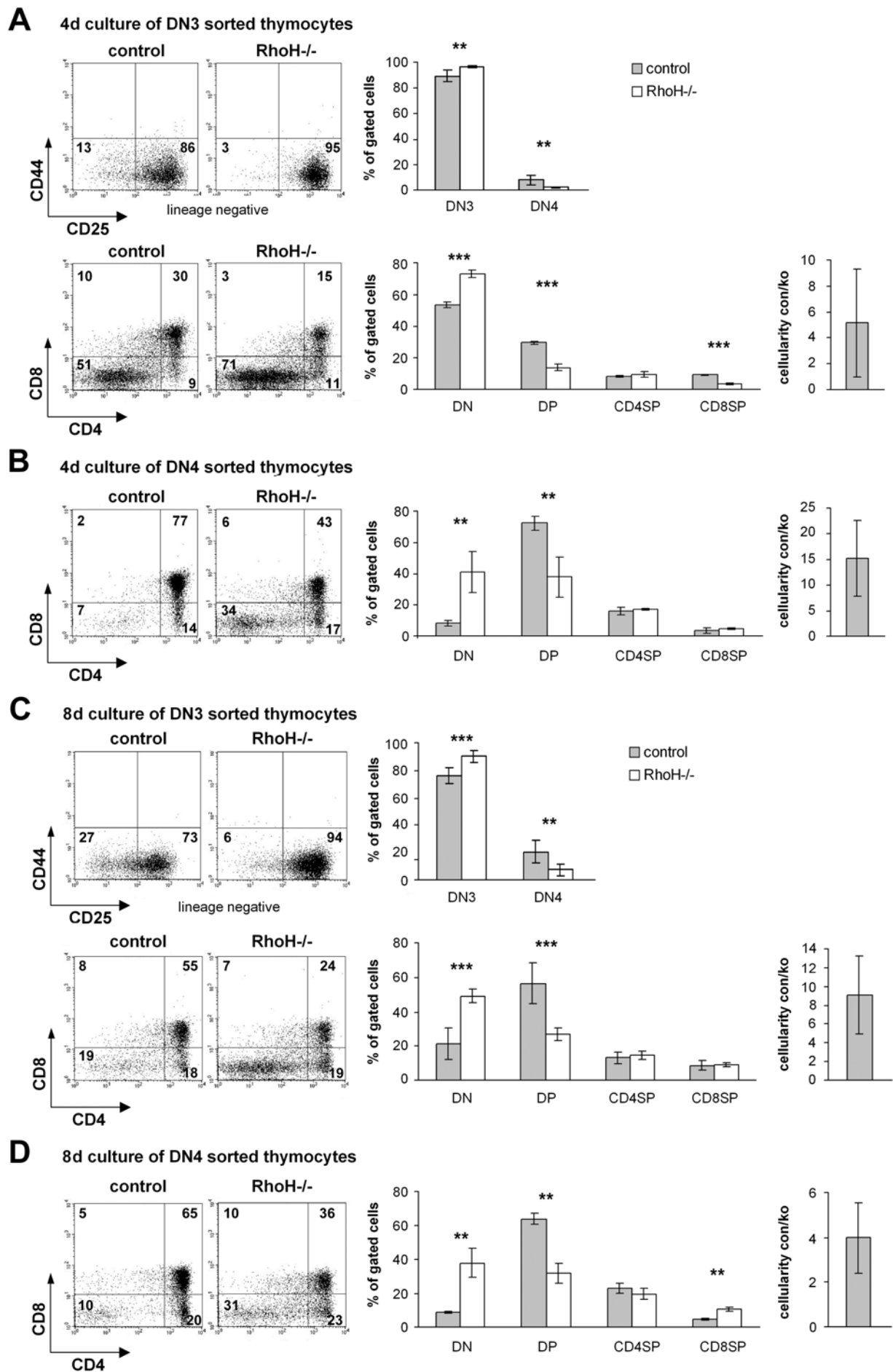
4.5.2   Defective positive selection of thymocytes

Since the aberrant expression of maturation markers TCRβ, CD5 and CD69 suggested an impaired positive selection of DP thymocytes into SP cells in the absence of RhoH, we analyzed positive selection of DP thymocytes into the CD4 lineage using an OT-II TCR transgenic model. We intercrossed RhoH-deficient mice backcrossed to C57BL6 with OT-II transgenic mice, which express an ovalbumin specific TCR restricted to MHC I-A^b as present in the RhoH-null mice and examined thymocyte subsets in these mice.

Control mice expressing OT-II TCR were expected to show an increase in CD4SP and decrease in DP and CD8SP thymocytes. Within the DN compartment, the DN4 population was supposed to be elevated and the DN3 population reduced.

In the OT-II TCR transgenic mice, the loci for the transgenic OT-II TCRβ and TCRα chain are already pre-rearranged, with the consequence that the rearrangement of the endogenous TCRβ and TCRα loci is largely suppressed and the OT-II TCRα and TCRβ chains are preferably expressed. OT-II TCRα and TCRβ pair and form together with CD3 the OT-II TCR, which is the predominant TCR expressed at the DN and later stages. The transgenic mice, however, are not on the RAG-/- background and express the recombination activating gene (RAG) enzyme, which is involved in the rearrangement of the *TCR* genes. Therefore, rearrangement of the loci for the endogenous TCRβ and TCRα chain can still occur, resulting in the endogenous pre-TCR and TCR expression at the DN and DP stage, respectively, although to a very low degree.

The assembly of and signaling through the OT-II TCR at the DN3 stage gives a positive signal for proliferation and survival, promoting further differentiation and resulting in the enlargement of the DN4 subset. At the DP stage of the thymocyte development, the low-affinity interaction between the OT-II-TCR on DP thymocytes and the MHC class II-self-antigen-complex on the thymic epithelial cells triggers TCR signaling that allows the development of CD4SP cells. CD8SP cells expressing OT-II TCR cannot be generated since OT-II TCR is MHC class II restricted and requires CD4 co-expression on a T cell for binding the antigen presenting cell.

FACS analysis of control mice expressing OT-II TCR confirmed our expectations. Control mice expressing OT-II TCR revealed a skewing to the CD4+ T cell subset and reduction of DP thymocytes (Figure 37A and Figure 26A). Very little CD8SP could be detected in mice expressing OT-II TCR (Figure 37A). Furthermore, the percentage of DN3 cells was decreased, while the DN4 population was increased (Figure 37B and Figure 26B). The ovalbumin TCR was expressed at the DN stage, as detected by Vα2 antibody recognizing the

TCRα chain: nearly 60% of DN cells in control mice expressed OT-II TCR (Figure 38A). Approximately 80% of DP thymocytes and nearly 100% of CD4SP cells carried OT-II-TCR (Figure 38A). In spleen, the skewing towards CD4 lineage was also detected and almost 100% of CD4+ splenic cells expressed OT-II-TCR (Figure 39).

In accordance to TCR signaling, the expression of CD5 increased in the transition from DN to DP and to CD4SP cells (Figure 38B), as well as the expression of the CD69 maturation marker rose on CD4SP cells in the control OT-II transgenic mice (Figure 38C).

A OT-II

	control		RhoH-/-	

(CD8 vs CD4 plots — control: 1.4, 44.8, 8.4, 45.4; RhoH-/-: 2.7, 70.7, 19.1, 7.5)

	control		RhoH-/-		
	average	stdev	average	stdev	
	x 10^6 cells				
cellularity	66,2	12,5	18,3	4,3	**
DN	5,3	1,7	3,6	0,9	
DP	36,9	1,3	12,9	3,1	***
CD4SP	26,6	11,7	1,3	0,3	*
CD8SP	0,7	0,1	0,2	0,1	***

B OT-II

	control		RhoH-/-	

(CD44 vs CD25 plots — control: 13.1, 3.1, 45.9, 37.9; RhoH-/-: 10.7, 2.8, 11.3, 75.2)

	control		RhoH-/-		
	average	stdev	average	stdev	
	x 10^5 cells				
DN1	7,8	3,4	4,1	1,6	
DN2	0,9	0,8	0,3	0,4	
DN3	5,6	8,5	7,9	6,5	
DN4	5,3	4,7	0,8	0,7	*

Figure 37. Defective positive selection in the absence of RhoH. (A) Thymocytes of 4-7 week old OT-II mice transgenic for an ovalbumin specific TCR, either expressing or not expressing RhoH were analyzed for the expression of CD4 and CD8 by FACS (upper panel). Quantification of absolute numbers of thymocyte subpopulations (lower panel; *: p< 0.05; **: p<0.01; ***: p<0.001; n=3/4). (B) Thymocytes of 4-7 week old OT-II mice transgenic for an ovalbumin specific TCR, either expressing or not expressing RhoH were gated for lineage negative (B220, CD4, CD8, NK1.1, Mac1, Gr-1, Ter119) cells and analyzed for the expression of CD25 and CD44. (DN1 (CD25-CD44+); DN2 (CD25+CD44+); DN3 (CD25+CD44-); DN4 (CD25-CD44-); upper panel). Quantification of absolute numbers of thymocyte subpopulations (lower panel; *: p< 0.05; n=3/4).

In contrast, RhoH-deficiency severely impaired generation of CD4SP cells in mice expressing the ovalbumin TCR, indicating a defect in positive selection (Figure 37A and Figure 26A). Moreover, no increase in DN4 population was observed, suggesting a defective β-selection, which controls the DN3 to DN4 transition (Figure 37B and Figure 26B). Consequently, no skewing towards CD4+ T cells in spleen was detected in RhoH-null mice expressing OT-II TCR (Figure 39).

The following data comprising the expression of TCRVα2, CD5 and CD69 on RhoH-deficient thymocytes confirm the assumption of impaired TCR signaling and defective positive selection. Among the DN cells, which upregulate Vα2 expression during β-selection,

RhoH-null mice showed a reduced amount of Vα2+ cells compared to controls (Figure 38A). Nearly all DP and CD4SP thymocytes expressed the ovalbumin specific TCR in mutant mice, although the expression level of Vα2 on DP cells was lower than in control OT-II transgenic mice and within the RhoH-deficient CD4SP cells and CD4+ splenocytes a population expressing lower Vα2 levels could be detected (Figure 38A and Figure 39).

Also in the presence of the ovalbumin TCR, the percentage of CD5low cells was higher on DN, DP and CD4SP thymocytes in RhoH-null mice compared to control transgenic mice (Figure 38B), and the relative amount of CD69high cells was lower on DP and CD4SP cells (Figure 38C).
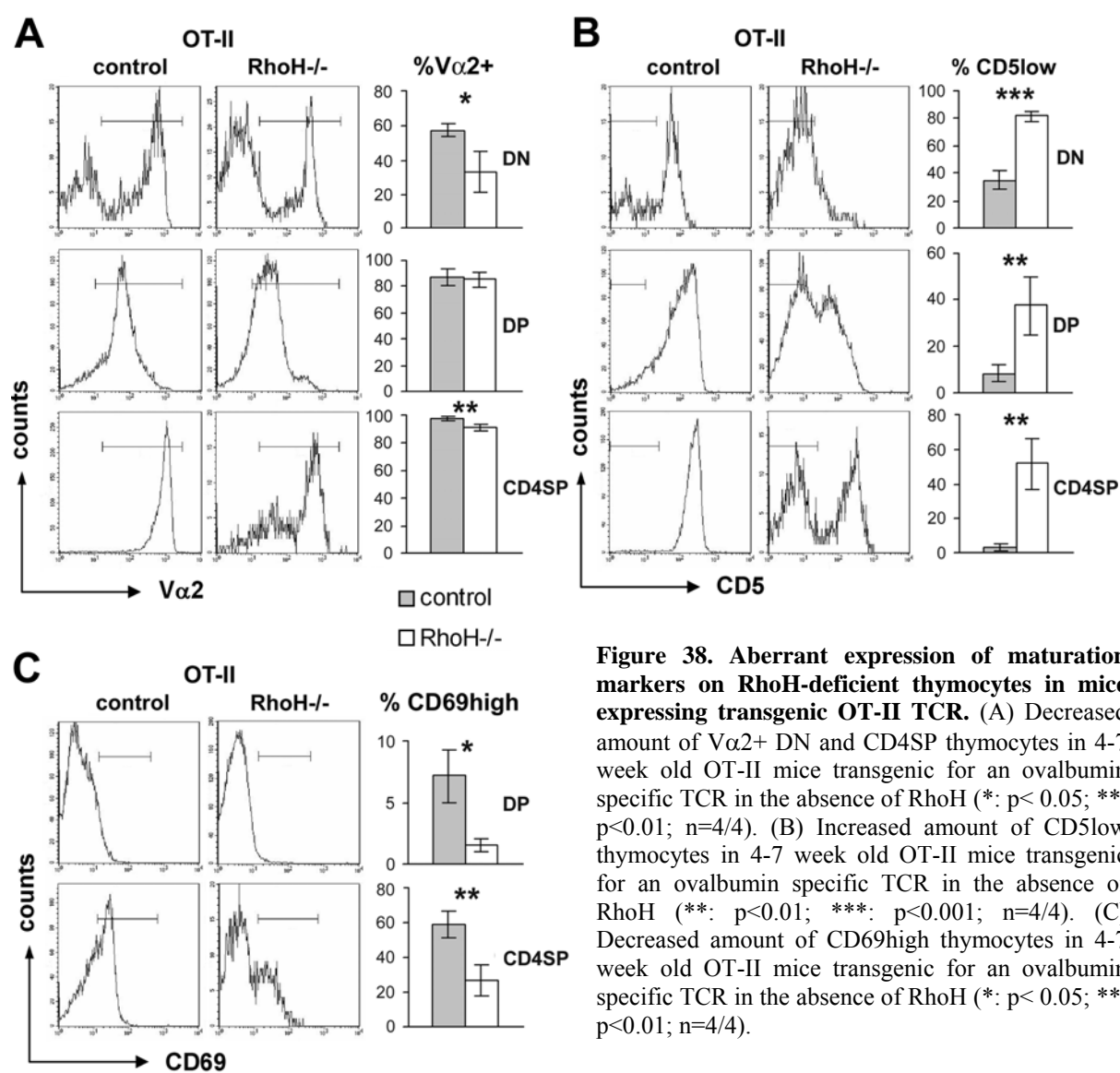
Figure 38. Aberrant expression of maturation markers on RhoH-deficient thymocytes in mice expressing transgenic OT-II TCR. (A) Decreased amount of Vα2+ DN and CD4SP thymocytes in 4-7 week old OT-II mice transgenic for an ovalbumin specific TCR in the absence of RhoH (*: $p < 0.05$; **: $p < 0.01$; n=4/4). (B) Increased amount of CD5low thymocytes in 4-7 week old OT-II mice transgenic for an ovalbumin specific TCR in the absence of RhoH (**: $p < 0.01$; ***: $p < 0.001$; n=4/4). (C) Decreased amount of CD69high thymocytes in 4-7 week old OT-II mice transgenic for an ovalbumin specific TCR in the absence of RhoH (*: $p < 0.05$; **: $p < 0.01$; n=4/4).
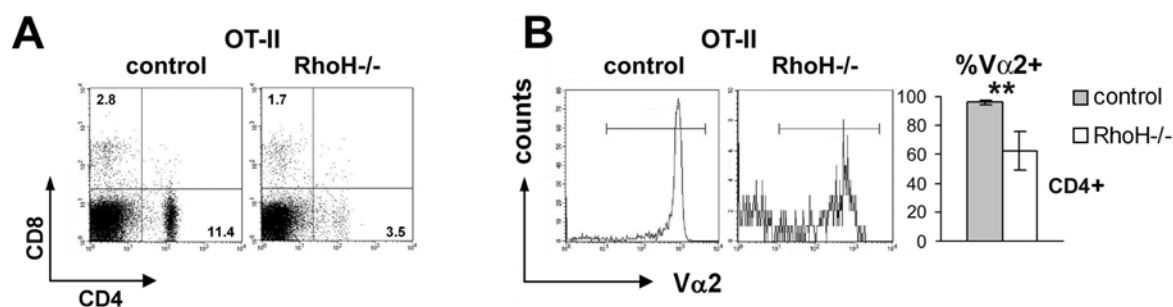
Figure 39. Reduced numbers of CD4+ splenocytes in mice expressing OT-II TCR in the absence of RhoH.
(A) Splenocytes of 4-7 week old OT-II mice transgenic for an ovalbumin specific TCR, either expressing or not expressing RhoH were analyzed for the expression of CD4 and CD8 by FACS. (B) Decreased amount of Vα2+ CD4+ splenocytes in 4-7 week old OT-II mice transgenic for an ovalbumin specific TCR in the absence of RhoH (*: $p < 0.05$; **: $p < 0.01$; n=4/4).

4.6 Biochemical analysis of signaling pathways in the absence of RhoH

4.6.1 Defective TCR signaling

The defects observed in the thymocyte development, in the expression of maturation markers and in the positive selection in RhoH-deficient mice are consistent with impaired TCR signaling. To test this possibility directly, we analyzed TCR signaling *in vitro*. We induced TCR signaling in FACS enriched preparations of DP and splenic CD4+ T cells by crosslinking biotinylated antibodies against CD3 or both CD3 and CD4 with streptavidin and investigated the activation of TCR signaling cascade by Western blot. In addition, we applied intracellular FACS staining to measure phosphorylation of signaling molecules in TCR-stimulated thymocyte preparations.

TCR engagement triggers as the earliest recognizable events the activation of the Src kinases lck and fyn, and ZAP70, a Syk-family kinase. Phosphorylation of lck at Y394 leads to activation of lck which in turn phosphorylates the ITAMs of CD3 and TCRζ molecules. ZAP70 is recruited to phosphorylated ITAMs and is phosphorylated by lck. After autophosphorylation at Y319, ZAP70 is activated and phosphorylates a number of proteins representing the distal events of TCR signaling. ZAP70-mediated phosphorylation of the scaffold protein LAT induces binding of various proteins, containing SH2-domains such as Gads/SLP-76/Vav1, Tec kinases, PLCγ1, PI-3K and Grb2. Together they form the LAT signalosome. Phosphorylation of the LAT-associated proteins initiates downstream events such as calcium influx or Erk activation.

We examined lysates of DP thymocytes and CD4+ splenic T cells in Western blot for tyrosine phosphorylated proteins (Figure 40). In control and mutant DP cells stimulation with CD3 and CD4 together resulted in a stronger tyrosine phosphorylation than treatment with CD3 alone

(Figure 40A). Although the pattern of tyrosine phosphorylated proteins was similar in control and mutant DP thymocytes and splenic CD4+ T cells, the extent of tyrosine phosphorylation of proteins visible at around 36, 50, 70 and 120 kD was reduced in RhoH-null cells (Figure 40). In the non-stimulated state the phosphorylated protein at 21 kD, which might correspond to phosphorylated TCRζ (p21ζ) chain, was absent in RhoH-deficient lysates (Figure 40).
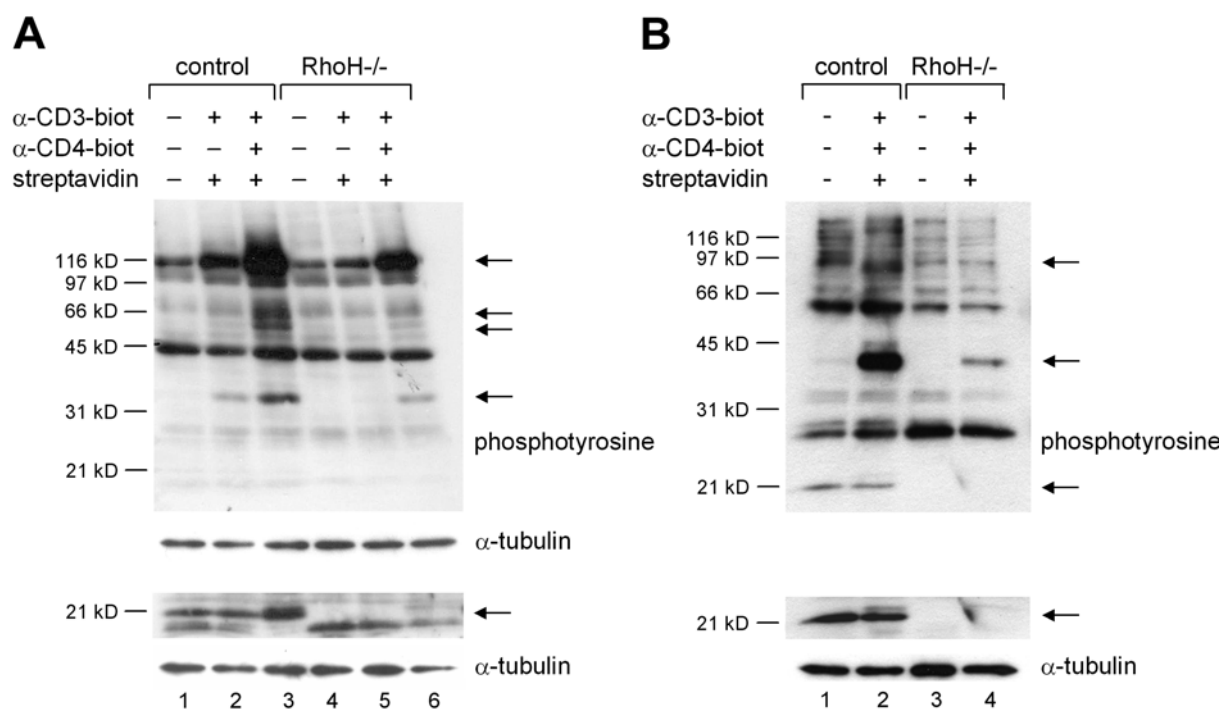
Figure 40. Impaired TCR-mediated tyrosine phosphorylation of RhoH-null DP thymocytes and CD4+ T cells. DP thymocytes (A) or CD4+ splenocytes (B) of 4-8 week old control and mutant mice were sorted by FACS or MACS beads, respectively. TCR signaling was stimulated as indicated for 5 min at 37°C. Total lysates were separated on SDS-PAGE (A; gradient gel) and analyzed by Western blot. Reduced tyrosine phosphorylation of proteins at around 21, 36, 50, 70 and 120 kD in RhoH-deficient DP (A) and splenic CD4+ T cells (B) after TCR activation. Representative results of 3 (A) or 1 (B) independent experiments.

4.6.2   Normal activation of proximal TCR signaling events

To determine in more detail, at which step of the TCR signaling cascade the absence of RhoH led to a reduction in activation, we measured the activation of different molecules involved in early and late events of TCR signaling.

In the absence of RhoH, TCR-induced phosphorylation of lck at Y505 was not altered in the absence of RhoH in DP and CD4SP cells (Figure 41A). Phosphorylation of Y505 occurs immediately after TCR engagement and negatively regulates lck. However, lck is simultaneously autophosphorylated at Y394, thus overriding this inhibition and leading to the active form of lck. TCR stimulation did not reveal any differences in ZAP70 phosphorylation

at Y319 in DP cells in the absence of RhoH (Figure 41C). Also in CD4SP cells, TCR dependent activation of ZAP70 did not require RhoH (Figure 41B). These data indicate that early events in TCR signaling, such as phosphorylation of lck and ZAP70, are not strongly affected by the loss of RhoH.

In CD4+ T cells, ZAP70 activates p38 MAPK independent of LAT (Salvador et al., 2005). In RhoH-null CD4SP thymocytes, p38 was weakly, but significantly, activated similar to controls (Figure 44C), suggesting that this downstream pathway of ZAP70 is normally intact in the absence of RhoH.
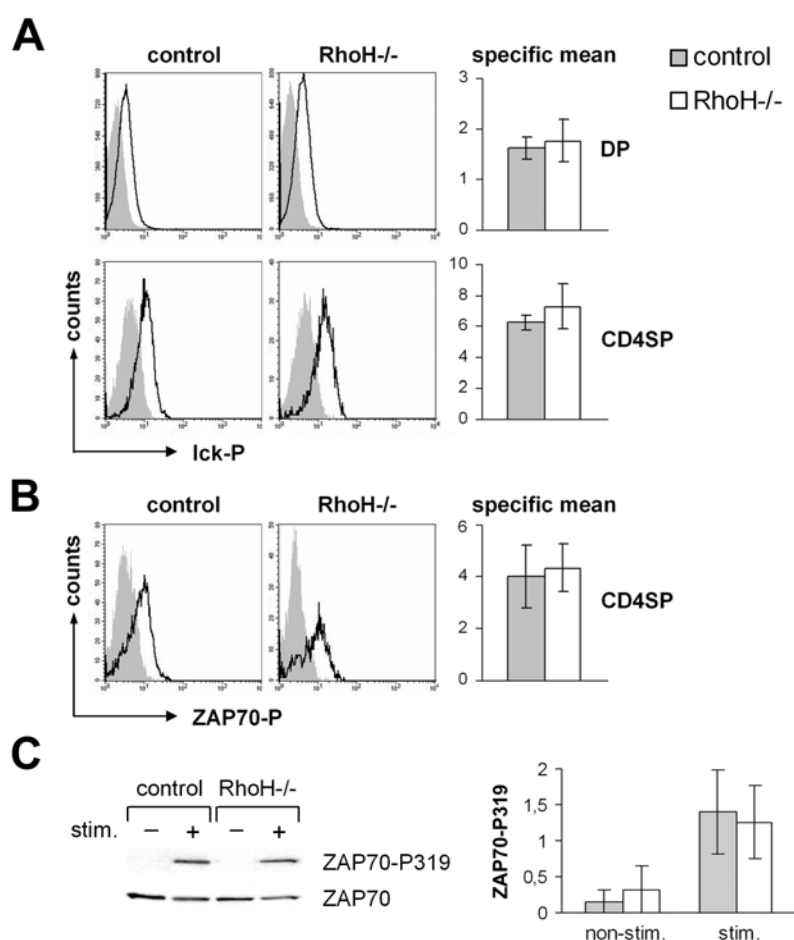
Figure 41. Normal TCR-mediated activation of the proximal events of TCR signaling in RhoH-deficient DP and CD4SP thymocytes. Thymocytes of 2 month old mice were stimulated with biotinylated antibodies CD3 and CD4 and streptavidin for 5 min at 37°C. Phosphorylation of lck(Y505) (A) and ZAP70(Y319)/Syk(Y352) (B) was measured by intracellular FACS. Different thymocyte populations were distinguished [histograms: filled (non-stimulated), line (stimulated)]. Differences between the mean of stimulated and non-stimulated (specific mean) cells are shown in bars (A, B; n=5/5). (C) DP thymocytes of 4-8 week old mutant mice were sorted by FACS. TCR signaling was induced as indicated by crosslinking of biotinylated CD3 and CD4 antibodies with streptavidin for 5 min at 37°C. Total lysates were analyzed by Western blot for ZAP70-P319 and ZAP70. Values are normalized to equal total amount of ZAP70 determined by Western blot. Bar graphs represent quantifications of 5 independent experiments.

4.6.3 Defective distal TCR signaling events

Although ZAP70 phosphorylation was normal, the ZAP70-mediated total tyrosine phosphorylation of LAT, a distal event of TCR signaling, was reduced in RhoH-null DP cells (Figure 42A). LAT has nine tyrosine residues which can be differentially phosphorylated allowing for a regulated binding of the SH2-domain containing proteins. Tyrosine phosphorylation of LAT at Y195, which is important for interaction of LAT with Gads/SLP-76 and indirectly

supporting the interaction of LAT with PLCγ1, was decreased in RhoH-deficient DP thymocytes (Figure 42B). Consequently, the phosphorylation of PLCγ1 at Y783, which is required for the activation of PLCγ1, was reduced in RhoH-null DP cells (Figure 42C). Also, the TCR-dependent phosphorylation of Vav1, recruited to LAT through Gads/SLP-76 binding, was lower in RhoH-mutant DP cells (Figure 42D).

However, the phosphorylation of Vav2, another member of Vav family, which is ubiquitously expressed in contrast to Vav1, was similar after TCR ligation in RhoH-deficient and control DP thymocytes (Figure 42E).
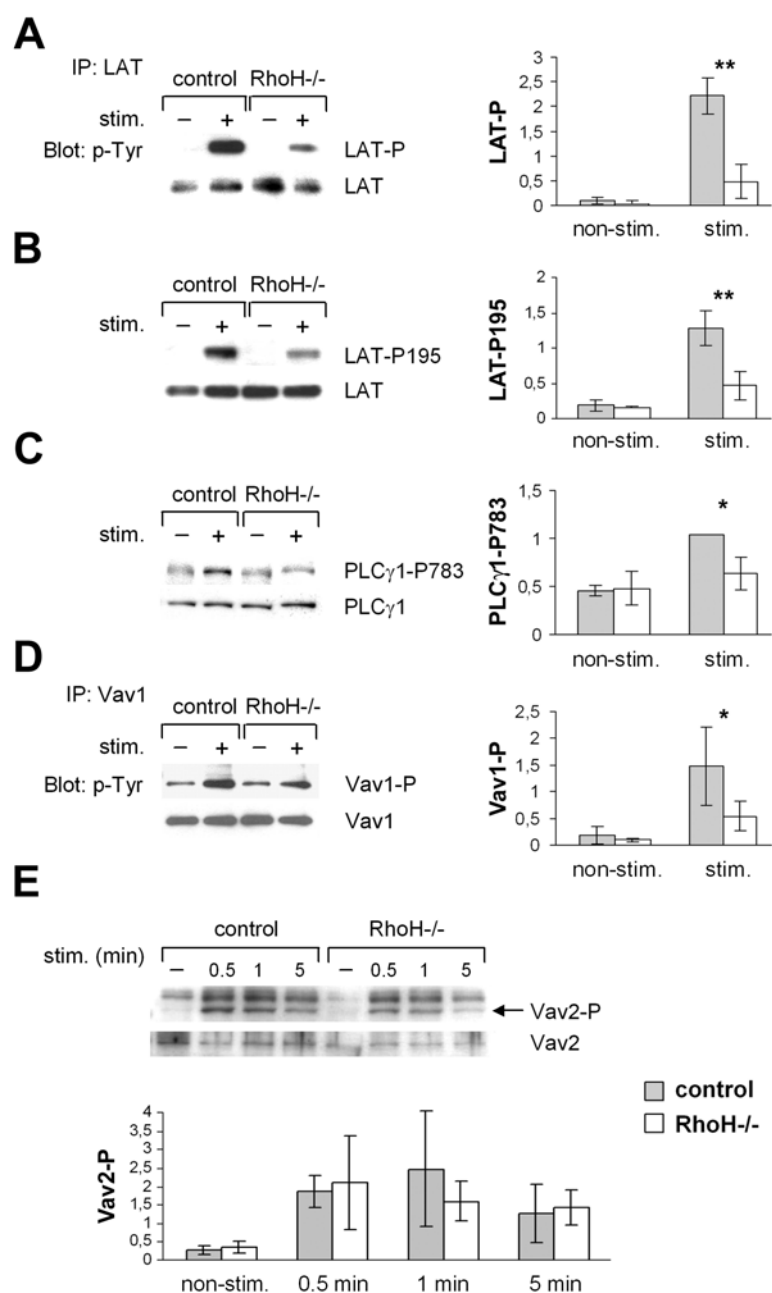
Figure 42. Impaired TCR-mediated activation of proteins forming the LAT-signalosome (distal events of TCR signaling) in RhoH-null DP thymocytes. DP thymocytes of 4-8 week old control and mutant mice were sorted by FACS or MACS microbeads. TCR signaling was induced as indicated by crosslinking of biotinylated CD3 and CD4 antibodies with streptavidin for 5 min (A-D) or indicated times (E) at 37°C. Total lysates were analyzed by Western blot for LAT-P195 (B), PLCγ1-P783 (C) and Vav2-P (E). Immunoprecipitations (IP) of LAT (A) and Vav1 (D) were blotted with anti-phosphotyrosine antibodies and reprobed with LAT (A) or Vav1 (D). Bar graphs represent quantifications of 3 (A-C), 4 (D) and 5 (E) independent experiments (*: $p<0.05$; **: $p<0.01$). All values are normalized to equal total amounts of the corresponding protein determined by Western blot.

4.6.4   Normal activation of Rac1 and Rac2

Despite the decreased TCR-induced activation of Vav1, which is important for the GEF activity of Vav1, activity of Rac1 and Rac2 after TCR activation was normal in RhoH-deficient DP cells (Figure 43). However, the basal level of Rac1 activity appeared to be higher in RhoH-null DP cells than in controls, suggesting either a compensatory upregulation of Rac1 activity in the absence of RhoH or an inhibition of basal Rac1 activity by RhoH (Figure 43A). Basal levels of active Rac2 were not significantly different between RhoH-mutant and control DP thymocytes (Figure 43B).
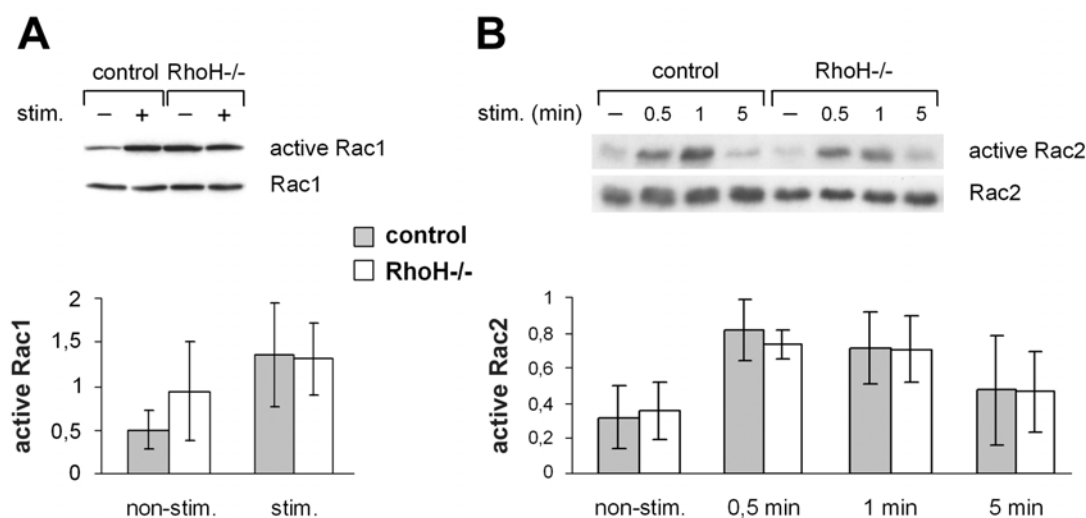
Figure 43. Normal TCR-mediated activation of Rac1 and Rac2 (downstream TCR signaling events) in RhoH-null DP thymocytes. DP thymocytes of 4-8 week old control and mutant mice were sorted by FACS or MACS microbeads. TCR signaling was induced as indicated by crosslinking of biotinylated CD3 and CD4 antibodies with streptavidin for 30 sec (A) or indicated times (B) at 37°C. Amounts of active Rac1 (A) and Rac2 (B) were determined by pulldown assays. Bar graphs represent quantifications of 10 (A) or 4 (B) independent experiments. All values are normalized to equal total amounts of the corresponding protein determined by Western blot.

4.6.5   Defective downstream TCR signaling events

We then tested TCR-dependent activation of Erk and calcium influx, which both require PLCγ1 activation and represent the downstream events. In the absence of RhoH, TCR-induced Erk phosphorylation was severely reduced in DP, CD4SP and CD8SP cells (Figure 44A, B). To assess TCR-induced calcium influx, thymocytes and splenocytes were loaded with the calcium-sensitive dye Fluo-4 and incubated with biotinylated antibodies against CD3. After induction of TCR signaling with streptavidin, the level of intracellular calcium was determined by FACS. Co-staining for CD4 and CD8 allowed us to distinguish DN, DP CD4SP and CD8SP cells. No strong calcium influx was detected in DN control and mutant

cells (Figure 45A). In DP, CD4SP and CD8SP cells, however, RhoH-deficient cells exhibited a significantly decreased percentage of cells responding to stimulation and a decreased mean fluorescence of all cells, indicating a partially impaired TCR-dependent calcium influx (Figure 45A). In addition, RhoH-deficient CD4+ and CD8+ splenocytes demonstrated a reduced stimulation of calcium influx after CD3 crosslinking, suggesting that RhoH is also important for TCR signaling in peripheral T cells (Figure 45B).

These data show that RhoH is required for TCR signaling downstream of ZAP70 in a cell autonomous manner, both in thymocytes and mature T cells.
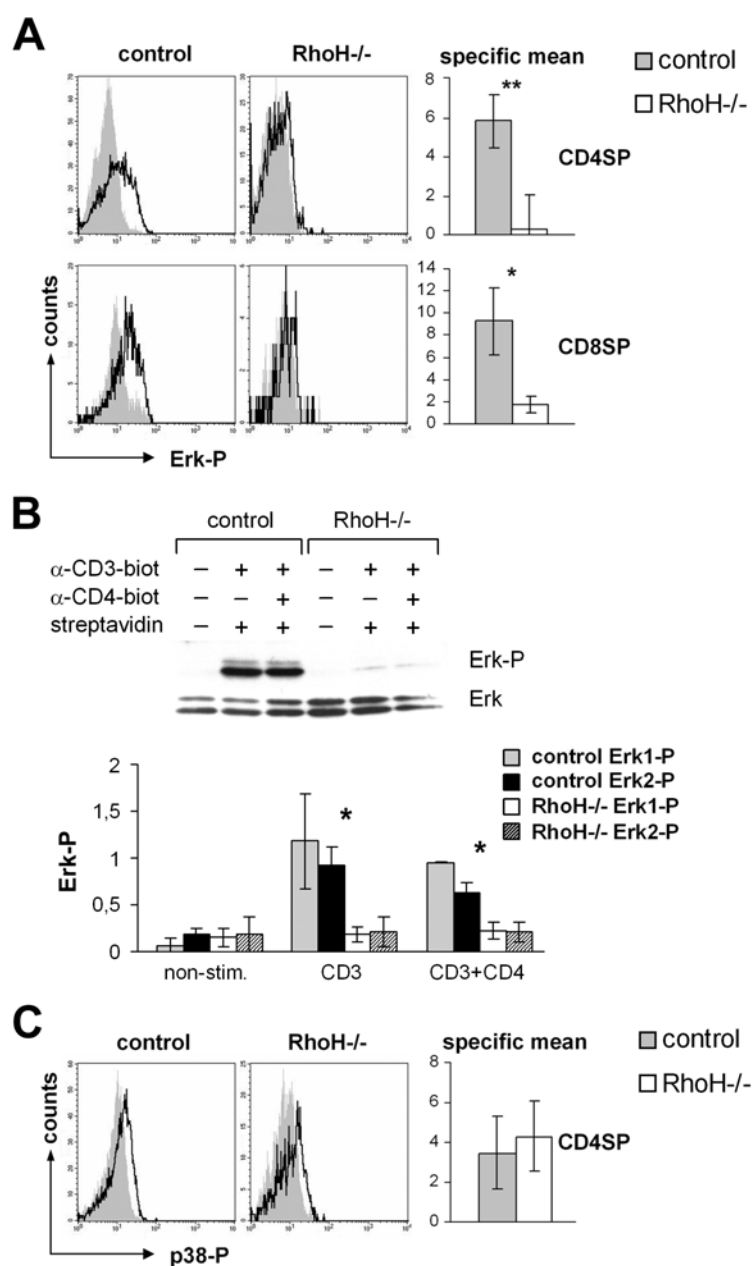
Figure 44. Impaired TCR-mediated activation of downstream TCR signaling events in RhoH-null DP and CD4SP thymocytes. Thymocytes of 2 month old mice were stimulated with biotinylated antibodies CD3 (A) or CD3 and CD4 (C) and streptavidin for 5 min at 37°C. Phosphorylation of Erk1/2 (T202/Y204) (A) and p38 MAPK (T180/Y182) (C) was measured by FACS. Different thymocyte populations were distinguished [histograms: filled (non-stimulated), line (stimulated)]. Differences between the mean of stimulated and non-stimulated (specific mean) cells are shown in bars [*: $p<0.05$; **: $p<0.01$; n=4/5 (A); n=5/5 (C)]. (B) DP thymocytes of 4-8 week old mutant mice were sorted by FACS. TCR signaling was induced as indicated by crosslinking of biotinylated CD3 and CD4 antibodies with streptavidin for 5 min at 37°C. Total lysates were analyzed by Western blot for Erk-P. Bar graphs represent quantifications of 3 independent experiments (*: $p<0.05$). All values are normalized to equal total amounts of the corresponding protein determined by Western blot.
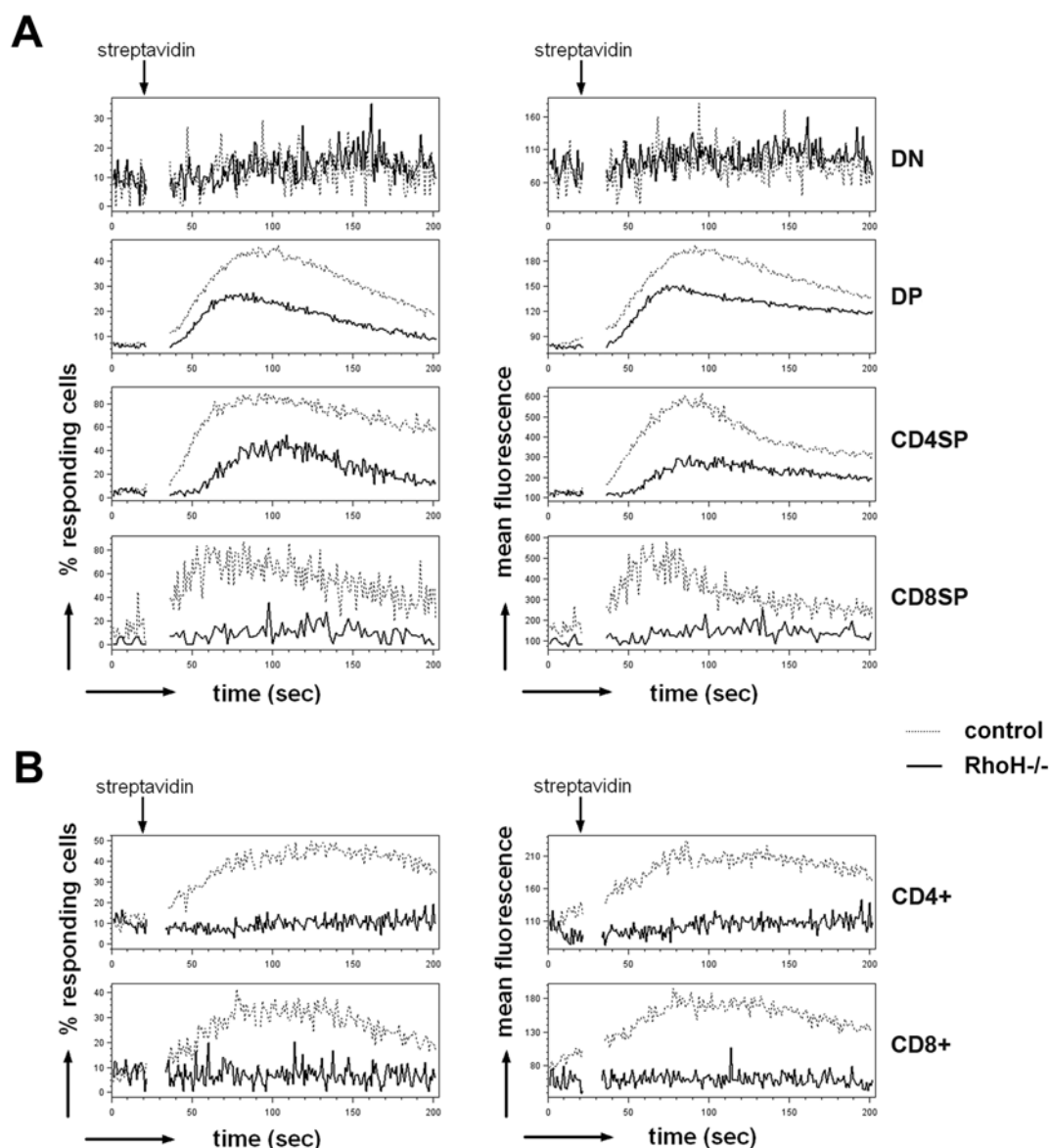
Figure 45. Defective calcium influx in RhoH-null thymocytes and mature T cells. Thymocytes (A) or splenocytes (B) of 2 month old mice were loaded with Fluo-4 and stained for CD4, CD8 and CD3. After warming up to 37°C, baseline Fluo-4 fluorescence was determined and TCR signaling was induced by crosslinking CD3 with streptavidin. Presented is the percentage of cells above threshold fluorescence (responding cells; left panel) and the mean fluorescence of all cells (right panel). Shown are representative results of 5 (A) or 2 (B) independent experiments.

4.7 Analysis of the immune response in the absence of RhoH

The reduced numbers of mature T cells and the impaired TCR signaling in thymocytes and splenic CD4+ T cells in the absence of RhoH suggested perturbed T cell dependent humoral immunity.

The primary immune response is triggered when a naïve T cell upon encounter with an antigen presented by a professional antigen presenting cell (APC), such as a DC, macrophage or B cell in the secondary lymphoid organ, is activated and becomes an effector T cell. DCs

are the most potent activators of T cells. CD8+ T cells recognize the processed antigen in the context of MHC class I on the APC and differentiate to cytotoxic T cells that can kill infected cells by releasing cytotoxins stored in special granula. CD4+ T cells bind antigens in the context of MHC class II and differentiate into the helper Th1 or Th2 cells. Th1 cells stimulate germ-killing activity of macrophages, while Th2 cells stimulate B cells to secrete antibodies. The effector T cells proliferate and either migrate to the site of the infection (as CD8+ T cells and Th1 cells) to remove pathogens or remain in the secondary lymphoid organs to activate B cells to produce antibodies (as Th2 cells). In the early phase of the immune response IgM is synthetized. This process is T cell independent. Later on, with the T cell help, class switching is initiated in B cells to produce IgG1, IgG2a, IgG2b, IgG3, IgE or IgA that have different functions in the immune response (Janeway et al., 2001). The class switch to a certain isotype depends on the cytokines produced by Th1 and Th2 cells. Th1 cells secrete IFN-γ, IL-2, TNF-α and TNF-β, favouring the class switch to IgG2a, IgG2b, IgG3 and IgA. Th2 cells generate IL-4, IL-5, IL-6 and IL-13, stimulating the production of IgG1 and IgE (Szabo et al., 2003). Thereby, these cells direct ongoing immune response through the secretion of cytokines. In germinal centres of lymphoid follicles, B cells activate SHM leading to affinity maturation of antibodies which can recognize the pathogens with higher affinity. During secondary immune response memory T and B cells, which develop at the time of the primary immune response, can counteract the pathogens with more efficiency.

To determine whether the loss of RhoH affects antibody production, we immunized control and RhoH-null mice with the T cell dependent (TD) antigen nitrophenyl-chicken-γ-globulin (NP$_{20}$-CG) and studied the development of the immune response. Immunization with NP$_{20}$-CG will lead mainly to a Th2 response, resulting in a production of IgG1 and to a lesser degree to a production of IgG2a and IgG3, characterizing a Th1 response.

RhoH was reported to be expressed stronger in Th1 subset of CD4+ T cells than in Th2 cells, another subset of CD4+ helper T cells, indicating that in the absence of RhoH, there might be a skewing of helper CD4+ T cells towards Th2 subset in the course of the immune response. The dominance of Th2 cells might lead to a shift in the secretion of cytokines towards Th2 type that in turn would induce a skewing of antibody isotypes towards IgG1. Therefore we compared the serum concentrations of NP$_{20}$-CG specific antibodies of IgG2a and IgG3 isotypes, which prevail in a Th1 response, with the concentration of antibodies of the IgG1 isotype, which is indicative of a Th2 response, at different time points after immunization. The NP$_{20}$-CG specific titers of antibodies were determined by means of ELISA.
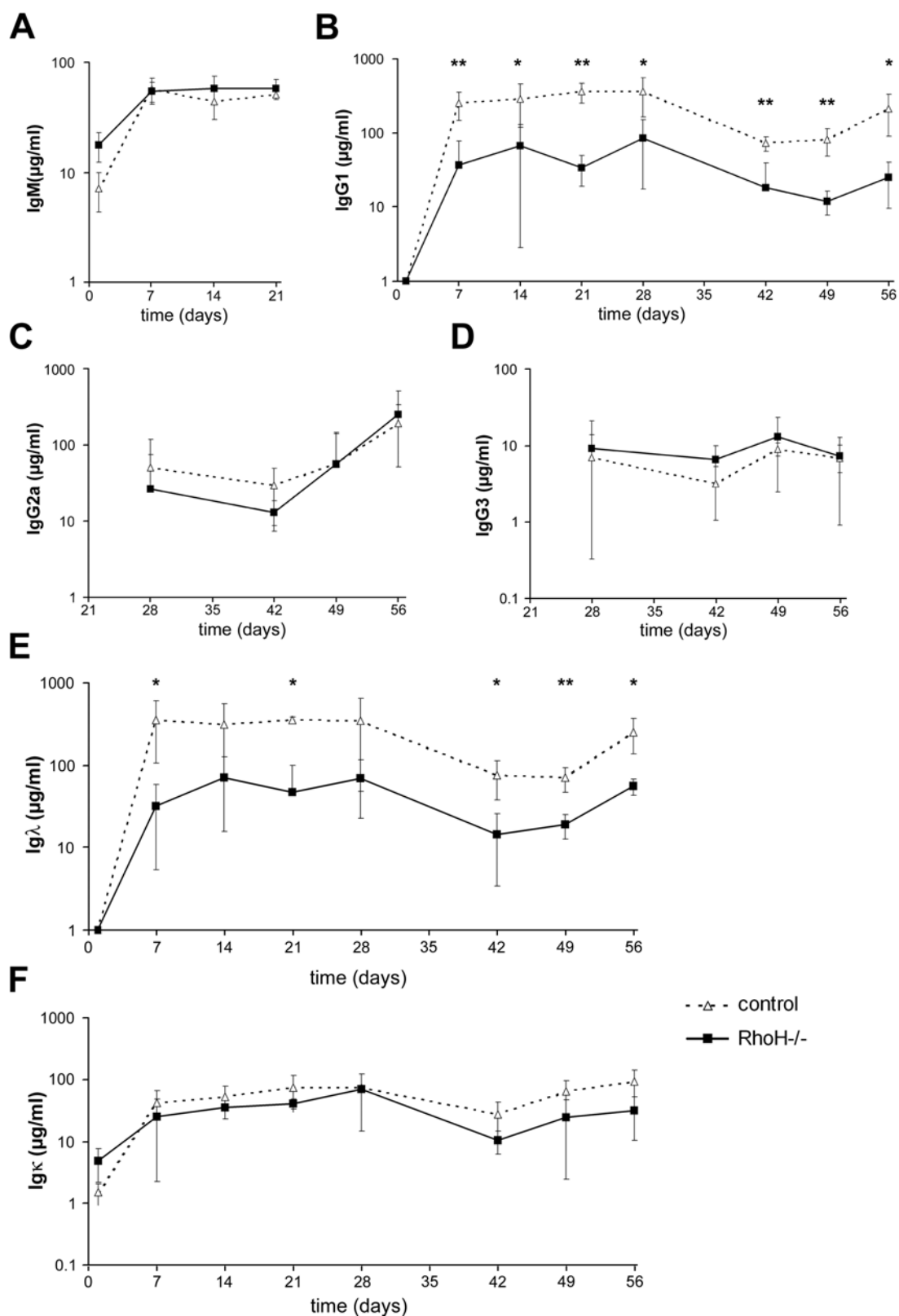
Figure 46. Impaired T cell dependent production of IgG1 and Igλ antibodies in RhoH-deficient mice. 2 month old control and RhoH-deficient mice were intraperitoneally injected with NP_{20}-CG and boosted on day 42. Production of NP_{20}-CG specific IgM (A) was determined by ELISA after 7, 14 and 21 days. Serum levels of NP_{20}-CG specific IgG2a (C) and IgG3 (D) were measured after 28, 42, 49 and 56 days. Response of NP_{20}-CG specific IgG1 (B), Igλ (E) and Igκ (F) antibodies was examined after 7, 14, 21, 28, 42, 49 and 56 days. [days 1-42: n=5/5; days 49-56: n=5/4); *: p<0.05; **: p<0.01; y axis is logarithmic].

The production of the IgM antibody, which is the first isotype to emerge in a humoral immune response and which does not require T cell help, was not changed after 7, 14 and 21 days in RhoH-null mice compared to controls (Figure 46A). IgM molecules form pentamers with 10 binding sites and therefore display high stickiness which could explain the relatively high levels of NP_{20}-CG specific IgM titer before the immunization in both RhoH-mutant and control mice (Figure 46A).

IgG production is dependent on T cell help. Before the NP_{20}-CG injection, IgG1 antibodies were below the detection threshold in RhoH-null and control mice (Figure 46B). During the primary response (day 1 to day 28) the IgG1 titer was induced and maintained at higher levels than IgM titers in control mice. At day 42 the titer fell and began to increase again during memory response in control mice (Figure 46B). In RhoH-deficient mice, the IgG1 antibody production followed the IgG1 response in control mice. However, the levels of IgG1 antibodies during initial response as well as after the boost immunization were reduced, demonstrating that the Th2 type and the memory response were affected (Figure 46B).

The titers of IgG2a and IgG3 were determined at the end of the initial immunization at day 28 and during the booster response at the days 42, 49 and 56. The production of IgG2a and IgG3 is T cell dependent. IgG3 levels were low at all time points and exhibited no significant differences between RhoH-null and control mice (Figure 46C, D). The titers of IgG2a antibodies increased in the course of the memory response and were similar in RhoH-mutant and control mice (Figure 46C, D). In contrast to our expectations, these data revealed no skewing towards a Th2 type response.

Next, we tested the production of immunoglobulin light chain Igκ and Igλ. The distribution of κ and λ light chains paired with the heavy chain depends on the mouse strain and the carrier protein bound to the hapten. The immunization with NP_{20}-CG elicits the production of λ chain over κ chain. In the mice on the mixed background C57BL6/129Sv the NP_{20}-CG immunogen induced predominantly Igλ antibodies. After the first NP_{20}-CG injection Igλ titers increased and were maintained at high levels during the primary reaction (Figure 46E). The Igλ titers decreased in the time from day 28 to day 42 and rose again during booster response in controls. The levels of Igλ were reduced during primary and memory response in the absence of RhoH (Figure 46E). The development of Igκ antibody response was similar to Igλ, however the Igκ levels were lower than those of Igλ. During the primary response, the Igκ titers were not different between control and RhoH-deficient mice, while during secondary response they were slightly, although not significantly, reduced in the absence of RhoH (Figure 46F).

Taken together, the T cell independent induction of IgM antibodies was not affected by the loss of RhoH, whereas the T cell dependent class switching to IgG1 and Igλ was impaired in the absence of RhoH. No indication of skewing to Th2 type response was observed.

4.8 β2-integrin-mediated adhesion in the absence of RhoH and T cell development in the absence of both RhoH and β2-integrin

4.8.1 Normal β2-integrin-mediated adhesion of RhoH-deficient cells

Previously, Cherry et al. reported that RhoH is required to maintain the integrin LFA-1 (αLβ2) in a non-adhesive state on lymphocytes (Cherry et al., 2004). LFA-1 is involved in lymphocyte migration, in the processes of eliciting an immune response and formation of immunological synapse.

To investigate whether the assigned function of RhoH leads to increased adhesiveness of thymocytes and thus participates in the defects observed in the thymocyte development in the absence of RhoH, we measured the adhesion of RhoH-null and control thymocytes to immobilized ICAM-1, one of the LFA-1 ligands. Adhesion of α4β1-integrin to VCAM-1 was assessed as a control for LFA-1-independent binding.

The adhesion assays were conducted in two series of experiments which differed slightly in the conditions. Manganese (Mn^{2+}) and PMA were applied to activate the integrins through "outside-in-signaling" and "inside-out-signaling", respectively. Mn^{2+} increases the integrin affinity by inducing the conformational change of the extracellular domain, while PMA stimulates activation of integrins through intracellular signals. To exclude the possible influence of the loss of already one RhoH allele on the cell adhesiveness, the binding of RhoH-null thymocytes was compared to that of wild type (+/+) and RhoH heterozygous (+/-) cells. Since no differences in adhesion between wild type and RhoH heterozygous thymocytes were observed at all conditions tested, the +/+ and +/- genotypes are referred as controls in the following section.

The basal binding to ICAM-1 determined in the medium or in the presence of magnesium (Mg^{2+}) was low both for RhoH-null and control thymocytes (Figure 47). The basal adhesion to VCAM-1 was a little higher than to ICAM-1 for RhoH-deficient and control thymocytes (Figure 47). In the presence of EDTA, that abrogates integrin-mediated binding, the adhesion to ICAM-1 and VCAM-1 of RhoH-mutant and control thymocytes was in the same range as the binding to ICAM-1 in the presence of Mg^{2+} (Figure 47B). Mn^{2+} (2mM) or PMA (100 ng/ml) activated RhoH-null thymocytes bound to ICAM-1 with an efficiency equal to control

cells (Figure 47A). Also at lower concentrations of Mn^{2+} (1 mM) or PMA (20 ng/ml), and at combination of Mn^{2+} and PMA, which has an additive effect on integrin activation, binding to ICAM-1 was similar in RhoH-deficient and control thymocytes (Figure 47B). This demonstrates that LFA-1 mediated adhesion of thymocytes is normally regulatable in the absence of RhoH, at least under the conditions tested. Adhesion to VCAM-1 was indistinguishable between control and mutant thymocytes, stimulated with Mn^{2+} or PMA (Figure 47).
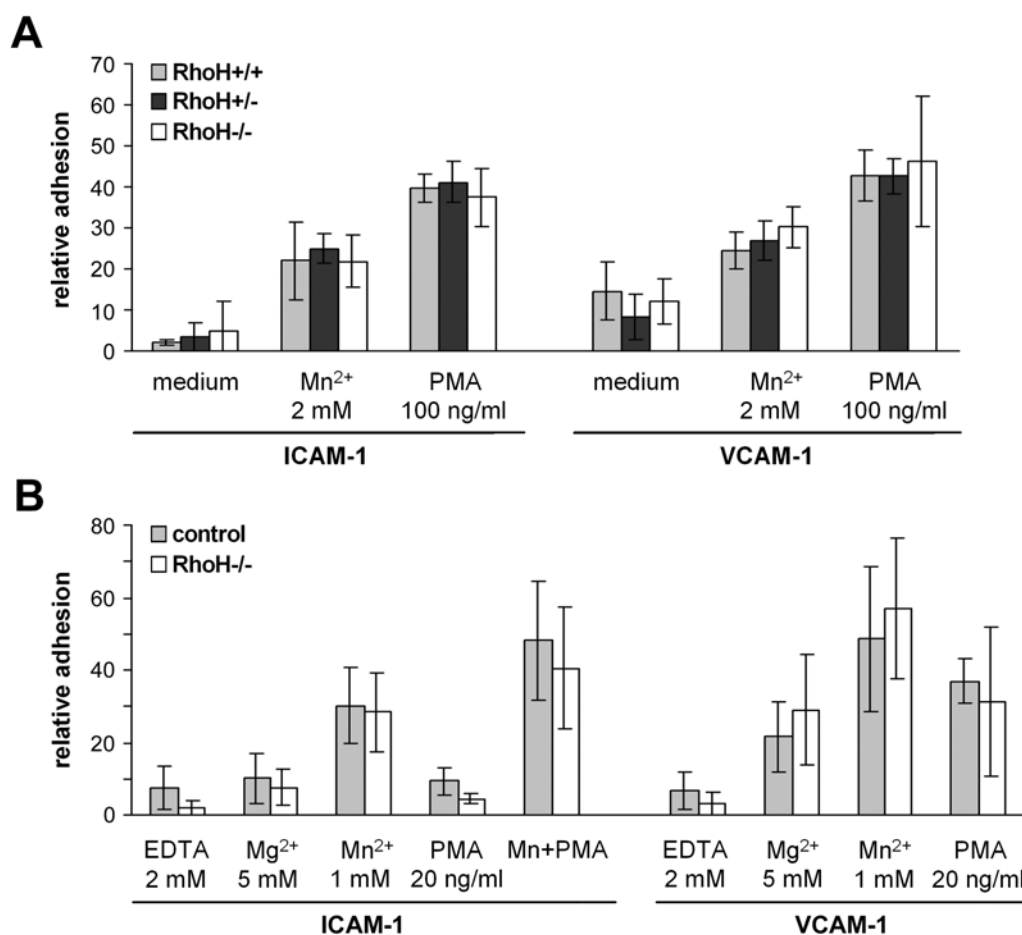
Figure 47. Normal adhesion of RhoH-null thymocytes to ICAM-1 and VCAM-1. (A) Relative adhesion of thymocytes from 4-8 week old mice to the immobilized αLβ2 ligand ICAM-1 and to the α4β1 ligand VCAM-1. Integrins were activated by treatment with 2 mM Mn^{2+} or 100 ng/ml PMA as indicated. Adhesion of wild type (RhoH+/+), heterozygous (RhoH+/-) and homozygous RhoH-null thymocytes (RhoH-/-) was indistinguishable at all conditions tested (n=1/2/3). This experiment was performed by Dr. Melanie Laschinger. (B) Relative adhesion of thymocytes from 4-8 week old mice to the immobilized αLβ2 ligand ICAM-1 and to the α4β1 ligand VCAM-1 is shown. Non-specific interaction was determined in the presence of EDTA. Different extents of integrin activation were achieved by treatment with 5 mM Mg^{2+}, 1 mM Mn^{2+}, 20 ng/ml PMA, and Mn^{2+} and PMA [ICAM-1 (EDTA: n=6/6; Mg: n=8/8; Mn: n=8/8; PMA: n=4/4; Mn+PMA: n=8/7); VCAM-1 (EDTA: n=6/6; Mg: n=8/7; Mn: n=8/7; PMA: n=4/4)].

In a more physiological setting, we furthermore examined the adhesion of T cells to the endothelial cell lines bEnd5 and bEndI1.1 (Reiss et al., 1998). To stimulate T cell adhesion, splenic cells were activated with Concanavalin A to T⁺ cell blasts. bEnd5 endothelial cells

express ICAM-1 and no VCAM-1. Upon treatment with TNF, bEnd5 cells upregulate expression of ICAM-1 and VCAM-1. bEndI1.1 endothelia cell line is ICAM-1-deficient and shows the same VCAM-1 expression profile before and after TNF treatment as bEnd5. RhoH-deficient and control T cells demonstrated low binding to bEnd5 cells, and even lower adhesion to ICAM-1-null bEndI1.1 cells. Both RhoH-null and control T cells revealed TNF-stimulated binding to bEnd5 endothelial cells which was not affected by a control antibody but which was partially inhibited by antibodies against LFA-1 or α4-integrin, respectively (Figure 48).

The binding of control and RhoH-null T cells to the ICAM-1-deficient cell line bEndI1.1 slightly increased upon treatment with TNF, but was much lower in comparison to adhesion to bEnd5 cells (Figure 48). This binding was based mainly on VCAM-1/α4β1-integrin interactions It was inhibited by antibodies against α4-integrin, resulting in a similar binding as under condition without TNF treatment, while remaining insensitive to control or LFA-1 antibody inhibition. These data suggest normal adhesion of LFA-1 to ICAM-1 in the absence of RhoH.
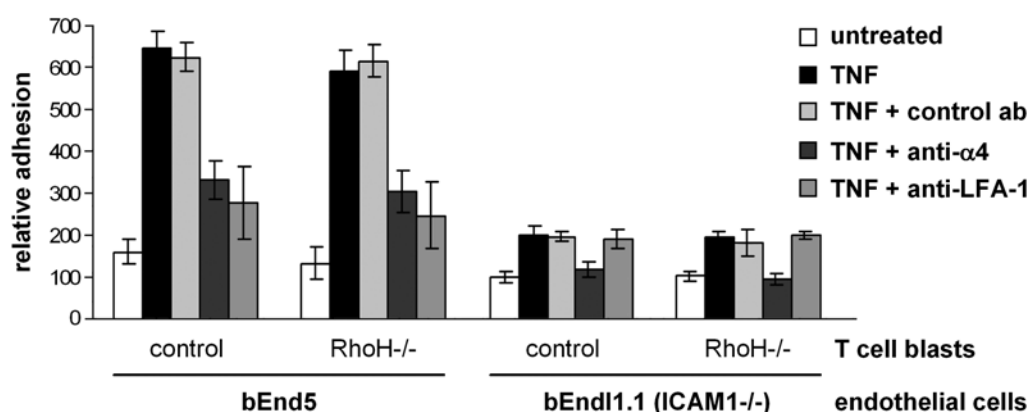
Figure 48. Normal adhesion of RhoH-null T cell blasts to the endothelial cells. Relative adhesion of T cell blasts to the endothelial cell line bEnd5 and the ICAM-1-deficient endothelial cell line bEndI1.1 (ICAM1-/-). Adhesion was stimulated by treating the endothelial cells with TNF. Antibodies against β2-integrin and LFA-1 were used to determine the specific contribution of these adhesion receptors to the attachment. An unrelated antibody was added as a control for non-specific effects. Wild type (RhoH+/+), heterozygous (RhoH+/-) and homozygous (RhoH-/-) RhoH-null T cell blasts showed indistinguishable adhesion at all conditions tested (n=2/2/4). This experiment was performed by Dr. Melanie Laschinger.

4.8.2   No rescue of thymocyte development by ablation of β2-integrin

To investigate by an alternative approach, whether RhoH-dependent modulation of β2-integrin function is involved in the defective thymocyte development in RhoH-null mice, we

crossed RhoH-deficient mice with mice lacking β2-integrin and analyzed T cell development in the absence of both RhoH and β2-integrin. If loss of RhoH indeed constitutively upregulated αLβ2 activity and thus contributed to the observed thymocyte phenotype, ablation of the *β2-integrin* gene would logically rescue the defect. However, we found that population sizes of DN, DP, CD4SP and CD8SP thymocytes were identical in RhoH-null and RhoH-β2-integrin-double knockout mice in comparison to controls (Figure 49), implying that the defective thymocyte development is not rescued through the inactivation of the *β2-integrin* gene. Furthermore, the increase of CD5low cells in different RhoH-null thymocyte populations was unaffected by the additional loss of β2-integrin (Figure 50). These data indicate that the impaired thymocyte development of the RhoH-null mice is independent of β2-integrin function.
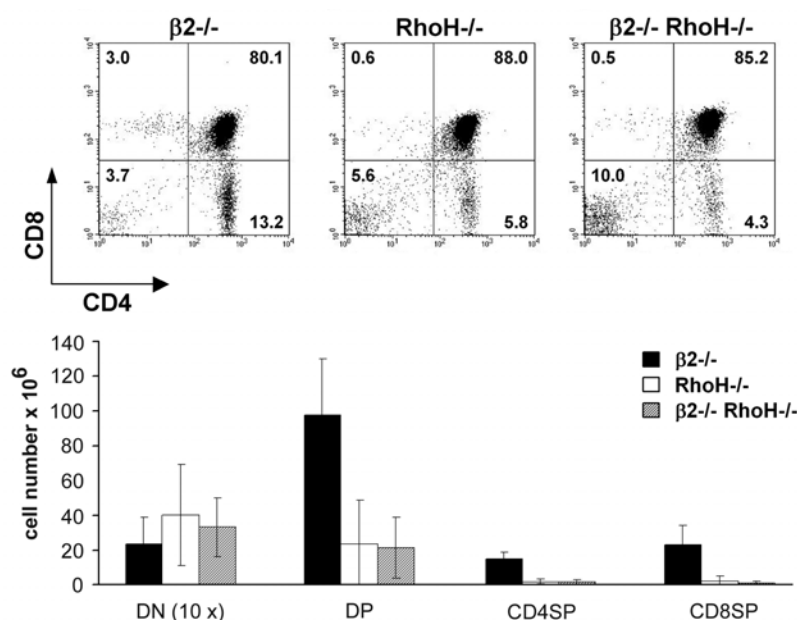
Figure 49. RhoH does not affect thymocyte development via regulation of β2-integrin-mediated adhesion. Thymocytes of 6-10 week old β2-integrin-null, RhoH-null and β2-RhoH-double knockout mice were analyzed for the expression of CD4 and CD8 by FACS. Bar graph presents the absolute cell numbers of each population (n=3/3/3).
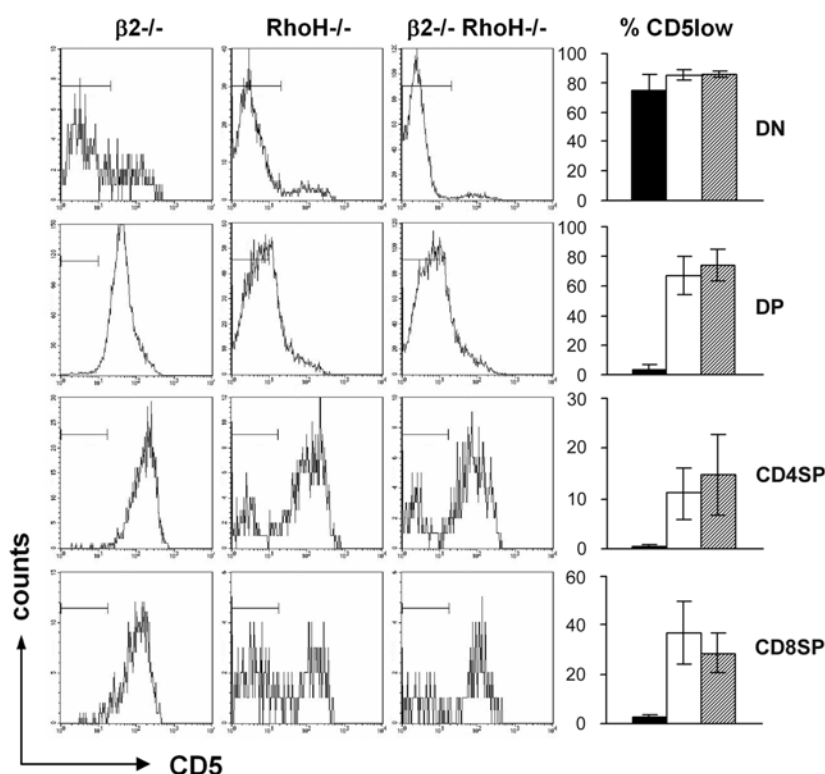
Figure 50. RhoH does not affect CD5 expression via regulation of β2-integrin-mediated adhesion. Expression of CD5 and amount of CD5low thymocytes in 6-10 week old β2-integrin-null, RhoH-null and β2-integrin-RhoH-double knockout mice (n=3/3/3). The percentages of cells marked in histograms are shown in bar graphs.

4.9 Identification of RhoH interaction partners

Analysis of TCR signaling in the RhoH-deficient thymocytes revealed that RhoH plays an important role downstream of ZAP70 and is required for efficient phosphorylation of the LAT signalosome. Our hypothesis is that RhoH associates with one of the members of the LAT signalosome and thereby contributes to its efficient phosphorylation. We therefore turned our attention to ZAP70, LAT and Vav1 as possible proteins which might interact with RhoH.

Normal phosphorylation of ZAP70 in the absence of RhoH indicated that RhoH is not necessary for ZAP70 activation, however it might bind to ZAP70 and only then ZAP70 can develop its full phosphorylation activity on the LAT signalosome. On the other hand, RhoH could have a stabilization effect on the LAT signalosome by binding to LAT or LAT-associated protein, e.g. Vav1. In the absence of RhoH this complex would be inefficiently formed, resulting in reduced phosphorylation. Vav1 is so far a favoured candidate, as it acts not only as an adaptor protein but also as a GEF for Rac1 and Cdc42. If RhoH activity is regulated, in contrast to the current model, Vav1 could activate RhoH and active RhoH could stabilize the LAT signalosome.

To test this, we performed pulldown assays and probed the immunoprecipitates for candidate proteins, mostly focussing on Vav1 and ZAP70.

4.9.1 Pulldown of RhoH binding partners using recombinant RhoH-GST

Since we did not possess a RhoH antibody, we used recombinantly expressed RhoH-GST in pulldown assays. RhoH-GST was immobilized on the glutathione sepharose beads (GS-beads) and incubated with thymocyte lysates. The immunoprecipitates were probed for Vav1 and ZAP70 in Western blot.

Expression and purification of RhoH-GST

Figure 51 monitors the expression, purification and binding of RhoH-GST fusion protein and GST protein to the GS-beads as demonstrated on a SDS-PAGE gel stained with Coomassie. GST protein was used in pulldown assays as a control for unspecific binding to the GST-tag. GST and RhoH-GST fusion protein (clone #6) expression could be induced by IPTG as shown by appearance of 26 kD and 47 kD band, respectively (lanes 1, 2, 3, 5), whereas the expression of RhoH-GST fusion protein, clone #4 could not be induced (lane 3).
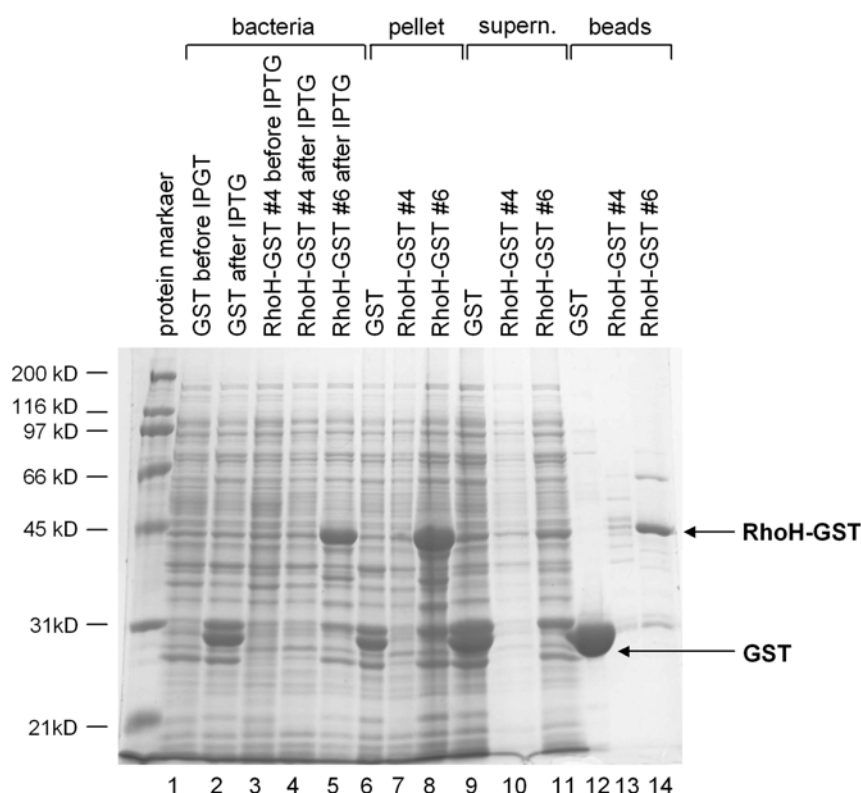
Figure 51. Expression and purification of RhoH-GST fusion protein. RhoH-GST (#4 and #6) and GST were transformed in *E.coli* and after reaching OD_{600} 0.5 their expression was induced by IPTG. The bacteria were harvested after 6 h growing at 26°C or o/n at 18°C and the RhoH-GST fusion protein (47 kD) and GST protein (26 kD) were purified. GST was found in the soluble fraction (supern. =supernatant), whereas RhoH-GST remained mainly in "inclusion bodies" (pellet). RhoH-GST and GST from the soluble fraction were bound to GS-beads and subsequently used in the pulldown assays.

During purification GST protein was detected in the supernatant (lane 9) and could be immobilized on the GS-beads very efficiently (lane 12). In contrast, RhoH-GST remained mainly insoluble in the "inclusion bodies" (lane 8) and therefore only a small amount of

RhoH-GST fusion protein could be bound to GS-beads (lane 14). A protein of approximately 70 kD, which associated with RhoH-GST, was likely a heat shock protein (Hsp70), suggesting that RhoH-GST was probably not properly folded and therefore mostly insoluble.

Scheme for RhoH-GST pulldown

As GEFs bind preferentially to the nucleotide-depleted state of GTPases compared to GTP- or GDP-bound states, we depleted RhoH-GST of nucleotides to possibly precipitate Vav1. Nucleotide-loaded conditions were used to precipitate ZAP70 as a possible effector (Figure 52). For the nucleotide-depleted condition, lysates were supplemented with EDTA to chelate magnesium, an essential cofactor for nucleotide binding (Figure 52). For nucleotide-loaded conditions, magnesium was added to maintain nucleotide binding (Figure 52). After washing the beads, the precipitates were resolved in the sample buffer and probed for Vav1 or ZAP70 (Figure 52).
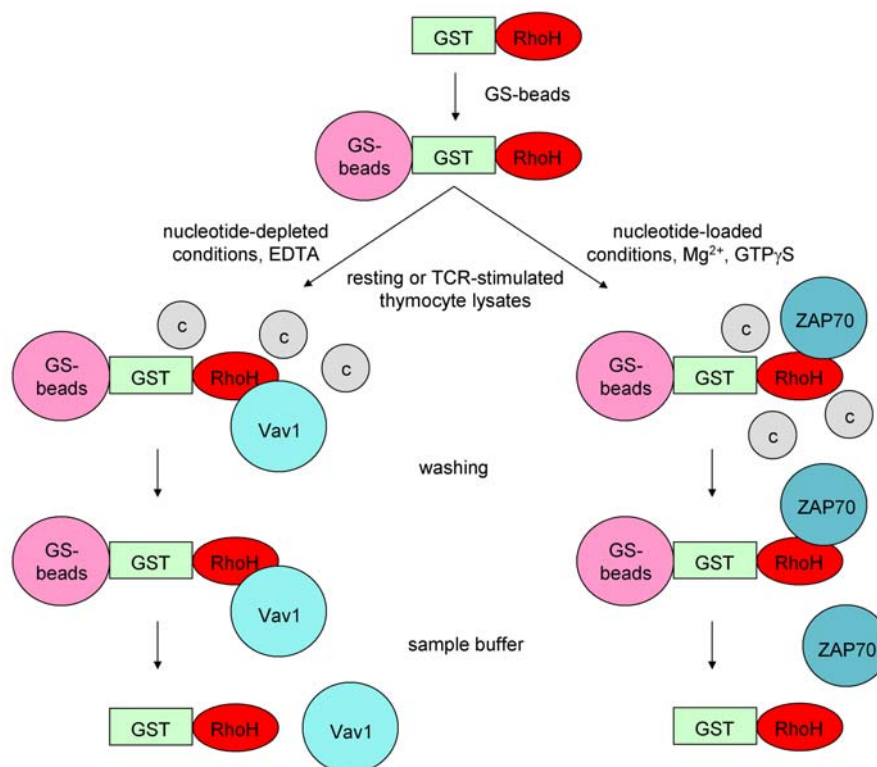
Figure 52. Scheme of the RhoH-GST pulldown. RhoH-GST bound to GS-beads are depleted of nucleotides by addition of EDTA (for GEF binding) or loaded with GTPγS in the presence of Mg^{2+} (for effector binding) and incubated with resting or TCR-stimulated thymocytes. After washing steps, the samples are denatured by adding sample buffer, and probed for Vav1 or ZAP70 in Western blot (c: non-specific proteins).

Since interaction of most proteins, that are involved in TCR signal transduction, is stimulated upon induction of TCR signaling, it could also be true for RhoH, that its association with Vav1 or ZAP70 is initiated or stabilized after TCR ligation. GEF activity of Vav1 is inhibited by an intramolecular binding of calponin homology domain to the cysteine-rich domain and is

restored by phosphorylation of the acidic domain upon TCR engagement (Tybulewicz, 2005). RhoH might bind to Vav1 upon TCR stimulation. To test these possibilities, we included the lysates of TCR-stimulated thymocytes. The stimulation of the thymocytes was verified in the Western blot probed for phosphotyrosine (data now shown).

RhoH-GST pulldown

A weak signal for Vav1 was detected in the precipitates of the nucleotide-depleted RhoH-GST fusion protein with resting thymocytes (Figure 53A, lane 3), whereas no signal with GST protein was observed (Figure 53A, lane 2). However, whether RhoH really interacts with Vav1 is vague, since an unspecific signal for Vav1 was both present in RhoH-GST and GST precipitates of TCR-stimulated thymocytes (Figure 53B, upper panel, lanes 1, 3). Similar pattern of an unspecific signal for ZAP70 was both visible in RhoH-GST and GST precipitates (Figure 53B, lower panel, lanes 2, 4). These data suggest that a possible interaction of RhoH with ZAP70 or Vav1 might be masked by an unspecific binding of these proteins to the GST-tag.
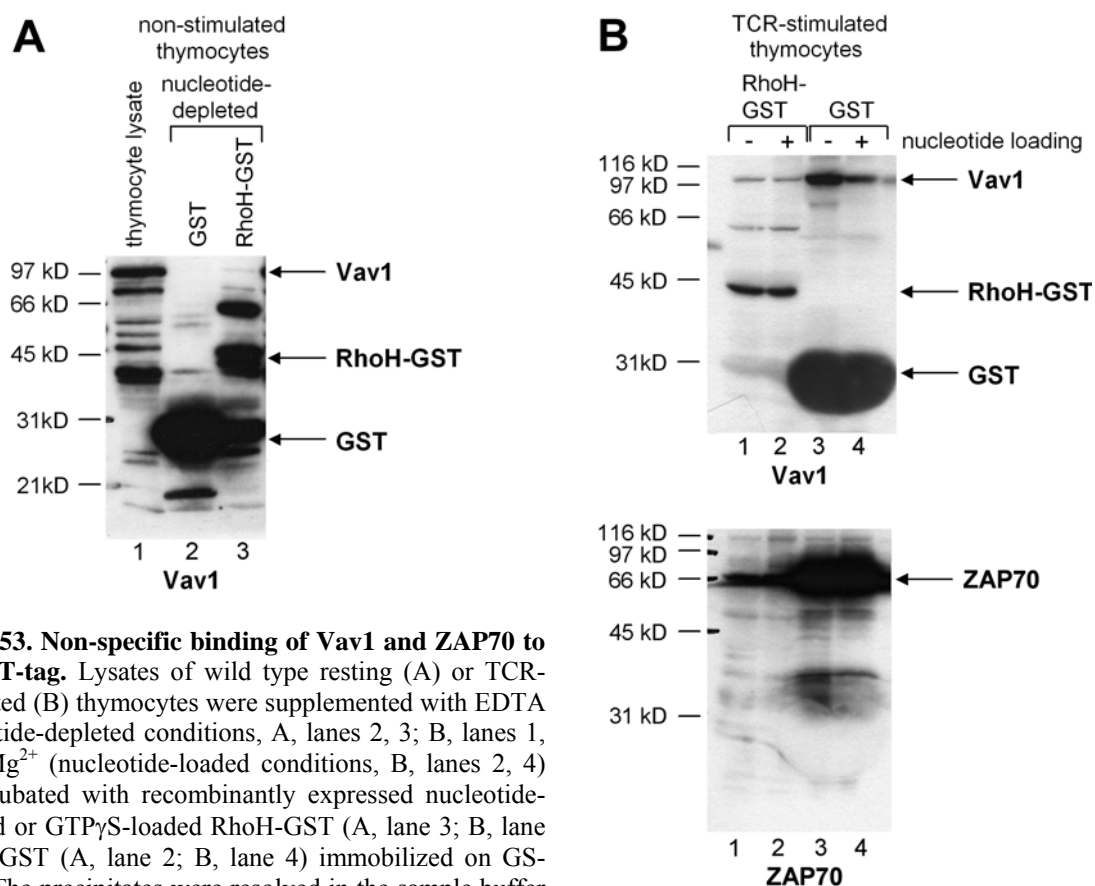
Figure 53. Non-specific binding of Vav1 and ZAP70 to the GST-tag. Lysates of wild type resting (A) or TCR-stimulated (B) thymocytes were supplemented with EDTA (nucleotide-depleted conditions, A, lanes 2, 3; B, lanes 1, 3) or Mg^{2+} (nucleotide-loaded conditions, B, lanes 2, 4) and incubated with recombinantly expressed nucleotide-depleted or GTPγS-loaded RhoH-GST (A, lane 3; B, lane 2) and GST (A, lane 2; B, lane 4) immobilized on GS-beads. The precipitates were resolved in the sample buffer and analyzed by Western blotting for Vav1 (A; B, upper panel) or ZAP70 (B, lower panel), after stripping the membrane.

4.9.2 Pulldown of RhoH binding partners using eukaryotically expressed RhoH-myc

To avoid an unspecific binding to the GST-tag and to reassure the correct folding of RhoH, we switched to eukaryotic myc-tag expression system. For pulldown of RhoH binding partners, myc-tagged RhoH was transfected in 293 cells (Figure 54A), immobilized on anti-myc-IgG beads and incubated with lysates of resting or TCR-stimulated thymocytes under nucleotide-depleted (Figure 54B, lanes 2, 3) or nucleotide-loaded (Figure 54B, lanes 4, 5) conditions.
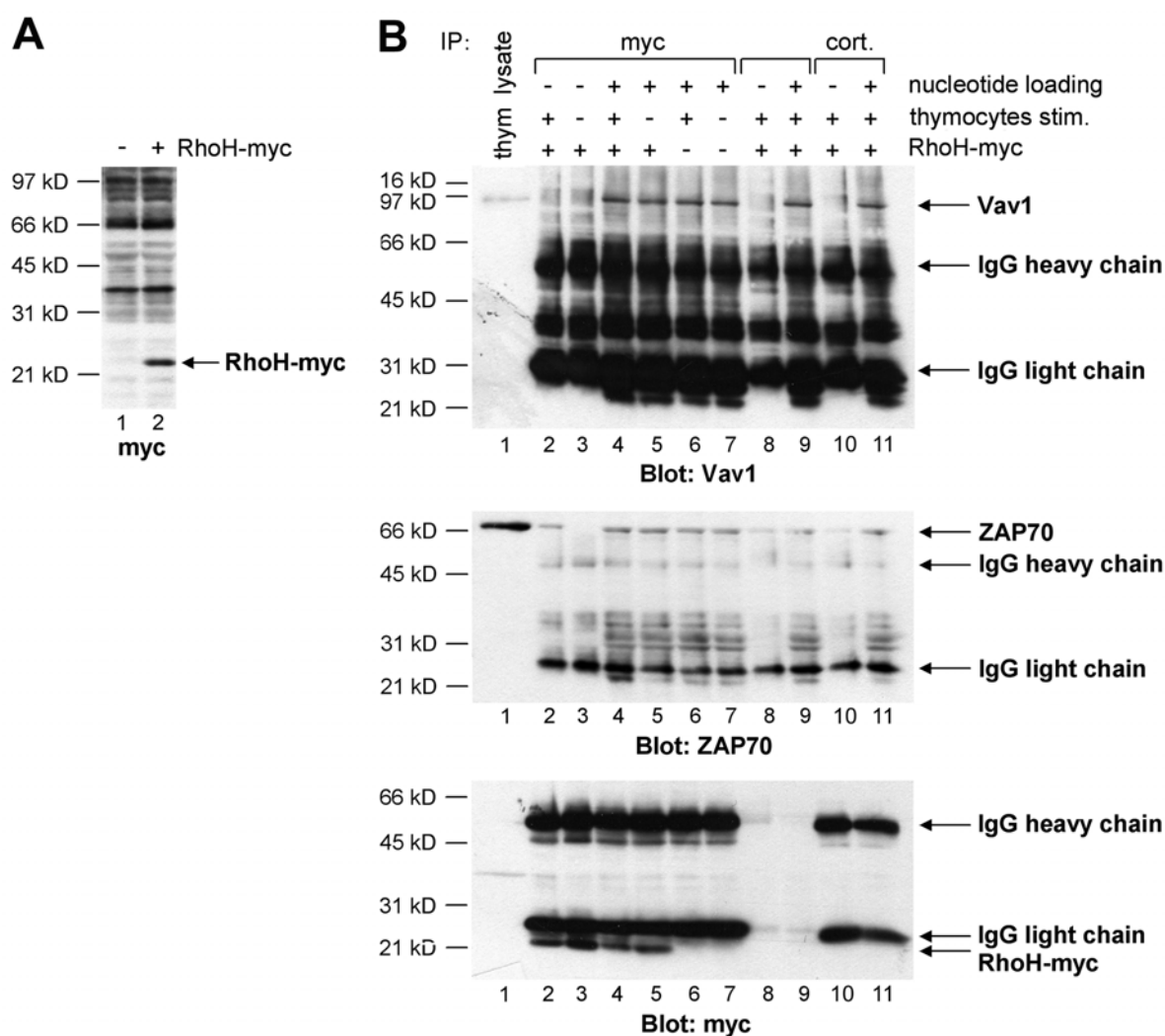
Figure 54. RhoH-myc does not bind specifically to Vav1 or ZAP70. (A) Lysates of 293 cells non-transfected or transfected with RhoH-myc were analyzed by Western blotting with myc-antibody. Lysates of wild type resting (B, lanes 3, 5, 7) or TCR-stimulated (B, lanes 2, 4, 6, 8-11) thymocytes were supplemented with EDTA (nucleotide-depleted conditions, B, lanes 2, 3, 8, 10) or Mg^{2+} (nucleotide-loaded conditions, B, lanes 4-6, 9, 11) and incubated with lysates of 293 cells non-transfected (B, lanes 6, 7) or transfected with RhoH-myc (B, lanes, 2-5, 8-11) and myc-antibody (nucleotide-depleted: B, lanes 2, 3; loaded with GTPγS: B, lanes 4-7) or only IgG beads (loaded with GTPγS: B, lanes 8, 9) or an unrelated cortactin-antibody (loaded with GTPγS: cort., B, lanes 10, 11). The precipitates were denatured in the sample buffer and analyzed by Western blotting for Vav1 (B, upper panel), ZAP70 (B, middle panel) and myc (B, lower panel), after stripping the membrane.

Under nucleotide-depleted conditions, Vav1 could not be precipitated with RhoH-myc neither from resting nor TCR-stimulated thymocytes (Figure 54B, lanes 2, 3). A signal for Vav1 obtained in the precipitates under nucleotide-loaded conditions (Figure 54B, upper panel, lanes 4, 5) appeared to be non-specific, as this signal was also present in the precipitates of non-transfected cells or samples containing no anti-myc antibody or an unrelated antibody during immunoprecipitation (Figure 54B, upper panel, lanes 6, 7, 9, 11). A signal for ZAP70 detected in the RhoH-myc-precipitates of TCR-stimulated and resting cells under nucleotide-loaded conditions (Figure 54B, middle panel, lanes 4, 5) appeared to be non-specific as well, since this signal was also present in immunoprecipitates of non-transfected cells (Figure 54B, middle panel, lanes 6, 7). If there would be a specific interaction between RhoH-myc and ZAP70 or Vav1, we would expect an increase in signal intensity when compared to a non-specific signal.

Probing the RhoH-myc precipitates for LAT did not result in a positive signal (data not shown). These results imply that RhoH does not interact with Vav1, ZAP70 or LAT under conditions tested.

4.9.3   Pulldown of RhoH binding partners using RhoH-Flag

The interaction between RhoH and predicted proteins as Vav1, ZAP70 and LAT could be weak and transient and maybe for this reason we were not able to detect this association. We reasoned that we might increase the chances of precipitating the possible interacting partners by using one system for RhoH expression and immunoprecipitation. We chose Jurkat TAg cell line (Northrop et al., 1993), derived from a human T cell leukemia, as a model system for T cells.

Jurkat TAg cells were transfected with RhoH-Flag (Figure 55, lanes 1, 2), and anti-Flag immunoprecipitations of TCR-stimulated or resting cells were performed. Samples with empty Flag-vector were used as a control for unspecific binding. We could not detect any specific signal for Vav1 or ZAP70 under nucleotide-depleted or nucleotide-loaded conditions, respectively (data not shown).
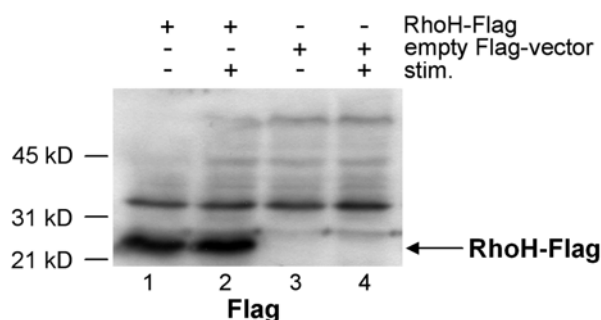
Figure 55. RhoH-Flag expression in Jurkat TAg cells. Jurkat TAg cells transfected with RhoH-Flag or empty Flag-vector were analyzed by Western blotting with Flag-antibody.

4.9.4   Pulldown of RhoH-binding partners using c.a. and d.n. RhoH-TAP-tag

Facing problems with immunoprecipitating ZAP70, Vav1 and LAT, we turned away from the "educative guess" approach, and initiated a more general approach by precipitating and identifying RhoH binding partners via mass spectrometry. RhoH was cloned into TAP-tag vector, which is used for tandem affinity purification (TAP) (Puig et al., 2001). TAP system is a two-step affinity purification method which allows for purifying protein complexes sufficiently clean to be analyzed by mass spectrometry. TAP tag consists of two IgG binding domains of *S. aureus A* (Protein A) and a calmodulin binding peptide separated by a TEV cleavage site.

We generated two RhoH mutants conjugated to a TAP-tag, which should be used along with the wild type RhoH-TAP-tag in the identification of binding proteins. Assuming that RhoH might be not GTPase-deficient, we mutated asparagine at the position 62 to leucine and threonine at the position 18 to asparagine (Figure 15), which leads in Rac1, Cdc42 and RhoA to a constitutive active [c.a.] (Li et al., 2003; Moreau et al., 2000; Khosravi-Far et al., 1994) or a dominant negative [d.n.] form (Ridley et al., 1992; Coghlan et al., 2000; Qiu et al., 1995), respectively. The c.a. form could be used to immunoprecipitate effector proteins (e.g. ZAP70, LAT) and the d.n. form could be used to fish putative GEFs (e.g. Vav1).

In preliminary experiments, we transfected both mutants into Jurkat TAg cells and performed immunoprecipitations under TCR-stimulated and resting conditions using IgG beads that bind to Protein A domain of the TAP-tag. However, we not able to precipitate neiter Vav1 nor ZAP70 with d.n. RhoH-T18N or c.a. RhoH-N62L mutants, respectively. Since the complete TAP-tag purification and mass spectrometry, require a lot of optimization steps and represent a new project, it could not be included in this PhD thesis because of time limitations.

4.9.5   C.a and d.n. RhoH do not affect TCR signaling in Jurkat TAg cells

The data of RhoH-deficient mice indicated that RhoH is a positive regulator of TCR signaling, suggesting that if RhoH activity was regulated, the c.a. form of RhoH could enhance TCR signaling upon stimulation or initiate signaling cascade without TCR ligation. On the other hand, the d.n. form of RhoH could decrease signaling upon TCR engagement by constitutive binding to an unknown GEF.

To examine these possibilities, we introduced the TAP-tagged wild type RhoH, c.a. RhoH-N62L and d.n. RhoH-T18N into Jurkat TAg cells. The lysates of TCR-stimulated and resting cells were investigated for phosphotyrosine in Western blot (Figure 56, middle panel). The

transfected proteins were examined by probing the lysates for Vav1 antibody, which contains an IgG, that binds to Protein A domain of the TAP-tag (Figure 56, upper panel). However, we did not observe any changes in the phosphotyrosine pattern between lysates of cells transfected with an empty TAP-tag vector, wild type RhoH, mutant forms of RhoH and lysates of non-transfected cells (Figure 56, middle panel). This implies that the aa substitutions do not modulate RhoH activity. It could be that the RhoH activity is not regulated as currently assumed. On the other side, it is also possible that the Jurkat TAg cell line, derived from leukemia cells, where a lot of pathways could be deregulated, is not the right system to study the RhoH activity.
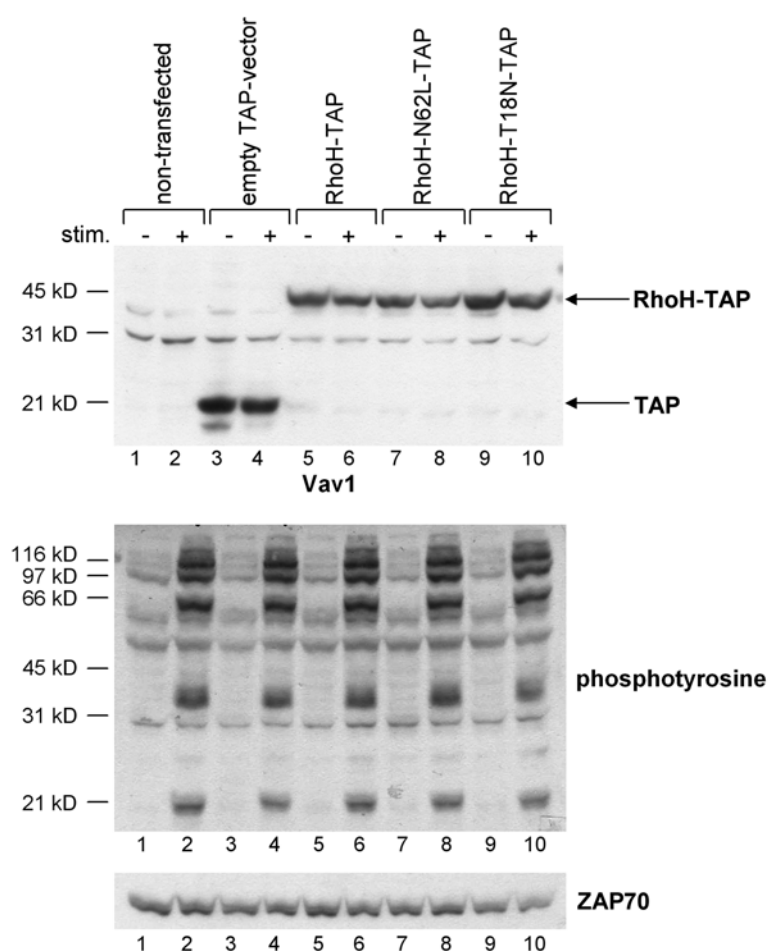
Figure 56. RhoH-N62L and RhoH-T18N mutant forms do not affect TCR signaling in Jurkat TAg cells. Empty TAP-tag-vector, RhoH-TAP-tag (wild type), RhoH-N62L-TAP-tag (c.a.) and RhoH-T18N-TAP-tag (d.n.) were transfected into Jurkat TAg cells. Lysates were analyzed by Western blotting with Vav1, which recognizes the Protein A domain of a TAP-tag via the IgG domain (upper panel), with phosphotyrosine (middle panel) and ZAP70 as a control for loading (lower panel).

5 Discussion

RhoH, first identified as a fusion transcript with LAZ3/BCL6 in a non-Hodgkin's lymphoma cell line, is a Rho GTPase, which is exclusively expressed in the hematopoietic system (Li et al., 2002; Gu et al., 2005a). In DLBCL and other lymphomas, *RhoH* was shown to accumulate mutations in the non-coding region as a result of a somatic hypermutation mechanism, suggesting that altered expression level might be involved in lymphoma formation (Preudhomme et al., 2000 ; Pasqualucci et al., 2001).

When this project was initiated, little was known about the function of RhoH based on one *in vitro* study (Li et al., 2002). In this study, RhoH was demonstrated to counteract other Rho GTPases and to have no intrinsic GTPase activity, indicating that RhoH is constitutively active (Li et al., 2002). More recent investigations using overexpression and RNA interference tools to alter expression levels assigned the functions of regulating integrin-mediated adhesion in Jurkat cells (Cherry et al., 2004) and proliferation and survival of HPCs to RhoH (Gu et al., 2005a). However, questions concerning the physiological role of RhoH in hematopoietic lineages remained unanswered.

To elucidate the function of RhoH in the hematopoietic system, RhoH-deficient mice, generated in our lab, were analyzed in this PhD project.

5.1 RhoH is a positive regulator of T cell development

The most obvious phenotype of the mice with *RhoH* gene ablation was seen in the pronounced reduction in thymocyte numbers. Since RhoH was shown to be expressed at the highest levels in the thymus, we suspected that RhoH might play a role in T cell differentiation or function.

Indeed, in the absence of RhoH, $\alpha\beta$ thymocyte development was partially blocked at the DN3 to DN4 stage and at the DN4 to DP transition, leading to an accumulation of DN3 thymocytes (s. 4.4.4.1). At this transition β-selection takes place, which ensures that only thymocytes that have generated a functional TCRβ chain can differentiate to DN4 and DP cells. A second partial block occurred at the transition from DP to CD4SP and CD8SP cells, where positive selection allows only MHC-restricted, self-tolerant thymocytes to develop further. Since both β-selection and positive selection are dependent on similar signaling cascades downstream of pre-TCR and TCR, our results indicated a possible role of RhoH in these signaling pathways. Aberrant expression of maturation markers, such as CD5, TCRβ and CD69 (s. 4.4.4.6)

suggested a defective pre-TCR and TCR signaling. Furthermore, analysis of TCR-stimulated RhoH-deficient thymocytes confirmed that TCR signaling was impaired in the absence of RhoH (s. 4.6).

The phenotype of the RhoH-deficient mice was surprising, as it differed strongly from what we anticipated to find based on previously published observations. As demonstrated in two studies, RhoH suppresses Rac1 activation and also Rac1-, Cdc42- and RhoA-mediated activation of NF-κB and p38 (Gu et al., 2005a; Li et al., 2002). We rather expected a disturbance of thymocyte development associated with a constitutive activation of Rac1, NF-κB or p38. However, constitutive activation of these proteins results in thymic differentiation disorders that are different from the defects observed in the thymocyte development in the absence of RhoH, suggesting that in thymocytes *in vivo*, RhoH is not crucial for regulation of these signaling molecules.

Constitutive activation of Rac1 increases proliferation of DN3 thymocytes and accelerates DN3 to DN4 transition by potentiation of pre-TCR signaling (Gomez et al., 2000). At later stages, constitutively active (c.a.) Rac1 enhances TCR signaling and thereby diverts positive selection to negative selection leading to decreased numbers of SP cells. Due to augmented TCR signaling, DP and SP thymocytes have a higher percentage of cells with upregulated expression of CD5 and CD69. In contrast, RhoH-deficient thymocytes revealed attenuated pre-TCR and TCR signaling (s. 4.6), resulting in a partial block from DN3 to DN4 and from DN4 to DP stages (s. 4.4.4.1) as well as in an impaired positive selection (s. 4.5.2). Although we observed an increased basal activation of Rac1 in the absence of RhoH (s. 4.6.4), the different phenotypes of c.a. Rac1 transgenic and RhoH-null mice suggest that the altered Rac1 activation is not contributing to the defective thymocyte development.

If RhoH-deficiency would cause constitutive activation of NF-κB in thymocytes, we would expect an increase of DN4 cells (Voll et al., 2000). NF-κB is activated through several receptors leading in a classical pathway to activation of the IκB kinase complex (IKKα, IKKβ, IKKγ), which phosphorylates IκB-α, the NF-κB inhibitor. Phosphorylated IκB-α is then ubiquitinylated and degraded by the proteasome, thus releasing NF-κB for translocation to the nucleus and activation of target genes (Siebenlist et al., 2005). Enhanced activation of NF-κB, as achieved by the expression of a c.a. IKKβ, provides a survival signal for the DN3 cells and leads to an increase in the DN4 population (Voll et al., 2000). In fact, we observed a decreased survival of DN4 thymocytes in RhoH-deficient mice.

The effect of augmented NF-κB activity on negative and positive selection was not examined in mice expressing c.a. IKKβ, but studies involving overexpression of the inhibitor IκB-α or

the d.n. form of IKK propose that NF-κB might be involved in both negative and positive selection by promoting apoptosis of autoreactive thymocytes and survival of positively selected cells (Siebenlist et al., 2005). All these effects were not observed in RhoH-null thymocytes.

Finally, if the consequence of ablation of the *RhoH* gene was elevated p38 MAP kinase activity, RhoH-deficient mice should show a progressive increase of thymus size, causing extinction of lung expansion and death of the mice around 5-6 months of age, as was shown for mice constitutively expressing MAP kinase kinase 6 (MKK6) in thymocytes, which specifically activates p38 (Diehl et al., 2000; Rincon and Pedraza-Alva, 2003).

Inactivation of p38 is required for the DN3 to DN4 transition. Persistent activation of p38 leads to a continuous accumulation of immature DN3 cells and an arrest in further development to DN4 and DP cells during fetal thymic differentiation, resulting in a complete absence of mature T cells in the periphery (Diehl et al., 2000; Rincon and Pedraza-Alva, 2003). Introduction of MKK6 into developing thymocytes forces deletion of DP cells, suggesting that p38 promotes negative selection. (Sugawara et al., 1998). Although we detected a significant increase of DN3 thymocytes in the absence of RhoH which could coincide with enhanced p38 activity, no complete arrest of thymocyte development occurred. Most importantly, we could not observe increased activation of p38 in RhoH-null DP cells (s. 4.6.5), making it unlikely that p38 activity is elevated in RhoH-deficient DN3 cells.

Taken together, the defects detected in the thymocyte development in RhoH-null mice did not match our expectations on the effect of RhoH deletion, thus establishing a novel role of RhoH as a positive regulator of T cell development.

5.2 RhoH regulates proliferation and survival of αβ thymocytes in a cell type and stage specific manner

Since overexpression of RhoH in HPCs was associated with suppressed proliferation and enhanced apoptosis, and decreased RhoH expression was connected to both increased proliferation and survival (Gu et al., 2005a; 2005b), we expected to observe both elevated proliferation and survival in the absence of RhoH. Contrary to this prognosis, proliferation of RhoH-null DN3 and DN4 cells was significantly reduced, whereas apoptosis of DN4, DP, CD4SP and CD8SP thymocytes was significantly increased in the absence of RhoH (s. 4.4.4.5). In CD4SP and CD8SP thymocytes, on the other hand, we detected higher proliferation in RhoH-mutant mice (s. 4.4.4.5). Hence, RhoH controls proliferation and survival differently in different hematopoietic cells and even at different stages of T cell development. It could be that within the stem cell compartment, RhoH maintains the size of

HPC population in a "steady-state" by repressing excessive proliferation and inducing apoptosis. After commitment to the T cell lineage, RhoH might act as a positive regulator of proliferation and survival by transducing pre-TCR and TCR signals leading to expansion and survival of DN and DP thymocytes. Finally, at the SP stage, RhoH appears to exert an independent influence on proliferation and survival, by diminishing the first and enhancing the latter. Against the hypothesis that RhoH negatively affects proliferation and survival of HPCs, which would foretell increased numbers of HPCs and probably also a higher amount of early thymocyte progenitors within the DN1 subset in the absence RhoH, is the finding that we obtained rather similar numbers of DN1 thymocytes in control and mutant mice (s. 4.4.4.1). To clarify this problem, proliferation and apoptosis of HPCs has to be investigated in RhoH-null mice.

At the end of the project presented in this thesis, another group published an analysis of RhoH-deficient mice, demonstrating similar results to our study (Gu et al., 2006). In contrast to our results, Gu and co-authors observed that while the DN4 thymocyte population was reduced, the proliferation of DN3, DN4 and SP thymocytes was not altered in the absence of RhoH (Gu et al., 2006). Slightly different assays applied by Gu et al. and our analysis might account for the discrepances in thymocyte proliferation between both studies (s. 3.9.1.2).

5.3 RhoH is not crucial for development of NK1.1+, γδ T, myeloid, erythroid and B cells

In contrast to αβ T cells, RhoH was not crucial for the development of NK1.1+ cells (s. 4.4.3) and γδ T lymphocytes (s. 4.4.4.2). However, RhoH might be involved in the early γδ T cell differentiation. We observed an incomplete block at the DN3 to DN4 transiton leading to an accumulation of DN3 γδ T cells in RhoH-deficient mice. Later stages of γδ T cell development appeared not be affected by the absence of RhoH.

Since RhoH expression is low in myeloid and erythroid lineages (Li et al., 2002, Gu et al., 2005a; Lahousse et al., 2004; s. 4.3), our finding that the development of granulocytes, monocytes and erythroblasts could occur normally in RhoH-deficient mice was expected (s. 4.4.1).

On the other hand, RhoH is expressed in B cells at levels similar to those in peripheral T cells (Li et al., 2002; Gu et al., 2005a; Lahousse et al., 2004; s. 4.3), suggesting that RhoH might play a similarly important role in B cell differentiation as in T cell development. However, no apparent disorders in B cell production were detected in RhoH-mutant mice (s. 4.4.2), suggesting that RhoH is not required for B cell maturation. B cell activation in RhoH-

deficient cells was not tested yet and it is still possible that RhoH plays an important role there. Future experiments will address this question.

RhoH-deficient mice did not develop any lymphomas. This finding is insofar intriguing with respect to B cells, as *RhoH* gene translocations and mutations in the non-coding region of *RhoH* gene have been observed in B cell type NHL and multiple myeloma (Dallery et al., 1995; Preudhomme et al., 2000; Pasqualucci et al., 2001; Gaidano et al., 2003; Deutsch et al., 2006; Bödor et al., 2005; Dijkman et al., 2006). Whether these mutations/translocations lead to a decreased or increased expression of RhoH is however not known.

Our data show that loss of RhoH expression is not sufficient to induce lymphoma formation within a year. Whether RhoH has any positive or negative influence on lymphoma formation, should be tested by crossing the RhoH-null mice to mice spontaneously developing B cell lymphoma. The effect on tumor frequency, onset, and progression should be examined. If RhoH is a tumour suppressor or an oncogene, RhoH-null mice will have more or less tumours, respectively.

5.4 RhoH is a positive regulator of TCR signaling

Normal phosphorylation of both lck at the inhibitory tyrosine and ZAP70 at Y319 in RhoH-null thymocytes after crosslinking of CD3 (s. 4.6.2), suggests that TCR signaling is not impaired at the level of ZAP70 activation. This notion is strengthened by the normal TCR-dependent activation of p38 in CD4SP cells (s. 4.6.5), since this activation is in T cells mediated by ZAP70 in a manner independent of LAT (Salvador et al., 2005). In contrast, phosphorylation of LAT, the LAT-associated proteins PLCγ1 and Vav1 (s. 4.6.3), activation of Erk and calcium influx (s. 4.6.5), which are downstream of PLCγ1, were dramatically reduced in RhoH-deficient thymocytes. RhoH, therefore, seems to specifically interfere with the LAT branch of ZAP70 signaling. The impaired TCR-dependent calcium influx in peripheral CD4+ and CD8+ T cells upon TCR stimulation indicates that RhoH is also important for TCR signaling in mature T cells and that loss of RhoH is not compensated for during development.

Taken together, our data indicate that RhoH is important for both pre-TCR and TCR signaling by facilitating phosphorylation of the LAT signalosome by ZAP70.

Lower expression levels of TCRβ detected on RhoH-null thymocytes might have partially contributed to the impaired TCR signaling. However, normal phosphorylation of lck and ZAP70 implies that decreased TCRβ surface levels are most likely the consequence rather than the cause of the defective TCR signaling.

Although we did not examine NF-κB activation in RhoH-deficient thymocytes, we are convinced that, contrary to our previous expectation, NF-κB is less activated in the absence of RhoH, since the pathway leading to NF-κB activation utilizes the LAT branch of TCR signaling (Siebenlist et al., 2005).

In our model RhoH could either bind directly to LAT or to a LAT-associated protein such as Vav1. By this interaction RhoH could stabilize the whole LAT signalosome, enabling its efficient phosphorylation through ZAP70 (Figure 57A). In another model, RhoH might interact directly with ZAP70 and this binding might be necessary for ZAP70 to unfold its full phosphorylation activity on the LAT signalosome, although it is not critical for normal autophosphorylation of ZAP70 (Figure 57B).
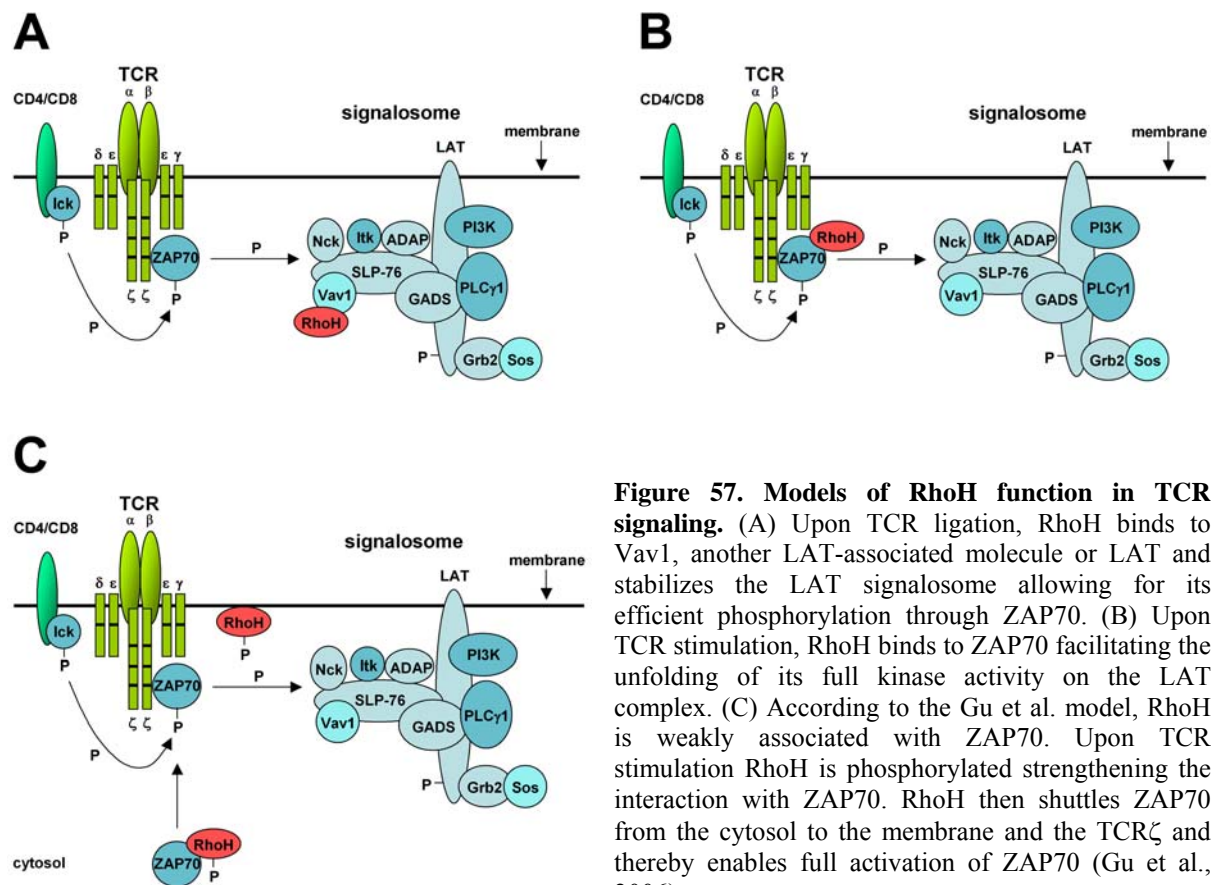
Figure 57. Models of RhoH function in TCR signaling. (A) Upon TCR ligation, RhoH binds to Vav1, another LAT-associated molecule or LAT and stabilizes the LAT signalosome allowing for its efficient phosphorylation through ZAP70. (B) Upon TCR stimulation, RhoH binds to ZAP70 facilitating the unfolding of its full kinase activity on the LAT complex. (C) According to the Gu et al. model, RhoH is weakly associated with ZAP70. Upon TCR stimulation RhoH is phosphorylated strengthening the interaction with ZAP70. RhoH then shuttles ZAP70 from the cytosol to the membrane and the TCRζ and thereby enables full activation of ZAP70 (Gu et al., 2006).

Gu and co-workers proposed a slightly different mechanism for RhoH in TCR signaling based on their observations that phosphorylation of ZAP70 itself was decreased after TCR stimulation, in contrast to our results (Gu et al., 2006). They suggested that the mild reduction in ZAP70 phosphorylation resulted from a disrupted recruitment of ZAP70 to the cell membrane after TCR activation (Gu et al., 2006). These data indicated that RhoH is important for ZAP70 phosphorylation and activation, contrary to our hypothesis. Since we showed normal ZAP70

phosphoryation by two independent techniques (FACS, Western blot; s. 4.6.2), we are confident that our data are correct.

Gu and co-authors suggested that attenuated phosphorylation and activation of ZAP70 might be explained by the failure of TCRζ phosphorylation in RhoH-deficient thymocytes (Gu et al., 2006). TCRζ contains three ITAMs and is constitutively phosphorylated at two distal ITAMs due to *in situ* TCR interactions with peptide-MHC complexes (Figure 58; Pitcher et al., 2003). This phospho-TCRζ (p21ζ) is constitutively bound by non-phosphorylated, inactive ZAP70 and migrates at an apparent size of 21 kD. Upon TCR crosslinking, the third ITAM in TCRζ is phosphorylated, leading to the 23 kD form of the TCRζ (p23ζ), and is then bound by ZAP70 (Figure 58). These events then result in phosphorylation and activation of ZAP70 by lck (Pitcher et al., 2003). Surprisingly, ZAP70 is not only bound to phosporylated TCRζ, it is also required for the phosphorylation of TCRζ, presumably by protecting it from dephosphorylation by phosphatases (Pitcher et al., 2003; Sozio et al., 2004).
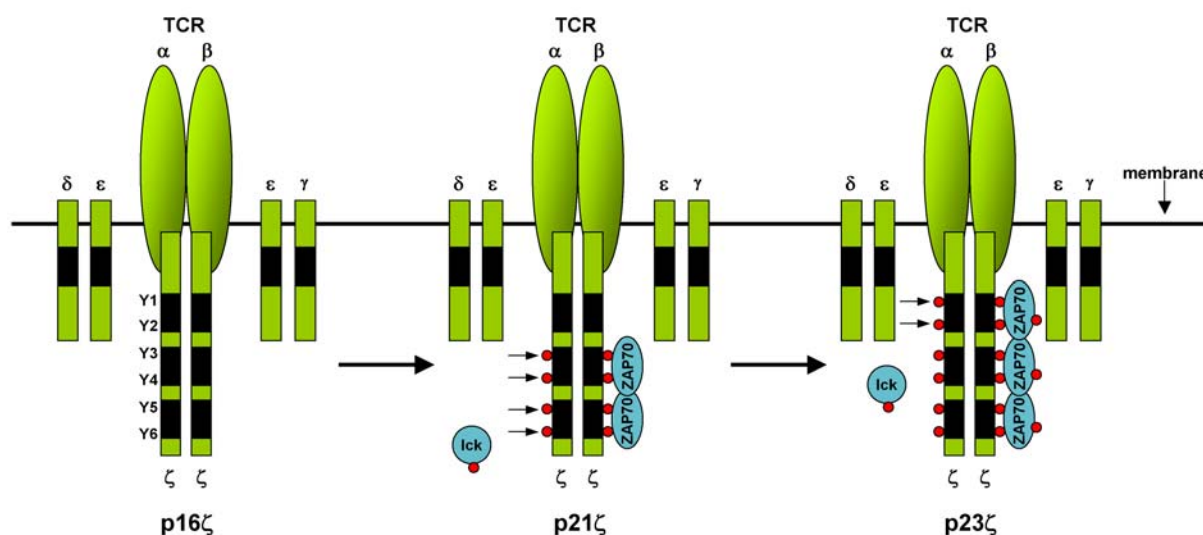
Figure 58. Stepwise model of TCRζ chain phosphorylation. Lck or fyn phosphorylates TCRζ (p16ζ) beginning with the distal tyrosine (Y6) of the ITAMs. Once Y3 is phosphorylated, two molecules of ZAP70 are bound, resulting in the 21 kD phosphorylated intermediate of TCRζ (p21ζ). Further phosphorylation of Y1 and Y2 in the ITAMs of TCRζ results in generation of a 23 kD form (p23ζ), which is then bound by a third molecule of ZAP70. Next, lck can phosphorylate and activate ZAP70 (a black rectangle indicates an ITAM, a red circle indicates phosphorylation; modified from Pitcher et al., 2003).

In RhoH-deficient DP thymocytes, p21ζ was absent under resting conditions and CD3 stimulation did not induce generation of the p23ζ form (Gu et al., 2006). In fact, we observed the absence of a phosphorylated protein at an apparent size of 21 kD in RhoH-deficient DP thymocytes and CD4+ splenocytes (s. 4.6.1) and speculated that the missing protein might be p21ζ. However, even when all tyrosines in the three TCRζ ITAMs are mutated to

phenylalanine so that no phosphorylation of TCRζ can occur, ZAP70 can still be phosphorylated normally (Pitcher et al., 2005). Also downstream signaling events such as phosphorylation of LAT and SLP-76 are not disturbed by the absence of p23ζ (Pitcher et al., 2005). Therefore, even if ZAP70 activation would be decreased in the absence of RhoH, this is unlikely to be explained by a decreased phosphorylation of TCRζ. The missing phosphorylated TCRζ forms in RhoH-deficient cells might be rather due to the increased phosphatase activity of PTPH1 (Sozio et al., 2004) or PTPN22 (Wu et al., 2006), which can dephosphorylate TCRζ. These phosphatases might be negatively regulated by RhoH.

Most interestingly, Gu and co-workers could show a direct interaction between RhoH and ZAP70, depending on a tyrosine phosphorylated ITAM-like sequence in RhoH (Gu et al., 2006; Figure 15). In resting T cells, RhoH and ZAP70 are weakly associated. Upon TCR engagement, RhoH is phosphorylated and the interaction between ZAP70 and RhoH is strengthened. Based on this finding, Gu and colleagues suggested that RhoH could shuttle ZAP70 from the cytoplasm to the plasma membrane, where ZAP70 then switches over to the TCRζ, and thereby enables full activation of ZAP70 upon TCR engagement (Figure 57C; Gu et al., 2006). In support of this idea, Gu et al. showed that RhoH-EGFP present in the cytoplasm could be targeted to the immunological synapse in normal T cells (Gu et al., 2006). Although we used several different methods, we could not show direct interaction between RhoH and ZAP70 (s. 4.9). However, these are negative results and it might be that we just never found the right conditions to detect an interaction between ZAP70 and RhoH.

Since we did not see any decrease in ZAP70 phosphorylation (s. 4.6.2), we also would not expect a reduced recruitment of ZAP70 to the TCR. What we would hypothesize to bring the different observations together is that early after TCR activation ZAP70 is recruited to the TCR complex and activated through phosphorylation by lck independent of RhoH. A RhoH-dependent event downstream of ZAP70 then leads to a reduced phosphorylation of TCRζ and a decreased presence of ZAP70 at the membrane. Assaying the membrane recruitment of ZAP70 at different time points after TCR crosslinking will tell whether this speculation is correct. In fact, Gu et al. examined TCR signaling after 10 min, while we tested it 5 min after TCR crosslinking (Gu et al., 2006; s. 3.11.6.1). Another difference is that Gu et al. used only CD3 antibody for crosslinking, while we applied CD3 and CD4 antibodies (s. 3.11.6.1), which should give a stronger signal.

Further studies are needed to resolve the discrepancies between our results and the results of Gu et al. with respect to ZAP70 phosphorylation and activation in RhoH-deficient thymocytes. To clearly show that the stimulation of ZAP70 kinase activity is either normal or

diminished in RhoH-deficient thymocytes, *in vitro* kinase assays of precipitated ZAP70 with an exogenous substrate have to be performed. It has also to be investigated by *in vitro* kinase experiments whether lck and fyn kinases are fully active, to exclude the possibility that the absence of p21ζ and p23ζ forms in RhoH-deficient thymocytes was due to impaired lck or fyn kinase activity. Furthermore, it will be important to explore the potential role of RhoH in the negative regulation of phosphatases, which dephosphorylate the ITAMs of TCRζ. Finally, the mechanisms by which RhoH stabilizes the LAT complex will have to be revealed. In this respect, it will be important to identify further RhoH binding partners.

Given that RhoH is expressed in B cells and that the BCR utilizes similar signal transduction machinery as the TCR, it is highly suggestive that RhoH might also be involved in BCR signaling (Koretzky et al., 2006; Simeoni et al., 2004; Wange, 2003). Moreover, the BCR is thought to supply important survival signals to B cell lymphomas (Küppers, 2005), where RhoH mutations and translocations were found. RhoH is often mutated in B cell type NHLs, which mostly depend on BCR expression, and rarely in B cell type HLs, which usually do not express the BCR (Küppers, 2005; Liso et al., 2006), providing an additional argument that RhoH might be important for BCR signaling. Therefore it would be of particular interest to examine BCR signaling in RhoH-deficient B cells. It will also be crucial to dissect whether RhoH is implicated in $\gamma\delta$ TCR signaling and signal transduction other than through the TCR, for example in chemokine or cytokine signaling in T lymphocytes.

5.5 Identification of RhoH interaction partners

As a link of RhoH to the LAT signalosome, we focussed on Vav1 because of striking similarities found between RhoH-null and Vav1-deficient mice. First, both mutant mice showed an accumulation of DN3 cells, while the numbers of DN1 and DN4 cells were relatively normal (s. 4.4.4.1; Turner et al., 1997). Second, both mutant mice revealed an approximately twofold reduction in the number of DP thymocytes and CD4SP and CD8SP cells were decreased even further (s. 4.4.4.1; Turner et al., 1997). Third, DP cells expressed lower levels of CD5 and less DP cells were TCRβhigh and CD69+ in both mice (s. 4.4.4.6; Turner et al., 1997). Fourth, activation of ZAP70 in DP cells after TCR activation was normal in both cases (s. 4.6.2). Fifth, phosphorylation of LAT (s. 4.6.3) and Erk and calcium influx (s. 4.6.5) stimulated by CD3 antibodies was severely decreased in DP cells of both mutant mice (Reynolds et al., 2004). Sixth, B cell development showed no apparent disorders in both cases (s. 4.4.2). However, immunization with TD antigen resulted in reduced IgG1 levels but similar IgM titer (s. 4.7; Gulbranson-Judge et al., 1999). Finally, $\gamma\delta$ T cells were present in

normal numbers in thymus and spleen when either RhoH or Vav1 was absent (s. 4.4.4.2; Swat et al., 2003).

Furthermore, Vav1 is a GEF for Rho GTPases and can bind to Cdc42, Rac1, and RhoA. Due to the structural similarity of RhoH with these protein family members, a direct interaction between Vav1 and RhoH is easily conceivable. If RhoH is constitutively active, as currently assumed (Li et al., 2002), we would suggest a model where activated Vav1 recruits RhoH to the TCR complex. This would enable further protein-protein interactions via RhoH leading to stabilization of the LAT signalosome and increased phosphorylation of LAT-associated proteins by ZAP70. Thereby, also phosphorylation of Vav1 would be increased in a positive feedback loop. If, however, RhoH is not constitutively active, but switching between a GDP- and GTP-bound form, Vav1 might activate RhoH by catalyzing the exchange of GDP to GTP. Like RhoH also the small GTPase Rap1 does not possess a detectable intrinsic GTPase activity due to mutation of a catalytic glutamine (Rubinfeld et al., 1991). However, Rap1 can hydrolyze GTP with the help of Rap1GAP which provides a catalytic asparagine (Daumke et al., 2004). It remains to be tested whether such a GAP exists for RhoH.

The fact that RhoH binds to GDIs (Li et al., 2002), which regulate Rho GTPase cycle along with GEFs and GAPs, seems to support the idea that RhoH activity is regulated and not constitutively active. If this is the case, mutants locking RhoH in the active state (N62L) could be used to co-precipitate effector proteins. On the other hand, mutants preventing dissociation of GEFs and interaction with effectors (T18N) could be used to precipitate GEFs, including Vav1. In addition, the latter mutants would provide a negative control for the precipitation of effectors with N62L form.

However, so far we have been unsuccessful in co-immunoprecipitating RhoH and Vav1 using recombinant RhoH-GST (s. 4.9.1) or RhoH-myc produced in 293 cells (s. 4.9.2), incubated with lysates from resting and stimulated thymocytes. Similarly, we were not able to precipitate Vav1 from Jurkat cells transfected with tagged RhoH (s. 4.9.3). We also could not detect co-precipitation of RhoH with ZAP70 or LAT (s. 4.9.1; 4.9.2; 4.9.3), other potential binding molecules. Also the use of the N62L and T18N mutants did not help to identify ZAP70, LAT and Vav1 as interaction partners of RhoH (s. 4.9.4). These data suggest that such interactions, if they are existent, are weak or transient.

More subtle lysis and immunoprecipitation conditions might be needed in order to be able to precipitate RhoH binding partners. We are therefore currently initiating a project involving double precipitation by TAP-tag technology and analysis of small amounts of RhoH binding molecules via mass spectrometry.

5.6   Crosstalk between RhoH and other Rho GTPases

RhoH was demonstrated to negatively affect Rac1 activation and Rac1 activity suggesting that RhoH might play a dual role both upstream and downstream of Rac1 in antagonizing both its activation and its effector pathways (Li et al., 2002; Gu et al., 2005a; Gu et al., 2005b). However, the mechanisms involved in these processes remained unclear. RhoH could bind a GAP, leading to inactivation of Rac1. This is similar to the mechanism proposed for Rnd proteins, which can activate p190Rho GAP and thus inhibit RhoA (Wennerberg et al., 2003). Another possibility would be that RhoH interacts with and inhibits the activity of a GEF. In order to suppress Rac1 signaling, RhoH could also bind and sequester a downstream target of Rac1 in a manner similar to RhoE. RhoE sequesters ROCK I, a downstream effector of RhoA, thus inhibiting RhoA signaling (Riento et al., 2003).

Because of the reported inhibitory function of RhoH on Rac1, we predicted that in the absence of RhoH, Rac1 activity would be upregulated. Indeed, basal Rac1 activity was increased in RhoH-null DP thymocytes (s. 4.6.4), suggesting that RhoH is a negative regulator of Rac1 activity in the resting state, and ablation of RhoH removes the inhibitory mechanism of Rac1 activation. On the other hand, increased Rac1 activity could be a compensatory change in response to the loss of RhoH. Against our expectation, Rac1 activity was not further enhanced in TCR-stimulated RhoH-deficient DP thymocytes, but was similar to that in control cells (s. 4.6.4), which argues against the hypothesis that RhoH antagonizes Rac1 activity. It could however be possible that in the absence of RhoH the activity of Rac1 in resting DP thymocytes reached its maximum, and could not be increased further. Vav1, a hematopoietic GEF for Rac1, is not a very probable candidate of being antagonized by RhoH, since activity of Vav1 was not raised in the resting state of RhoH-deficient thymocytes and even reduced after TCR ligation (s. 4.6.3).

It is unlikely that the increased basal activity of Rac1 in RhoH-null DP thymocytes is the reason for the impaired thymocyte development. As mentioned before, constitutive activation of Rac1 should rather result in "augmented" TCR signaling (s. 5.1). Constitutively active Rac1 can rescue the defective DN3 to DN4 transition in Vav1-null thymocytes and increase the expression of TCRβ, CD5 and CD69 on DP and CD4SP cells (Gomez et al., 2000; 2001) opposite to the phenotype of RhoH-deficient cells (s. 4.4.4.1; 4.4.4.6). Conceivably, the different phenotypes are explained by the fact that the level of active Rac1 is much lower in RhoH-deficient thymocytes than in thymocytes overexpressing the constitutively active mutant form of Rac1 (Gomez et al., 2000; 2001).

To address the possible contribution of increased basal activity of Rac1 in RhoH-mutant thymocytes to the defective T cell development, RhoH-null mice could be intercrossed with mice with deficiency for Rac1 in the hematopoietic system and examined to see whether thymocyte development can be restored.

It should also be noted that Rac2 activation was not altered in RhoH-deficient DP thymocytes (s. 4.6.4), suggesting a differential regulation of Rac1 and Rac2 and that there might be no crosstalk between RhoH and Rac2.

Analysis of activation of other Rho GTPases such as RhoA or Cdc42 in thymocytes deficient for RhoH will shed more light on the crosstalk between RhoH and other members of the Rho GTPase family.

5.7 Can RhoH-deficiency cause autoimmunity?

In RhoH-deficient mice expressing a transgenic OT-II TCR, positive selection into the CD4 lineage was abrogated due to impaired TCR signaling (s. 4.5.2). Positive selection requires weak TCR signaling and ensures that no autoreactive thymocytes, which induce strong TCR signaling upon antigen binding, can enter the periphery. However, in RhoH-deficient mice expressing OT-II TCR, attenuated TCR signaling was not sufficient to rescue thymocytes from death by neglect and to initiate positive selection. In RhoH-mutant mice carrying no transgenic OT-II TCR, mature T cells could still be generated, though in reduced numbers, since DP thymocytes express TCRs of different affinities. Thymocytes with TCRs of high affinity, which would normally initiate a strong TCR signaling upon ligand engagement and would be deleted by negative selection, are now positively selected in RhoH-null mice, and thus most likely represent the detected SP cells.

In mice with decreased TCR signaling it has been observed that positively selected potentially autoreactive T cells can emigrate into the periphery, where they are activated by self-antigens (Cope, 2004). Indeed, in the absence of RhoH increased amount of splenic and lymph node CD4+ and CD8+ T cells exhibited an activated phenotype of CD62L^{low}CD44^{high} (s. 4.4.4.3), which could constitute an autoreactive T cell pool, suggesting that these cells are not efficiently removed during thymocyte development. Supporting the idea that altered signal transduction through the TCR changes the thresholds in thymic selection, leading to positive selection of otherwise negatively selected autoimmune T cells, is the recent publication on the SKG mice, which spontaneously develop arthritis due to self-reactive T cells. These cells escape thymic negative selection by attenuated TCR signaling, caused by a point mutation in the *ZAP70* gene (Sakaguchi et al., 2003; Cope, 2004). This could also be true for RhoH-

deficient mice. Although we did not notice any obvious signs of autoimmune disease, it will be important to test whether autoimmune T cells in RhoH-mutant mice are present in the periphery, whether RhoH-deficient mice have an increased susceptibility to autoimmune diseases, and whether reduced levels of RhoH are found in patients suffering from autoimmune illnesses.

5.8 RhoH is important for T cell dependent immune response

After immunization of RhoH-deficient mice with the T cell dependent antigen, we detected normal IgM levels, but reduced IgG1 and Igλ titers during primary and memory response (s. 4.7). These results signify that RhoH is important for T cell dependent antibody production.

Since RhoH-null T and B cells could localize normally to the B and T cell areas within peripheral lymphoid organs, we can exclude that the impaired immune response was caused by the inability of RhoH-deficient lymphocytes to be recruited to these structures.

Isotype switching is controlled by cell-cell contacts between B and T cells via CD40-CD40L, B7.1/B7.2-CD28 and ICOS-ICOS ligand interactions, and by cytokines secreted by CD4+ helper T cells. Mice deficient for CD40, OCA-B, and Vav1 are not able to switch isotype and produce only IgM (Kawabe et al., 1994; Kim et al., 1996; Gulbranson-Judge et al., 1999). As discussed above, we would consider Vav1 to be the most likely candidate for regulation of class switching via the same pathway as RhoH.

RhoH-deficient T cells exhibited defective TCR signaling (s. 4.6), suggesting that they are unable to secrete cytokines and upregulate co-stimulatory molecules that are essential for B cell activation and class switching. Whether this might be the reason for the defective immune response, could be analyzed by *in vitro* stimulation assays of T cells with wild type antigen presenting cells, examining proliferation, cytokine production and cell surface expression of co-stimulatory receptors.

It is also possible that cell-cell contacts between B and T cells in the absence of RhoH cannot be formed effectively, attenuating B lymphocyte stimulation.

Alternatively, significantly reduced T cell numbers in secondary lymphoid organs of RhoH-mutant mice can activate less B cells and diminished numbers of activated B cells may account for the decreased immune response.

Another hypothesis for the reduced antibody levels could be a decreased intrinsic ability of RhoH-deficient B cells to be activated or to induce isotype switching. RhoH might transduce signals through the BCR or accessory molecules and thus serve as a positive regulator of B cell activation. To investigate whether RhoH-null B cells can be activated and initiate class

switching normally, *in vitro* stimulation of B cells could be performed and the secreted antibodies examined by ELISA. An *in vivo* approach to dissect B cell activation and antibody production by T helper cells could be the immunization of mice with a T cell independent antigen, such as NP-Ficoll, and analysis of antibody titers. If B lymphocytes can be activated and undergo isotype switching normally, similar antibody levels should be detected in sera from RhoH-deficient and control mice.

Given that RhoH expression was shown to be higher in Th1 than in Th2 cells (Li et al., 2002), we predicted a skewing towards Th2 response after immunization with a T cell dependent antigen, which would manifest in an increase of Th2 type antibody levels over Th1 type immunoglobulins. In contrast, we detected reduced levels of Th2 type antibody IgG1 in RhoH-deficient mice (s. 4.7). Levels of Th1 type antibodies were similarly low in both control and RhoH-null mice (s. 4.7). It has to be noted that the NP_{20}-CG antigen used in this immunization study induces predominantly Th2 type antibody IgG1, and to a lower extent Th1 antibodies. Therefore, no clear statement can be made regarding RhoH role in Th1 response. Other immunogens have to be applied which can induce a Th1 response to resolve this question.

Finally, RhoH might also have a function in DCs. Rescue of the defect by adoptive transfers of B, T cells and DCs into RhoH-mutant mice and induction of an immune response will prove which cell types are functionally defective in the absence of RhoH.

5.9   RhoH is not crucial for β2-integrin mediated adhesion

Adhesion plays an important role in development, migration and biological function of hematopoietic cells and implicates adhesion molecules such as cadherins, selectins, ICAMs, and integrins, whose activity and cell surface expression is tightly regulated by chemokines/cytokines.

Integrins are family of 24 transmembrane proteins, which consist of an α and a β subunit and mediate binding to extracellular matrix molecules, soluble substances and cellular receptors (Hynes, 2002). LFA-1 (αLβ2-integrin) is expressed on all leukocytes, with highest expression on lymphocytes, and binds to ICAM-1, -2 and -3. LFA-1 mediated adhesion in leukocytes is tightly regulated and LFA-1 becomes activated only upon chemokine stimulation (Springer TA, 1990).

RhoH was suggested to be important to keep leukocytes in the non-adhesive state, since in Jurkat cells and human peripheral blood lymphocytes, RhoH was found to negatively regulate

LFA-1-mediated adhesion (Cherry et al., 2004). By which mechanism RhoH affects LFA-1 adhesiveness, was not studied.

According to the information on a suppressive role of RhoH on the LFA-1 integrin, we expected increased LFA-1 adhesion in cells lacking RhoH. If increased LFA-1 activity would be the major consequence of RhoH-deficiency, then we would expect normal cellularity of BM and thymus, enlarged spleen and reduced lymph nodes with no alterations in T cell development (Semmrich et al., 2005). These observations did not correspond to the phenotype of RhoH-deficient mice. In contrast to the anticipated elevated LFA-1 binding capacity, we detected normal adhesion of RhoH-null thymocytes to immobilized ICAM-1 (s. 4.8.1). This binding could be stimulated with Mn^{2+}, PMA or a combination of both (s. 4.8.1). Furthermore, RhoH-deficient T cell blasts could adhere normally to endothelial cells and adhesion could be stimulated upon TNF treatment of endothelial cells (s. 4.8.1). These results suggest that RhoH might not be required for the regulation of LFA-1 adhesiveness.

Our results do not rule out a more subtle role for RhoH in cell adhesion and cell-cell-contacts *in vivo*. For example, altered frequency or duration of conjugate formation between thymocytes and thymic stroma could contribute to abnormal positive or negative selection in the absence of RhoH. However, such subtle changes in LFA-1 dependent adhesion would not explain the cell autonomous defect in TCR signaling in DP thymocytes *in vitro* (s. 4.6). Moreover, deletion of β2-integrin in addition to RhoH did not modulate impaired thymocyte development of RhoH-deficient mice (s. 4.8.2), suggesting that β2-integrin is not involved in this defect.

5.10   Future prospects

By analysis of RhoH-deficient mice we showed in this study a crucial role of RhoH in T cell development and pre-TCR and TCR signaling.

Future studies should address the role of RhoH in BCR signaling, since it shares several organizational features and molecules with TCR signaling. Completely unknown is also the role of RhoH for the function of γδ T cells, NK cells, mast cells and neutrophils.

The remaining central task for future research will be the identification of further RhoH binding partners. Discovery of new molecules binding to RhoH will help to resolve open questions in the mechanism of RhoH function in TCR signaling. In addition, it might shed light on posttranscriptional regulation of RhoH besides the reported TCR-mediated phosphorylation (Gu et al., 2006), and will reveal whether RhoH can hydrolyze GTP in the presence of a special GAP and whether it can be activated by GEFs.

With respect to the mutations that have been found in the *RhoH* gene in a number of lymphomas, it will be of particular significance to investigate whether RhoH is promoting or inhibiting lymphoma formation in mouse lymphoma models. Special focus will be on leukemia stem cells, since RhoH was reported to have an inhibitory effect on proliferation and survival of normal HSCs (Gu et al., 2005a).

Finally, it will be interesting to analyze whether RhoH-deficient mice develop autoimmune disorders.

6 References

Albagli, O., Dhordain, P., Deweindt, C., Lecocq, G., and Leprince, D. (1995). The BTB/POZ domain: a new protein-protein interaction motif common to DNA- and actin-binding proteins. *Cell Growth Differ* 6: 1193-1198.

Alberola-Ila, J., and Hernandez-Hoyos, G. (2003). The Ras/MAPK cascade and the control of positive selection. *Immunol Rev* 191: 79-96.

Ashwell, J. D. (2006). The many paths to p38 mitogen-activated protein kinase activation in the immune system. *Nat Rev Immunol* 6: 532-540.

Azzam, H. S., Grinberg, A., Lui, K., Shen, H., Shores, E. W., and Love, P. E. (1998). CD5 expression is developmentally regulated by T cell receptor (TCR) signals and TCR avidity. *J Exp Med* 188: 2301-2311.

Barnden, M. J., Allison, J., Heath, W. R., and Carbone, F. R. (1998). Defective TCR expression in transgenic mice constructed using cDNA-based alpha- and beta-chain genes under the control of heterologous regulatory elements. *Immunol Cell Biol* 76: 34-40.

Berg, L. J., Finkelstein, L. D., Lucas, J. A., and Schwartzberg, P. L. (2005). Tec family kinases in T lymphocyte development and function. *Annu Rev Immunol* 23: 549-600.

Bhandoola, A., and Sambandam, A. (2006). From stem cell to T cell: one route or many? *Nat Rev Immunol* 6: 117-126.

Bishop, A. L., and Hall, A. (2000). Rho GTPases and their effector proteins. *Biochem J* 348 Pt 2: 241-255.

Bodor, C., Bognar, A., Reiniger, L., Szepesi, A., Toth, E., Kopper, L., and Matolcsy, A. (2005). Aberrant somatic hypermutation and expression of activation-induced cytidine deaminase mRNA in mediastinal large B-cell lymphoma. *Br J Haematol* 129: 373-376.

Bokoch, G. M. (2003). Biology of the p21-activated kinases. *Annu Rev Biochem* 72: 743-781.

Bokoch, G. M. (2005). Regulation of innate immunity by Rho GTPases. *Trends Cell Biol* 15: 163-171.

Burridge, K., and Wennerberg, K. (2004). Rho and Rac take center stage. *Cell* 116: 167-179.

Cancelas, J. A., Lee, A. W., Prabhakar, R., Stringer, K. F., Zheng, Y., and Williams, D. A. (2005). Rac GTPases differentially integrate signals regulating hematopoietic stem cell localization. *Nat Med* 11: 886-891.

Carlyle, J. R., Michie, A. M., Furlonger, C., Nakano, T., Lenardo, M. J., Paige, C. J., and Zuniga-Pflucker, J. C. (1997). Identification of a novel developmental stage marking lineage commitment of progenitor thymocytes. *J Exp Med* 186: 173-182.

Ceredig, R., and Rolink, T. (2002). A positive look at double-negative thymocytes. *Nat Rev Immunol* 2: 888-897.

Chardin, P. (2006). Function and regulation of Rnd proteins. *Nat Rev Mol Cell Biol* 7: 54-62.

Cherry, L. K., Li, X., Schwab, P., Lim, B., and Klickstein, L. B. (2004). RhoH is required to maintain the integrin LFA-1 in a nonadhesive state on lymphocytes. *Nat Immunol* 5:

961-967.

Clements, J. L. (2003). Known and potential functions for the SLP-76 adapter protein in regulating T-cell activation and development. *Immunol Rev* 191: 211-219.

Coghlan, M. P., Chou, M. M., and Carpenter, C. L. (2000). Atypical protein kinases Clambda and -zeta associate with the GTP-binding protein Cdc42 and mediate stress fiber loss. *Mol Cell Biol* 20: 2880-2889.

Cope, A. P. (2004). Altered signalling thresholds in T lymphocytes cause autoimmune arthritis. *Arthritis Res Ther* 6: 112-116.

Corre, I., Gomez, M., Vielkind, S., and Cantrell, D. A. (2001). Analysis of thymocyte development reveals that the GTPase RhoA is a positive regulator of T cell receptor responses in vivo. *J Exp Med* 194: 903-914.

Cotteret, S., and Chernoff, J. (2006). Nucleocytoplasmic shuttling of Pak5 regulates its antiapoptotic properties. *Mol Cell Biol* 26: 3215-3230.

Cotteret, S., Jaffer, Z. M., Beeser, A., and Chernoff, J. (2003). p21-Activated kinase 5 (Pak5) localizes to mitochondria and inhibits apoptosis by phosphorylating BAD. *Mol Cell Biol* 23: 5526-5539.

Croker, B. A., Tarlinton, D. M., Cluse, L. A., Tuxen, A. J., Light, A., Yang, F. C., Williams, D. A., and Roberts, A. W. (2002). The Rac2 guanosine triphosphatase regulates B lymphocyte antigen receptor responses and chemotaxis and is required for establishment of B-1a and marginal zone B lymphocytes. *J Immunol* 168: 3376-3386.

Dallery, E., Galiegue-Zouitina, S., Collyn-d'Hooghe, M., Quief, S., Denis, C., Hildebrand, M. P., Lantoine, D., Deweindt, C., Tilly, H., Bastard, C., and et al. (1995). TTF, a gene encoding a novel small G protein, fuses to the lymphoma-associated LAZ3 gene by t(3;4) chromosomal translocation. *Oncogene* 10: 2171-2178.

Daumke, O., Weyand, M., Chakrabarti, P. P., Vetter, I. R., and Wittinghofer, A. (2004). The GTPase-activating protein Rap1GAP uses a catalytic asparagine. *Nature* 429: 197-201.

DerMardirossian, C., and Bokoch, G. M. (2005). GDIs: central regulatory molecules in Rho GTPase activation. *Trends Cell Biol* 15: 356-363.

Deutsch, A. J., Aigelsreiter, A., Staber, P. B., Beham, A., Linkesch, W., Guelly, C., Brezinschek, R. I., Fruhwirth, M., Emberger, W., Buettner, M., *et al.* (2007). MALT lymphoma and extranodal diffuse large B-cell lymphoma are targeted by aberrant somatic hypermutation. *Blood* 109: 3500-3504.

Di Santo, J. P. (2006). Natural killer cell developmental pathways: a question of balance. *Annu Rev Immunol* 24: 257-286.

Diebold, B. A., Fowler, B., Lu, J., Dinauer, M. C., and Bokoch, G. M. (2004). Antagonistic cross-talk between Rac and Cdc42 GTPases regulates generation of reactive oxygen species. *J Biol Chem* 279: 28136-28142.

Diehl, N. L., Enslen, H., Fortner, K. A., Merritt, C., Stetson, N., Charland, C., Flavell, R. A., Davis, R. J., and Rincon, M. (2000). Activation of the p38 mitogen-activated protein kinase pathway arrests cell cycle progression and differentiation of immature thymocytes in vivo. *J Exp Med* 191: 321-334.

Dijkman, R., Tensen, C. P., Buettner, M., Niedobitek, G., Willemze, R., and Vermeer,

M. H. (2006). Primary cutaneous follicle center lymphoma and primary cutaneous large B-cell lymphoma, leg type, are both targeted by aberrant somatic hypermutation but demonstrate differential expression of AID. *Blood* <u>107</u>: 4926-4929.

Ebinu, J. O., Bottorff, D. A., Chan, E. Y., Stang, S. L., Dunn, R. J., and Stone, J. C. (1998). RasGRP, a Ras guanyl nucleotide- releasing protein with calcium- and diacylglycerol-binding motifs. *Science* <u>280</u>: 1082-1086.

Etienne-Manneville, S., and Hall, A. (2002). Rho GTPases in cell biology. *Nature* <u>420</u>: 629-635.

Forget, M. A., Desrosiers, R. R., Gingras, D., and Beliveau, R. (2002). Phosphorylation states of Cdc42 and RhoA regulate their interactions with Rho GDP dissociation inhibitor and their extraction from biological membranes. *Biochem J* <u>361</u>: 243-254.

Gaidano, G., Pasqualucci, L., Capello, D., Berra, E., Deambrogi, C., Rossi, D., Maria Larocca, L., Gloghini, A., Carbone, A., and Dalla-Favera, R. (2003). Aberrant somatic hypermutation in multiple subtypes of AIDS-associated non-Hodgkin lymphoma. *Blood* <u>102</u>: 1833-1841.

Galandrini, R., Henning, S. W., and Cantrell, D. A. (1997). Different functions of the GTPase Rho in prothymocytes and late pre-T cells. *Immunity* <u>7</u>: 163-174.

Ghiaur, G., Lee, A., Bailey, J., Cancelas, J. A., Zheng, Y., and Williams, D. A. (2006). Inhibition of RhoA GTPase activity enhances hematopoietic stem and progenitor cell proliferation and engraftment. *Blood* <u>108</u>: 2087-2094.

Gillis, S., and Watson, J. (1980). Biochemical and biological characterization of lymphocyte regulatory molecules. V. Identification of an interleukin 2-producing human leukemia T cell line. *J Exp Med* <u>152</u>: 1709-1719.

Gomez, M., Kioussis, D., and Cantrell, D. A. (2001). The GTPase Rac-1 controls cell fate in the thymus by diverting thymocytes from positive to negative selection. *Immunity* <u>15</u>: 703-713.

Gomez, M., Tybulewicz, V., and Cantrell, D. A. (2000). Control of pre-T cell proliferation and differentiation by the GTPase Rac-I. *Nat Immunol* <u>1</u>: 348-352.

Gordon, M. S., Kanegai, C. M., Doerr, J. R., and Wall, R. (2003). Somatic hypermutation of the B cell receptor genes B29 (Igbeta, CD79b) and mb1 (Igalpha, CD79a). *Proc Natl Acad Sci U S A* <u>100</u>: 4126-4131.

Gu, Y., Chae, H. D., Siefring, J. E., Jasti, A. C., Hildeman, D. A., and Williams, D. A. (2006). RhoH GTPase recruits and activates Zap70 required for T cell receptor signaling and thymocyte development. *Nat Immunol* <u>7</u>: 1182-1190.

Gu, Y., Filippi, M. D., Cancelas, J. A., Siefring, J. E., Williams, E. P., Jasti, A. C., Harris, C. E., Lee, A. W., Prabhakar, R., Atkinson, S. J., *et al.* (2003). Hematopoietic cell regulation by Rac1 and Rac2 guanosine triphosphatases. *Science* <u>302</u>: 445-449.

Gu, Y., Jasti, A. C., Jansen, M., and Siefring, J. E. (2005a). RhoH, a hematopoietic-specific Rho GTPase, regulates proliferation, survival, migration, and engraftment of hematopoietic progenitor cells. *Blood* <u>105</u>: 1467-1475.

Gu, Y., Zheng, Y., and Williams, D. A. (2005b). RhoH GTPase: a key regulator of hematopoietic cell proliferation and apoptosis? *Cell Cycle* <u>4</u>: 201-202.

Gulbranson-Judge, A., Tybulewicz, V. L., Walters, A. E., Toellner, K. M., MacLennan, I. C., and Turner, M. (1999). Defective immunoglobulin class switching in Vav-deficient mice is attributable to compromised T cell help. *Eur J Immunol* <u>29</u>: 477-487.

Gupta, S., Fanzo, J. C., Hu, C., Cox, D., Jang, S. Y., Lee, A. E., Greenberg, S., and Pernis, A. B. (2003a). T cell receptor engagement leads to the recruitment of IBP, a novel guanine nucleotide exchange factor, to the immunological synapse. *J Biol Chem* <u>278</u>: 43541-43549.

Gupta, S., Lee, A., Hu, C., Fanzo, J., Goldberg, I., Cattoretti, G., and Pernis, A. B. (2003b). Molecular cloning of IBP, a SWAP-70 homologous GEF, which is highly expressed in the immune system. *Hum Immunol* <u>64</u>: 389-401.

Hall, A. (1998). Rho GTPases and the actin cytoskeleton. *Science* <u>279</u>: 509-514.

Hayday, A. C., and Pennington, D. J. (2007). Key factors in the organized chaos of early T cell development. *Nat Immunol* <u>8</u>: 137-144.

Hayes, S. M., and Love, P. E. (2007). A retrospective on the requirements for gammadelta T-cell development. *Immunol Rev* <u>215</u>: 8-14.

He, X., and Kappes, D. J. (2006). CD4/CD8 lineage commitment: light at the end of the tunnel? *Curr Opin Immunol* <u>18</u>: 135-142.

Henning, S. W., Galandrini, R., Hall, A., and Cantrell, D. A. (1997). The GTPase Rho has a critical regulatory role in thymus development. *Embo J* <u>16</u>: 2397-2407.

Hestdal, K., Ruscetti, F. W., Ihle, J. N., Jacobsen, S. E., Dubois, C. M., Kopp, W. C., Longo, D. L., and Keller, J. R. (1991). Characterization and regulation of RB6-8C5 antigen expression on murine bone marrow cells. *J Immunol* <u>147</u>: 22-28.

Hynes, R. O. (2002). Integrins: bidirectional, allosteric signaling machines. *Cell* <u>110</u>: 673-687.

Janeway, C. A.; Travers, P.; Walport, M.; Shlomchik, M. (2001). Immunobiology. Garland Science

Ihara, K., Muraguchi, S., Kato, M., Shimizu, T., Shirakawa, M., Kuroda, S., Kaibuchi, K., and Hakoshima, T. (1998). Crystal structure of human RhoA in a dominantly active form complexed with a GTP analogue. *J Biol Chem* <u>273</u>: 9656-9666.

Jaffe, A. B., and Hall, A. (2005). Rho GTPases: biochemistry and biology. *Annu Rev Cell Dev Biol* <u>21</u>: 247-269.

Kappes, D. J., He, X., and He, X. (2005). CD4-CD8 lineage commitment: an inside view. *Nat Immunol* <u>6</u>: 761-766.

Karnoub, A. E., Symons, M., Campbell, S. L., and Der, C. J. (2004). Molecular basis for Rho GTPase signaling specificity. *Breast Cancer Res Treat* <u>84</u>: 61-71.

Kawabe, T., Naka, T., Yoshida, K., Tanaka, T., Fujiwara, H., Suematsu, S., Yoshida, N., Kishimoto, T., and Kikutani, H. (1994). The immune responses in CD40-deficient mice: impaired immunoglobulin class switching and germinal center formation. *Immunity* <u>1</u>: 167-178.

Khosravi-Far, R., Chrzanowska-Wodnicka, M., Solski, P. A., Eva, A., Burridge, K., and Der, C. J. (1994). Dbl and Vav mediate transformation via mitogen-activated protein kinase pathways that are distinct from those activated by oncogenic Ras. *Mol Cell Biol*

14: 6848-6857.

Kim, C., and Dinauer, M. C. (2001). Rac2 is an essential regulator of neutrophil nicotinamide adenine dinucleotide phosphate oxidase activation in response to specific signaling pathways. *J Immunol* 166: 1223-1232.

Kim, U., Qin, X. F., Gong, S., Stevens, S., Luo, Y., Nussenzweig, M., and Roeder, R. G. (1996). The B-cell-specific transcription coactivator OCA-B/OBF-1/Bob-1 is essential for normal production of immunoglobulin isotypes. *Nature* 383: 542-547.

Kodama, H., Nose, M., Niida, S., Nishikawa, S., and Nishikawa, S. (1994). Involvement of the c-kit receptor in the adhesion of hematopoietic stem cells to stromal cells. *Exp Hematol* 22: 979-984.

Kondo, M., Wagers, A. J., Manz, M. G., Prohaska, S. S., Scherer, D. C., Beilhack, G. F., Shizuru, J. A., and Weissman, I. L. (2003). Biology of hematopoietic stem cells and progenitors: implications for clinical application. *Annu Rev Immunol* 21: 759-806.

Koretzky, G. A., Abtahian, F., and Silverman, M. A. (2006). SLP76 and SLP65: complex regulation of signalling in lymphocytes and beyond. *Nat Rev Immunol* 6: 67-78.

Kronenberg, M. (2005). Toward an understanding of NKT cell biology: progress and paradoxes. *Annu Rev Immunol* 23: 877-900.

Kuppers, R. (2005). Mechanisms of B-cell lymphoma pathogenesis. *Nat Rev Cancer* 5: 251-262.

Ladi, E., Yin, X., Chtanova, T., and Robey, E. A. (2006). Thymic microenvironments for T cell differentiation and selection. *Nat Immunol* 7: 338-343.

Lahousse, S., Smorowski, A. L., Denis, C., Lantoine, D., Kerckaert, J. P., and Galiegue-Zouitina, S. (2004). Structural features of hematopoiesis-specific RhoH/ARHH gene: high diversity of 5'-UTR in different hematopoietic lineages suggests a complex post-transcriptional regulation. *Gene* 343: 55-68.

Li, B., Yu, H., Zheng, W., Voll, R., Na, S., Roberts, A. W., Williams, D. A., Davis, R. J., Ghosh, S., and Flavell, R. A. (2000). Role of the guanosine triphosphatase Rac2 in T helper 1 cell differentiation. *Science* 288: 2219-2222.

Li, Q., Ho, C. S., Marinescu, V., Bhatti, H., Bokoch, G. M., Ernst, S. A., Holz, R. W., and Stuenkel, E. L. (2003). Facilitation of Ca(2+)-dependent exocytosis by Rac1-GTPase in bovine chromaffin cells. *J Physiol* 550: 431-445.

Li, X., Bu, X., Lu, B., Avraham, H., Flavell, R. A., and Lim, B. (2002). The hematopoiesis-specific GTP-binding protein RhoH is GTPase deficient and modulates activities of other Rho GTPases by an inhibitory function. *Mol Cell Biol* 22: 1158-1171.

Liso, A., Capello, D., Marafioti, T., Tiacci, E., Cerri, M., Distler, V., Paulli, M., Carbone, A., Delsol, G., Campo, E., *et al.* (2006). Aberrant somatic hypermutation in tumor cells of nodular-lymphocyte-predominant and classic Hodgkin lymphoma. *Blood* 108: 1013-1020.

Lores, P., Morin, L., Luna, R., and Gacon, G. (1997). Enhanced apoptosis in the thymus of transgenic mice expressing constitutively activated forms of human Rac2GTPase. *Oncogene* 15: 601-605.

Macian, F. (2005). NFAT proteins: key regulators of T-cell development and function. *Nat Rev Immunol* 5: 472-484.

Meller, N., Merlot, S., and Guda, C. (2005). CZH proteins: a new family of Rho-GEFs. *J Cell Sci* <u>118</u>: 4937-4946.

Moon, S. Y., and Zheng, Y. (2003). Rho GTPase-activating proteins in cell regulation. *Trends Cell Biol* <u>13</u>, 13-22.

Moreau, V., Frischknecht, F., Reckmann, I., Vincentelli, R., Rabut, G., Stewart, D., and Way, M. (2000). A complex of N-WASP and WIP integrates signalling cascades that lead to actin polymerization. *Nat Cell Biol* <u>2</u>: 441-448.

Muschen, M., Re, D., Jungnickel, B., Diehl, V., Rajewsky, K., and Kuppers, R. (2000). Somatic mutation of the CD95 gene in human B cells as a side-effect of the germinal center reaction. *J Exp Med* <u>192</u>: 1833-1840.

Na, S., Li, B., Grewal, I. S., Enslen, H., Davis, R. J., Hanke, J. H., and Flavell, R. A. (1999). Expression of activated CDC42 induces T cell apoptosis in thymus and peripheral lymph organs via different pathways. *Oncogene* <u>18</u>: 7966-7974.

Nagasawa, T. (2006). Microenvironmental niches in the bone marrow required for B-cell development. *Nat Rev Immunol* <u>6</u>: 107-116.

Nassar, N., Cancelas, J., Zheng, J., Williams, D. A., and Zheng, Y. (2006). Structure-function based design of small molecule inhibitors targeting Rho family GTPases. *Curr Top Med Chem* <u>6</u>: 1109-1116.

Nel, A. E. (2002). T-cell activation through the antigen receptor. Part 1: signaling components, signaling pathways, and signal integration at the T-cell antigen receptor synapse. *J Allergy Clin Immunol* <u>109</u>: 758-770.

Nel, A. E., and Slaughter, N. (2002). T-cell activation through the antigen receptor. Part 2: role of signaling cascades in T-cell differentiation, anergy, immune senescence, and development of immunotherapy. *J Allergy Clin Immunol* <u>109</u>: 901-915.

Northrop, J. P., Ullman, K. S., and Crabtree, G. R. (1993). Characterization of the nuclear and cytoplasmic components of the lymphoid-specific nuclear factor of activated T cells (NF-AT) complex. *J Biol Chem* <u>268</u>: 2917-2923.

Ohno, H. (2006). Pathogenetic and clinical implications of non-immunoglobulin ; BCL6 translocations in B-cell non-Hodgkin's lymphoma. *J Clin Exp Hematop* <u>46</u>: 43-53.

Okkenhaug, K., Bilancio, A., Emery, J. L., and Vanhaesebroeck, B. (2004). Phosphoinositide 3-kinase in T cell activation and survival. *Biochem Soc Trans* <u>32</u>: 332-335.

Palacios, E. H., and Weiss, A. (2004). Function of the Src-family kinases, Lck and Fyn, in T-cell development and activation. *Oncogene* <u>23</u>: 7990-8000.

Palmer, E. (2003). Negative selection--clearing out the bad apples from the T-cell repertoire. *Nat Rev Immunol* <u>3</u>: 383-391.

Pasqualucci, L., Migliazza, A., Basso, K., Houldsworth, J., Chaganti, R. S., and Dalla-Favera, R. (2003). Mutations of the BCL6 proto-oncogene disrupt its negative autoregulation in diffuse large B-cell lymphoma. *Blood* <u>101</u>: 2914-2923.

Pasqualucci, L., Neumeister, P., Goossens, T., Nanjangud, G., Chaganti, R. S., Kuppers, R., and Dalla-Favera, R. (2001). Hypermutation of multiple proto-oncogenes in B-cell diffuse large-cell lymphomas. *Nature* <u>412</u>: 341-346.

Peng, H. Z., Du, M. Q., Koulis, A., Aiello, A., Dogan, A., Pan, L. X., and Isaacson, P. G. (1999). Nonimmunoglobulin gene hypermutation in germinal center B cells. *Blood* <u>93</u>: 2167-2172.

Pennington, D. J., Silva-Santos, B., and Hayday, A. C. (2005). Gammadelta T cell development--having the strength to get there. *Curr Opin Immunol* <u>17</u>: 108-115.

Pitcher, L. A., Mathis, M. A., Young, J. A., DeFord, L. M., Purtic, B., Wulfing, C., and van Oers, N. S. (2005). The CD3 gamma epsilon/delta epsilon signaling module provides normal T cell functions in the absence of the TCR zeta immunoreceptor tyrosine-based activation motifs. *Eur J Immunol* <u>35</u>: 3643-3654.

Pitcher, L. A., Young, J. A., Mathis, M. A., Wrage, P. C., Bartok, B., and van Oers, N. S. (2003). The formation and functions of the 21- and 23-kDa tyrosine-phosphorylated TCR zeta subunits. *Immunol Rev* <u>191</u>: 47-61.

Porritt, H. E., Rumfelt, L. L., Tabrizifard, S., Schmitt, T. M., Zuniga-Pflucker, J. C., and Petrie, H. T. (2004). Heterogeneity among DN1 prothymocytes reveals multiple progenitors with different capacities to generate T cell and non-T cell lineages. *Immunity* <u>20</u>: 735-745.

Preudhomme, C., Roumier, C., Hildebrand, M. P., Dallery-Prudhomme, E., Lantoine, D., Lai, J. L., Daudignon, A., Adenis, C., Bauters, F., Fenaux, P., *et al.* (2000). Nonrandom 4p13 rearrangements of the RhoH/TTF gene, encoding a GTP-binding protein, in non-Hodgkin's lymphoma and multiple myeloma. *Oncogene* <u>19</u>: 2023-2032.

Puig, O., Caspary, F., Rigaut, G., Rutz, B., Bouveret, E., Bragado-Nilsson, E., Wilm, M., and Seraphin, B. (2001). The tandem affinity purification (TAP) method: a general procedure of protein complex purification. *Methods* <u>24</u>: 218-229.

Qiu, R. G., Chen, J., McCormick, F., and Symons, M. (1995). A role for Rho in Ras transformation. *Proc Natl Acad Sci U S A* <u>92</u>: 11781-11785.

Reiss, Y., Hoch, G., Deutsch, U., and Engelhardt, B. (1998). T cell interaction with ICAM-1-deficient endothelium in vitro: essential role for ICAM-1 and ICAM-2 in transendothelial migration of T cells. *Eur J Immunol* <u>28</u>: 3086-3099.

Reynolds, L. F., de Bettignies, C., Norton, T., Beeser, A., Chernoff, J., and Tybulewicz, V. L. (2004). Vav1 transduces T cell receptor signals to the activation of the Ras/ERK pathway via LAT, Sos, and RasGRP1. *J Biol Chem* <u>279</u>: 18239-18246.

Ridley, A. J., Paterson, H. F., Johnston, C. L., Diekmann, D., and Hall, A. (1992). The small GTP-binding protein rac regulates growth factor-induced membrane ruffling. *Cell* <u>70</u>: 401-410.

Riento, K., Guasch, R. M., Garg, R., Jin, B., and Ridley, A. J. (2003). RhoE binds to ROCK I and inhibits downstream signaling. *Mol Cell Biol* <u>23</u>: 4219-4229.

Rincon, M., and Pedraza-Alva, G. (2003). JNK and p38 MAP kinases in CD4+ and CD8+ T cells. *Immunol Rev* <u>192</u>: 131-142.

Roberts, A. W., Kim, C., Zhen, L., Lowe, J. B., Kapur, R., Petryniak, B., Spaetti, A., Pollock, J. D., Borneo, J. B., Bradford, G. B., *et al.* (1999). Deficiency of the hematopoietic cell-specific Rho family GTPase Rac2 is characterized by abnormalities in neutrophil function and host defense. *Immunity* <u>10</u>: 183-196.

Rosenbauer, F., and Tenen, D. G. (2007). Transcription factors in myeloid development:

balancing differentiation with transformation. *Nat Rev Immunol* 7: 105-117.

Rossman, K. L., Der, C. J., and Sondek, J. (2005). GEF means go: turning on RHO GTPases with guanine nucleotide-exchange factors. *Nat Rev Mol Cell Biol* 6: 167-180.

Rubinfeld, B., Munemitsu, S., Clark, R., Conroy, L., Watt, K., Crosier, W. J., McCormick, F., and Polakis, P. (1991). Molecular cloning of a GTPase activating protein specific for the Krev-1 protein p21rap1. *Cell* 65: 1033-1042.

Saiki, R. K., Gelfand, D. H., Stoffel, S., Scharf, S. J., Higuchi, R., Horn, G. T., Mullis, K. B., and Erlich, H. A. (1988). Primer-directed enzymatic amplification of DNA with a thermostable DNA polymerase. *Science* 239: 487-491.

Sakaguchi, N., Takahashi, T., Hata, H., Nomura, T., Tagami, T., Yamazaki, S., Sakihama, T., Matsutani, T., Negishi, I., Nakatsuru, S., and Sakaguchi, S. (2003). Altered thymic T-cell selection due to a mutation of the ZAP-70 gene causes autoimmune arthritis in mice. *Nature* 426: 454-460.

Salvador, J. M., Mittelstadt, P. R., Guszczynski, T., Copeland, T. D., Yamaguchi, H., Appella, E., Fornace, A. J., Jr., and Ashwell, J. D. (2005). Alternative p38 activation pathway mediated by T cell receptor-proximal tyrosine kinases. *Nat Immunol* 6: 390-395.

Scharffetter-Kochanek, K., Lu, H., Norman, K., van Nood, N., Munoz, F., Grabbe, S., McArthur, M., Lorenzo, I., Kaplan, S., Ley, K., et al. (1998). Spontaneous skin ulceration and defective T cell function in CD18 null mice. *J Exp Med* 188: 119-131.

Schmitt, T. M., and Zuniga-Pflucker, J. C. (2002). Induction of T cell development from hematopoietic progenitor cells by delta-like-1 in vitro. *Immunity* 17: 749-756.

Schmitt, T. M., and Zuniga-Pflucker, J. C. (2006). T-cell development, doing it in a dish. *Immunol Rev* 209: 95-102.

Swanson, B. J., Murakami, M., Mitchell, T. C., Kappler, J., and Marrack, P. (2002). RANTES production by memory phenotype T cells is controlled by a posttranscriptional, TCR-dependent process. *Immunity* 17: 605-615.

Schwartz, M. (2004). Rho signalling at a glance. *J Cell Sci* 117: 5457-5458.

Semmrich, M., Smith, A., Feterowski, C., Beer, S., Engelhardt, B., Busch, D. H., Bartsch, B., Laschinger, M., Hogg, N., Pfeffer, K., and Holzmann, B. (2005). Importance of integrin LFA-1 deactivation for the generation of immune responses. *J Exp Med* 201: 1987-1998.

Shen, H. M., Peters, A., Baron, B., Zhu, X., and Storb, U. (1998). Mutation of BCL-6 gene in normal B cells by the process of somatic hypermutation of Ig genes. *Science* 280: 1750-1752.

Shinohara, M., Terada, Y., Iwamatsu, A., Shinohara, A., Mochizuki, N., Higuchi, M., Gotoh, Y., Ihara, S., Nagata, S., Itoh, H., et al. (2002). SWAP-70 is a guanine-nucleotide-exchange factor that mediates signalling of membrane ruffling. *Nature* 416: 759-763.

Siebenlist, U., Brown, K., and Claudio, E. (2005). Control of lymphocyte development by nuclear factor-kappaB. *Nat Rev Immunol* 5: 435-445.

Simeoni, L., Kliche, S., Lindquist, J., and Schraven, B. (2004). Adaptors and linkers in T and B cells. *Curr Opin Immunol* 16: 304-313.

Socolovsky, M., Nam, H., Fleming, M. D., Haase, V. H., Brugnara, C., and Lodish, H. F. (2001). Ineffective erythropoiesis in Stat5a(-/-)5b(-/-) mice due to decreased survival of early erythroblasts. *Blood* 98: 3261-3273.

Sommers, C. L., Samelson, L. E., and Love, P. E. (2004). LAT: a T lymphocyte adapter protein that couples the antigen receptor to downstream signaling pathways. *Bioessays* 26: 61-67.

Sozio, M. S., Mathis, M. A., Young, J. A., Walchli, S., Pitcher, L. A., Wrage, P. C., Bartok, B., Campbell, A., Watts, J. D., Aebersold, R., *et al.* (2004). PTPH1 is a predominant protein-tyrosine phosphatase capable of interacting with and dephosphorylating the T cell receptor zeta subunit. *J Biol Chem* 279: 7760-7769.

Springer, T. A. (1990). Adhesion receptors of the immune system. *Nature* 346: 425-434.

Sugawara, T., Moriguchi, T., Nishida, E., and Takahama, Y. (1998). Differential roles of ERK and p38 MAP kinase pathways in positive and negative selection of T lymphocytes. *Immunity* 9: 565-574.

Swat, W., Dessing, M., von Boehmer, H., and Kisielow, P. (1993). CD69 expression during selection and maturation of CD4+8+ thymocytes. *Eur J Immunol* 23: 739-746.

Swat, W., Xavier, R., Mizoguchi, A., Mizoguchi, E., Fredericks, J., Fujikawa, K., Bhan, A. K., and Alt, F. W. (2003). Essential role for Vav1 in activation, but not development, of gammadelta T cells. *Int Immunol* 15: 215-221.

Szabo, S. J., Sullivan, B. M., Peng, S. L., and Glimcher, L. H. (2003). Molecular mechanisms regulating Th1 immune responses. *Annu Rev Immunol* 21: 713-758.

Takahama, Y. (2006). Journey through the thymus: stromal guides for T-cell development and selection. *Nat Rev Immunol* 6: 127-135.

Talts, J. F., Brakebusch, C., and Fassler, R. (1999). Integrin gene targeting. *Methods Mol Biol* 129: 153-187.

Tcherkezian, J., and Lamarche-Vane, N. (2007). Current knowledge of the large RhoGAP family of proteins. *Biol Cell* 99: 67-86.

Turner, M., Mee, P. J., Walters, A. E., Quinn, M. E., Mellor, A. L., Zamoyska, R., and Tybulewicz, V. L. (1997). A requirement for the Rho-family GTP exchange factor Vav in positive and negative selection of thymocytes. *Immunity* 7: 451-460.

Tybulewicz, V. L. (2005). Vav-family proteins in T-cell signalling. *Curr Opin Immunol* 17: 267-274.

Valencia, A., Chardin, P., Wittinghofer, A., and Sander, C. (1991). The ras protein family: evolutionary tree and role of conserved amino acids. *Biochemistry* 30: 4637-4648.

Van Hennik, P. B., and Hordijk, P. L. (2005). Rho GTPases in hematopoietic cells. *Antioxid Redox Signal* 7: 1440-1455.

Vetter, I. R., and Wittinghofer, A. (2001). The guanine nucleotide-binding switch in three dimensions. *Science* 294: 1299-1304.

Vincent, S., Jeanteur, P., and Fort, P. (1992). Growth-regulated expression of rhoG, a new member of the ras homolog gene family. *Mol Cell Biol* 12: 3138-3148.

Voll, R. E., Jimi, E., Phillips, R. J., Barber, D. F., Rincon, M., Hayday, A. C., Flavell, R.

A., and Ghosh, S. (2000). NF-kappa B activation by the pre-T cell receptor serves as a selective survival signal in T lymphocyte development. *Immunity* 13: 677-689.

Walmsley, M. J., Ooi, S. K., Reynolds, L. F., Smith, S. H., Ruf, S., Mathiot, A., Vanes, L., Williams, D. A., Cancro, M. P., and Tybulewicz, V. L. (2003). Critical roles for Rac1 and Rac2 GTPases in B cell development and signaling. *Science* 302: 459-462.

Wang, H. R., Zhang, Y., Ozdamar, B., Ogunjimi, A. A., Alexandrova, E., Thomsen, G. H., and Wrana, J. L. (2003). Regulation of cell polarity and protrusion formation by targeting RhoA for degradation. *Science* 302: 1775-1779.

Wange, R. L. (2003). The missing link(er): a return to symmetry in antigen receptor signaling? *Mol Interv* 3: 75-78, 50.

Wennerberg, K., and Der, C. J. (2004). Rho-family GTPases: it's not only Rac and Rho (and I like it). *J Cell Sci* 117: 1301-1312.

Wennerberg, K., Forget, M. A., Ellerbroek, S. M., Arthur, W. T., Burridge, K., Settleman, J., Der, C. J., and Hansen, S. H. (2003). Rnd proteins function as RhoA antagonists by activating p190 RhoGAP. *Curr Biol* 13: 1106-1115.

Wennerberg, K., Rossman, K. L., and Der, C. J. (2005). The Ras superfamily at a glance. *J Cell Sci* 118: 843-846.

Werlen, G., Hausmann, B., Naeher, D., and Palmer, E. (2003). Signaling life and death in the thymus: timing is everything. *Science* 299: 1859-1863.

Wu, X., and Frost, J. A. (2006). Multiple Rho proteins regulate the subcellular targeting of PAK5. *Biochem Biophys Res Commun* 351: 328-335.

Wu, J., Katrekar, A., Honigberg, L. A., Smith, A. M., Conn, M. T., Tang, J., Jeffery, D., Mortara, K., Sampang, J., Williams, S. R., *et al. (2006). Identification of substrates of human protein-tyrosine phosphatase PTPN22. *J Biol Chem* 281: 11002-11010.

Xiong, N., and Raulet, D. H. (2007). Development and selection of gammadelta T cells. *Immunol Rev* 215: 15-31.

Yamashita, I., Nagata, T., Tada, T., and Nakayama, T. (1993). CD69 cell surface expression identifies developing thymocytes which audition for T cell antigen receptor-mediated positive selection. *Int Immunol* 5: 1139-1150.

Yang, L., Wang, L., Geiger, H., Cancelas, J. A., Mo, J., and Zheng, Y. (2007). Rho GTPase Cdc42 coordinates hematopoietic stem cell quiescence and niche interaction in the bone marrow. *Proc Natl Acad Sci U S A* 104: 5091-5096.

Yu, H., Leitenberg, D., Li, B., and Flavell, R. A. (2001). Deficiency of small GTPase Rac2 affects T cell activation. *J Exp Med* 194: 915-926.

Zuniga-Pflucker, J. C. (2004). T-cell development made simple. *Nat Rev Immunol* 4: 67-72.

Acknowledgments

It would have never been possible to carry out this work without the help of many people to whom I am very grateful. I would like to express my sincere gratitude to:

Prof. Dr. Cord Brakebusch, my supervisor, for giving me the opportunity to work on this project, for his excellent teaching, expert advice, for being very supportive throughout my work and for critically reading my thesis.

Prof. Dr. Reinhard Fässler for giving me the possibility to work in his department.

Prof. Dr. Charles N. David, for accepting to be my "Doktorvater" at the university and for his support and for reviewing this thesis in such a short time.

Prof. Dr. Michael Schleicher, the 2nd referee of my thesis, Prof. Dr. Elisabeth Weiß, Prof. Dr. Jörg Nickelsen, Prof. Dr. Kirsten Jung and Dr. Angelika Böttger, the members of my thesis committee, for agreeing to review my work.

Prof. Dr. Karin Scharffetter-Kochanek, Dr. Thorsten Peters, Per Thor Straten and Dr. Joachim Ellwart for fruitful collaboration.

Dr. Wolfgang Klinkert and Tania Køllgaard for great help and patience with FACS sorting.

Dr. Michael Sixt for helping with FACS sorting and stimulating discussions.

Prof. Dr. Ari Waisman and Claudia Utthoff-Hachenberg for helping with ELISA assays.

Dr. Melanie Laschinger, Dr. Monika Semmrich and Prof. Dr. Bernhard Holzmann for helping with adhesion assays in such a short time and for great collaboration.

All members of the "old and new Cord's group", for creating a nice atmosphere in the lab, for a lot of discussions, help, for all the fun we had together and for being friends. I am very grateful to Anna, Martina, Gerd, Ola, Hanni, Sebastian, Uschi, Dan, Esben, Marie, Ben. Sahar for helping with mice, Richard for critically reading my thesis, and especially Tine and Xunwei who also came to Copenhagen. I would like to say a special "thank you" to Tine for reading my thesis.

Finally, my very special thanks go to my parents and my brother for their continuous support and to Klaus for his understanding, support and patience.

Curriculum vitae

Personal information

Name:	Tatjana Dorn
Date of birth:	27.01.79
Place of birth:	Nowokuznetsk, Russia
Nationality:	German

Education

01/2007 – 07/2007   **University of Copenhagen, BRIC, Copenhagen, Denmark**

PhD student in the group of Prof. Dr. Cord Brakebusch

02/2006 – 01/2007   **University of Copenhagen, Dept. of Molecular Pathology, Copenhagen, Denmark**

PhD student in the group of Prof. Dr. Cord Brakebusch

01/2004 – 01/2006   **Max-Planck-Institute of Biochemistry, Martinsried, Germany**

PhD student in the junior research group of Prof. Dr. Cord Brakebusch in the Dept. of Molecular Medicine, headed by Prof. Dr. Reinhard Fässler

11/1998 –11/2003   **Diploma in Biology, Ludwig-Maximilians-University, Munich, Germany**

Diploma student in the group of Prof. Dr. Rudolf Grosschedl, Gene Center, Munich, Germany

09/1995 – 07/1998   **Abitur, A.B. von Stettensches Institut, secondary school, Augsburg, Germany**

09/1994 – 07/1995   **Europäisches Gymnasium, secondary school, Berchtesgaden, Germany**

11/1993 – 07/1994   **Hauptschule, general secondary school, Rosshaupten, Augsburg, Germany**

09/1986 – 10/1993   **primary and secondary school, Nowokuznetsk, Russia**